UNIVERSITAT DE BARCELONA

An integrated assessment of nanoparticle exposures in the ceramic industry

Apostolos Salmatonidis

ADVERTIMENT. La consulta d’aquesta tesi queda condicionada a l’acceptació de les següents condicions d'ús: La difusió d’aquesta tesi per mitjà del servei TDX (**www.tdx.cat**) i a través del Dipòsit Digital de la UB (**diposit.ub.edu**) ha estat autoritzada pels titulars dels drets de propietat intel·lectual únicament per a usos privats emmarcats en activitats d’investigació i docència. No s’autoritza la seva reproducció amb finalitats de lucre ni la seva difusió i posada a disposició des d’un lloc aliè al servei TDX ni al Dipòsit Digital de la UB. No s’autoritza la presentació del seu contingut en una finestra o marc aliè a TDX o al Dipòsit Digital de la UB (framing). Aquesta reserva de drets afecta tant al resum de presentació de la tesi com als seus continguts. En la utilització o cita de parts de la tesi és obligat indicar el nom de la persona autora.

ADVERTENCIA. La consulta de esta tesis queda condicionada a la aceptación de las siguientes condiciones de uso: La difusión de esta tesis por medio del servicio TDR (**www.tdx.cat**) y a través del Repositorio Digital de la UB (**diposit.ub.edu**) ha sido autorizada por los titulares de los derechos de propiedad intelectual únicamente para usos privados enmarcados en actividades de investigación y docencia. No se autoriza su reproducción con finalidades de lucro ni su difusión y puesta a disposición desde un sitio ajeno al servicio TDR o al Repositorio Digital de la UB. No se autoriza la presentación de su contenido en una ventana o marco ajeno a TDR o al Repositorio Digital de la UB (framing). Esta reserva de derechos afecta tanto al resumen de presentación de la tesis como a sus contenidos. En la utilización o cita de partes de la tesis es obligado indicar el nombre de la persona autora.

WARNING. On having consulted this thesis you’re accepting the following use conditions: Spreading this thesis by the TDX (**www.tdx.cat**) service and by the UB Digital Repository (**diposit.ub.edu**) has been authorized by the titular of the intellectual property rights only for private uses placed in investigation and teaching activities. Reproduction with lucrative aims is not authorized nor its spreading and availability from a site foreign to the TDX service or to the UB Digital Repository. Introducing its content in a window or frame foreign to the TDX service or to the UB Digital Repository is not authorized (framing). Those rights affect to the presentation summary of the thesis as well as to its contents. In the using or citation of parts of the thesis it’s obliged to indicate the name of the author.

PhD Thesis

Apostolos Salmatonidis

2019

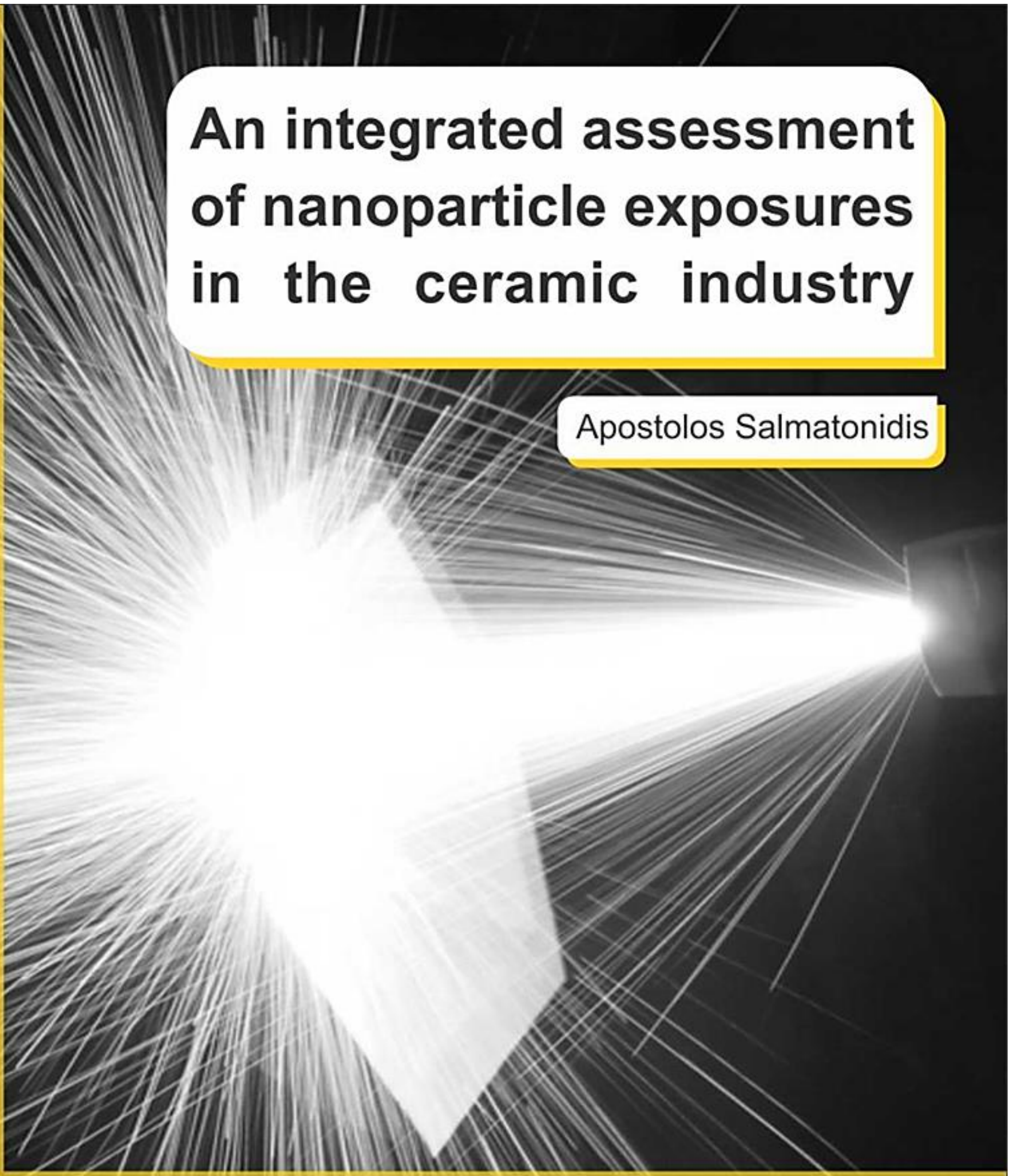

An integrated assessment of nanoparticle exposures in the ceramic industry

Apostolos Salmatonidis

UNIVERSITAT DE BARCELONA

CSIC

Faculty of Chemistry

Doctoral program "Analytical Chemistry and the Environment"

An integrated assessment of nanoparticle exposures in the ceramic industry

Apostolos Salmatonidis

PhD Thesis

Barcelona, July 2019

Supervisors	**Tutor**
Dr. María del Mar Viana Rodríguez	
(IDAEA-CSIC)	Dr. Ángeles Sahuquillo Estrugo
Prof. Dr. Eliseo Monfort Gimeno	(UB, Faculty of Chemistry)
(ITC-UJI)	

To the beacons of my life

Artemis, Konstantinos, Mar

‘‘ἕν οἶδα, ὅτι ούδέν οἶδα’’

free interpretation: “I know one thing, that I know nothing”

attributed to: **Socrates** (Greek philosopher, ca. 470-399 BC)

Summary

Exposure to nanoparticles has been associated with adverse effects on human health. When the exposure route is inhalation, nanoparticles can cause pulmonary inflammation which may be more severe than from fine particles, while significant associations between nanoparticles and cardiovascular morbidity have also been also observed. Consequently, industrial processes which release airborne nanoparticles into workplace air have become an issue of growing concern with regard to occupational exposure and potential health hazards for workers. Nanoparticles emitted by industrial activities may be engineered and used as input/output in a process, or formed unintentionally as a result of a given industrial activity and are referred to as process-generated nanoparticles. The latter have high probability to be released from high energy processes (e.g. thermal) and to impact exposure in various scenarios at diverse industrial settings.

The present PhD Thesis has three main objectives: to identify nanoparticle sources in industrial settings and characterize their release mechanisms, to characterize the different exposure scenarios, and to assess the effectiveness of mitigation strategies for exposure reduction. These objectives were addressed by applying an integrated assessment of nanoparticle exposures in real-world scenarios. All of the industrial scenarios studied were related to the ceramic industry (e.g. laser ablation of ceramic tiles, thermal spraying of ceramic coatings). The results obtained are presented in the form of four scientific papers.

The first scientific publication (1) identified pulsed laser ablation of ceramic tiles as a source of process-generated nanoparticles. This work studied the mechanisms controlling nanoparticle formation and release during ablation of different types of ceramic tiles. High particle number concentrations were detected (3.5×10^{4} to 2.5×10^{6} cm^{-3}) for all of the tiles and with both lasers assessed (near- and mid-infrared). Different particle release mechanisms were identified: during ablation with the near-IR laser particles were emitted through melting and nucleation, while emissions from the mid-IR laser were attributed to melting and mechanical shockwaves. Particle number and mass emissions were dependent on the tile surface characteristics as well as the laser parameters.

The second publication (2) characterized nanoparticle emissions and their impact on exposure during thermal spraying of ceramic coatings in a real-world industrial scenario. High particle number ($>10^{6}$ cm^{-3}; 30–40 nm) and mass (60–600 μgPM_1 m^{-3}) concentrations were recorded inside the spraying booths, which impacted exposure in the worker area (10^{4}–10^{5} cm^{-3}, 40–65 nm; 44–87 μgPM_1 m^{-3}). Irregularly-shaped, metal-containing particles (Ni, Cr, W) were sampled from the worker

area and a direct link between the spraying activity and exposure was established. In terms of particle number count, 90% of the particles were nanoparticles with sizes 26–90 nm. The third publication (3) discussed the hygroscopic properties of these nanoparticles, which were monitored online with an HTDMA. The nanoparticles emitted were found to take up moderate amounts of water when exposed to elevated relative humidity (87% RH), with their hygroscopicity being distinguishably lower compared to that of the atmospheric background aerosol particles present in the workplace air. Thus, particle hygroscopicity was identified as a useful metric to discriminate process-generated from background particles in workplace air.

Finally, the fourth scientific publication (4) quantified the effectiveness of mitigation strategies implemented during four different exposure scenarios under real-world settings. The nanoparticle removal efficiency of source enclosure combined with local exhaust ventilation was quantified to range between 65-99%, The highest efficiency was achieved by the combined use of a strong local exhaust ventilation with full enclosure (99.8%), tested during thermal spraying. Source substitution achieved a 91.5% reduction of exposure concentrations in the worker breathing zone, lower than the expected 100% due to interference from simultaneous sources. Mask respirators managed to reduce worker exposure by 86.7%, whereas source isolation reached maximum efficiency of 84.4%. The results highlight the interdependence of different mitigation strategies (e.g., LEV and source enclosure), which are frequently implemented simultaneously in real-world industrial scenarios. The mitigation measures for exposure reduction have proven to be more efficient when tailored to each specific industrial scenario.

The combination of key information and analyses deriving from the experimental scenarios assessed allowed to extract conclusions and recommendations with direct application to the industrial sector under study.

Resumen

La exposición a nanopartículas se asocia con efectos adversos en la salud humana. En consecuencia, las actividades industriales que liberan nanopartículas al aire en entornos laborales se han convertido en un problema de creciente relevancia desde el punto de vista de salud ocupacional y de los riesgos potenciales para la salud de los trabajadores. Las nanopartículas emitidas por actividades industriales pueden diseñarse y utilizarse como materia prima en procesos industriales, o formarse involuntariamente como resultado de una actividad industrial dada (estas últimas, denominadas con frecuencia nanopartículas de proceso). Las nanopartículas de proceso tienen una alta probabilidad de liberarse durante actividades altamente energéticas (por ejemplo, procesos térmicos) y de generar situaciones de exposición laboral en diversos escenarios y entornos industriales.

La presente tesis doctoral tiene tres objetivos principales: identificar fuentes de emisión de nanopartículas en entornos industriales y caracterizar sus mecanismos de liberación, caracterizar los diferentes escenarios de exposición, y evaluar la efectividad de las estrategias de mitigación para la reducción de la exposición. Estos objetivos se abordaron mediante la aplicación de una evaluación integrada de la exposición a nanopartículas en escenarios industriales reales (no en laboratorio). Todos los escenarios industriales estudiados estaban relacionados con procesos térmicos asociados a la industria cerámica (por ejemplo, ablación por láser de baldosas cerámicas, proyección térmica de recubrimientos cerámicos). Los resultados obtenidos se presentan en forma de cuatro publicaciones científicas.

La primera publicación científica (1) identificó la ablación por láser pulsado de baldosas cerámicas como una fuente de nanopartículas de proceso. La segunda publicación (2) describió las emisiones de nanopartículas y su impacto en la exposición durante la proyección térmica de recubrimientos cerámicos en un escenario industrial. La tercera publicación (3) analizó las propiedades higroscópicas de estas nanopartículas, que se monitorearon en línea con un HTDMA. Finalmente, la cuarta publicación científica (4) cuantificó la efectividad de las estrategias de mitigación implementadas en cuatro escenarios de exposición diferentes, en entornos industriales bajo condiciones reales de operación.

La combinación de información clave y de los análisis derivados de los escenarios experimentales evaluados permitió extraer conclusiones y recomendaciones con aplicación directa al sector industrial cerámico.

Contents

Table of Contents

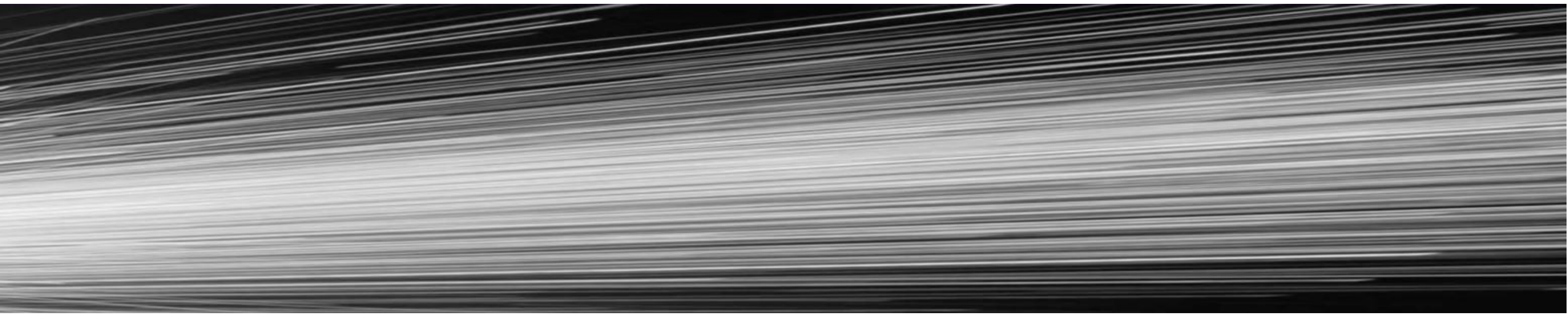

Chapter 1. **Introduction**

1. Introduction

1.1. Air pollution and health

1.1.1. Air pollution – history and health effects

Air pollution has been accompanying human activity since the ancient times, when concerns were raised by Roman philosopher and statesman Seneca[1] in A.D. 61. Lawsuits over smoke pollution were presented in Roman courts, when the jurist Titus Aristo declared that "*a cheese shop could not discharge smoke into the buildings above it*". The first legislative action against pollution was adopted in Constantinople by the Byzantine emperor Justinian in 535 AD, where clean air was declared as a birthright: "*by the law of nature these things are common to mankind – the air, running water, the sea*". "*Fumifugium*" was the first systematic report written by John Evelyn in 1661, which explicitly associated the burning of coal in London with poor air quality and health effects: "the capital's 'otherwise wholesome and excellent Aer' is corrupted by *a 'Hellish cloud of seacoal' and so its inhabitants 'breathe nothing but an impure and thick Mist accompanied with a fulginous and filthy vapor' corrupting the lungs and provoking coughs and catarrh*". Furthermore, drastic mitigation measures were proposed, such as the relocation of industrial buildings from the center of the city to regions where smoke could be diverted from urban areas by wind currents (Jenner, 1995). More recent events such as the infamous London Smog in 1952 led to the implementation of air quality limit values such as the UK Clean Air Act in 1956.

Environmental factors, in particular ambient air pollution pose risks with health implications. At present, ambient air pollution is associated with millions of premature deaths globally every year (WHO, 2016). In areas of the globe with high levels of ambient air pollution, such as India, one out of every eight deaths could be attributed to air pollution (Balakrishnan et al., 2019). Recent studies demonstrated that chronic exposure to high levels of airborne particulate matter impairs vascular function, which can lead to myocardial infarction, arterial hypertension, stroke, and heart failure (Lelieveld et al., 2019). Air pollution was responsible in 2015 for 19% of all cardiovascular deaths worldwide, 24% of ischemic heart disease deaths, 21% of stroke deaths, and 23% of lung cancer deaths (Landrigan, 2017). Sensitive population groups such as children and infants are most vulnerable to air pollutants (Kim and American Academy of Pediatrics Committee on Environmental Health, 2004). There is evidence linking air pollution with adverse effects on different birth outcomes

---

[1] Seneca the Younger (c. 4 BC-65 AD)

(Šrám et al., 2005), whereas respiratory symptoms, preterm birth, infant mortality, deficits in lung growth and asthma are also associated with air pollution (Kim and American Academy of Pediatrics Committee on Environmental Health, 2004). Lelieveld et al. (2015) predicted that under the current circumstances premature mortality will increase in Europe and the Americas mainly in urban areas; while large increases are estimated in Southeast Asia and the Western Pacific, will lead to a global growth of premature mortality to 6.6 million in 2050.

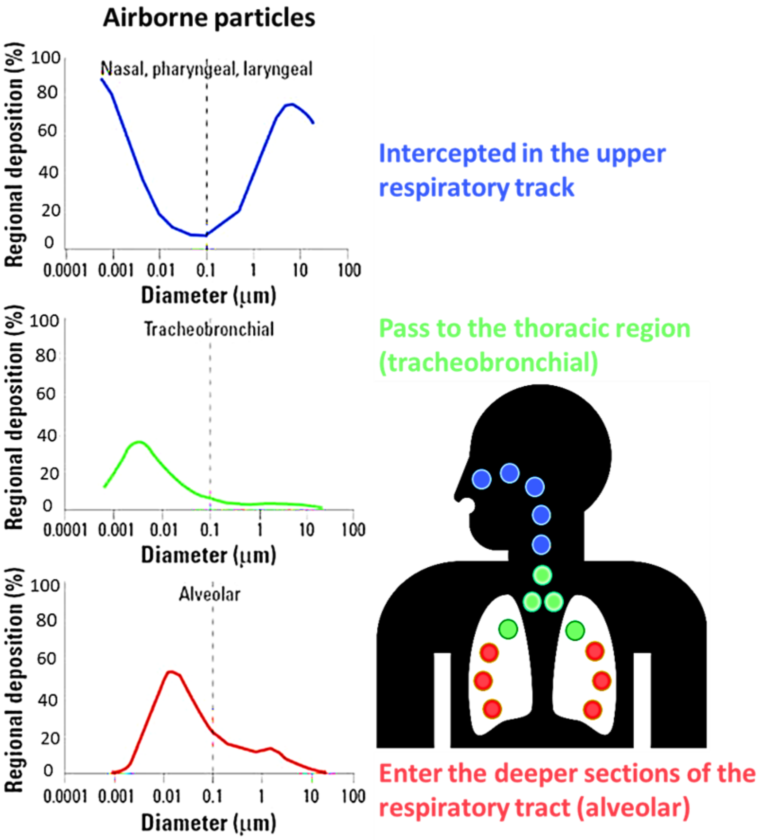

Figure 1.1. Regional deposition of inhaled particles in the human respiratory tract in terms of number, according to the International Commission on Radiological Protection (ICRP, 1994). Modified from Oberdörster et al. (2005).

1.1.2. Aerosols inhalation and toxicological response

Airborne particles (aerosols) penetrate into different regions of the human respiratory tract as a function of their size (Figure 1.1), which results in the fact that particles smaller than 100 nm can be deposited in the deeper parts of the respiratory tract (Oberdörster et al., 2005a) and even translocate to other organs through the bloodstream. Pope et al. (1995) associated air pollution with respiratory disease and cardiopulmonary mortality based on epidemiological evidence. Ferin et al. (1992) demonstrated that particles below 2.5 μm are responsible for pulmonary retention in rats, while Donaldson et al. (2002) reported that inhalation of particles smaller than 100 nm could lead to attacks of airways disease and systemic effects. Thereafter, numerous studies linked these particles (i.e. smaller than 100 nm) to adverse health effects mainly due to exposure through inhalation (Araujo et al., 2008; Hoek et al., 2010; Ibald-Mulli et al., 2002; Knibbs et al., 2011; Landrigan et al., 2017; Oberdörster and Utell, 2002). Inhaled nanoparticles are deposited in the respiratory tract mainly through diffusion (displacement due to collisions); whereas other mechanisms such as inertial impaction, gravitational sedimentation, interception affect larger particles and do not contribute to nanoparticle deposition (Oberdörster et al., 2005a).

Toxicological assessments of particles were carried out to understand the mechanisms leading to different morbidity cases (Donaldson et al., 2001b). The mechanism driving toxicological response to particles smaller than 100 nm can be summarized in different stages (Donaldson et al. (2001a):

- Impaired phagocytosis, when alveolar macrophage molecules are unable to clear lungs from particles, leads to particle accumulation.
- Increased interaction of the accumulated particles with the epithelium and the high oxidative stress due to particles' large surface area.
- Mediators (cytokine and chemokine) released due to oxidative stress, is considered a pro-inflammatory state which may lead to inflammation.

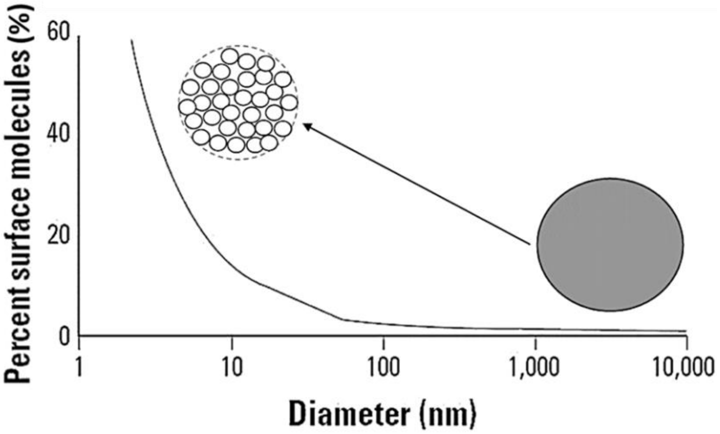

Figure 1.2. Ratio of surface to total molecules (surface of molecules) as a function of size. Surface area increases as the size (diameter) of particles decreases. Modified from Oberdörster et al. (2005).

Particle surface area increases exponential below 100 nm (Figure 1.2), and may significantly affect toxicity responses and induction of oxidative stress (Oberdörster et al., 2005b). Although it can be very challenging to measure particles bellow 10 nm, it is also very relevant because the surface area of particles >10 nm increases sharply (Figure 1.2). The deposited surface area can be a predictor of pulmonary inflammation (Donaldson et al., 2002). Particle inhalation is related with risk of cardiovascular disease through inflammation and with induced acute phase response (Saber et al., 2014). The acute phase response is the systemic response to acute and chronic inflammatory states caused by e.g. bacterial infection. Drivers of acute phase response are associated with risk of cardiovascular disease, including asthma and air pollution exposure (Gabay and Kushner, 1999). A direct connection between particle inhalation and acute phase response was also proven in experiments with human volunteers (Monsé et al., 2018).

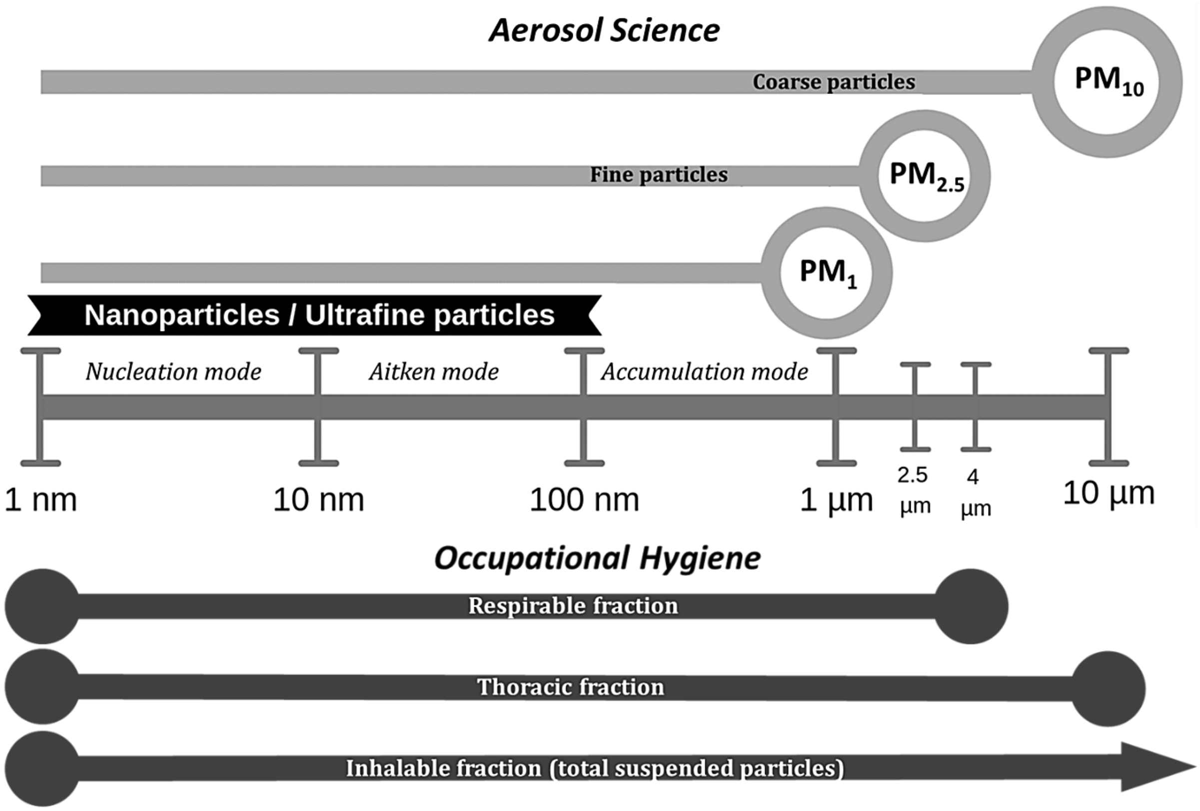

Figure 1.3. Particle classification based on their size (d_{50}).

1.2. Nanoparticles – definition and classification

1.2.1. Definition of nanoparticles particles based on their size

In the atmosphere, the complex and dynamic mixture of solid and liquid particles from natural and anthropogenic sources is known as aerosols (Hinds, 1999). Primary particles are those emitted directly to the atmosphere, while secondary particles are formed in the atmosphere from gaseous precursors. Airborne particulate matter (PM) can be classified based on the size distribution of airborne particles, specifically by the mass median diameter (d_{50}), as (Figure 1.3):

- PM_{10}: particles with d_{50} =10 µm. The fraction between 2.5 and 10 µm is frequently referred to as coarse particles. The sum of PM_{10} and particles with diameter >10 µm is known as total suspended particles (TSP). Furthermore, this fraction of particles is referred as thoracic in occupational hygiene nomenclature (Jiménez et al., 2011).
- PM_4: particles with d_{50} =4 µm. It is also referred as respirable fraction and is considered very relevant from the occupational health point of view (ACGIH, 1995; CEN, 1993; ISO, 1995).
- $PM_{2.5}$: particles with d_{50} =2.5 µm. It is widely used in environmental and ambient air quality studies.
- PM_1: particles with d_{50} =1 µm. It is the mass concentration fraction of the smallest particles suspended in air.
    - Accumulation mode particles: with diameters between 100 nm and 1 µm, accumulation mode particles typically have a long atmospheric residence time (Hinds, 1999; Harrison et al., 2000) and they include e.g. aged secondary aerosols and smog particles (Seinfeld & Pandis, 2006).
- Nanoparticles (NP): the prefix "*nano*", which comes from the Greek word "*νάνος*" meaning *dwarf*, is used to describe a very small magnitude (10^{-9}) of a metric: for time a nanosecond is 10^{-9} seconds, for size a nanometer is 10^{-9} meters (nm), etc. Therefore, materials in the nanometer range are referred to as nanomaterials. More specifically, according to 2011/696/EU Commission Recommendation on the definition of nanomaterial, a material containing particles with one or more external dimensions in the size range 1-100 nm can be classified as nanomaterial (EU, 2011). Consequently, particles with dimensions (e.g. diameter) in the size range 1-100 nm can also be referred to as nanoparticles, although other definitions are also available (Boverhof et al., 2015; Savolainen et al., 2010b). For comparison, interatomic distances – space between atoms – are only one order of magnitude smaller (10^{-10} m; Ångstroms).

- Ultrafine particles (UFPs): particles with diameter <100 nm, therefore including the Aitken (10-100 nm) and nucleation modes (1-10 nm).
    - Aitken mode particles: with diameters between 10-100 nm, Aitken mode particles originate from primary emissions (e.g., soot) and from coagulation/condensation of nucleation mode particles (Hinds, 1999; Kulmala et al., 2004; Seinfeld & Pandis, 2006).
    - Nucleation mode particles: particles with diameters <10 nm and formed from gaseous precursors, and which rapidly grow by condensation or coagulation with other particles (Hinds, 1999; Kulmala et al., 2004; Seinfeld & Pandis, 2006).

Thus, it is noticeable that ultrafine particles (UFPs) and nanoparticles (NPs) are equivalent in terms of particle diameter. Each term is used typically in a different research field: while the term UFPs is frequently used in aerosol research, e.g. covering ambient air quality, the term “nanoparticle” is often used in nanotechnology, indoor/workplace studies and regulation (e.g., EU, 2011). In the present Thesis the term nanoparticle (NP) will be used to refer to particles with diameter <100 nm.

1.2.2. Origin and types of nanoparticles in the air – anthropogenic & natural

Aerosols deriving from natural sources are dominant in the atmosphere at global scale in terms of mass concentration (<80%), while human activities contribute with a relatively small fraction (Deepshikha and Srinivasan, 2010; Voiland, 2010). Natural phenomena can produce nanoparticles, which are then released to the environment, with varying chemical composition and morphology depending on their sources. A large portion of atmospheric coarse and fine aerosols originate from dust transport; specifically, African mineral dust contributes to increased PM concentrations in southern Europe (Pey et al., 2013; Viana et al., 2014). Volcanic eruptions release gases (CO_2, SO_2 and HCl) and water vapors (von Glasow, 2010), but also significant amounts of particulate matter including nanoparticles (Buzea et al., 2007). Wildfires are an increasingly relevant phenomenon, during which carbonaceous emissions including nanoparticles are generated (Buzea et al., 2007). Secondary aerosols (<100nm; from nucleation processes) are emitted from seas and oceans around the world (O’Dowd and De Leeuw, 2007). All of the above natural sources are potential nanoparticle emitters (Sadik, 2013).

Anthropogenic[2] nanoparticle sources, on the other hand, involve human activities. When nanoparticles are intentionally manufactured they are known as engineered nanoparticles (ENPs;

---

[2] *Anthropos – Greek word for human (Άνθρωπος)*

Table 1.1), which are particles synthesized with specific characteristics (i.e. size, shape, chemical composition) and properties (e.g. optical, catalytic, surface chemistry) and for defined purpose or application. At the nanoscale, quantum-mechanical phenomena, Brownian motion, surface and interface interactions are much more pronounced than in the case of the macroscale, hence, the novel properties of nanomaterials. Nowadays, nanotechnology is a growing field and is gradually transforming a broad range of industrial sectors (cosmetics, electronics, automotive, construction, pharmaceutical and biomedicine; Schaming and Remita, 2015).

Aside from nanotechnology, nanoparticles may be formed and released unintentionally as a result of human activities, e.g., during high-energy thermal or mechanical industrial activities (mechanical machining of surfaces, thermal processes, combustion; Table 1.1). These particles are known as incidental, process-generated (PGNPs) or non-engineered (n-ENPs), and as a result of their unintentional formation they have no predetermined size, morphology or chemical composition. The vast variability of physical and chemical characteristics of these nanoparticles is not fully understood yet, because they strongly depend on the emission source and on the respective activity; and therefore, create a knowledge gap. Examples are diesel exhaust (soot) and combustion particles (BéruBé et al., 2007; D'Anna, 2009; Mills et al., 2011), fumes from different welding processes (Brand et al., 2013b; Cena et al., 2015; Graczyk et al., 2015; Jenkins et al., 2005; Lehnert et al., 2012; Sowards et al., 2008; Zimmer and Biswas, 2001) and rubber vulcanization (van Broekhuizen, 2017). In addition, mechanical processes such abrasion (Bello et al., 2009), gridding (Zimmer and Maynard, 2002), shredding (Raynor et al., 2012), drilling (van Broekhuizen et al., 2011) and sanding (van Broekhuizen, 2017) release PGNPs. Moreover, PGNPs are emitted by printing technologies e.g. during laser printing (Koivisto et al., 2010; Morawska et al., 2009) and 3D-printing (Gu et al., 2019; Stephens et al., 2013; Zhou et al., 2015). Furthermore, PGNPs are released during asphalt working (Elihn et al., 2008), metal casting (Evans et al., 2008) and also from high energy processes (Fonseca et al., 2016a, 2015; Salmatonidis et al., 2019a, 2018). The emission mechanisms and the physical-chemical properties of unintentionally-released nanoparticles are strongly dependent on the features of the industrial process generating them. Consequently, the broad variety of industrial activities and potential nanoparticle emission sources result in a large variability of potential nanoparticle emissions and associated health hazards.

Table 1.1. Examples of potential sources of nanoparticles in workplaces.

Engineered Nanoparticles (ENPs)	Nanomaterial production	Synthesis of nanoparticles in gas-phase (fire reactor, spark discharge)
	Nanomaterial application	Spray of nanoparticle suspensions and dispersions; Handling of nanoparticle powders
Process-Generated Nanoparticles (PGNPs)	Mechanical processes	Gridding; Milling; Abrasion (sanding, cutting); Machining; Shredding
	Combustion processes	Internal combustion engines (diesel, gasoline, gas); Incineration, Power plants (coal)
	Conventional thermal processes	Metal casting; Welding (metal, plastic); Sintering; Rubber manufacturing (vulcanization); Asphalt works
	High-energy processes	Laser (ablation, cutting, engraving, cladding); Plasma cutting; Plasma spraying

1.2.3. Nanoparticle sources and impacts on occupational exposure

Exposure is defined as the contact between an agent and a target. For inhalation exposure, this contact takes place through the nose and open mouth over an exposure period (Zartarian et al., 2005). Estimations suggest that 2 million workers will be employed in nanotechnology industries by 2020 (NIOSH, 2013), and this increase in production and use of nanomaterials drives a potential for increased exposure of workers to nanomaterials (Invernizzi, 2011). Along with the new technology arise unknown aspects, many of them concerning occupational safety and health. In addition, nanoparticles are unintentionally formed and released during diverse industrial activities, where occupational risks also occur. Numerous research studies have been carried out to expand knowledge about the effects of nanomaterials (Schulte et al., 2016, 2014). Kuhlbusch et al. (2018) in their study on nanomaterial exposures expressed a straightforward concept: a risk is only present if an exposure is possible. Savolainen et al. (2010b, 2010a) pointed out the need to characterize the different ENM exposure scenarios, along with ENM characteristics, and use these data for health risk assessment with a special emphasis on occupational environments. Literature reviews on ENPs occupational exposures show that exposures occur more frequently during ENP application and handling activities such as cleaning and maintenance (Ding et al., 2017), collection/harvesting, spraying and finishing, as well as during those involving feeding into a process and handling of powders (Basinas et al., 2018; Debia et al., 2016).

In industrial sectors unrelated to nanotechnology, exposures to unintentionally-released nanoparticles occur during different types of activities (e.g. thermal, combustion, mechanical; (Fonseca et al., 2014; Salmatonidis et al., 2018, 2019a; Van Broekhuizen et al., 2012b; Viana et al., 2017). Other examples are mechanical processes such as grinding of bulk materials (e.g. ceramic, metallic, wood; (Zimmer and Maynard, 2002), sanding operations (Göhler et al., 2010) or even dry cutting of composite materials (Bello et al. (2009). Conventional heating processes have also been observed to generate nanoparticle emissions, such as metal casting (Evans et al., 2008), rubber manufacturing (Kim et al., 2013) and molding of polymers (van Broekhuizen, 2017). The same is true for welding methods, where high concentrations both in terms of mass and number were released (Brand et al., 2013a, 2013b), for which significant impacts on exposure were reported (Lehnert et al., 2012). In ambient air, asphalt workers are exposed to nanoparticles, among other pollutants, originating from asphalt fumes (Elihn et al., 2008), and nanoparticles are also released as combustion byproducts from diesel and petrol engines (Burtscher, 2005; Donaldson et al., 2005). A literature review (Viitanen et al., 2017) presented results according to which occupational exposure to incidental nanoparticles may be significantly higher than exposure to background concentrations.

In the case of emissions of process-generated nanoparticles, emission mechanisms may differ significantly between processes and result in the release of markedly different nanoparticle number concentrations and chemical composition, which are two drivers of health effects along with exposure duration and frequency. Indoor workplaces vary significantly in terms of infrastructure (size and geometry of the facilities), mitigation strategies implemented, and number of workers. Moreover, several activities are frequently carried out simultaneously, increasing the complexity of source identification. This variety of activities, infrastructure and operating conditions, results in the need for tailored and dedicated exposure assessments under the different industrial scenarios. However, case specific exposure assessments are scarce and further research is necessary to fill this gap. Finally, in ambient air, occupational exposure to nanoparticles may occur during e.g. asphalt works, welding, or sanding of surfaces, where the effect of background aerosols (e.g. traffic) might be significant.

1.2.4. Exposure assessment & characterization

Two basic conditions define exposure scenarios: (i) the emission source which drives the release mechanisms; and (ii) the interaction between the particles and the target (worker), in particular through the breathing air (Zartarian et al., 2005). Once exposure occurs, the characterization of the exposure scenario becomes the next concern. Typically, exposure assessment strategies and approaches are based on different aerosol metrics (Table 1.2), in order to address the complexity of exposure to nanoparticles (Brouwer et al., 2004; Maynard and Aitken, 2007). The measurement of the particular aerosol metrics can be performed either by real-time monitoring (online) or by sampling and posterior analysis of the samples (offline). While particle mass concentration is commonly used for ambient coarse and fine particles (Allen et al., 1997; Chow, 1995; Eleftheriadis et al., 2014; Manoli et al., 2002; Querol et al., 2007, 2004a, 2004b; Viana et al., 2014, 2008), metrics used in nanoparticle exposure assessments are biologically-relevant metrics such as surface area (Oberdörster et al., 2005b; Schmid and Stoeger, 2017; Stoeger et al., 2006; Warheit et al., 2006) and especially particle number concentration (Brouwer, 2010; Koivisto et al., 2012a; Tsai et al., 2009; Van Broekhuizen et al., 2012a).

Table 1.2. Particle metrics typically used in particle exposure assessment

Metrics	Units	Measurement
Particle number concentration	# / cm^3	online
Mass concentration	μg / m^3	online / offline
Surface area concentration	μg^2 / cm^3	online
Size & size distribution	nm	online
Chemical characterization	μg/m^3, ppm	offline
Structural & morphological characterization	not standardized	offline

A critical point for exposure characterization is the discrimination of nanoparticles emitted by a specific source from background aerosols (e.g., traffic soot) or from secondary sources (e.g., activities running in parallel). A typically used approach for this purpose is the near-field/far-field approach (Koivisto et al., 2015), according to which emissions monitoring takes place simultaneously in two locations: the source (near-filed) and the background (far-field). The comparative analysis of the two datasets, in terms of a specified metric (particle number/mass concentration) can indicate the potential impact of the source on worker exposure. An alternative route to identify the potential exposure risk of a source is based on the concept of statistical significance (Kaminski et al., 2015). According to the latter, the background particle number concentration is determined during non-activity periods in the worker area. Subsequently, particle number concentrations in the worker area are monitored and, if greater than the background concentration plus three times the geometric standard deviation of the background concentration, then the emissions are considered to significantly impact exposure. Towards a harmonization of exposure assessments, a tiered approach comprising of 3 tiers (initial, basic and expert) has been internationally recognized as standard procedure (OECD, 2015).

1.3. Nanoparticle exposure in the ceramic industry

Ceramic manufacturing is one of the most ancient fabrication practices on the planet. There is evidence that cobalt nanoparticles were unintentionally used in glass matrix since the Neolithic era as pigment (Colomban, 2013). Hence, nanoparticles have been present for centuries in ceramic production processes. Lycurgus Cup[3] is a famous glasswork from the Roman period, which takes a different color when illuminated from outside (green) and from inside (red). This is a combined effect of metallic nanoparticles (50-100 nm), in particular red transmission due to the absorption of gold and green reflectance due to the scattering of silver nanoparticles (Schaming and Remita, 2015). Thus, artisans working with ceramics throughout history were probably unintentionally exposed to nanoparticles.

Nowadays, as discussed above, the means to monitor and characterize the impact of different industrial activities on worker exposure have been developed, allowing the identification of potential health hazards. Sanfélix et al. (2018) demonstrated that a number of processes emit nanoparticles in the ceramic industry. Incidental nanoparticles can be emitted from different processes applied in the ceramic industry such as traditional pottery (Voliotis et al., 2014), ceramic tile sintering (Fonseca et al., 2016a) and novel methods such as thermal spraying (Salmatonidis et al., 2019a), laser ablation of ceramic tiles (Fonseca et al., 2015; Salmatonidis et al., 2018). Controlled experiments at pilot-plant scale demonstrated the relevance of adequately implemented mitigation strategies for exposure

---

[3] Fourth century CE

reduction in the case of thermal spraying (Viana et al., 2017). Hence, the literature review associated the processing of ceramic materials at high energy stages with unintentional nanoparticle emissions.

1.4. Mitigation measures & risk management

1.4.1. Mitigation strategies

The efficient implementation of targeted mitigation strategies is key for exposure reduction. When the emission source is clearly identified, exposure mitigation measures can be designed and applied with a specific focus. Fonseca et al. (2014) found clear evidence of exposure risk to carbon nanotubes (CNTs) during their manufacturing without local exhaust ventilation (LEV), while for the same case no significant exposure was detected when LEV was implemented. Kuhlbusch et al. (2011) describe several cases of worker exposure in nanotechnology workplaces despite the implementation of mitigation measures. During application, processing and handling of ENMs the emission sources can be identified and mitigation measures can be effectively implemented (Fonseca et al., 2018). Moreover, Koivisto et al. (2017) demonstrated that a library comprising quantitative release data from the processing of products containing ENMs could help predict exposure through modelling-based assessments.

Viitanen et al. (2017) assessed publications dealing with industrial sources of PGNPs particles and exposure concentrations in workplaces, concluded that real exposures (e.g. in welding and metal industry) were more than hundred times greater than those resulting from background aerosols. The obtained results of measurements were not conclusive enough to draw general conclusions with regard to exposure. Hence, addressing PGNPs release is challenging because of the complexity linked to source identification and isolation. Correspondingly, a number of real-world emission sources are difficult to be enclosed or contained; thus, implementing effective mitigation strategies becomes increasingly difficult (van Broekhuizen, 2017). Another limitation for designing efficient mitigation strategies are the large variability of industrial processes and their diverse implementation in each specific industrial plant.

A number of studies discussed the efficiency of PPE (e.g. protective gloves, clothes, filtering facepieces respirators, masks) against nanoparticle exposures (Kim et al., 2006, 2007; Lee et al., 2007; Myojo et al., 2017; Tsai et al., 2010). A recent review that quantified the efficiency of PPE and engineering controls (e.g. LEV) for reducing nanoparticle exposures in controlled scenarios such as laboratories, reported that the available data are inconclusive (Goede et al., 2018). A review of this literature showed that studies focused on PGNPs are less frequent than for engineered nanoparticles, and the little information about the effectiveness of applied technical measures refers mostly to laboratory-scale. Consequently, the data regarding the efficiency of nanoparticle exposure mitigation measures in real world facilities, at an industrial scale, are scarce and not standardized. Thus, a clear research gap is evidenced regarding the efficiency of mitigation strategies in real-world facilities at industrial scale.

1.4.2. Occupational risk management & hierarchy of controls

The requirement of the employer to provide a safe and healthy workplace was instructed by different organizations (EU, 1989; U.S.C., 1970) and defined based on previous experience (Schulte et al., 2014). In the framework of traditional industrial hygiene, the concept of the hierarchy of controls was developed (Halperin, 1996). Up-to-date risk management approaches are based on the hierarchy of controls (E.U., 2014; Schulte et al., 2008). In Table 1.3 the different levels of the hierarchy are classified by priority. The source elimination is the highest in hierarchy and is based rather on a prevention philosophy, or control of the hazard as close to the source as possible. The substitution of the source suggests the replacement of the emitter by a non-hazardous counterpart, depending on the type of the source (process or material) this may include the implementation of a new technology or a safer substance. The engineering controls include two type of measures: (i) the improvement of facilities design and the development of safer processes; and (ii) different types of extraction (local, central), ventilation and dilution (natural, forced). The administrative controls are policies which intent to limit exposure to a hazard by minimizing the potential duration of exposure, and through the establishment of good work practices. The use of personal protective equipment (PPE) is the lowest in the hierarchy because is meant to have complementary application in the cases where measures higher in the hierarchy cannot be used or where they are only partially effective. PPE include devices for protection against inhalation exposure (e.g. masks, respirators, helmets), but also gloves and clothing as protection to dermal exposure.

Table 1.3. Hierarchy of controls according to Schulte et al., 2008

I.	Source elimination	
II.	Source substitution	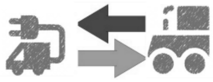
III.	Source enclosure	
IV.	Administrative controls	
V.	Engineering controls	
VI.	Personal protective equipment	

1.5. Legislation & Regulations

From a legislative point of view, the available toxicological and epidemiological data do not allow to establish occupational exposure limits (OEL) for the control of nanoparticle exposures in work environments (Kaluza et al., 2013; Van Broekhuizen et al., 2012a). The fact that a unique, harmonized definition for nanomaterials is not available (Boverhof et al., 2015; EU, 2011; Savolainen et al., 2010b), contributes to this ambiguity. Different regulatory agencies define different limit values for certain nanomaterials (Table 1.4), evidencing a lack of harmonization. In the absence of defined OELs, the precautionary approach is proposed, and in addition a set of nano-reference values (NRVs), referring particle number concentration, has been proposed (Van Broekhuizen et al., 2012a).

Table 1.4. Occupational Exposure Limits (OEL) for specific nanomaterials adopted by different agencies

Nanomaterials	**OEL / regulatory boards**		
	SER[a]	ECHA[b]	NIOSH[c]
Nano-TiO_2	-	-	0.3 mg/cm^3
Nano-fibers	0.01 fibers/cm^3	-	0.001 mg/cm^3
Nano-SiO_2 (fumes)	-	0.3 mg/cm^3	-
Biopersistent nanomaterial (density > 6×10^3 kg/cm^3)	$2*10^4$ /cm^3	-	-
Biopersistent nanomaterial (density < 6×10^3 kg/cm^3)	$4*10^4$ /cm^3	-	-

[a] *Social and Economic Council (Netherlands)*

[b] *European Chemical Agency (EU)*

[c] *National Institute for Occupational Safety and Health (USA)*

In the case of exceeding these reference values, it is recommended to adopt preventive and corrective measures to reduce exposure levels, which should be tailored to the needs of each specific scenario. In this sense, the International Council on Nanotechnology reviewed exposure control strategies implemented by industries worldwide and proposed a set of "best practices" to establish risk assessment frameworks (Conti et al., 2008; Gerritzen et al., 2006; WHO, 2017).

1.6. Gap analysis and motivation

Based on the literature review presented above, 3 main research gaps were identified which are the drivers of the present PhD Thesis:

1. Nanoparticles emitted unintentionally during the course of industrial activities have a major potential to generate workplace exposure impacts and risks. However, their emission mechanisms and the vast variability of physical-chemical properties of these nanoparticles are not fully characterized. This is because they strongly depend on the industrial activities generating nanoparticle release, which rapidly evolve based on innovative technologies and which also vary significantly from one plant to another. Thus, real-world studies on

nanoparticle formation and release mechanisms are necessary to contribute to the understanding of the drivers of workplace exposure.

2. Similarly, the impacts of such nanoparticle release mechanisms on workplace exposure are potentially large and highly variable. The combination of operating conditions (parametrization of the industrial activity under study) and workplace setup (dimensions, ventilation, air exchange rates, etc.) determine potential exposure risks. As a result, case-specific and real-world workplace exposure assessments are necessary to contribute to the growing body of literature on process-generated nanoparticle exposures.
3. Finally, exposures may be mitigated by means of a large variety of technological and non-technological measures. Their efficiency is, once again, dependent on a large number of parameters ranging from the design to the implementation of the measures, and their operating conditions tailored to the specific industrial activity under study. Whereas data are available in the literature on the effectiveness of mitigation strategies at laboratory scale, data on their implementation in real-world settings are scarce.

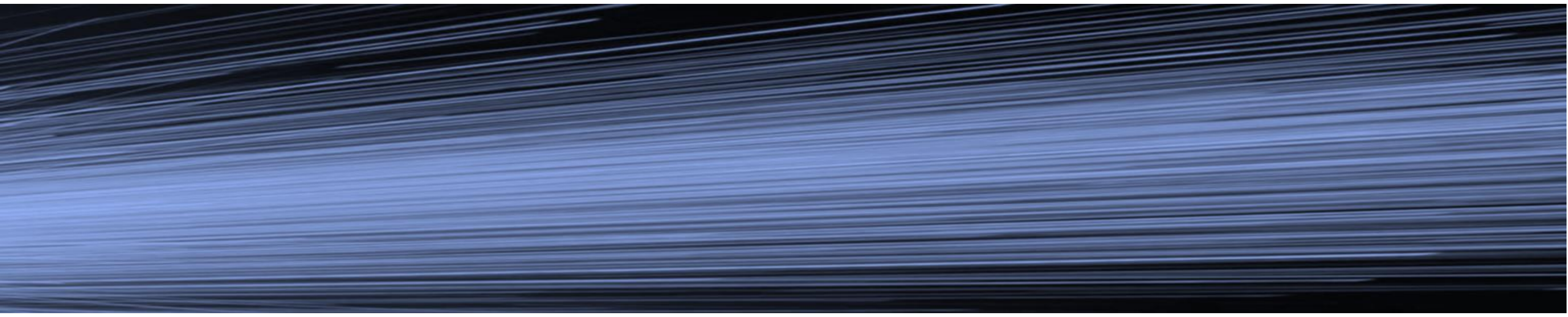

Chapter 2. **Scope, objectives and structure**

2. Scope, objectives and structure

2.1. Scope and objectives

A number of processes and activities in the ceramic industry unintentionally release nanoparticles and their inhalation can lead to potential health hazards. As described in the Gap Analysis (section 1.6), real-world and case-specific approaches are necessary to minimize or prevent nanoparticle exposures in occupational settings. This requires a holistic approach comprising three key types of information: emission mechanisms, exposure characterization, and mitigation measures.

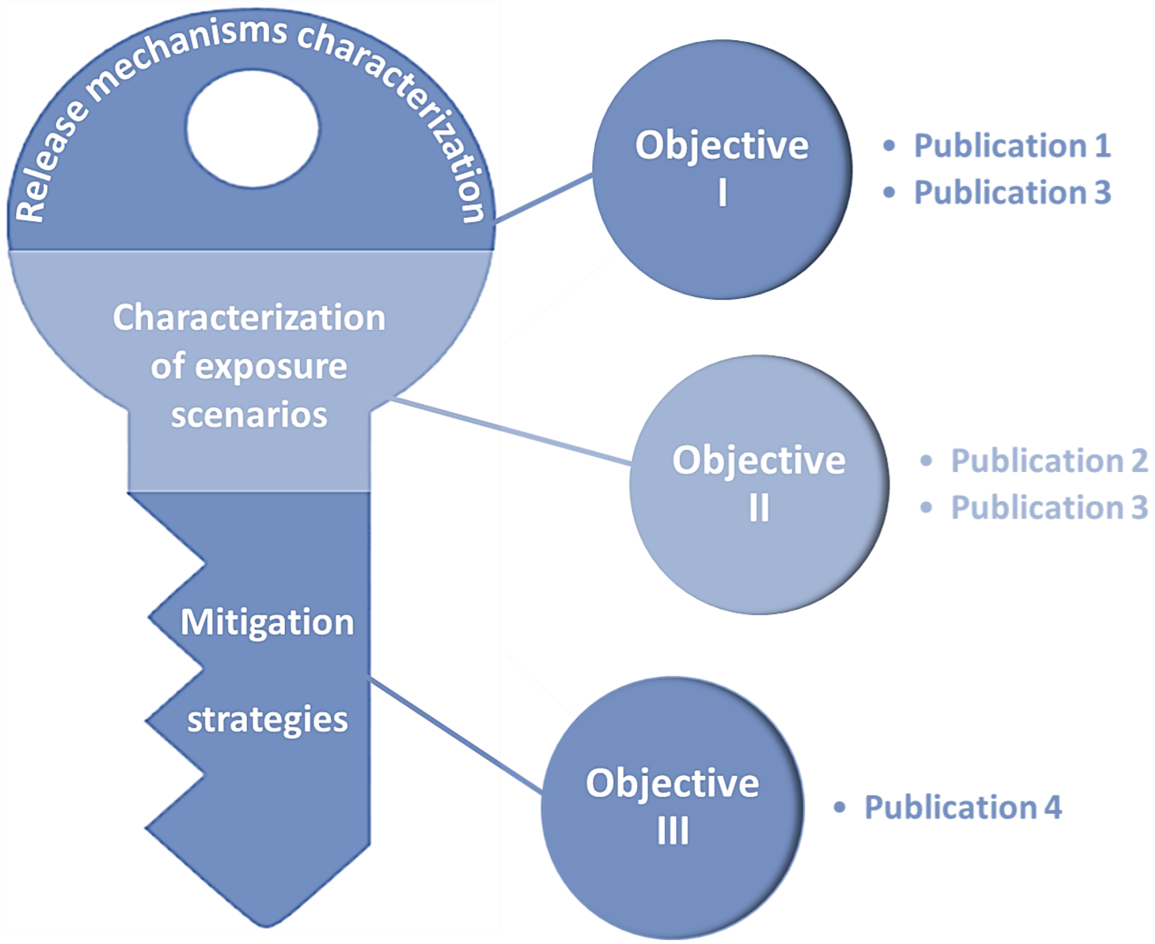

Figure 2.1. Schematic illustration of the integrated assessment proposed, its different stages and the scientific publications.

An integrated assessment is proposed in this PhD Thesis to reduce the risks and contribute to the nanosafety of industrial processes by restricting exposure. This assessment comprises three stages (Figure 2.1), each one covering a distinct research objective:

I. Identification of nanoparticle emission sources followed by the characterization of nanoparticle formation and release mechanisms. This is greatly depended on the energy footprint of each industrial activity, as high energy processes (e.g. thermal) are more probable to release high nanoparticles concentrations and relative low concentrations of coarse particles. Moreover, the properties (thermal/optical, microstructure, crystallinity, dustiness, etc.) of the input materials used in each industrial process (raw/target materials, feedstock, etc.) can influence the emission mechanism and particle release.

II. Identification and characterization of nanoparticle exposure scenarios in terms of particle size, number, mass concentrations and physicochemical properties. In order to ensure compatibility across scenarios, harmonized protocols should be implemented. A source oriented assessment is of importance here to discriminate nanoparticles released from specific activities from background aerosols, or from emissions originating from secondary processes. Moreover, additional properties such as the hygroscopicity of the emitted nanoparticles can be monitored online, providing important information regarding the behavior of nanoparticles as well as indicating their source. A comprehensive exposure analysis also includes the characterization of the emitted nanoparticles in terms of morphology (shape and size), composition, physicochemical properties and microstructure (e.g. crystallinity). The characterization of aerosols released is usually an offline procedure, samples are collected on-site and thereafter analyzed. Morphology (shape and size), and elemental composition are the main nanoparticle characteristics evaluated.

III. Design and implementation of tailored mitigation strategies, with optimal efficiency in exposure reduction. Different emission sources and diverse exposure scenarios creates the necessity for tailored mitigation strategies. Assessing and evaluating the information acquired from the previous stages, appropriate mitigation strategies can be designed The effectiveness of each mitigation measure applied is evaluated in order to guarantee its optimal efficiency and assure minimum occupational risks.

2.2 Thesis structure

The Introduction chapter (1) provides general information on aerosols, nanoparticle emissions from industrial process, their associated health impacts, exposure assessment and methods to reduce occupational risks. The current chapter (2), describes the scope, objective and structure of the present Thesis. In chapter 3 the methodology followed during experimental measurements, measurement principles, techniques and data treatment are described. The Results chapter (4) is comprised of four scientific publications (3 of them published, one of them under review) in peer-viewed international journals. Subsequently, the Discussion chapter (5) provides an integrated interpretation of the research findings. The main conclusions are drawn and presented in chapter 6, while the limitations of the current work and future research needs are discussed in chapter 7. The References followed by the Acknowledgements concludes this Thesis. Each one of the scientific publications included in this PhD Thesis addresses at least one research objective as follows:

- *Scientific publication 1*

Nanoparticle formation and emission during laser ablation of ceramic tiles; Apostolos Salmatonidis, Mar Viana, Noemí Pérez, Andrés Alastuey, Germán F. de la Fuente, Luis Alberto Angurel, Vicenta Sanfélix, Eliseo Monfort; Journal of Aerosol Science, 126 (2018) 152–168; DOI: https://doi.org/10.1016/j.jaerosci.2018.09.006

Objective: this publication addresses the first (I) objective of the Thesis.

The mechanisms determining NP emissions during laser ablation of ceramic tiles are characterized in this publication by correlating fundamental ablation phenomena with particle release. A parametric study was designed to assess the influence of material properties (composition, structural characteristics), laser sources (wavelength) as well as process parameters (pulse duration, frequency) on NP formation and emissions in terms of size, particle number and mass concentration. The ultimate goal of the present work was to increase the understanding of the mechanisms governing NP formation during laser ablation, which may provide insights for improved exposure assessments and facilitate the design of more efficient exposure mitigation measures.

- *Scientific publication 2*

Workplace Exposure to Nanoparticles during Thermal Spraying of Ceramic Coatings; Apostolos Salmatonidis, Carla Ribalta, Vicenta Sanfélix, Spyridon Bezantakos, George Biskos, Adriana Vulpoi, Simon Simion, Eliseo Monfort and Mar Viana; Annals of work exposures and health, 63, 1 (2019) 91-106; DOI: https://doi.org/10.1093/annweh/wxy094

Objective: this publication addresses the second (II) objective of the Thesis.

In indoor air and more specifically in industrial settings, unintentionally emitted NPs pose an occupational risk since they are generated and released to the worker area, with potential to impact workers' health. Hazards and risks need to be dealt with by means of both technological and non-technological mitigation strategies. The aim of this work was to assess NP release and characterize exposure scenarios during thermal spraying of ceramic coatings onto metallic surfaces and their impact on inhalation exposure, under real-world operating conditions in an industrial setting.

- *Scientific publication 3*

Hygroscopic behavior of ultrafine particles emitted during thermal spraying; Apostolos Salmatonidis, Mar Viana, George Biskos, Spyridon Bezantakos; Journal of Aerosol Science (under review)

Objective: this publication addresses the second (II) and first (I) objectives of the Thesis.

A Hygroscopic Tandem Differential Mobility Analyzer was used to probe the hygroscopicity of nanoparticles (i.e., their ability to take up water upon exposure to elevated humidity) in a thermal spraying facility. This is an intrinsic aerosol property which define the deposition behavior of inhaled aerosol particles in the human respiratory system, and consequently the associated health effects. Emitted NPs could be discriminated from background aerosols based on differences of their hygroscopicities. Primary particle size and number determined by the HTDMA measurements were compared with those observed by transmission electron microscopy (TEM). Furthermore, emission mechanisms during thermal spraying are identified.

- *Scientific publication 4*

Effectiveness of nanoparticle exposure mitigation measures in industrial settings; Apostolos Salmatonidis, Vicenta Sanfélix, Pablo Carpio, Lech Pawłowski, Mar Viana, Eliseo Monfort; International Journal of Hygiene and Environmental Health, 222 (2019) 926–935; DOI: https://doi.org/10.1016/j.ijheh.2019.06.009

Objective: this publication addresses the third (III) objective of the Thesis.

The last article aimed to quantify the efficiency of mitigation measures for NP exposure reduction implemented under real-world operating conditions in the ceramic industry. These measures included: ventilation, source enclosure, source substitution and source isolation. The efficiency of the measures was assessed following a case study approach. Exposure reductions were characterized in terms of particle number concentrations. Thus, this work is expected to fill a current knowledge gap on exposure mitigation strategies by contributing with quantitative data on the effectiveness of specific mitigation strategies.

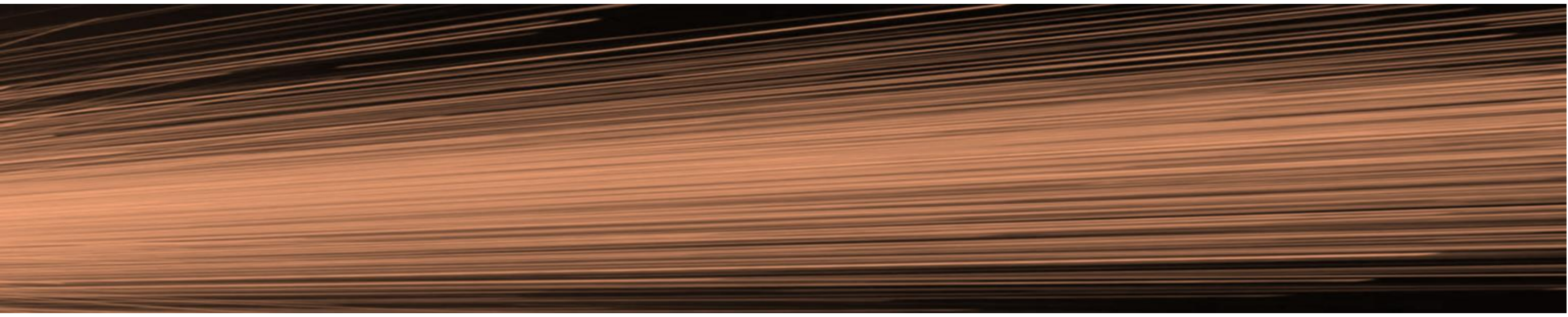

Chapter 3. **Methodology**

3. Methodology

3.1. Measurement principles, instrumentation, and particle characterization techniques

3.1.1. Real-time aerosol measurements – Online instruments

A range of monitoring instruments was used for the experimental sections of the work presented in this PhD Thesis, and is summarized in Table 3.1. The operating principles of each of the instruments and techniques used are described.

Condensation Particle Counters

Condensation Particle Counters (CPC) monitor particle number concentrations down to the nanometer size range, since their detection efficiency for small particles is better than those of optical particle counters (McMurry, 2000a). Within the instrument, particles are enlarged due to supersaturation and the subsequent condensation of a vapors to reach the diameter at which they can be optically detected and the number concentration quantified for particles larger than the instrument's lower detection diameter (Liu and Kim, 1977; Wiedensohlet et al., 1997). The lower detection diameter is determined by the Kelvin diameter, the supersaturation diffusion coefficient of the condensable gas and the particle material (Stolzenburg and McMurry, 1991). The upper and lower detection limits are specific for each CPC type. In addition to their environmental applications, CPCs have been used to detect snorkeling diesel submarines and also as "people sniffer" during the Vietnam war (McMurry, 2000b).

CPCs operate with continuous aerosol flows which allow them to count each single particle (Agarwal and Sem, 1980; Wiedensohlet et al., 1997). In alcohol-based CPCs the aerosol flow is saturated with vapors of a liquid (mainly butanol) in a slightly heated saturator. The temperature of the butanol-aerosol mixture is decreased by 17-27°C in the condenser of the CPC, where vapors supersaturate and condense onto the particles which grow to droplets of several µm in diameter. The droplet flow is focused in a nozzle and introduced into a counting optical detector. The droplets pass a laser beam, each single particle creates a light pulse, and pulses with an amplitude above a certain threshold are counted. The particle number concentration can be calculated for a given aerosol flow rate. Instead of alcohol, water can also be used for the measurement of sub-micrometer aerosol particles following a slightly different approach but the same principle (Hermann et al., 2007). The aerosol flow is saturated with water vapor and temperature equilibrated in a cooled saturator. The flow passes through a condenser with heated walls, which contain water, producing an elevated vapor pressure. The water vapors diffuse faster to the center of the aerosol flow than the heat from the walls and thus supersaturate it. The particles grow quickly to droplets of a detectable size and are counted by an optical detector.

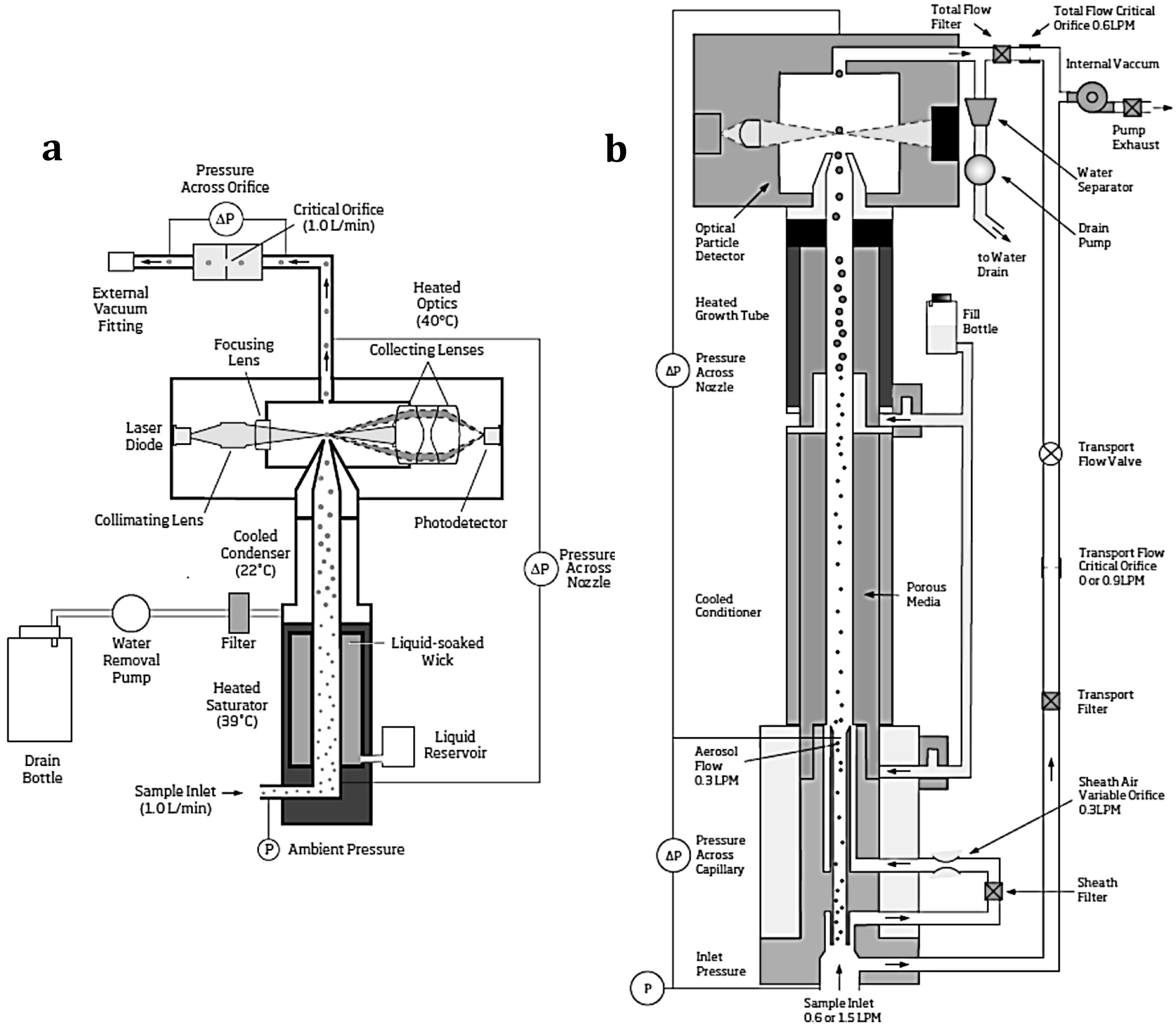

Figure 3.1. Schematic illustration of working principle of (a) alcohol – butanol CPC, (b) water CPC. Source: TSI Inc. (www.tsi.com),TSI models (a) 3776 and (b) 3788.

In the experimental measurements a butanol CPC (TSI model 3775) was used as a single counter to monitor total particle number concentration in the range of 4 nm–3 μm with 1-min resolution (publications 1 & 4). A butanol CPC TSI model 3376 (2.5-3μm; publication 1) and a butanol CPC TSI model 3010 (10nm-3µm; publication 3) were also used as part of more complex measurement set-ups.

Differential Mobility Analyzer

The working principle of a Differential Mobility Analyzer (DMA) is based on the capacity of electrically charged particles to move in an electric field according to their electrical mobility (Flagan, 1998). The electrical mobility depends mainly on particle size and electrical charge, as smaller particles have higher electrical mobility (Hinds, 1999; Liu and Pui, 1974b). Higher electrical charge also leads to higher electrical mobility (Knutson and Whitby, 1975). In constant temperature and pressure conditions and assuming that all particles carry only one electrical charge, the electrical mobility is a function of particle size (Flagan, 1998; Liu and Pui, 1974a, 1974b). The fundamental working principal can be described with the plate capacitor model (Figure 3.2), whereby an electric field is applied between the plates (vertically), a laminar particle-free sheath air flow Q_{sh} is led through the capacitor (parallel) and the aerosol flow Q_A (parallel) is fed into the capacitor close to plate 1 (Knutson and Whitby, 1975; Liu and Pui, 1974b). Applying an appropriate voltage can select particles with specific mobility and thus, of certain size.

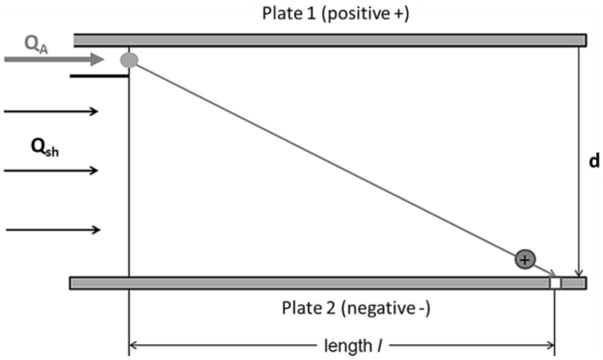

Figure 3.2. Working principal of DMAs based on the plate capacitor model. Source: modified from (Chen et al., 2019)

Hewitt (1957) introduced the design for cylindrical DMAs, which are capacitors that are composed by an inner rod-electrode and an outer electrode with given radius (McMurry, 2000a; Winklmayr et al., 1991). Aerosol particles are classified due to their electrical mobility in the DMA, after which a volume flow of monodisperse aerosol with particles of a defined mobility are led out of the DMA through a slit at the end of the inner electrode/rod (Figure 3.3). The size resolution depends on the ratio of the volume flow rates Q_A/Q_{Sh}; with increasing ratio, the size resolution improves (Flagan, 1998; Hinds, 1999). DMAs are core components of several measurement instruments such as generators for monodisperse aerosols, Mobility Particle Size Spectrometers (SMPS, DMPS, TDMPS) and Tandem DMAs (Volatility, Hygroscopicity). For the experimental measurements carried out in the framework of this Thesis two custom-made long-DMAs manufactured by the Cyprus Institute (Salmatonidis et al., 2019b) were used (publication 3). In addition, a nano-DMA TSI Model 3085, which is optimized for the size range below 20 nm, but it covers a broad range of particle diameters (2-150 nm) was also used (publication 1).

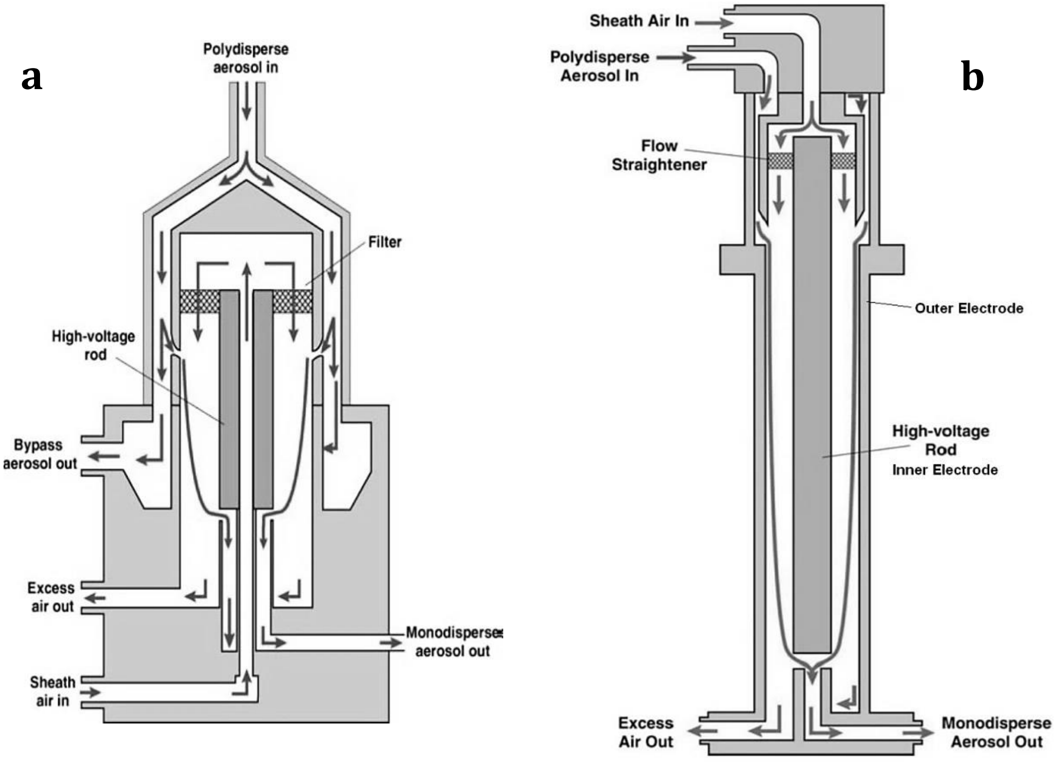

Figure 3.3. (a) nano-DMA TSI model 3085 and (b) long-DMA TSI model 3081. Source: TSI Inc. (www.tsi.com).

Scanning Mobility Particle Size spectrometer

The main components of a Scanning Mobility Particle Sizer (SMPS) are: the pre-impactor which eliminates coarser particles, a bipolar diffusion charger (X-ray or nuclear source) to charge the particles, a DMA where the voltage is continuously increased and a CPC as a counter. SMPS spectrometers can measure particle number size distributions for a given size range, which depends on the DMA-geometry, the sheath air flow rate and the downstream CPC (Flagan, 1998; Knutson and

Whitby, 1975; McMurry, 2000a). Longer DMAs can detect larger particles (10-800 nm) while higher sheath air flow rates and shorter nano-DMAs can be used to measure smaller particles (3-100 nm) (Chen et al., 1996). The particle number concentration is monitored as a function of time, while for each SMPS system the relationship between electrical mobility and time (time between DMA entrance and CPC detection) must be determined. The metric measured is an electrical mobility distribution, which is converted to particle number size distribution by a computer inversion routine (Hagen and Alofs, 1983; Hoppel, 1978). The complete inversion routine must incorporate the bipolar charge distribution for multiple charge correction, the size dependent DMA transfer function and the measured electrical mobility distribution (Alofs and Balakumar, 1982; McMurry, 2000a). Finally, the calculated size distribution has to be corrected for the CPC counting efficiency curve, and the internal losses due to particle diffusion (inlet and sampling tubes), which can be calculated by the method of the equivalent pipe length (Wiedensohler et al., 2012). A TSI model 3080 SMPS (Figure 3.4) comprising a TSI 3776 CPC and a TSI 3085 nano-DMA was used in the experimental measurements (publication 1) to monitor particle size distribution from 3-100 nm with a 3-min resolution.

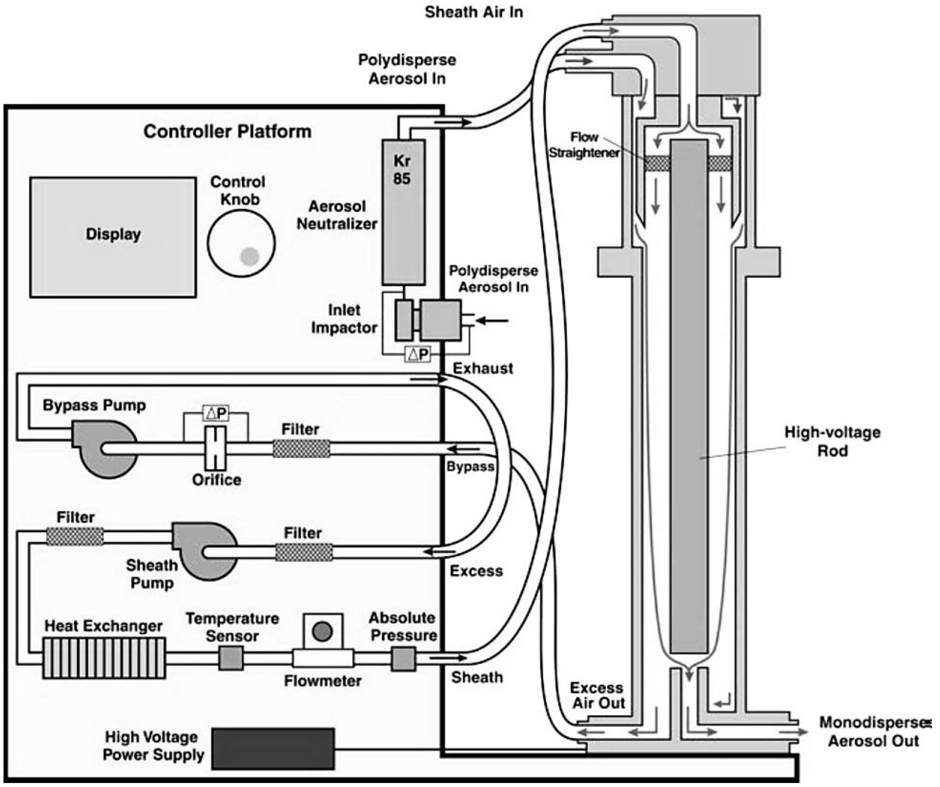

Figure 3.4. SMPS TSI model 3080. Source: TSI Inc. (www.tsi.com).

Optical instruments

Optical Particle Sizers (OPS) and photometers monitor the ability of aerosols to scatter light of a certain source (Hinds, 1999). The general principal is that light scattered by particles is measured in a certain volume under a fixed angle (e.g. 90°; Figure 3.5). Particle sizing is achieved when a fraction of the scattered light is converted to a voltage pulse of proportional intensity, which is assigned to a specific particle size according to pulse height analysis (Gebhart, 2001). Light scattered from a measurement volume depends on aerosol properties such as particle shape, size distribution and the aerosol refractive index. An assumption of particle density is necessary in order to convert the measured values to mass concentration. Optical instruments require calibration with well-defined aerosol particles (e.g., latex particles). When equipped with size selective inlet conditioners, optical particle sizers can provide size-segregated particle mass concentrations. The latter describes the Dusttrak DRX (TSI model 8533), which was used in the experimental measurements to monitor size-segregated particle mass concentrations from 0.1-15 μm with 1-minute resolution (publication 1). In addition, a mini Laser Aerosol Spectrometer (GRIMM model 11-R) was used to measure particles in the size range 0.25-32 μm, and report total and size-segregated particle mass concentrations in 31 channels with a 6-second time resolution (publications 2 & 4).

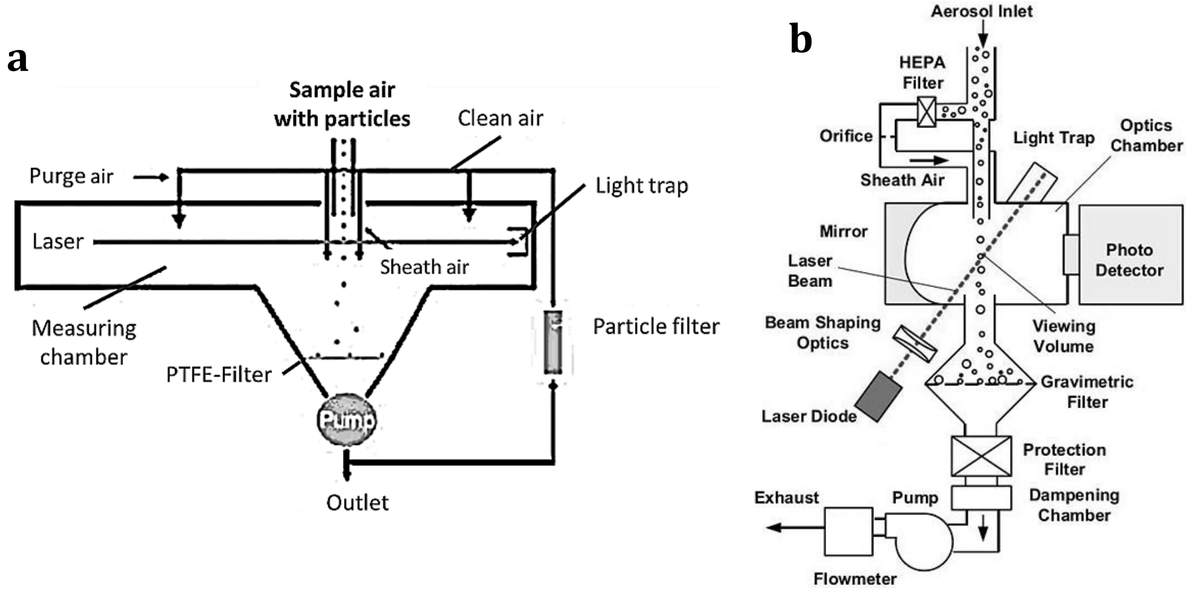

Figure 3.5. Operating principles of two optical counters used in this PhD Thesis: (a) GRIMM mini-LAS 11-R device concept, Source: GRIMM (www.GRIMM-aerosol.com); (b) Dusttrak DRX operating principal, Source: TSI Inc. (www.tsi.com).

Unipolar diffusion charger (corona-based)

The need for compact, portable, autonomous (battery-operated) instruments and personal monitors led to the development of unipolar diffusion chargers. The corona charger is a small enough and energy efficient component to be incorporated in miniaturized particle counters/sizers. It is implemented in different instruments following diverse designs, with the main function to substitute radioactive or X-ray neutralizers of the stationary instruments. Such is the case of the NanoScan-SMPS (TSI 3910; Table 3.1) where particles charged by the corona are classified in 13 channels (10-420 nm) according to their mobility diameters by a radial DMA (Zhang et al., 1995) and subsequently counted by an incorporated isopropanol-CPC, resembling the working principle of a standard SMPS (Fonseca et al., 2016b; Tritscher et al., 2013).

The Diffusion Size Classifier-miniature (DiSCmini by TESTO) used in this Thesis, is a portable instrument which can also be used as a personal monitor (Asbach et al., 2017). It uses an ion trap to remove the ion excess of the corona charged particles and subsequently two stages of electrometers (diffusion, filter) are used. DiSCmini´s monitors particles in the range 10-700 nm (size, number; Table 3.1), as a function of the instrument's calibration curve for monodisperse aerosols (Fierz et al., 2011).It can provide data with a range of time resolutions (1 second-1 hour).

The Wide Range Aerosol Spectrometer (MiniWRAS by GRIMM) is a combination of an OPC and an electrical mobility spectrometer. The OPC measures the size distribution from 250 nm to 32 μm in 31 size channels (Table 3.1). The number of particles is determined by the number of stray light pulses per period, while the particle size determines the amplitude of the scattered light. For each size channel the particle number is measured, and under the assumption that particles are spherical the mass distribution can also be calculated. Smaller particles (10-193 nm) are charged with a corona charger, after which the particles go into a collecting-precipitation electrode, where they are separated according to their electrical mobility and finally measured (1-min resolution) with a Faraday cup electrometer (GRIMM Aerosol Technik GmbH).

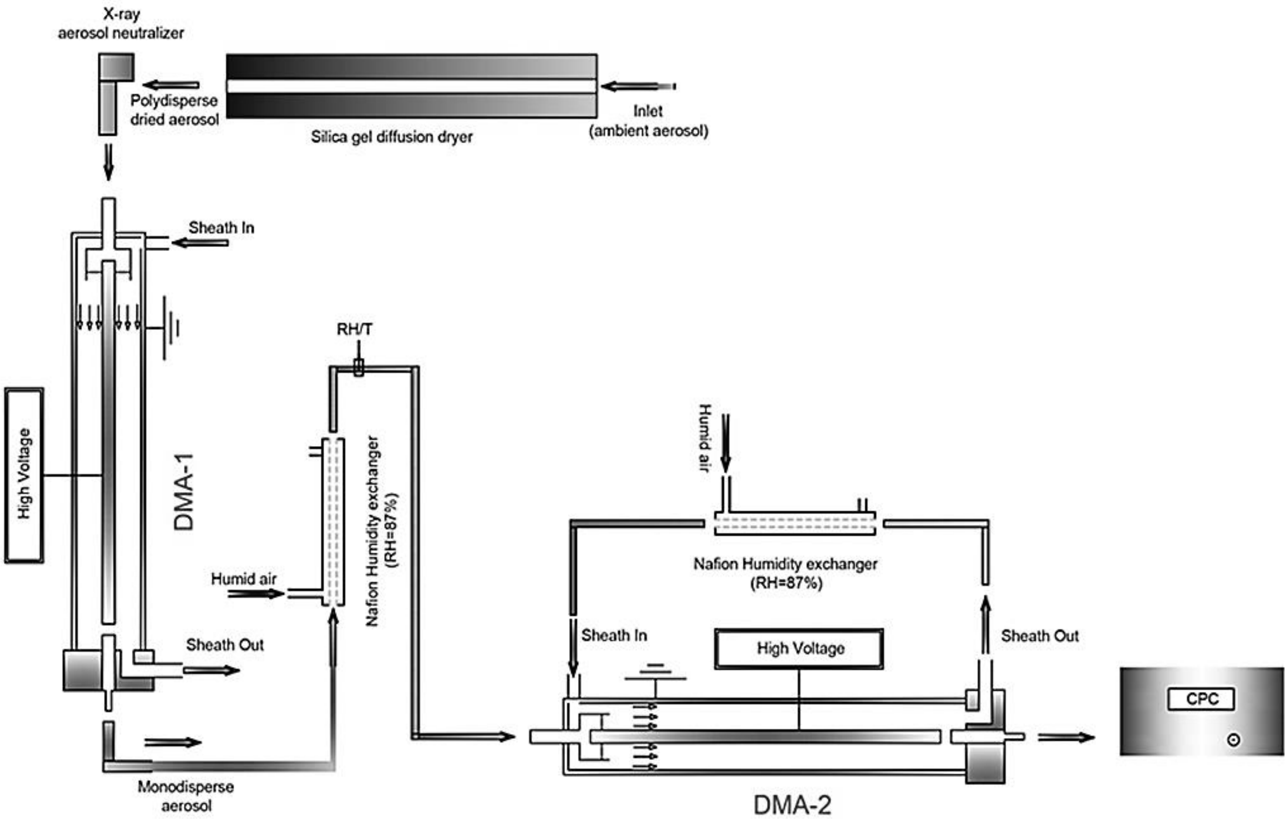

Figure 3.6. Schematic illustration of the HTDMA working principle. Source: (Salmatonidis et al., 2019b)

Hygroscopicity Tandem Differential Mobility Analyzer

A Hygroscopicity Tandem Differential Mobility Analyzer (HTDMA) was developed following the principles of Rader and McMurry (1986), in the framework of the CERASAFE project (www.cerasafe.eu) by Cyprus Institute (CyI) and was used in monitoring campaigns in this PhD Thesis (publication 4). The instrument consisted of two custom-made DMAs, one commercial CPC (TSI 3010) and two custom-made humidity exchangers (Figure 3.6). The first DMA (DMA-1) of the system was used for selecting nearly monodisperse dried particles, which were then exposed to elevated RH conditions, before their size distribution was measured by the second DMA (DMA-2) and the CPC as a standard SMPS. The system was operated with sheath and aerosol flow rates of 3.0 and 0.3 L/min, respectively, and for both of them the RH was controlled to 87%. The sampling time of the instrument and the voltage of DMA-1 can be periodically changed (e.g. every 6 min.) in order to sequentially select particles having different dry electrical mobility diameters (e.g. 30 or 90 nm; Table 3.1).

Table 3.1. Characteristics of the online instruments used in the experimental part of this work.

Instrument type	**Size range (nm)**	**Particle metric**	**Manufacturer-Model**	**Used in PhD publications**
CPC	2.5-3000	Particle number	TSI: 3775, 3776, 3010	1, 3, 4
SMPS	3-100	Size distribution	TSI 3080	1
NanoScan SMPS	10-420	Size distribution	TSI 3910	1, 2, 3, 4
DiSCmini	10-700	Size, Number, LDSA	TESTO	1, 2, 3, 4
DustTrak DRX	100-15000	PM_x	TSI 8533	1
Mini-LAS	250-32000	Mass distribution	GRIMM model 11-R	2, 4
Mini-WRAS	10-35000	Size & mass distribution	GRIMM model 1371	1, 2, 4
HTDMA	30 & 90	Particle size	Custom – CyI	3

3.1.2. Characterization techniques – offline measurements

Samples were collected on electron microscopy grids (Agar scientific Quantifoil 200 Mesh Au) for offline morphological and physicochemical characterization. The sampling set-up was composed by a Leland pump (SKC Inc.) operating at a flowrate of 5 liters/minute, connected to a cassette (SKC inlet diameter 1/8 inch and filter support pads of diameter 25mm) to which the TEM grid was attached.

Electron Microscopy

Electron microscopy is an advanced characterization method that can provide multiple information for particles in the micro as well as nanoscale. Morphology (shape and size) of single particles, their composition, agglomeration/aggregation state, and crystallinity are some of the characteristics which can be analyzed. Electron microscopy is based on the property of electrons to interact with matter by generating a variety of excitation phenomena with characteristic radiations and energies, which, if collected, are a key source of information. The type of interaction is directly related to the sample thickness, the energy of the electron beam and the material itself (Williams and Carter, 2009). Different types of electrons and electromagnetic radiation species are emitted, due to the elastic and inelastic scattering of the beam electrons from the atoms of the sample (Figure 3.7a). Modern electronic microscopes are equipped with detectors and collectors of the different types of radiation emitted, and through specialized software extract essential particle information.

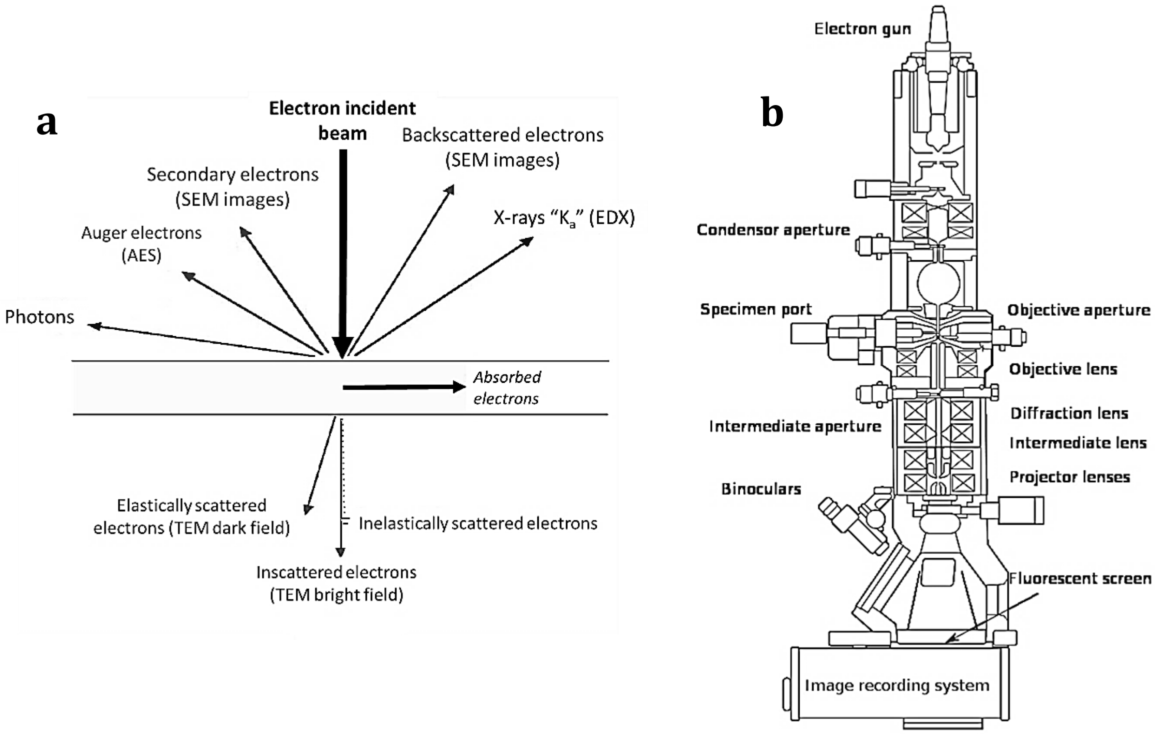

Figure 3.7. (a) Phenomena taking place during the incidence of the electron beam; (b) TEM scheme. Source modified from (Williams and Carter, 2009).

The Transmission Electron Microscope (TEM) consists of three main parts: the light source, the objective lens system and the magnification system. As light source an electron gun emitting a high energy beam is used. The beam is aligned by a system of condenser lenses and aperture. The objective lens, where the image of the sample is created with a basic magnification (×50-100), is a fundamental component of the TEM. The magnification system consists of electromagnetic lenses (first and second intermediate), which are iron-core coils producing magnetic fields, and an intermediate aperture. TEM can achieve magnifications in the order of $\times10^6$. The inelastically scattered electrons of the incident beam (Figure 3.7a), which retain a large proportion of their original energy and exit the lower surface of the sample (transmission), are the main contributors to the TEM image (Williams and Carter, 2009). When the energy of the electrons of the incident beam is large enough to excite an electron in an inner shell, ejecting it, it creates an electron hole. Subsequently, an electron from an outer shell (higher-energy) fills the hole and the difference in energy between the higher-energy shell and the lower-energy shell may be released in the form of an X-ray known as K_a (Figure 3.7a). The energy of the X-ray emitted, equal to the energy difference of the two shells, is characteristic of the element from which it is emitted. Hence, it can provide information on the composition of the sample by the stoichiometric Energy Dispersive X-ray analysis (EDX/EDS).

The particles sampled during the experimental campaigns were characterized in terms of morphology (size, shape) and elemental composition at the Scientific and Technological Centers of the University of Barcelona (CCiTUB), using JEOL JEM 2100 Transmission Electron Microscope with a LaB6 thermionic filament., coupled with an EDX spectrometer (Oxford Instruments INCA x-sight), with Si (Li) detector. The TEM images were acquired using a Gatan Orius CCD camera and processed with the "ImageJ" software, version 1.52f.

X-ray diffraction

X-ray diffraction (XRD) is used in the study of matter and crystalline solids. The characteristic feature of crystals is their periodic structure. When an X-ray beam impacts on a crystal surface it is partially scattered by the atoms of the first crystal plane, another part is scattered from the second plane, and the process continues resulting in constructive interference (Figure 3.8). Braggs law: $n\lambda=2d\sin\theta$ (where λ is the X-ray wavelength) allows the calculation of lattice spacing (d) when the angles "θ", under which the constructively interfering X-rays leave the crystal, are known (Epp, 2016; Warren, 1990). Diffractometers are instruments consisting of an X-ray source, the sample holder (stage) and a detector (Figure 3.8a). In modern instruments the individual parts can move in a circular trajectory, in order to perform measurements under a range of angles. X-ray diffraction peaks are formed when constructive interference of monochromatic X-rays beam scattered at specific angles from each set of lattice planes in a sample. The peak intensities are determined by the atomic positions within the lattice planes. Consequently, the X-ray diffraction pattern is the fingerprint of periodic atomic arrangements in a given material. Information on structures, phases, preferred crystal orientations (texture), average grain size and crystallinity can be obtained (Kohli, 2012).

The powder XRD data were collected in the IDAEA-CSIC X-Ray laboratory by using a Bruker D8 Advance diffractometer with CuKa1 radiation source (1.5405 Å) and a graphite monochromator. The diffractograms were obtained from 5° to 120° 2θ with a step of 0.02° and a counting time of 10 s. The crystalline phase identification was carried out by using the computer program ''EVA' (Produced by

Bruker). The software TOPAS 2.1. (Bruker AXS TOPAS, General profile and structure analysis software for powder diffraction data, V2.0, Bruker AXS, Karlsruhe, Germany, 2000.) with the fundamental parameter approach was used for Rietveld refinement. The optimized parameters were background coefficients, zero-shift error, peak shape parameters, cell parameters and isotropic thermal factors. The values of the pattern dependents on the disagreement factor (R_{wp}), and the statistical reliability factor of Bragg (RB) which were evaluated and they indicated that fits were satisfactory (Young, 1993).

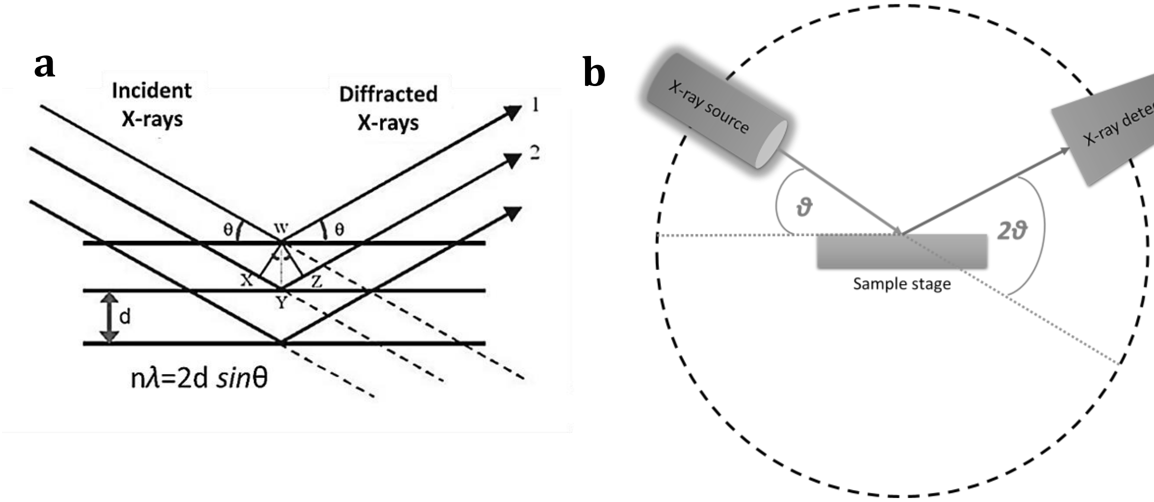

Figure 3.8. (a) Principal of X-Ray diffraction and Bragg´s law, (b) basic parts and principal of a diffractometer. Source: modified from (Epp, 2016)

3.2 Monitoring strategy

In industrial settings, different activities (i.e., potential particle emission sources) may take place with diverse periodicity. The combination of production processes and how often are performed depends on each industry’s production planning (e.g. commercial orders, customer needs, market behavior, etc.). As a result, exposure monitoring could require time-intensive and costly full-shift particle monitoring. Alternatively, task-based exposure assessments may be carried out, which provide specific information on overall worker exposure (Ramachandran, 2008) and can facilitate the design of appropriate control measures as well as provide necessary data for modeling purposes (Brouwer et al., 2012).

Task-based exposure assessments focus on a specific activity/process, and should be carried out over a representative period of time. Assessments may focus on the breathing zone of one individual using portable instruments (OJIMA, 2012). However, when several workers were affected in a worker area, a stationary monitoring set-up at breathing height (ca. 0.7-1.5 m) is preferable. Other options are the near field (NF)/far field (FF) approach, described by (Brouwer et al., 2009) and used by (Demou et al., 2009; Fonseca et al., 2018; Koivisto et al., 2010, 2012b, 2015, 2016; Koponen et al., 2015; Ribalta et al., 2019) among others, to distinguish nanoparticles from background aerosols (i.e. ambient particles from other than the studied sources inside or outside the workplace). The impact of the studied source (near field) on exposure concentrations in the worker area (far field) may be monitored in real-time. Depending on the scenario, discrimination of background aerosols may be achieved either by monitoring particle metrics before and after the activity, or by simultaneously monitoring particle metrics at the source and at a background location. Workplace exposure monitoring strategies applied in this Thesis followed internationally-recognized standard procedures (OECD.82, 2017) based on a tiered approach (Brouwer et al., 2012).

A multi–instrument approach was applied for all the exposure scenarios assessed as suggested by Fonseca (2016) and Brouwer et al., (2012). However, the different instruments can have different features and specifications (e.g. working principles, measurement ranges and metrics, time resolutions etc.; Asbach et al., 2016). Therefore, the compatibility of the resulting data needs to be validated through inter-comparisons of the specific instruments. In this work, inter-comparisons were carried out prior to the measurements at an air quality monitoring station in Barcelona (Spain), using ambient air aerosols and stationary instruments as references. The proper functioning of the instruments was ensured and data were considered compatible when R^2 coefficients were ≥0.9.

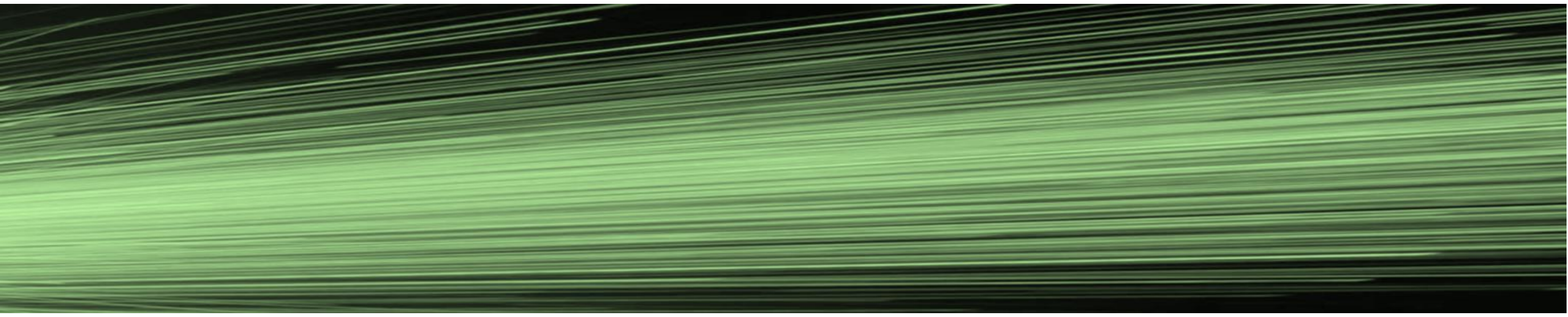

Chapter 4. **Results**

4. Results

The results of the present PhD Thesis are presented in this section in the form of four scientific publications as submitted to peer-reviewed journals. The publications follow the order of the objectives of this PhD Thesis, as presented in Chapter 2. Publication 1 addresses the first objective “identification of nanoparticle sources and characterization of emission mechanisms” during laser ablation of ceramic tiles. Publications 2 and 3 tackle the second objective “characterization of exposure scenarios” by studying thermal spraying at an industrial scale. The third objective regarding “exposure mitigation strategies” is addressed in publication 4.

4.1. Scientific publication 1

Nanoparticle formation and emission during laser ablation of ceramic tiles

Apostolos Salmatonidis[a,d], Mar Viana[a], Noemí Pérez[a], Andrés Alastuey[a], Germán F. de la Fuente[b], Luis Alberto Angurel[b], Vicenta Sanfélix[c], Eliseo Monfort[c]

[a] *Institute of Environmental Assessment and Water Research, Spanish Research Council (IDÆA-CSIC), 08034, Barcelona, Spain.*

[b] *Aragón Materials Science Institute (ICMA - Universidad de Zaragoza, CSIC), 50018, Zaragoza, Spain.*

[c] *Institute of Ceramic Technology (ITC)- AICE - Universitat Jaume I, 12006 Castellón, Spain.*

[d] *University of Barcelona, Faculty of Chemistry, Department of Chemical Engineering and Analytical Chemistry, 08028, Barcelona, Spain.*

Published in: Journal of Aerosol Science, 2018, Volume 126, Pages 152-168

DOI: https://doi.org/10.1016/j.jaerosci.2018.09.006

The following is a pre-print version, which was produced by the author, of an article published in Journal of Aerosol Science (Elsevier): Submitted on 14 May 2018; revised on 12 July 2018; accepted on 21 September 2018. Available online at: https://doi.org/10.1016/j.jaerosci.2018.09.006

Nanoparticle formation and emission during laser ablation of ceramic tiles

Apostolos Salmatonidis[a,d]*, Mar Viana[a], Noemí Pérez[a], Andrés Alastuey[a], Germán F. de la Fuente[b],
Luis Alberto Angurel[b], Vicenta Sanfélix[c], Eliseo Monfort[c]

[a] *Institute of Environmental Assessment and Water Research, Spanish Research Council (IDÆA-CSIC), 08034, Barcelona, Spain.*

[b] *Aragón Materials Science Institute (ICMA - Universidad de Zaragoza, CSIC), 50018, Zaragoza, Spain.*

[c] *Institute of Ceramic Technology (ITC)- AICE - Universitat Jaume I, 12006 Castellón, Spain.*

[d] *University of Barcelona, Faculty of Chemistry, Department of Chemical Engineering and Analytical Chemistry, 08028, Barcelona, Spain.*

**corresponding author: Apostolos Salmatonidis, apostolos.salmatonidis@idaea.csic.es*

Abstract

Pulsed laser ablation (PLA) is a widely used technology, for surface structuring and tile decoration in the ceramic industry. During PLA, nanoparticles (NP <100 nm) are unintentionally released and may impact exposure. This work aims to understand the mechanisms controlling NP formation and release during ablation of different types of ceramic tiles, using different laser setups (near-IR and mid-IR). The measurements took place at laboratory and pilot-plant-scale, with varying laser wavelength, frequency, velocity, and pulse duration. In total, the combination of 4 types of ceramic tiles and 2 lasers was assessed. Particle number concentration and size distribution (SMPS with nano-DMA, DiSCmini, butanol-CPC) and particle mass concentration (DustTrak-DRX) were monitored. Samples were also collected for morphological and chemical characterization (TEM/EDX). High particle number concentrations were detected ($3.5*10^4/cm^3$ to $2.5*10^6/cm^3$) for all of the tiles and under both laser setups. Particle formation (<10 nm) by nucleation was detected, and secondary amorphous SiO_2 nanoparticles (>10 nm) were formed and released during ablation of the porcelain tiles. Different release mechanisms were identified: during ablation with the near-IR laser particles were emitted through melting and nucleation, while emissions from the mid-IR laser were attributed to melting and mechanical shockwaves. Particle number and mass emissions were dependent on the tile surface characteristics (e.g., porosity, crystallinity) and chemical properties. This work is potentially relevant from the point of view of exposure mitigation strategies in industrial facilities where PLA is carried out.

Keywords: nanoparticles, ceramic industry, laser ablation, formation mechanisms

1. Introduction

Laser ablation is a technology with widespread applications at global scale, examples of which are precision microfabrication (Sugioka, Meunier, & Pique, 2010), surface structuring (Lahoz, de la Fuente, Pedra, & Carda, 2011) characterization and analytical techniques (Russo, Mao, Gonzalez, Zorba, & Yoo, 2013). Pulsed laser ablation (PLA), in particular, is a state-of-the-art method used for ceramic tile processing in order to achieve designs with enhanced durability and aesthetic properties (Pascual et al., 2005). However, this technology is known to generate nanoparticle (NP, <100 nm) emissions to workplace air and the environment (A. S. Fonseca et al., 2015, 2016). Based on current literature, understanding the sources and mechanisms controlling the formation and release of process-generated nanoparticles (PGNP) in industrial settings is becoming increasingly relevant, in order to minimize potential hazards (Hameri, Lahde, Hussein, Koivisto, & Savolainen, 2009; van Broekhuizen, 2012; Viitanen, Uuksulainen, Koivisto, Hämeri, & Kauppinen, 2017). Adverse health effects of NPs have been extensively described in the literature (Heal, Kumar, & Harrison, 2012), and the main exposure route to NPs is inhalation. Specifically, Oberdörster (2001) showed that in certain cases NP can cause severer pulmonary inflammation than fine particles, while Weichenthal (2012) observed significant associations between NP and acute cardiovascular morbidity. Consequently, numerous industrial processes which generate NP emissions have received increasing attention in recent years (Curwin & Bertke, 2011; Demou, Peter, & Hellweg, 2008; Ana Sofia Fonseca et al., 2014; Gandra, Miranda, Vilaa, Velhinho, & Teixeira, 2011; Gómez, Irusta, Balas, & Santamaria, 2013; Koivisto et al., 2012; van Broekhuizen, 2012). Pfefferkorn et al (2009) described the potential for exposure to ultrafine aerosols during industrial welding operations, and Viana et al. (2017) reported analogous potential during atmospheric thermal spraying. Additionally, Voliotis et al. (2014) proved that traditional ceramic production processes emit particles <100 nm, and awareness was raised towards this specific industrial sector.

In order to characterize and minimize exposure, the mechanisms generating particle emissions must be understood. During laser ablation intense electromagnetic fields interact with matter and atoms are selectively driven off by thermal or non-thermal mechanisms (Phipps, 2007). NP emissions during PLA can be mainly associated with three phenomena:

- Nucleation: atoms, ions and clusters which emanate from the plasma plume (Noël, Hermann, & Itina, 2007), can act as nuclei and through different growth routes (coalescence, diffusional, coagulation) form secondary particles (Polte, 2015). Gaseous precursors which may originate from direct sublimation (solid-to-gas) and from evaporation of melt (liquid-to-gas), can condensate and form new particles (A. S. Fonseca et al., 2015).
- Melt expulsion (droplets): Temperature differences between the surface and the body of the material create localised pressure gradients (Czotscher & Vollertsen, 2016; Zhigilei, Lin, & Ivanov, 2009), which force droplets of melt to get extruded from the tile, cool down rapidly and, due to surface tension, form spherical particles.
- Shockwaves: Mechanical shockwave cracking of grains can contribute to the emission of primary particles. Particle removal is associated to ablation and poor thermal resistance, which is typical for porcelain tiles (Lahoz et al., 2011). Thermal shock and the consequent ejection of micro-scaled grains occurs due to differences in thermal expansion coefficients

(Pascual-Cosp, Ramírez del Valle, Garciá-Fortea, & Sánchez-Soto, 2002; Pascual-Cosp, Ramírez Del Valle, García Fortea, & Sánchez Soto, 2001; Pascual et al., 2005).

In addition to these, particle aggregation and agglomeration mechanisms are also determinants of particle size distribution after formation and emission (Koch & Friedlander, 1989; Lushnikov, Maksimenko, & Pakhomov, 1989; Sivayoganathan, Tan, & Venkatakrishnan, 2012).

The current study aims to characterize the mechanisms determining NP emissions during PLA of ceramic tiles by correlating fundamental ablation phenomena with particle release. A parametric study was designed to assess the influence of material properties (composition, structural characteristics), laser sources (wavelength) as well as process parameters (pulse duration, frequency) on NP formation and emissions in terms of size, particle number and mass concentration. The ultimate goal of the present work was to increase the understanding of the mechanisms governing NP formation during laser ablation, which may facilitate the design of more efficient exposure mitigation measures.

2. Materials and methods

The laser ablation experiments took place at the Materials Science Institute of Aragón "ICMA" (CSIC-University of Zaragoza) in Zaragoza (Spain), with an overall duration of 5 working days.

Table 1. Ceramic tiles under study (Abbreviations, 1st letter: Glaze, 2nd letter: Tile, 3rd letter: Colour)

Abbreviation	Full Name	Tile	Porous	Main Components**
UPG	Unglazed Porcelain Grey	Porcelain stoneware	no	71% SiO_2, 19% Al_2O_3
UAW	Unglazed Alumina White	Alumina	yes	97% Al_2O_3
UBW	Unglazed Biscuit White	Non-sintered/biscuit porcelain	yes	70% SiO_2, 20% Al_2O_3
GER	Glazed Earthenware Red	Earthenware	yes	57% SiO_2, 12% ZnO

*The chemical composition refers only to the glaze, and not the body of the GER tile, since that was the part processed by the laser; **The full chemical characterization can be found in Table S1 in Supplementary material.

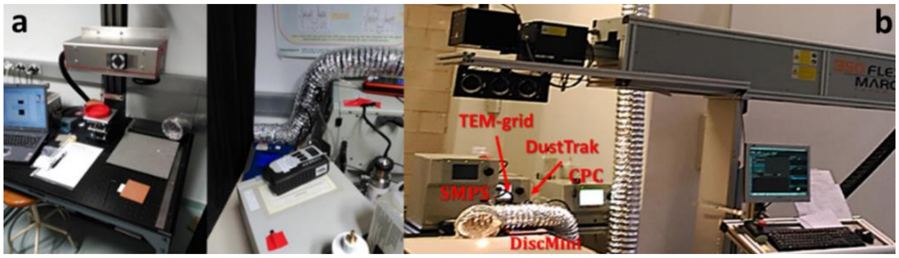

Figure 1. Experimental setup of (a) the laboratory-scale with the near-IR laser, and (b) the pilot-plant with the mid-IR laser. The distribution of the different particle monitoring instrumentation is presented.

2.1 Tile and laser combinations

Four different ceramic tiles were used as target materials (Table 1). Porcelain stoneware (UPG; 71% SiO_2, 19% Al_2O_3; Table S1 in Supplementary Material) is currently the ceramic tile of highest commercial interest, as it exhibits higher technical and functional performance and greater versatility, allowing this tile to be used in both indoor and outdoor environments (International Organization for Standardization, 2012; Sánchez, García-Ten, Sanz, & Moreno, 2010). Porous ceramics (e.g. alumina, UAW; 97% Al_2O_3; Table S1), on the other hand are used in high temperature applications such as thermal insulation in the cement, steel, aluminium, iron-alloy and petrochemical industries (Salomão, Bôas, & Pandolfelli, 2011). Glaze is a vitreous coating (56% SiO_2, 12% ZnO, 7% ZrO_2; Table S1) that seals the inherent porosity of the tile`s body material and serves as a colorant or waterproofing agent and it was a component of the earthenware tiles studied in this work. Each target material has different chemical composition as shown in Table S1 (Supplementary material). Furthermore, the different optical properties of the tiles result in very different absorbance of the incident energy, which means that the laser treatment efficiency will vary depending on the material itself. In addition, this efficiency strongly depends on the laser wavelength. Therefore, two different laser systems with different wavelengths were used:

A. Near-IR laser (Easy Laser, Model: YLPM-1-4x200-20-20, Ytterbium fiber laser, Wavelength: 1064 nm, nominal power 20 W) at laboratory scale, with which the UPG, UAW and UBW tiles were processed (Fig. 1a).

B. Mid-IR laser (Easy Laser, Model: 350 Flexi Marcatex, Slab-type CO_2 laser, Wavelength: 10.6 μm, nominal power 350 W) at pilot-plant scale, used to process the UPG, UBW and GER tiles (Fig. 1b). Although, the UAW tiles were optically compatible with this laser, strong thermal stresses were generated inducing tile fracture. Hence, the UAW tiles were not processed with this laser.

Mid-IR lasers (i.e. CO_2) are widely used in industrial applications for cutting and welding, while n-IR lasers are generally used for engraving (Andreeta, Cunha, Vales, Caraschi, & Jasinevicius, 2011). Applications include scribing, engraving, and marking of a wide variety of materials, including glass and ceramics. Finally, the difference in power between these lasers was considered advantageous as they allowed for the assessment of NP formation at two different scales (laboratory and pilot plant, Fig. 1).

2.2 Experimental

In order to ensure the reproducibility of the results all experiments were performed in triplicate and consisted of 20-minutes ablation followed by a 10-minutes settle-down time. Localized air extraction was installed close to the target tiles (Fig. 1), both in the laboratory and the pilot plant, at a distance of approximately 10 centimetres from the initial point of the laser beam. The extraction intensities for all the experiments were kept at a constant flow speed of 3.5 m/s. The laser beam started marking from an initial point and covered a rectangular surface with a continuous parallel line movement. The tile surface treated by the laser was always untreated, i.e., the laser always moved towards the untreated part of each tile and there was no spatial overlap from one laser shot to another. The spacing between lines is shown in Table S2 in Supplementary Material.

Laser ablation was carried out under two energy settings with the near-IR laser: high and low, detailed process parameters are listed in Table S2 in Supplementary material. In the case of "high energy" configuration higher pulse durations were used. These two different energy settings were used to observe the effects of processing parameters on the same target materials, under the same laser wavelength. Table 2 summarizes the sequence of experiments. As opposed to the near-IR laser, only one set of laser processing parameters was applied for the target tiles with the mid-IR laser. However, in the case of GER samples a low energy set of process parameters were also applied. The reason for that was to study the effect of the energy input to the excessively high emissions in this particular case (GER).

Table 2. Experimental sequence

Date	Energy settings	Tile	Comments
		Near-IR laser	
07-02-2017	Low	UPG	-
07-02-2017	Low	UAW	2 different tiles (1st +2nd rep., 3rd rep.)
07-02-2017	Low	UBW	Heating switched on
08-02-2017	High	UPG	-
08-02-2017	High	UAW	3 different tiles-different for each repetition
08-02-2017	High	UBW	-
		Mid-IR laser	
09-02-2017	Standard	UBW	Filter extraction with the same flow
10-02-2017	Standard	UPG	1st repetition – briefly stopped
10-02-2017	Standard	GER	-
10-02-2017	Low	GER	In addition to the standard energy settings

2.3 *Real-time measurements*

Particle monitoring was carried out simultaneously in four different locations, using the following instrumentation:

1) Emission source
   - Scanning Mobility Particle Sizer (TSI SMPS 3080, TSI 3776 CPC) with a nano-DMA (Differential Mobility Analyser) to monitor particle size distribution from 3nm to 100 nm with a 3-minute resolution.
   - Butanol Condensation Particle Counter (TSI model 3775) to monitor total particle number concentration in the range of 4 nm – 3 μm with 1-minute resolution.
   - Miniature diffusion size classifier "DiSCmini" (TESTO AG), which detects particles ranging from 10 nm to 700 nm, monitoring total particle number, mean particle diameter and lung deposited surface area.
   - DustTrak DRX Aerosol Monitor (TSI model 8533), simultaneously monitoring size-segregated particle mass concentrations from 0.1 to 15 μm. The instrument was set to a 1-minute resolution.
   - Samples were collected on TEM grids (Agar scientific Quantifoil 200 Mesh Au) for offline morphological and physicochemical characterization. A Leland pump (SKC Inc.) with a flow

of 5 litters/minute was connected with a cassette (SKC inlet diameter 1/8 inch and filter support pads of diameter 25mm) to which the TEM grid was attached.

2) Near Field
    - Electrical mobility spectrometer (Nanoscan-SMPS, TSI model 3910) to monitor particle size distribution. The size range of the instrument is 10 nm - 420 nm and the time resolution 1 minute.
    - Optical Particle Sizer (TSI model 3330) monitoring particle optical size distribution in the 0.3-10 µm range, with 1-minute time resolution.
    - Miniature diffusion size classifier "DiSCmini" (TESTO AG), see above.
    - Samples were also collected on TEM grids, see above.

3) Far-Field
    - Mini Wide Range Aerosol Spectrometer (GRIMM mini-WRAS) monitoring particle size diameter from 10 nm – 35 µm. This instrument also provides PM_1, $PM_{2.5}$ and PM_{10} mass concentrations.
    - Miniature diffusion size classifier "DiSCmini" (TESTO AG), see above.
    - DustTrak DRX Aerosol Monitor (TSI model 8533)

4) Outdoor
    - Miniature diffusion size classifier "DiSCmini" (TESTO AG), see above.
    - DustTrak DRX Aerosol Monitor (TSI model 8533), see above.

The emission source measurements for both lasers were performed inside the extraction tube at a distance of approximately 0.5 m from the incident laser beam. It is not possible to provide a precise distance since the laser beam was moving away from the extraction tube during the process. At the emission source all the instruments used inlets with tubing no longer than 10 cm. For the DiSCmini transparent conductive "Tygon" tubing was used (Asbach et al., 2016), while conductive silicone tubing was used for the rest of the instruments. In the near-field, far-field and outdoor locations no tubing was used for any of the online instruments. The potential limitations of the Dusttrak monitors were taken into account (Rivas et al., 2017).

3. Results

In this section time series of the different experimental cycles, categorized by laser and energy settings, are described in terms of particle size distribution, particle number as well as mass concentration. The results presented correspond to the emission source only, given that the data collected in the near-field and far-field locations did not show any significant impacts from NP emissions in the worker area or in the background. The lack of impact was due to the high efficiency of the exposure mitigation mechanisms in place in this industrial setup (localized extraction). Thus, under the conditions assessed in this work, no significant impact on worker exposure was detected.

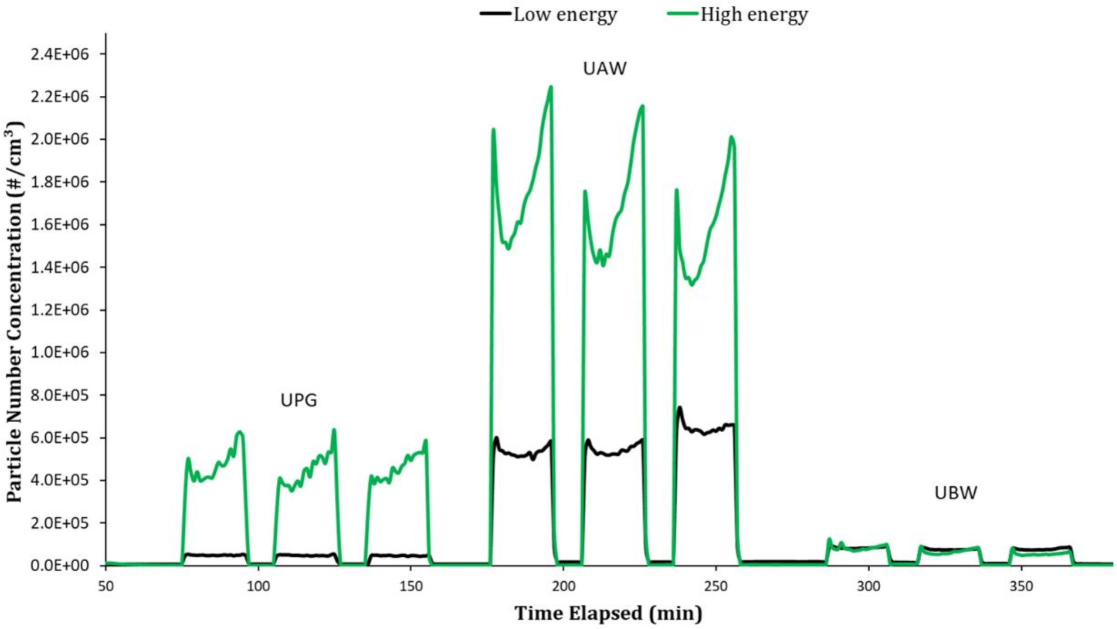

Figure 2. Particle number concentrations (4 nm -3µm) during low energy and high energy ablation of the different tiles with the near-IR laser.

3.1 Near-IR laser

3.1.1 Experiments carried out under low energy settings

The time series of particle number concentration (N) in the size range 4nm-3µm of three different tiles (UPG, UAW and UBW) are shown in Fig. 2. Emissions in terms of particle number (N) were evident in all cases as soon as the laser beam hit the target, and for the entire duration of the ablation run (20 minutes). Likewise, once the laser beam stopped, a rapid drop of N occurred allowing clear separation of each repetition. The highest emissions were registered during the ablation of UAW tiles ($6.1*10^5/cm^3$), which released almost 6 times more particles than UBW ($7.6*10^4/cm^3$) and 11 times more than UPG ($4.6*10^4/cm^3$). The UBW showed higher emissions than UPG, but still in the same order of magnitude. The mean particle diameters in the range 10-700 nm (DiSCmini) were 59.6, 69.9 and 84.7 nm for the UPG, UAW and UBW tiles respectively.

The UPG and the UBW exhibited a very high reproducibility over their repetitions, while in the case of UAW the last repetition showed higher emissions in terms of particle number concentration than the first two. The reason behind this difference is that the two first repetitions were performed on the two opposite sides of the same tile (front and back), while the third one was performed on a different tile. Even though tiles of the same material (α-alumina) were used, crystallographic analysis of different UAW tiles showed that in some cases there was a minor phase of $MgAl_2O_4$ (spinel, Fig. S1) which may have affected the emissions. The ablation of UAW tiles requires melting at 2050ºC (Nedialkov, Atanasov, Sawczak, & Sliwinski, 2003) which is lower than the $MgAl_2O_4$ spinel melting point (2135ºC). Therefore, it may be concluded that a potentially higher melting temperature resulted in lower NP emissions.

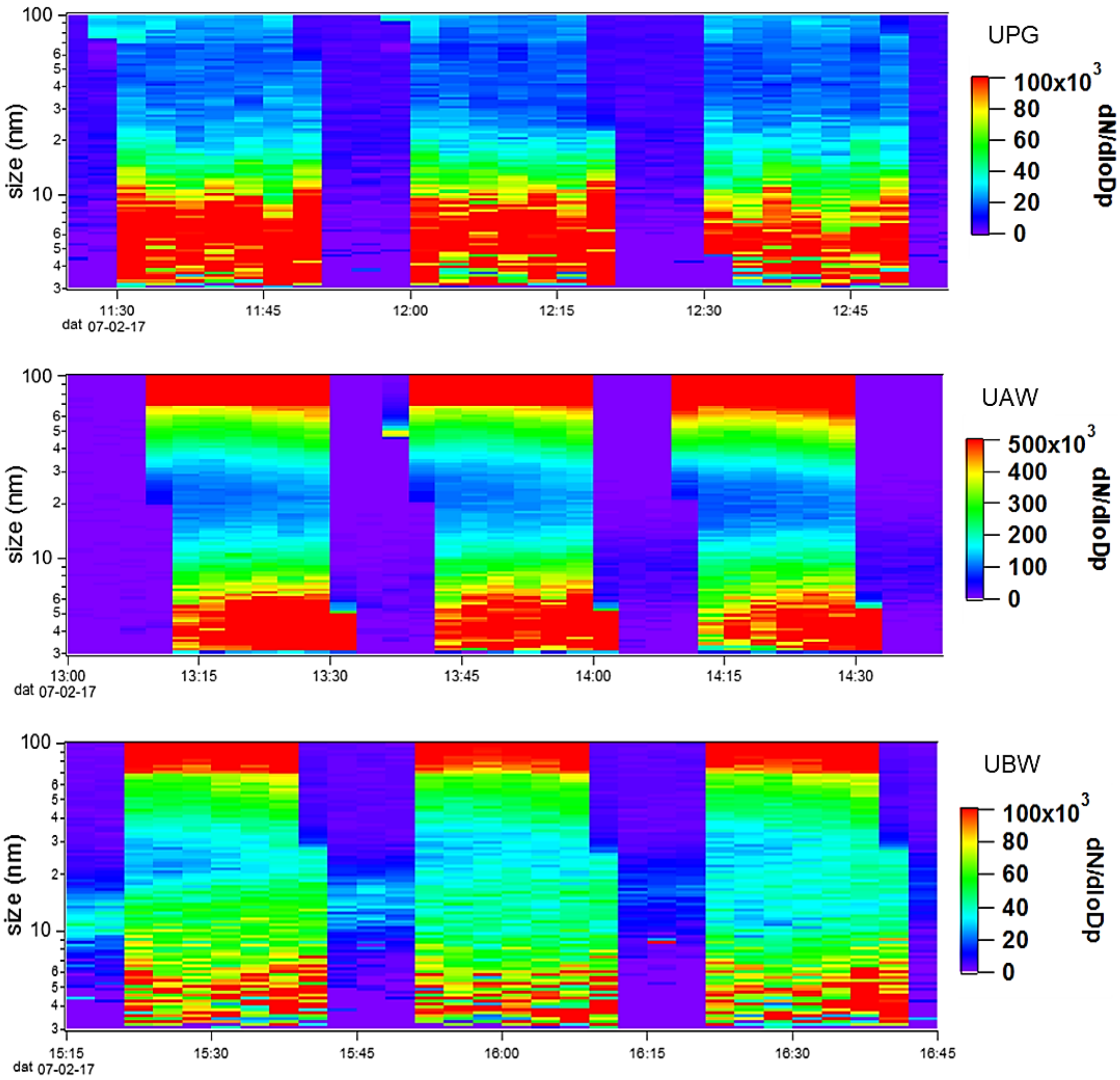

Figure 3. Size distribution (3-100 nm) of particles emitted during ablation with the near-IR laser under low energy settings

In order to explain the differences in the emissions of the different tiles their particle size distribution patterns were assessed (Fig. 3). During the ablation of UPG tiles under low energy settings, high NP concentrations in the size bins <10 nm were recorded (80-100 $*10^3/cm^3$), evidencing nanoparticle emissions. The small sizes of NP detected suggest that they may source from nucleation from atoms and ions (Noël et al., 2007) as well as from gaseous precursors (A. S. Fonseca et al., 2015, 2016). As described above, in this scenario gaseous precursor emissions may originate from direct sublimation and from evaporation of the melt (cf. section 4). Hence, nucleation through different routes may be identified as the dominant emission mechanism during ablation of UPG tiles.

In the case of the UAW tiles, two separate modes with high concentration of different sized particles may be observed. The first mode, from 3 to 10 nm (300-500 $10^3/cm^3$), can be attributed to particle nucleation. As Nedialkov et al. (2003) found strong evidence of melt during pulsed laser ablation of alumina, the second mode from 40 to 100 nm (300-500 $10^3/cm^3$) can be attributed to the direct emissions of molten droplets (cf. section 4). Based on Figure 3 it may be concluded that two mechanisms, melting and nucleation, had similar contributions to the emissions of alumina in the size range 3-100 nm.

The particles emitted during ablation of the UBW tiles consisted mainly of primary NPs (>40 nm), with a relatively minor contribution from nucleation. The irregular emission pattern for particles <5 nm could have been influenced by instrumentational noise. The emission of nanoparticles (40-100 nm), similar to the case of UAW, can be attributed to the melt expulsion from the surface of the irradiated tile. The melt formed and continued to be heated was then evaporated and the resulting vapours could have condensed to form <10 nm NPs (Fig. 3). The particle concentrations in the size range >40 nm (60-100 $10^3/cm^3$) suggests that the dominant mechanism in this case was primary emissions due to melting of the tile surface.

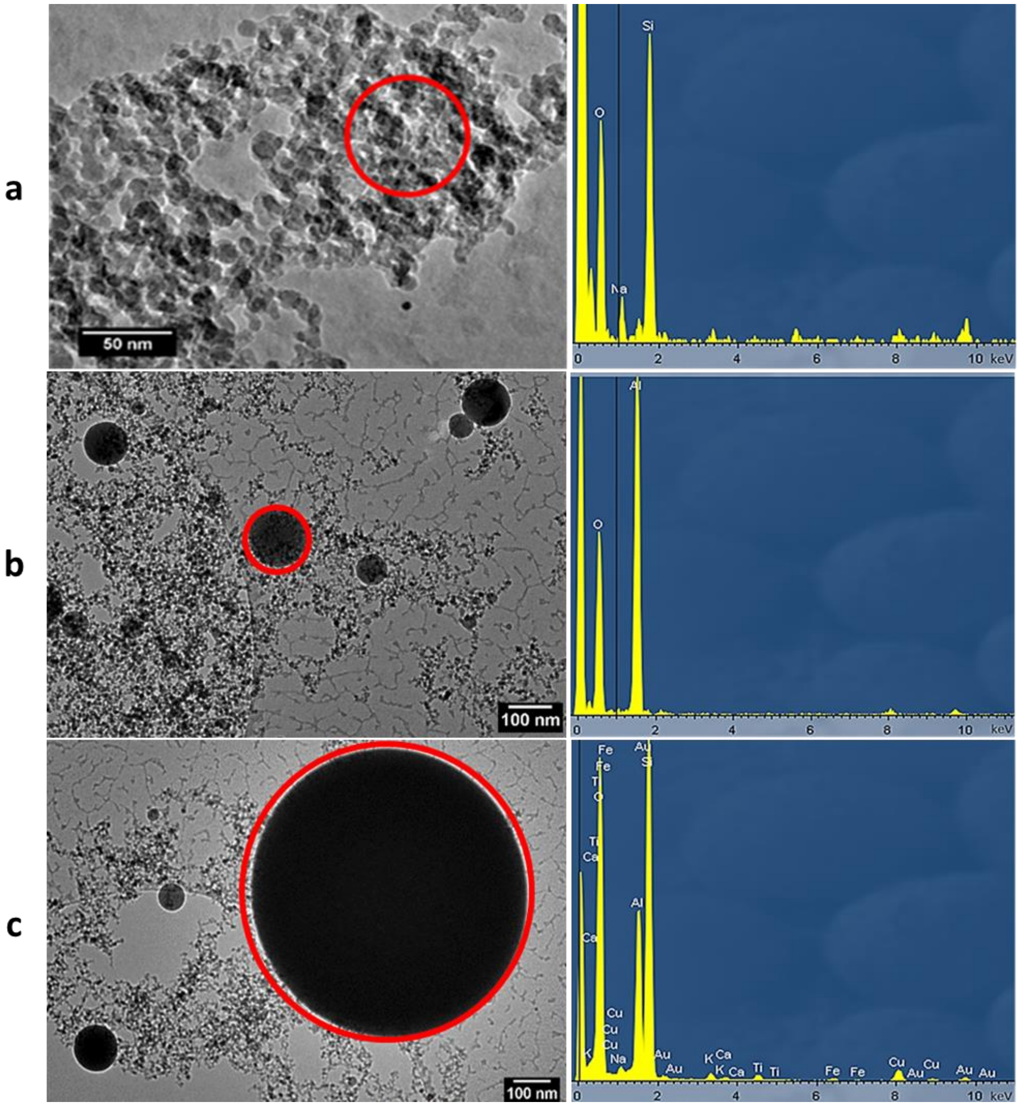

Figure 4. TEM images (right) and EDX spectra (left) of particles released during ablation under low energy settings, sourcing from: UPG (a), UAW (b), UBW (c) tiles

The TEM analysis of the particles collected during ablation of the different tiles is presented in Fig. 4. The main components of porcelain are silica and alumina (over 90%, Table S1). Nanoparticles released from UPG ablation (Fig. 4a) were mainly silica nanoparticles, with traces of sodium, which is a minor component in porcelain. The newly formed silica nanoparticles with diameters Dp ≤10 nm were in agreement with the SMPS size distribution and the nucleation mechanism proposed. The UAW tiles (Fig. 4b) released spherical particles originating from the ejection of melt droplets (>40 nm), as well as nanoparticles formed by the condensation of melt vapours (<10 nm), which is consistent with the size distribution (Fig. 3). Similar is the case for the UBW (Fig. 4c), for which larger and spherical particles were detected (>40 nm), alongside with smaller NPs (<10 nm). As shown in Figure 4, agglomerates were also detected originating from the emission process or as a sampling artefact on the TEM grids. Due to the high particle concentrations monitored it was expected that particle aggregation and agglomeration should have taken place under this kind of particle emission scenario (Max L. Eggersdorfer, Kadau, Herrmann, & Pratsinis, 2012; Maximilian L. Eggersdorfer & Pratsinis, 2014).

Particle mass concentrations were also monitored under low energy settings in four different size ranges (Fig. 5). UAW tiles released the highest mass concentrations during ablation. Contributions from the different mass size fractions can be clearly distinguished, confirming that particles of different sizes were emitted. The PM_1/PM_{10} ratio for the UAW tiles was 87.5%, indicating that the main contributor to emissions was PM1. UPG and UBW tiles exhibited relatively low emissions in terms of mass, with all PM fractions contributing respectively less than 25 μg/m³.

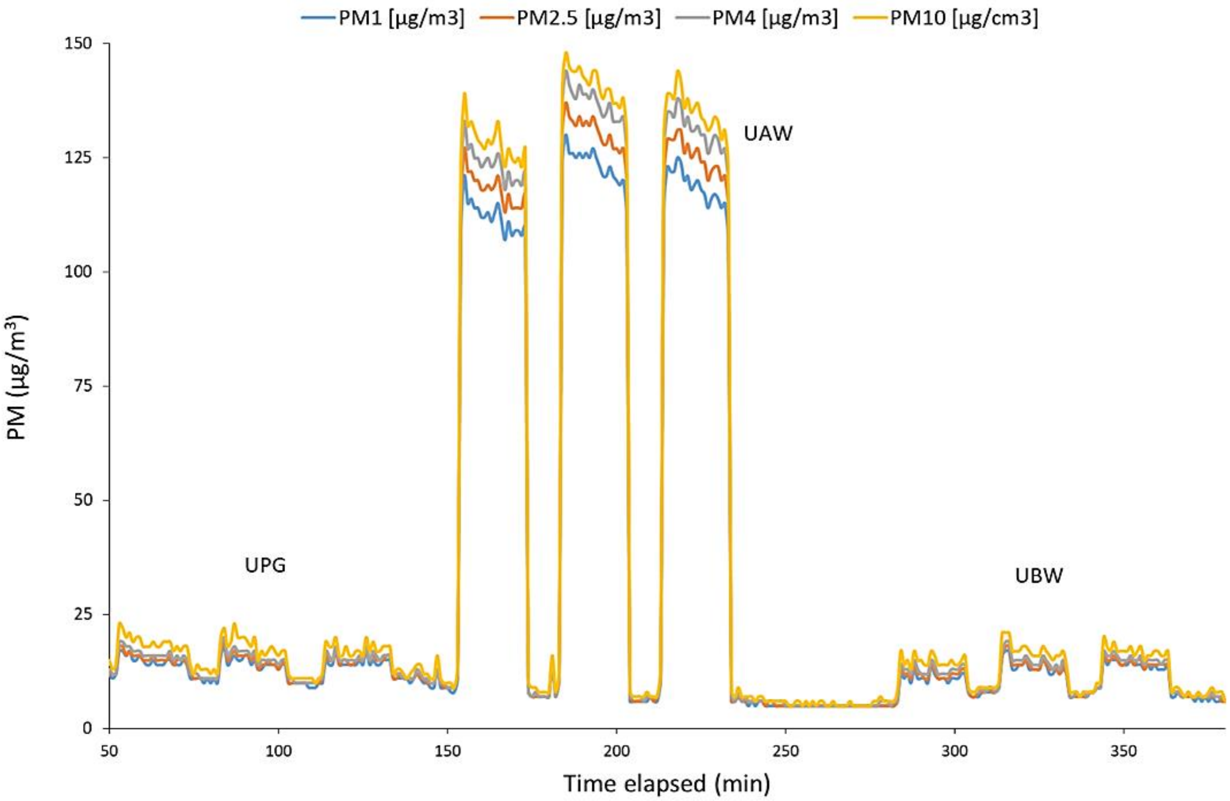

Figure 5. Particle mass concentrations during ablation with the near-IR laser under low energy settings

For both of these materials the ratio PM$_1$/PM$_{10}$ was approximately the same (≈80%), indicating a slightly higher contribution from larger particles (PM$_{10}$) than the UAW tiles, probably originated from the ejection of grains due to generation of shockwaves. For porcelain tiles differences in thermal expansion coefficients between the matrix (glassy phase in the case of porcelain) and dispersed particles (quartz and alumina) or crystalline phases formed during this thermal process (mullite), producing strong compressive stresses on the glassy phase (Carty & Senapati, 1998). Specifically, for both the UPG and UBW tiles the presence of cracks around quartz particles was observed (Fig. S3), which suggests that under mechanical aggression these particles could be easily dislodged. Even though the grain ejection mechanism has a very limited contribution to the emissions in terms of particle number, the few large particles emitted may have a significant impact in terms of particle mass concentration.

Table 3. Particle concentrations and mean diameters monitored during ablation with the near-IR laser.

Target Tile		**Particle number concentration (N)**	**Particle number concentration (N)**	**Mean diameter**	**Particle number concentration (N)**	**Mean diameter**	**PM$_{2.5}$**
		4 nm-3 µm	10-700 nm	10-700 nm	3-100 nm	3-100 nm	
		CPC (#/cm^3)	DiSCmini (#/cm^3)	DiSCmini (nm)	SMPS (#/cm^3)	SMPS (nm)	DustTrak DRX (µg/m^3)
				Low energy settings			
UPG	Average	$4.56*10^{4}$	$3.69*10^{4}$	59.6	$8.48*10^{4}$	14.7	15.2
	St.dev.	$8.81*10^{3}$	$6.94*10^{3}$	2.8	$9.73*10^{3}$	2.0	1.4
	Max	$5.30*10^{4}$	$5.54*10^{4}$	66.8	$1.08*10^{5}$	19.2	19.0
UAW	Average	$4.85*10^{5}$	$9.07*10^{5}$	69.9	$5.03*10^{5}$	32.8	133
	St.dev.	$9.64*10^{4}$	$1.40*10^{5}$	7.9	$4.41*10^{4}$	3.2	13.9
	Max	$6.13*10^{5}$	$1.28*10^{6}$	86.1	$5.85*10^{5}$	39.3	143
UBW	Average	$7.60*10^{4}$	$1.50*10^{5}$	84.7	$9.13*10^{4}$	31.7	13.6
	St.dev.	$1.50*10^{4}$	$2.06*10^{4}$	2.6	$8.13*10^{3}$	0.9	1.6
	Max	$9.13*10^{4}$	$1.82*10^{5}$	89.3	$1.11*10^{5}$	33.8	18.0
				High energy settings			
UPG	Average	$4.54*10^{5}$	$4.86*10^{5}$	81.5	$5.61*10^{5}$	25.1	44.3
	St.dev.	$8.01*10^{4}$	$7.33*10^{4}$	7.3	$1.09*10^{5}$	1.6	3.7
	Max	$6.29*10^{5}$	$6.48*10^{5}$	95.1	$7.58*10^{5}$	28.4	59.0
UAW	Average	$1.69*10^{6}$	$2.40*10^{6}$	36.1	$9.02*10^{5}$	46.9	181
	St.dev.	$2.45*10^{5}$	$2.32*10^{5}$	2.0	$1.61*10^{5}$	1.6	7.6
	Max	$2.24*10^{6}$	$2.70*10^{6}$	39.9	$1.19*10^{6}$	50.5	205
UBW	Average	$6.90*10^{4}$	$7.08*10^{4}$	109	$1.02*10^{5}$	22.5	5.8
	St.dev.	$1.63*10^{4}$	$2.12*10^{4}$	16.8	$3.04*10^{4}$	1.7	2.5
	Max	$1.23*10^{5}$	$1.38*10^{5}$	144	$1.64*10^{5}$	24.5	18.0

3.1.2 Experiments carried out under high energy settings

Higher energy settings were expected to have a major effect on ablation as higher temperatures, more intense and expanded plasmas, were introduced.

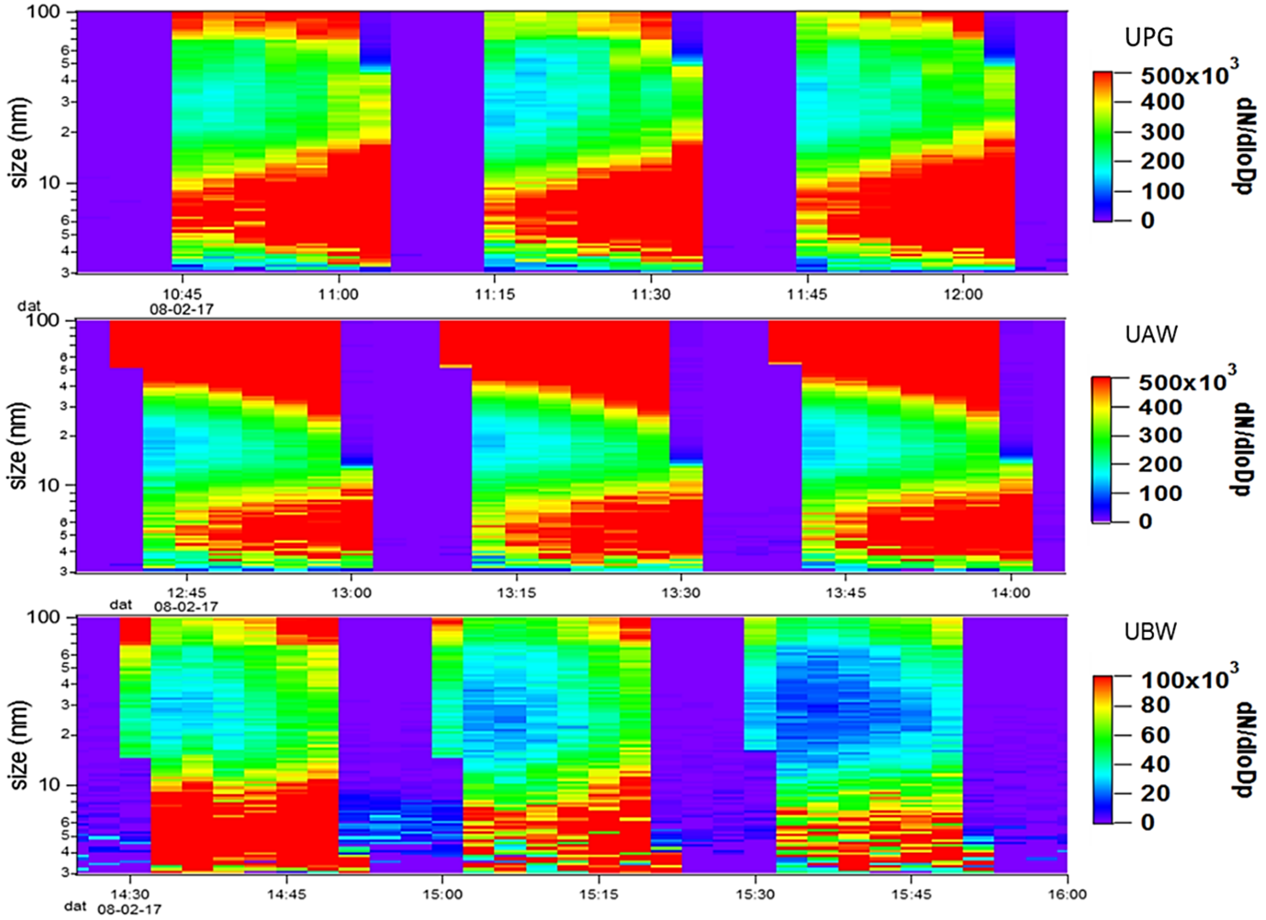

Figure 6. Size distribution (3-100 nm) of particles emitted during ablation with the near-IR laser under high energy settings

NP emissions in terms of particle number concentration were much higher under high energy settings in comparison to low energy settings for UAW and UPG tiles, while they were in the same range for UBW (Fig. 2). A good reproducibility was achieved and the patterns were similar to the ones obtained from the lower energy settings experiments. Specifically, for UAW tiles particle number concentrations under high energy settings increased by approximately a factor of three ($1.7*10^6/cm^3$) and for UPG by one order of magnitude ($4.5*10^5/cm^3$) compared to low energy settings. In the size range 10-700 nm mean diameters for the UPG and UBW tiles (Fig. S2 in Supplementary material) increased by approximately 20nm from the respective low energy values (Table 3) indicating a similar change in the particle release mechanisms for this size range.

In terms of particle size distribution (3-100 nm, Fig. 6), different patterns were observed. NPs released from UPG tiles showed high concentrations in the size range 3-15 nm, which were interpreted as sourcing from new particle formation. This mechanism is similar to the one described for the low energy settings (Section 3.1.1), although with higher concentrations. The latter may be explained by the fact that more intense and expanded plasma plume released larger amount of nuclei, which led to a higher number of newly formed particles (cf. section 4). In addition, higher rates of gaseous emissions were also expected due to higher energy, leading to enhanced new particle formation. Finally, the increased temperatures probably resulted in the melting of the surface of the tile and this led to the ejection of small droplets (30-100 nm, 300-500*10^3/cm^3) due to the pressure gradient. As a result, Fig. 6-UPG shows the prevalence of new particle formation, with a shift of the specific mode to larger particle diameter over time compared to low energy settings (from 5-10 nm to 3-20 nm), together with a higher contribution of NPs in the >60 nm size bins probably originating from emission of droplets (500*10^3/cm^3). One trait of these emissions, detected also for UAW under high-energy settings (Figure 6), was the evolution of particle number concentrations as a function of time, with increasing numbers of particles between approximately 3-10 nm and 30-60 nm. A similar pattern was observed for GER tiles with the mid-IR laser (Figure 10), for particles between 20-40 nm. These patterns could be related to new particle formation, growth, agglomeration, or linked to sampling artefacts, but the data available at present is not sufficient to extract robust conclusions. Further research would be necessary to understand this temporal pattern which was observed for a subset of laser-tile combinations.

The high energy settings had a similar influence on the UAW tiles, and a shift towards primary emissions was observed. Under low energy settings the dominant formation mechanism was melting for UAW tiles (Fig. 3), and this became even more evident with the increased energy input (Fig. 6). The presence of NPs <10 nm (3.1*10^8/cm^3) was also detected, but their relative contribution was much lower than that of particles in the 30-100 nm size range (7.2*10^8/cm^3).

A completely different pattern in terms of particle size distribution was observed for the UBW tiles. While NPs >70 nm dominated emissions under the low energy settings (100*10^3/cm^3, Fig. 3), when higher energy was applied the results showed dominance of NPs <10 nm (100*10^3/cm^3, Fig. 6). As the plasma plume was expanded it favoured a higher rate of new particle formation, but at the same time it hindered the energy transfer from the laser to the surface of the tile, thus limiting the expulsion of melt droplets (>70 nm).

NPs formed during high energy ablation conditions were collected on TEM grids (Fig. 7). Particles released during the ablation of the UPG tiles were mainly consisting of silica (Fig. 8a), while the coarser spherical particles had similar composition to the tile (Table S1 in Supplementary material). The silica content of the UPG tiles was much higher than that of alumina (Table S1) and porcelain tiles have typically free silica, whilst alumina is combined with other compounds mainly forming mullite and abundant in vitreous silica phases (Sánchez et al., 2010; Sanchez, Orts, Garcia-Ten, & Cantavella, 2001). Thereafter, silica rich vapours formed and condensed, promoting silica to emerge as the phase that dominated particle nucleation during UPG processing. Furthermore, oxides lose oxygen at high melting temperatures, consequently they become reduced and may decompose partially, which is also the case for silica where the suboxide (SiO_x) forms upon melting and reacts in air to form nanosized SiO_2 (Fricke-Begemann, Meinertz, Weichenhain-Schriever, & Ihlemann, 2014; Saxena, Agarwal, & Kanjilal, 2011; Slaoui, Fogarassy, Fuchs, & Siffert, 1992; Zhang, Lifshitz, & Lee, 2003). Two types of alumina particles can be seen in Fig. 7b: NPs originating from nucleation (Dp <10 nm), and larger spherical particles from the droplets of molten material. Similar results were obtained for UBW tiles (Fig. 7c).

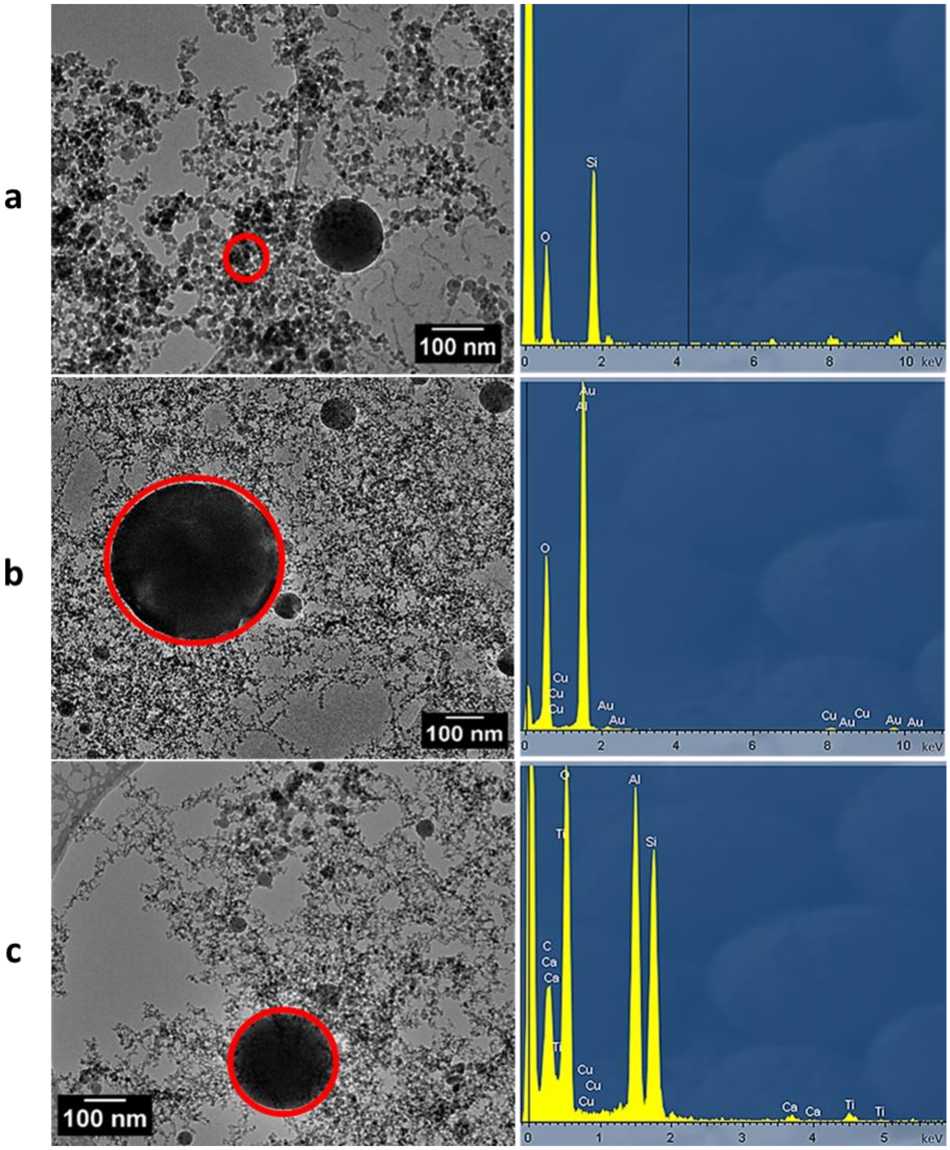

Figure 7. TEM images (left) and EDX spectra (right) of particles released during ablation under high energy settings, sourcing from: UPG (a), UAW (b), UBW (c) tiles

To conclude, even though the two porcelain tiles (UPG and UBW) had similar chemical composition (Table S1), differences in their NP emissions were observed. Specifically, SiO_2 NPs were formed and released in the case of UPG but not from the UBW tiles. This may be explained by the fact that the two porcelain tiles had different microstructures (Fig. S3 in Supplementary material). While the surface of the UPG tile shows agglomerates of grains in a vitreous (amorphous) matrix, the UBW tiles exhibit a more homogenous surface. Based on the above, it was interpreted that as the laser moved onto the surface of the UPG tile it would have melted and evaporated the different components, and consequently released species with different chemical composition than the matrix. Conversely, in the case of UBW tile all of the species emitted – and thus NPs – had the same chemical composition.

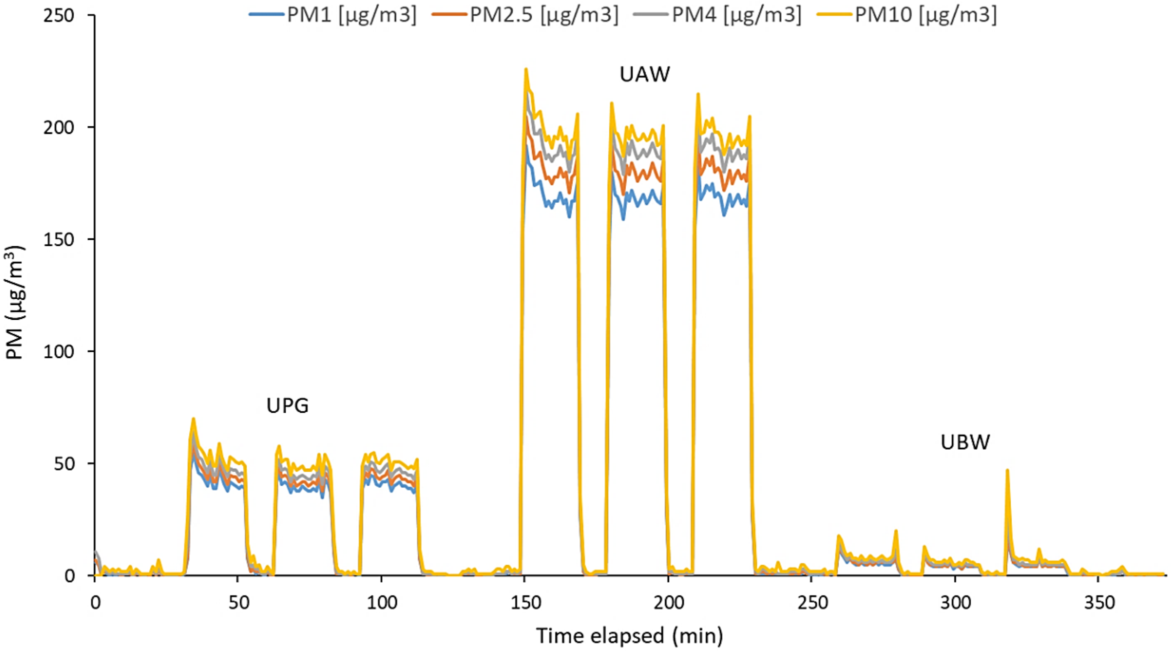

Figure 8. Particle mass concentrations during ablation with the near-IR laser under high energy settings

Particle mass concentrations are shown in Fig. 8, where $PM_{2.5}$ emissions from UPG tiles (44 µg/m^3) were higher by a factor of 3 when compared to the low energy settings (Table 3). Hence, higher energy laser processing results in increased particle mass as well as number concentrations. The situation was different for UBW tiles, where a reduction was observed for particle mass concentrations, and $PM_{2.5}$ values (5.8 µg/m^3) decreased by a factor of two when compared to the low energy settings (Table 3). The PM_1/PM_{10} ratio also decreased to 64%, indicating a relatively higher contribution of coarser particles to emissions in particle mass. Due to the high temperatures achieved with the laser different chemical reactions and transformations were induced: the porous UBW tiles released nanosized particles from the homogenous melt, while in the case of dense porcelain tiles (UPG) thermal shock results in ejection of grains due to differences in thermal expansion coefficients (Lahoz et al., 2011; Pascual-Cosp et al., 2002, 2001). Therefore, the UPG released more particle mass than the UBW and these results are also in agreement with those obtained for particle number concentrations (Fig. 2).

Finally, particle mass concentrations for UAW tiles were similar under low and high energy settings, as was also the PM_1/PM_{10} ratio (86%). The relative shift in particle size distribution observed for NPs emitted during ablation of this kind of tile did not have an impact on particle mass concentrations, given that the major concentration of particles monitored had diameters 3-100 nm.

3.2 Mid-IR laser

Particle number concentrations emitted from the UPG tiles (Fig. 9) were slightly lower ($2.37*10^5$ /cm^3) when compared to the n-IR laser (high energy,$4.54*10^5$/cm^3), but still in the same order of magnitude. However, particle emissions in the range 3-100 nm (Figure 10) were low and closer (1000/cm^3) to the instrument's detection limit than for other types of tiles, which might explain the irregular pattern observed (Figure 10, top). This might also be explained by the fact that mechanisms which would have formed nanoparticles (e.g. nucleation) were minor contributors to the emissions. Particle number concentrations in the range 3-100 nm were the lowest of all the cases studied and mean particle diameter in the range 10-700 nm was larger (160 nm, Table 4) than in the case of the near-IR laser. Thus, the dominant ablation mechanism for this kind of tile was attributed to grain ejection due to shockwaves, which would have released small numbers of coarser particles (Figures 10 and 12).

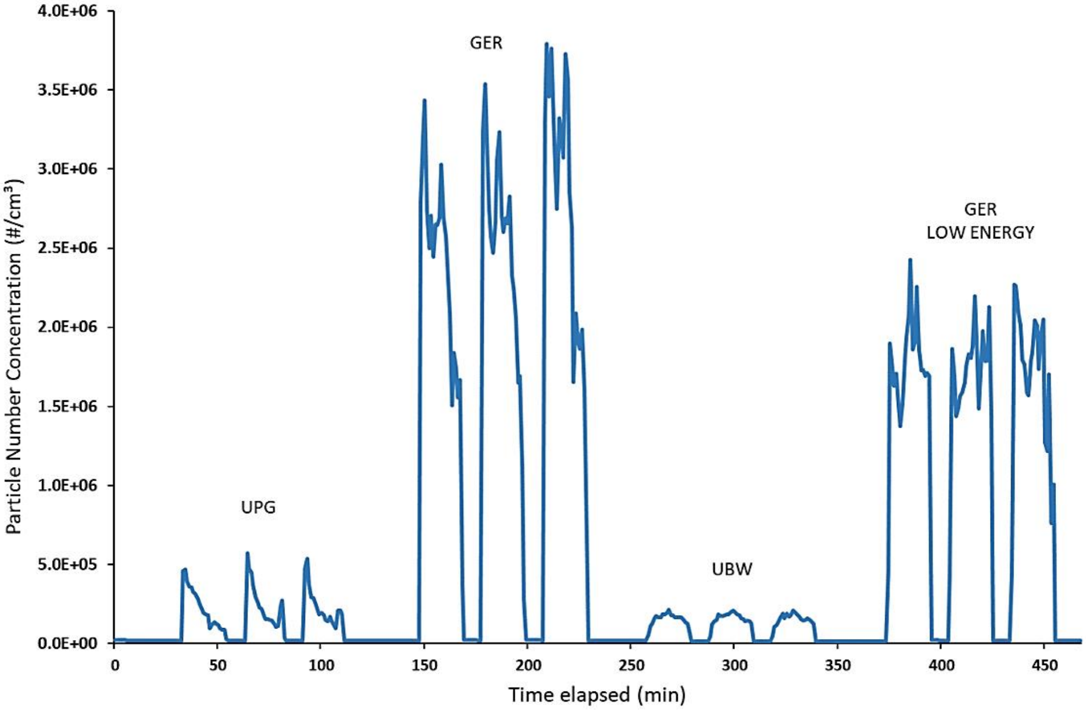

Figure 9. Particle number concentrations (size range 4nm-3µm) during ablation of the different types of tiles with the md-IR laser

In the case of UBW tiles, particle number concentrations increased from the n-IR (high energy) to the mid-IR laser ablation (from $6.9*10^4$/cm^3 to $1.59*10^5$/cm^3; Table 3 and 4 respectively). However, the particle size distribution in the range 3-100 nm (Fig. 10) showed a very different pattern suggesting different ablation mechanisms. In the n-IR case (Fig. 6) nucleation was the dominant mechanism with a minor contribution of melting, while in the case of mid-IR laser there was a more uniform release of NPs in all size bins. Thus, no dominant NP formation mechanism was identified, it can rather be interpreted that a combination of mechanisms was contributing similarly to the emissions in this specific size range (3-100 nm). Finally, particle emissions during ablation of the GER tiles were noticeable due to the unexpectedly high concentrations monitored (2.6*10^6/cm^3; Fig. 9). GER was ablated under two energy settings aiming to understand these emissions. The high particle number concentrations were almost one order of magnitude higher than for any of the other materials, even under the lower energy settings.

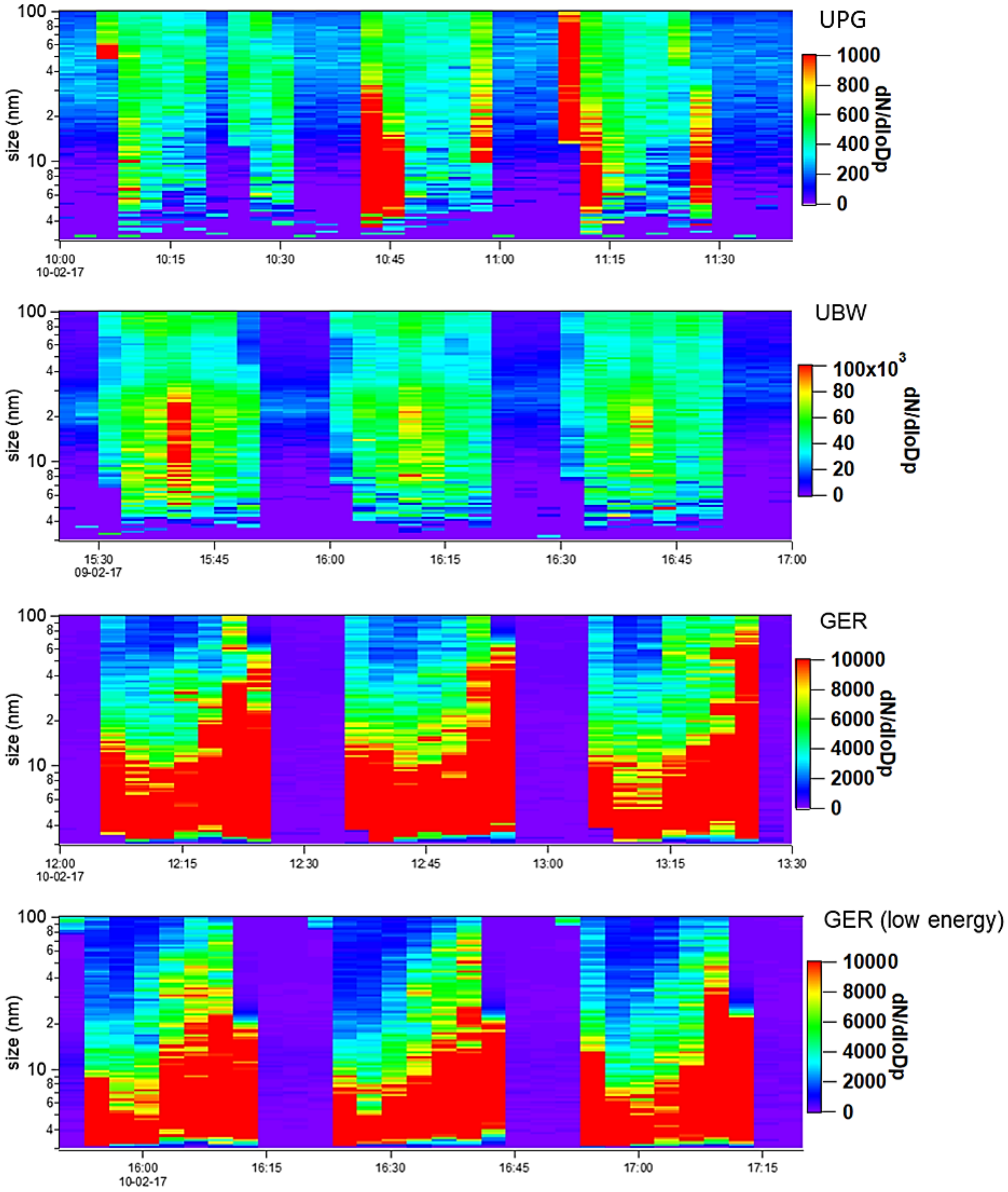

Figure 10. Size distribution (3-100 nm) of particles emitted during ablation with the mid-IR laser

The particle size distribution patterns (3-100 nm; Fig. 10) were very similar and reproducible for both energy settings, and dominated by NPs <20 nm with an increasing contribution of <40 nm NPs as the tile was being ablated. This would suggest a strong influence of nucleation and new particle formation processes. In addition, during ablation it is expected that the glaze, the main difference with the previous materials, would have molten and generated the ejection of droplets of different sizes in this case mainly >100 nm. Thus, these particles would have been outside the scanning range of the SMPS system used in this work, but not of the CPC (4nm-3µm, Fig. 9). These coarser particles were detected by TEM and are shown in Fig. 11.

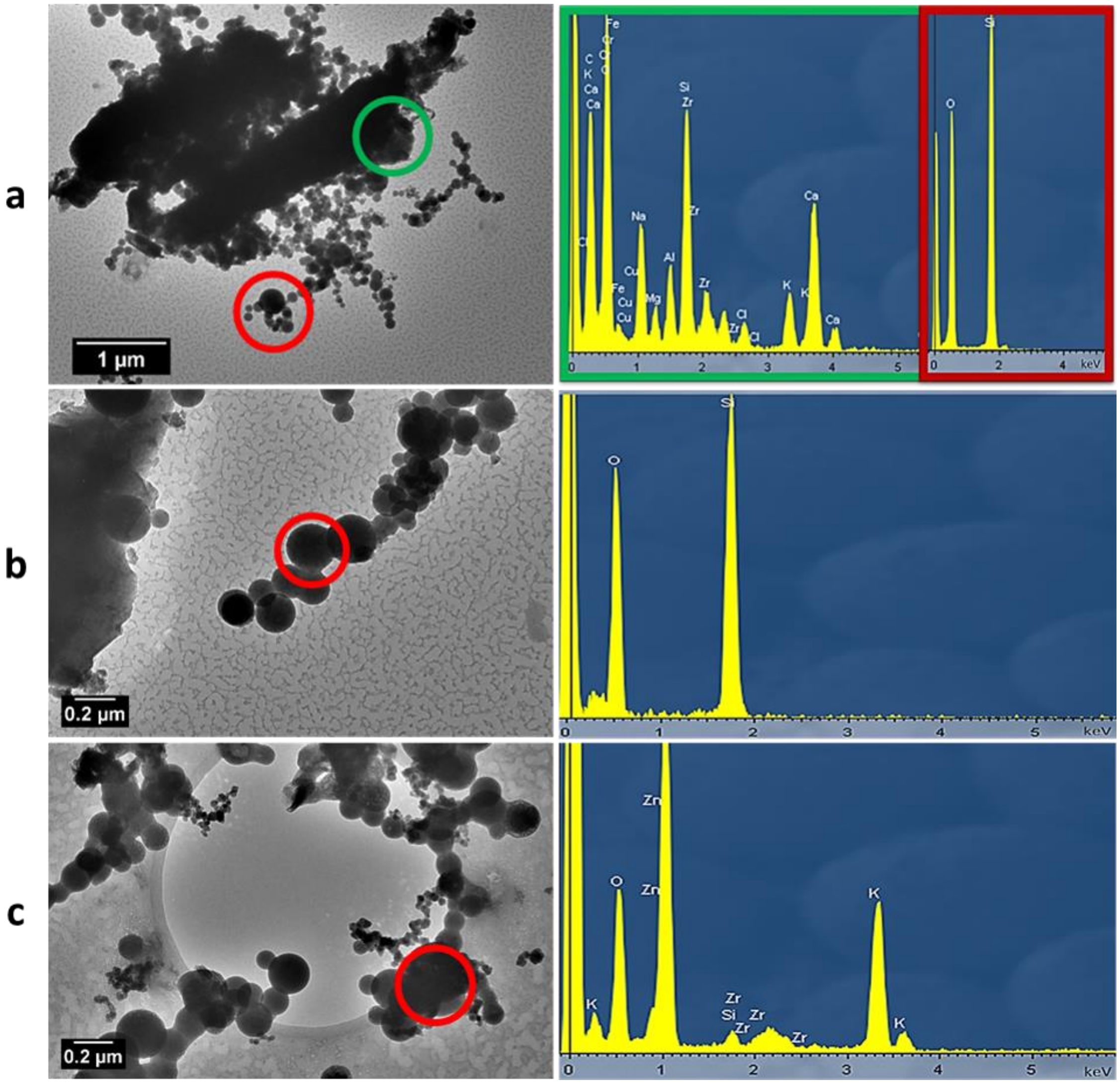

Figure 11. TEM images (left) and EDX spectra (right) of particles released during ablation using mid-IR laser, sourcing from UPG (a), UBW (b), GER (c) tiles

TEM images of particles emitted during ablation with the mid-IR laser are shown in Fig. 11. As evidenced by the shape and size of the particles emitted (Fig. 11a), coarse grains of UPG tiles were released due to the mechanical shockwave mechanism. EDX analysis of the smaller spherical particles (Fig. 11a marked in red) showed that they consist of SiO_2, probably originating from the evaporation of silica, as was described in section 3.1.2. The case is similar for UBW tiles (Fig. 11b), where spherical particles were also present. The formation of silica particles during the ablation of the UBW occurred during irradiation with the mid-IR laser, while this effect was not observed with the near-IR laser. The higher energy transmitted to the surface of the same tiles, as well as the different wavelength of the radiation, may create a more extensive heat-affected zone and modify the formation and release mechanisms, a fact that can be observed in the shape and size of the particles emitted (Fig. 11). Finally, different types of particles were identified during ablation of GER tiles (Fig. 11c): spherical and relatively coarser particles (>200 nm) originating from melt ejection, while irregular aggregates and NPs <20 nm are attributed to nucleation processes. The majority of the particles consisted mainly of zinc oxide, which is in the glassy phase of the glaze (Aparici, Moreno, Escardino, Amoros, & Mestre, 1994).

Table 4. Particle concentrations and mean diameters monitored during ablation with the mid-IR laser

Target Tile		**Particle number concentration (N)**	**Particle number concentration (N)**	**Mean diameter**	**Particle number concentration (N)**	**Mean diameter**	**$PM_{2.5}$**
		4 nm-3 µm	10-700 nm	10-700 nm	3-100 nm	3-100 nm	
		CPC (#/cm^3)	DiSCmini (#/cm^3)	DiSCmini (nm)	SMPS (#/cm^3)	SMPS (nm)	DustTrak DRX (µg/m^3)
UPG	Average	$2.37*10^5$	$1.70*10^5$	97.4	$4.94*10^4$	29.4	171
	St.dev.	$1.24*10^5$	$1.16*10^5$	35.6	$3.22*10^4$	5.9	134
	Max	$5.73*10^5$	$5.13*10^5$	187	$1.49*10^5$	38.6	674
UBW	Average	$1.59*10^5$	$1.62*10^5$	96.7	$6.64*10^4$	28.1	727
	St.dev.	$3.29*10^4$	$3.07*10^4$	8.2	$1.28*10^4$	2.1	231
	Max	$2.14*10^5$	$2.20*10^5$	110	$1.03*10^5$	32.7	1160
GER	Average	$2.62*10^6$	$1.47*10^6$	48.5	$2.03*10^6$	12.8	4450
	St.dev.	$6.48*10^5$	$5.58*10^5$	7.5	$1.96*10^6$	3.9	2259
	Max	$3.79*10^6$	$2.70*10^6$	61.5	$6.76*10^6$	18.8	11900
GER (low energy settings)	Average	$1.76*10^6$	$8.39*10^5$	68.1	$2.63*10^6$	12.4	3119
	St.dev.	$2.97*10^5$	$1.56*10^5$	10.1	$5.64*10^6$	4.4	2062
	Max	$2.43*10^6$	$1.45*10^6$	97.1	$2.45*10^7$	18.9	10400

High particle mass concentrations (up to $PM_{2.5}$ 11900 µg/m^3) with irregular emission patterns were recorded for the GER tiles, which varied as a function of the energy settings (Figure 12). The shockwave mechanism was attributed as the main contributor to these emissions. For UBW tiles mass concentrations were higher by 2 orders of magnitude (Table 4) than those monitored with the near-IR laser, while only by a factor of 2 in terms of particle number concentration. This fact confirms the change in the dominant emission mechanism from nucleation and droplets expulsion with the near-IR laser, to the mechanical shockwave with the mid-IR laser. For the UPG tiles, particle number concentrations decreased by a factor of 2 while particle mass concentrations increased by a factor of 4 with the mid-IR laser when compared to values obtained with the n-IR laser (Tables 3 and 4). The above offer a validation on the relevance of the mechanical shockwave mechanism with mid-IR PLA of ceramic tiles.

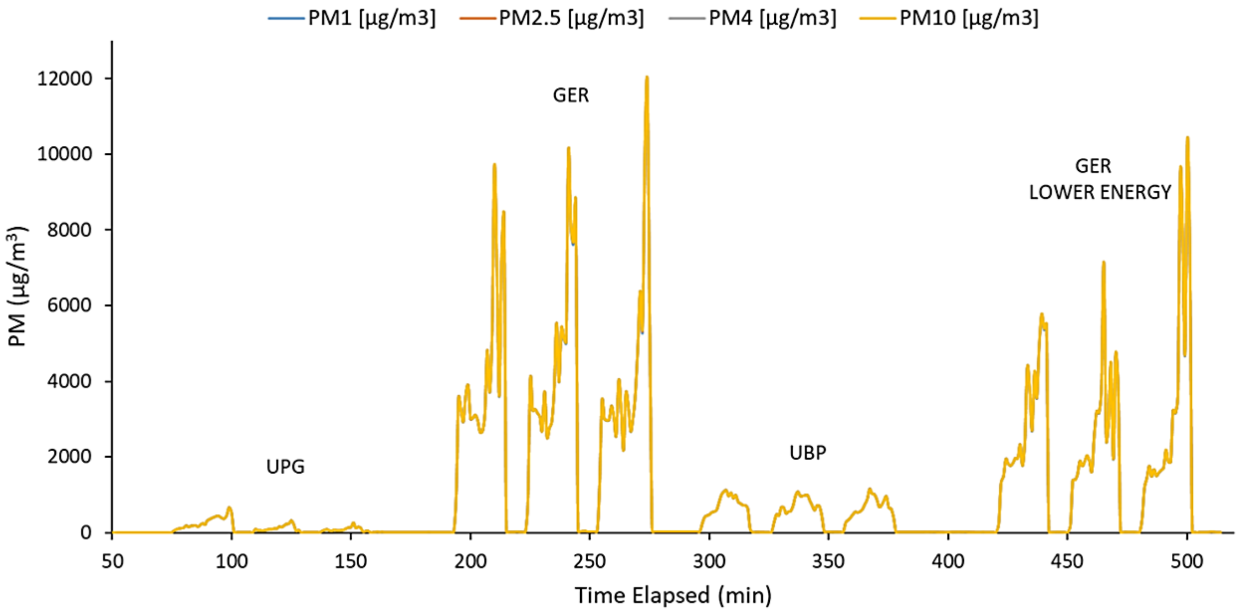

Figure 12. Particle mass concentrations of the emissions, for the different tiles and energy settings during ablation with the mid-IR laser

4. Discussion

Particle formation mechanisms during PLA of ceramic tiles were proposed by correlating measured particle number concentrations and size distributions with ablation phenomena described in the ceramic literature. Parameters found to influence particle emissions were laser type and energy settings, as well as the type of tile and their surface characteristics (chemical and physical). The mechanisms which contributed to particle emissions in this study are summarised in Figure 13, including the relationship between the dominant particle emission mechanisms and the types of laser used. Based on the results presented in the previous section, particle nucleation was the dominant mechanism in terms of particle number emissions in the size range 3-20 nm, while high emissions in terms of particle mass concentrations were attributed to mechanical shockwaves (>100 nm). Conversely, tile melting contributed to particle mass and number emissions given that it may generate droplets with a wide range of particle diameters (with a mean diameter around 40 nm). It should be noted that the melting mode comprises also agglomerates and aggregates of smaller particles, as evidenced in Figures 4 and 11. Due to high surface energy the smaller nanoparticles have a strong tendency to rapidly form agglomerates in order to reach a more stable state (Max L.

Eggersdorfer et al., 2012; Polte, 2015). Agglomerates can have a wide range of sizes depending on the primary size of the particles as well as the number of clustered particles. Further research is necessary to distinguish between the contributions solely from the melting mechanism and from nanoparticle agglomeration. Finally, with regard to the influence of the type of laser, nucleation and melting were observed with the near-IR laser whereas melting and mechanical shockwaves were more present in the case of the mid-IR laser.

Table 5. Emission mechanisms identified and their characteristics during PLA of different ceramic tiles

Energy Settings	Emission characteristics	UPG	UAW	UBW	GER
			Near-IR Laser		
Low	N$_p$ – CPC (#/cm^3)	$4.6*10^4$	$4.9*10^5$	$7.6*10^4$	-
	Mean D$_p$ – SMPS (nm)	14.7	32.8	31.7	-
	N$_p$ – SMPS (#/cm^3)	$8.5*10^4$	$5.0*10^5$	$9.1*10^4$	-
	PM$_{2.5}$ (µg/m^3)	15.2	133	13.6	-
	Dominant mechanism	Nucleation	Nucleation, Melting	Melting	-
High	N$_p$ – CPC (#/cm^3)	$4.5*10^5$	$1.7*10^6$	$6.9*10^4$	-
	Mean D$_p$ – SMPS (nm)	25.1	46.9	22.5	-
	N$_p$ – SMPS (#/cm^3)	$5.6*10^5$	$9.0*10^5$	$1.0*10^5$	-
	PM$_{2.5}$ (µg/m^3)	44.3	181	5.8	-
	Dominant mechanism	Nucleation, Melting	Nucleation, Melting	Nucleation	-
			Mid-IR Laser		
Standard	N$_p$ – CPC (#/cm^3)	$2.4*10^5$	-	$1.6*10^5$	$2.6*10^6$
	Mean D$_p$ – SMPS (nm)	29.4	-	28.1	12.8
	N$_p$ – SMPS (#/cm^3)	$4.9*10^4$	-	$6.6*10^4$	$2.0*10^6$
	PM$_{2.5}$ (µg/m^3)	171	-	727	44450
	Dominant mechanism	Shockwave	-	Combined[a]	Combined[a]
Low	N$_p$ – CPC (#/cm^3)	-	-	-	$1.8*10^6$
	Mean D$_p$ – SMPS (nm)	-	-	-	12.4
	N$_p$ – SMPS (#/cm^3)	-	-	-	$2.6*10^6$
	PM$_{2.5}$ (µg/m^3)	-	-	-	3119
	Dominant mechanism	-	-	-	Combined[a]

[a] Combined contribution from nucleation, melting and shockwaves.

Table 5 links the particle emission characteristics observed with the emission mechanisms proposed, for all the combinations of tiles and laser parameters. For the near-IR laser, total particle number concentrations (measured with CPC) increased by one order of magnitude (10^4 to 10^5/cm^3, and 10^5 to 10^6/cm^3) with increasing energy (from low to high) for two of the three tiles (UPG and UAW, respectively), while the UBW tile showed a slightly different pattern with similar total particle emissions for both energy settings (10^4/cm^3). When looking strictly at the 3-100 nm size range (measured with SMPS), particle number concentrations did show an increasing trend for all of the materials with increasing energy input. Mean particle diameter increased for UPG and UAW from the low to the high energy inputs, while the UBW tiles showed again a different trend (with decreasing particle diameter). Furthermore, for particle mass concentrations (PM$_{2.5}$ in Table 5) emissions from

UPG and UAW tiles with the n-IR laser increased from lower to higher energies, while they decreased for the UBW tiles (in accordance with the dominant mechanism). The same was observed regarding the dominant mechanisms proposed for particle emission: the UPG and UAW tiles followed an evolution, from low to high energy inputs, from nucleation-dominated emissions to melting, and finally mechanical shockwave (Figure 13). Conversely, the UBW tiles showed a prevalence of melting with low energy inputs, and of nucleation for the high energy settings, which suggests that higher energy inputs were necessary to generate the adequate conditions for nucleation, for this type of tiles.

Given that the UPG and UBW tiles have a similar chemical composition (Table 1), these results suggest that tile physical properties such as microstructure (i.e. crystallinity, Figure S6 in Supplementary material), optical properties (colour) or porosity play a relevant role in particle emissions. Hence, it may be concluded that the type of material, as well as the laser parameters, affect particle emissions during PLA of ceramic tiles. The different patterns observed for the UBW tiles when compared to the UPG and UAW tiles require further research, in order to understand the differences detected. However, it should be noted that UBW is typically an intermediate product in the ceramic industry, and not as relevant from a particle emission and workplace exposure perspective as the other materials, much more generally used in the industry.

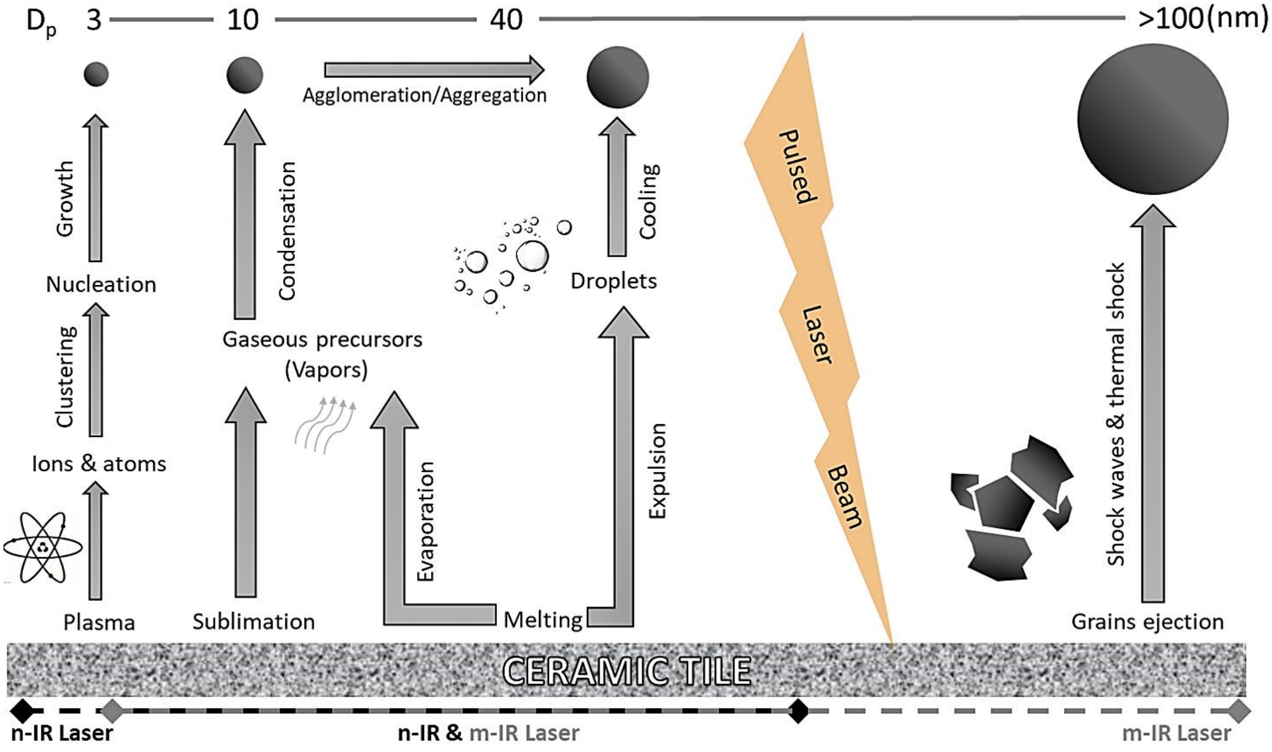

Figure 13. Schematic illustration of NP formation and release mechanisms during PLA of ceramic tiles

5. Conclusions

This work presents an interdisciplinary study, which aims to establish a connection between aerosol research, laser ablation and ceramic technology, with potential implications for human health. NP emissions were monitored during pulsed laser ablation (PLA) of ceramic tiles with the aim to understand the mechanisms behind particle formation and release. The assessment of particle number concentrations and size distributions evidenced that particle formation was directly connected with ablation phenomena. Four different types of tiles (unglazed porcelain, unglazed alumina, unglazed biscuit porcelain and glazed earthenware) and two lasers (near-IR and mid-IR) were used. Irrespective of the combination of laser and tile used, high concentrations of NPs were released during PLA of ceramic tiles. The ceramic tile composition, physicochemical properties, and surface microstructure are parameters which affect particle release during PLA. In terms of particle number, emissions were higher during the ablation of unglazed alumina (UAW) and glazed earthenware (GER). SiO_2 and Al_2O_3 particles (>10 nm) were formed through different nucleation pathways during ablation of the ceramic tiles.

Although a combination of mechanisms was seen to contribute to particle number emissions, the dominant ones were nucleation and melting with the near-IR laser, whereas they were melting and mechanical shockwaves for the mid-IR laser. Melting and the subsequent ejection of droplets in the range 40-700 nm were found to have a significant contribution in terms of particle number concentration. Nucleation generated particles <20 nm, and mechanical shockwaves released particles >100 nm. Thus, the ablation of tiles for which the dominant mechanism was nucleation resulted in high particle number concentrations, whereas for tiles dominated by mechanical shockwaves high particle mass concentrations were monitored. These results are potentially relevant from the point of view of exposure mitigation strategies in industrial facilities where PLA is carried out. The localized extraction system implemented in the scenarios assessed proved to be an efficient mitigation measure, as it prevented particle release to the worker area.

6. Acknowledgements

The authors kindly acknowledge Mr. Carlos Borrell and Mr. Carlos Estepa for their help during the experimental work and Dr Natalia Moreno for the XRD measurements. The current work was carried out in the framework of the CERASAFE project (www.cerasafe.eu), with the support of SIINN ERA-NET (project id: 16), and is funded by the Spanish MINECO (PCIN-2015-173-C02-01). Partial support from project MAT2016-79866-R (AEI/FEDER, UE) is acknowledged.

REFERENCES

Andreeta, M. R. B., Cunha, L. S., Vales, L. F., Caraschi, L. C., & Jasinevicius, R. G. (2011). Bidimensional codes recorded on an oxide glass surface using a continuous wave CO2 laser. *Journal of Micromechanics and Microengineering*, *21*(2), 025004. https://doi.org/10.1088/0960-1317/21/2/025004

Aparici, J., Moreno, A., Escardino, A., Amoros, J. L., & Mestre, S. (1994). Study of Opacification in Zirconium Ceramic Glazes Used in Single-Fired Wall Tile Manufacture. In *Study of Opacification in Zirconium Ceramic Glazes Used in Single-Fired Wall Tile Manufacture* (pp. 35–45). Castellon de la plana, Spain: QUALICER 94.

Asbach, C., Kaminski, H., Lamboy, Y., Schneiderwind, U., Fierz, M., & Todea, A. M. (2016). Silicone sampling tubes can cause drastic artifacts in measurements with aerosol instrumentation based on unipolar diffusion charging. *Aerosol Science and Technology*, *50*(12), 1375–1384. https://doi.org/10.1080/02786826.2016.1241858

Carty, W. M., & Senapati, U. (1998). Porcelain - Raw materials, processing, phase evolution, and mechanical behavior. *Journal of the American Ceramic Society*, *81*(1), 3–20. https://doi.org/10.1111/j.1151-2916.1998.tb02290.x

Curwin, B., & Bertke, S. (2011). Exposure characterization of metal oxide nanoparticles in the workplace. *Journal of Occupational and Environmental Hygiene*, *8*(10), 580–587. https://doi.org/10.1080/15459624.2011.613348

Czotscher, T., & Vollertsen, F. (2016). Analysis of melting and melt expulsion during nanosecond pulsed laser ablation. *Physics Procedia*, *83*, 53–61. https://doi.org/10.1016/j.phpro.2016.08.007

Demou, E., Peter, P., & Hellweg, S. (2008). Exposure to manufactured nanostructured particles in an industrial pilot plant. *Annals of Occupational Hygiene*, *52*(8), 695–706. https://doi.org/10.1093/annhyg/men058

Eggersdorfer, M. L., Kadau, D., Herrmann, H. J., & Pratsinis, S. E. (2012). Aggregate morphology evolution by sintering: Number and diameter of primary particles. *Journal of Aerosol Science*, *46*, 7–19. https://doi.org/10.1016/j.jaerosci.2011.11.005

Eggersdorfer, M. L., & Pratsinis, S. E. (2014). Agglomerates and aggregates of nanoparticles made in the gas phase. *Advanced Powder Technology*, *25*(1), 71–90. https://doi.org/10.1016/j.apt.2013.10.010

Fonseca, A. S., Maragkidou, A., Viana, M., Querol, X., Hämeri, K., de Francisco, I., … de la Fuente, G. F. (2016). Process-generated nanoparticles from ceramic tile sintering: Emissions, exposure and environmental release. *Science of the Total Environment*, *565*, 922–932. https://doi.org/10.1016/j.scitotenv.2016.01.106

Fonseca, A. S., Viana, M., Querol, X., Moreno, N., de Francisco, I., Estepa, C., & de la Fuente, G. F. (2015). Ultrafine and nanoparticle formation and emission mechanisms during laser processing of ceramic materials. *Journal of Aerosol Science*, *88*, 48–57. https://doi.org/10.1016/j.jaerosci.2015.05.013

Fonseca, A. S., Viitanen, A. K., Koivisto, A. J., Kangas, A., Huhtiniemi, M., Hussein, T., … Hameri, K. (2014). Characterization of exposure to carbon nanotubes in an industrial setting. *Annals of Occupational Hygiene*, *59*(5), 586–599. https://doi.org/10.1093/annhyg/meu110

Fricke-Begemann, T., Meinertz, J., Weichenhain-Schriever, R., & Ihlemann, J. (2014). Silicon suboxide (SiOx): laser processing and applications. *Applied Physics A: Materials Science and Processing*, *117*(1), 13–18. https://doi.org/10.1007/s00339-014-8236-3

Gandra, J., Miranda, R., Vilaa, P., Velhinho, A., & Teixeira, J. P. (2011). Functionally graded materials produced by friction stir processing. *Journal of Materials Processing Technology*, *211*(11), 1659–1668. https://doi.org/10.1016/j.jmatprotec.2011.04.016

Gómez, V., Irusta, S., Balas, F., & Santamaria, J. (2013). Intense generation of respirable metal nanoparticles from a low-power soldering unit. *Journal of Hazardous Materials*, *256–257*, 84–89. https://doi.org/10.1016/j.jhazmat.2013.03.067

Hameri, K., Lahde, T., Hussein, T., Koivisto, J., & Savolainen, K. (2009). Facing the key workplace challenge: Assessing and preventing exposure to nanoparticles at source. *Inhalation Toxicology*, *21*, 17–24. https://doi.org/10.1080/08958370902942525

Heal, M. R., Kumar, P., & Harrison, R. M. (2012). Particles, air quality, policy and health. *Chemical Society Reviews*, *41*(19), 6606. https://doi.org/10.1039/c2cs35076a

International Organization for Standardization. (2012). International Organization for Standardization 13006: Ceramic tiles - Definitions, classification, characteristics and marking. USA: ISO.

Koch, W., & Friedlander, S. K. (1989). The effect of particle coalescence on the surface area of a coagulating aerosol. *Journal of Aerosol Science*, *20*(8), 891–894. https://doi.org/https://doi.org/10.1016/0021-8502(89)90719-2

Koivisto, A. J., Lyyränen, J., Auvinen, A., Vanhala, E., Hämeri, K., Tuomi, T., & Jokiniemi, J. (2012). Industrial worker exposure to airborne particles during the packing of pigment and nanoscale titanium dioxide. *Inhalation Toxicology*, *24*(12), 839–849. https://doi.org/10.3109/08958378.2012.724474

Lahoz, R., De La Fuente, G. F., Pedra, J. M., & Carda, J. B. (2011). Laser engraving of ceramic tiles. *International Journal of Applied Ceramic Technology*, *8*(5), 1208–1217. https://doi.org/10.1111/j.1744-7402.2010.02566.x

Lushnikov, A. A., Maksimenko, V. V, & Pakhomov, A. V. (1989). Fractal aggregates from laser plasma. *Journal of Aerosol Science*, *20*(8), 865–870. https://doi.org/10.1016/0021-8502(89)90713-1

Nedialkov, N. N., Atanasov, P. A., Sawczak, M., & Sliwinski, G. (2003). Ablation of ceramics with ultraviolet, visible, and infrared nanosecond laser pulses. In *Proc. SPIE 5120, XIV International Symposium on Gas Flow, Chemical Lasers, and High-Power Lasers* (Vol. 5120, pp. 703–708). https://doi.org/10.1117/12.515847

Noël, S., Hermann, J., & Itina, T. (2007). Investigation of nanoparticle generation during femtosecond laser ablation of metals. *Applied Surface Science*, *253*(15), 6310–6315. https://doi.org/10.1016/j.apsusc.2007.01.081

Oberdörster, G. (2001). Pulmonary effects of inhaled ultrafine particles. *International Archives of Occupational and Environmental Health*, *74*(1), 1–8. https://doi.org/10.1007/s004200000185

Pascual-Cosp, J., Ramírez del Valle, A. J., Garciá-Fortea, J., & Sánchez-Soto, P. J. (2002). Laser cutting of high-vitrified ceramic materials: Development of a method using a Nd:YAG laser to avoid catastrophic breakdown. *Materials Letters*, *55*(4), 274–280. https://doi.org/10.1016/S0167-577X(02)00377-4

Pascual-Cosp, J., Ramírez Del Valle, A. J., García Fortea, J., & Sánchez Soto, P. J. (2001). Thermal evolution of a ceramic material processed using a Nd-YAG laser. *Boletin de La Sociedad Espanola de Ceramica y Vidrio*.

Pascual, A., Fortanet, E., Carda, J. B., Pavlov, R., Pedra, J. M., De La Fuente, G. F., … Lahoz, R. (2005). Ceramic tile decoration by laser technology. In *CFI Ceramic Forum International* (Vol. 82). Castellon de la plana, Spain.

Pfefferkorn, F. E., Bello, D., Haddad, G., Park, J. Y., Powell, M., McCarthy, J., … Hoover, M. D. (2009). Characterization of exposures to airborne nanoscale particles during friction stir welding of aluminum. *Annals of Occupational Hygiene*, *54*(5), 486–503. https://doi.org/10.1093/annhyg/meq037

Phipps, C. (2007). *Laser Ablation and its Applications*. (E. W. T. Rhodes, E. B. a Adibi, T. Asakura, T. W. Hansch, T. Kamiya, F. Krausz, … W. T. Rhodes, Eds.), *Springer Series in Optical Sciences* (Vol. 129). USA: Springer. https://doi.org/10.1007/978-0-387-30453-3

Polte, J. (2015). Fundamental growth principles of colloidal metal nanoparticles – a new perspective. *CrystEngComm*, *17*(36), 6809–6830. https://doi.org/10.1039/C5CE01014D

Rivas, I., Mazaheri, M., Viana, M., Moreno, T., Clifford, S., He, C., … Querol, X. (2017). Identification of technical problems affecting performance of DustTrak DRX aerosol monitors. *Science of the Total Environment*, *584–585*, 849–855. https://doi.org/10.1016/j.scitotenv.2017.01.129

Russo, R. E., Mao, X., Gonzalez, J. J., Zorba, V., & Yoo, J. (2013). Laser ablation in analytical chemistry. *Analytical Chemistry*, *85*(13), 6162–6177. https://doi.org/10.1021/ac4005327

Salomão, R., Bôas, M. O. C. V., & Pandolfelli, V. C. (2011). Porous alumina-spinel ceramics for high temperature applications. *Ceramics International*, *37*(4), 1393–1399. https://doi.org/10.1016/j.ceramint.2011.01.012

Sánchez, E., García-Ten, J., Sanz, V., & Moreno, A. (2010). Porcelain tile: Almost 30 years of steady scientific-technological evolution. *Ceramics International*, *36*(3), 831–845. https://doi.org/10.1016/j.ceramint.2009.11.016

Sanchez, E., Orts, M. J., Garcia-Ten, J., & Cantavella, V. (2001). Porcelain tile composition effect on phase formation and end products. *American Ceramic Society Bulletin*, *80*(6), 43–49.

Saxena, N., Agarwal, A., & Kanjilal, D. (2011). Effect of thermal annealing on the formation of silicon nanoclusters in SiOXfilms grown by PLD. *Physica B: Condensed Matter*, *406*(11), 2148–2151. https://doi.org/10.1016/j.physb.2011.03.019

Sivayoganathan, M., Tan, B., & Venkatakrishnan, K. (2012). Effect of mega-hertz repetition rate on the agglomerated particle size of femtosecond synthesized nanostructures. *Optical Materials Express*, *2*(8), 987–995. https://doi.org/10.1364/OME.2.000987

Slaoui, A., Fogarassy, E., Fuchs, C., & Siffert, P. (1992). Properties of silicon dioxide films prepared by pulsed-laser ablation. *Journal of Applied Physics*, *71*(2), 590–596. https://doi.org/10.1063/1.350411

Sugioka, K., Meunier, M., & Pique, A. (2010). *Laser Precision Microfabrication*. (K. Sugioka, M. Meunier, & A. Piqué, Eds.) (Vol. 135). Berlin, Heidelberg: Springer Berlin Heidelberg. https://doi.org/10.1007/978-3-642-10523-4

van Broekhuizen, P. (2012). *Nano Matters - Building Blocks for a Precautionary Approach*. University of Amsterdam, Amsterdam. Retrieved from https://dare.uva.nl/search?identifier=84997b8a-0640-409e-9017-c716ad8e1995

Viana, M., Fonseca, A. S., Querol, X., López-Lilao, A., Carpio, P., Salmatonidis, A., & Monfort, E. (2017). Workplace exposure and release of ultrafine particles during atmospheric plasma spraying in the ceramic industry. *Science of the Total Environment*, *599–600*, 2065–2073. https://doi.org/10.1016/j.scitotenv.2017.05.132

Viitanen, A. K., Uuksulainen, S., Koivisto, A. J., Hämeri, K., & Kauppinen, T. (2017). Workplace measurements of ultrafine particles-A literature review. *Annals of Work Exposures and Health*, *61*(7), 749–758. https://doi.org/10.1093/annweh/wxx049

Voliotis, A., Bezantakos, S., Giamarelou, M., Valenti, M., Kumar, P., & Biskos, G. (2014). Nanoparticle emissions from traditional pottery manufacturing. *Environ. Sci.: Processes Impacts*, *16*(6), 1489–1494. https://doi.org/10.1039/C3EM00709J

Weichenthal, S. (2012). Selected physiological effects of ultrafine particles in acute cardiovascular morbidity. *Environmental Research*, *115*, 26–36. https://doi.org/10.1016/j.envres.2012.03.001

Zhang, R.-Q., Lifshitz, Y., & Lee, S.-T. (2003). Oxide-Assisted Growth of Semiconducting Nanowires. *Advanced Materials*, *15*(78), 635–640. https://doi.org/10.1002/adma.200301641

Zhigilei, L. V., Lin, Z., & Ivanov, D. S. (2009). Atomistic modeling of short pulse laser ablation of metals:

Connections between melting, spallation, and phase explosion. *Journal of Physical Chemistry C*, *113*(27), 11892–11906. https://doi.org/10.1021/jp902294m

Supplementary material

Nanoparticle formation and emission during laser ablation of ceramic tiles

Apostolos Salmatonidis, Mar Viana, Noemí Pérez, Andrés Alastuey, Germán F. de la Fuente, Luis Alberto Angurel, Vicenta Sanfélix, Eliseo Monfort

Table S1. Chemical characterisation of the tiles under study.

UBW		**UAW**		**UPG**		**Glaze***	
Component	**Content (w_t%)**	**Component**	**Content (w_t%)**	**Component**	**Content (w_t%)**	**Component**	**Content (w_t%)**
SiO_2	70.2	Al_2O_3	97.3	SiO_2	70.6	SiO_2	55.7
Al_2O_3	19.8	SiO_2	1.3	Al_2O_3	18.9	ZnO	12.0
Na_2O	5.8	MgO	0.5	Fe_2O_3	1.0	CaO	10.2
K_2O	1.29	Na_2O	0.2	Na_2O	3.7	ZrO_2	7.0
CaO	0.71	CaO	0.04	K_2O	1.9	Al_2O_3	4.3
TiO_2	0.62	Fe_2O_3	0.03	CaO	0.6	K_2O	3.9
Fe_2O_3	0.51	K_2O	0.03	MgO	0.2	B_2O_3	3.6
MgO	0.35	BaO	0.03	TiO_2	0.9	MgO	2.5
P_2O_5	0.13	TiO_2	0.01	MnO	0.01	HfO_2	0.14
BaO	0.03	MnO	0.01	P_2O_5	0.3	Na_2O	0.10
ZrO_2	0.03	P_2O_5	0.01	Cr_2O_3	0.3	Fe_2O_3	0.05
SrO	0.02			ZrO_2	1.0	TiO_2	0.05
MnO	0.01					PbO	0.03
						P_2O_5	0.03
						BaO	0.01
						Li_2O	<0.01
						SrO	<0.01

*The chemical composition refers only to the glaze, and not the body of the GER tile, since that was the part processed by the laser

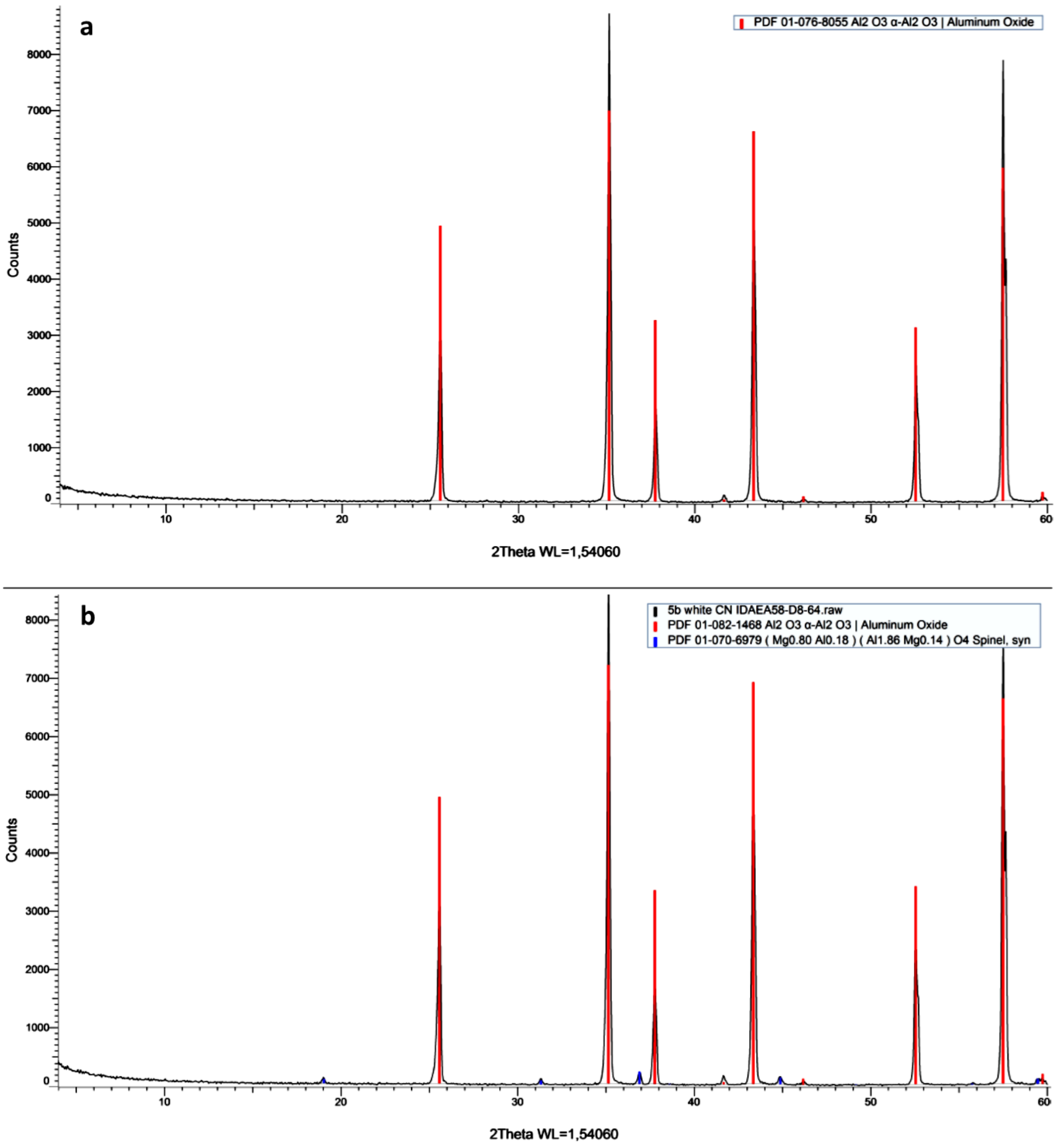

Figure S1. X-ray powder diffraction pattern of UAW α-Alumina tiles, (a) pure α-Alumina and (b) the tile with dominant phase of α-Alumina and a minor phase (trace) of spinel MgAlO

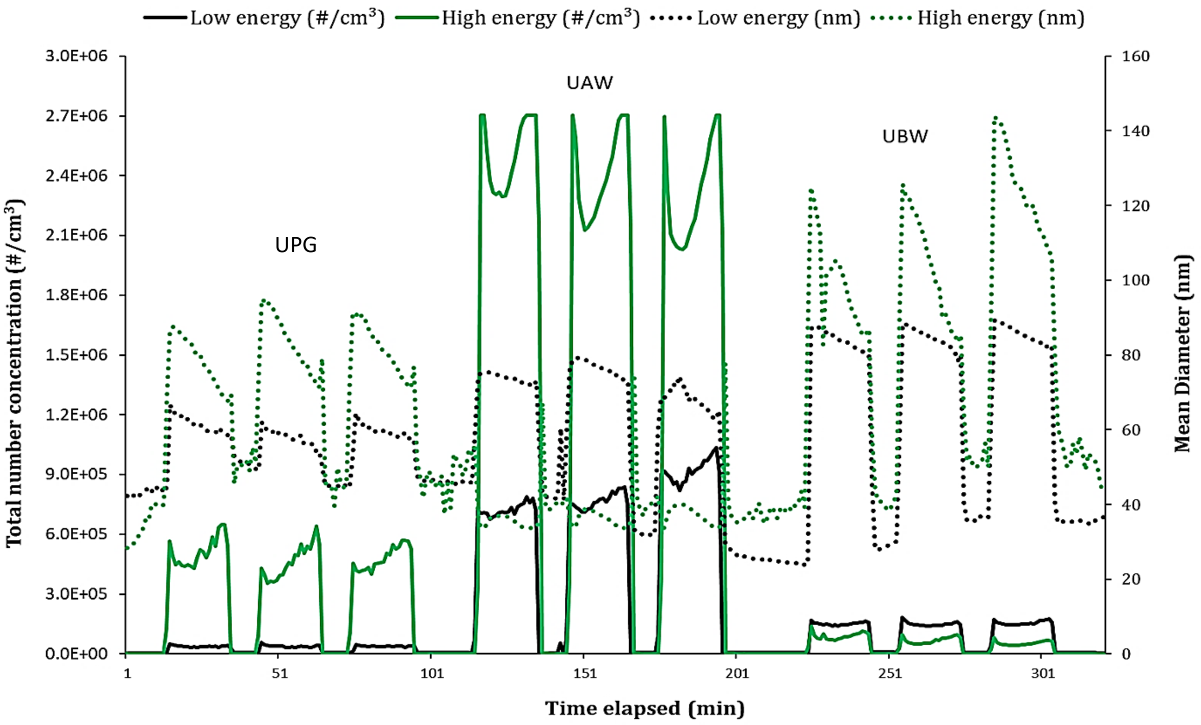

Figure S2. Mean particle diameter (nm) and number concentration (10-700 nm) for low and high energy settings, monitored with DiSCmini.

Table S2. Laser parameters and energy settings applied for the two laser set-ups.

Energy settings	**Near-IR laser**		**Mid-IR laser**	
	Low	**High**	**Standard**	**Low**
Laser power (W)	11.5	20		
Duty cycle (%)			30	15
Spacing between lines (mm)	0.02	0.03	0.8	0.8
Laser velocity (m/min)	1.5	1.5	4	4
Frequency (kHz)	20	25	20	15
Pulse duration (ns)	100	200	50000	66667

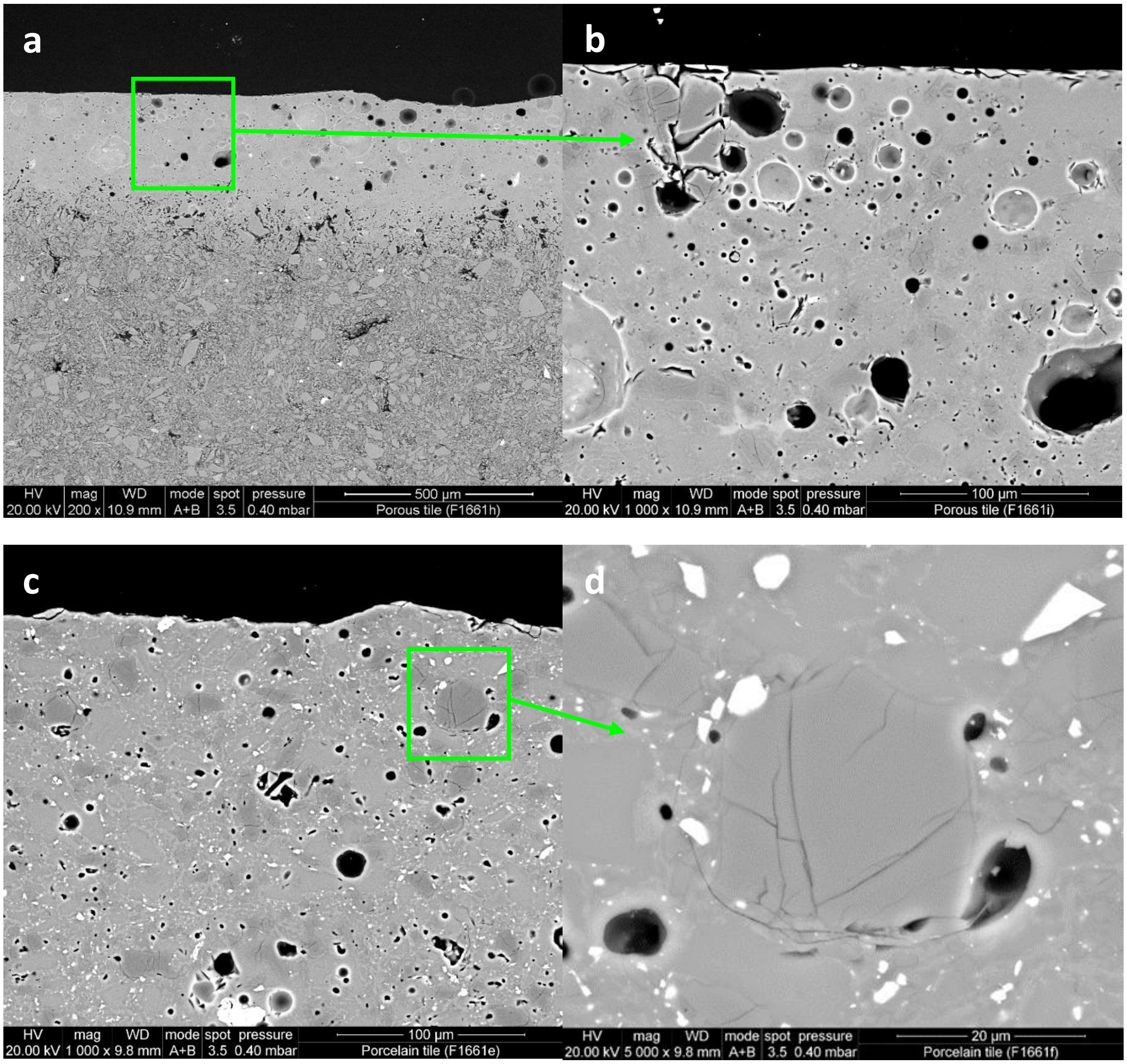

Figure S3. SEM images of the surfaces of untreated porcelain tiles. UBW (a,b) and UPG (c,d)

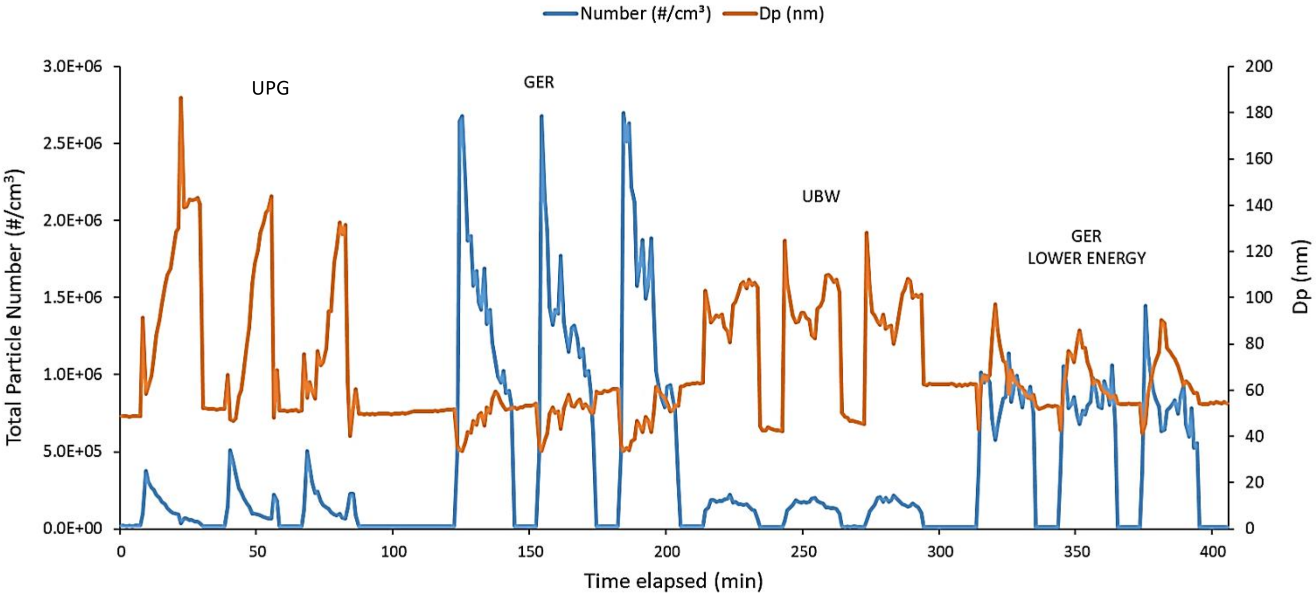

Figure S4. Mean particle diameter (nm) and total particle number concentration (10-700 nm) for the different tiles and energy settings during ablation with the mid-IR laser.

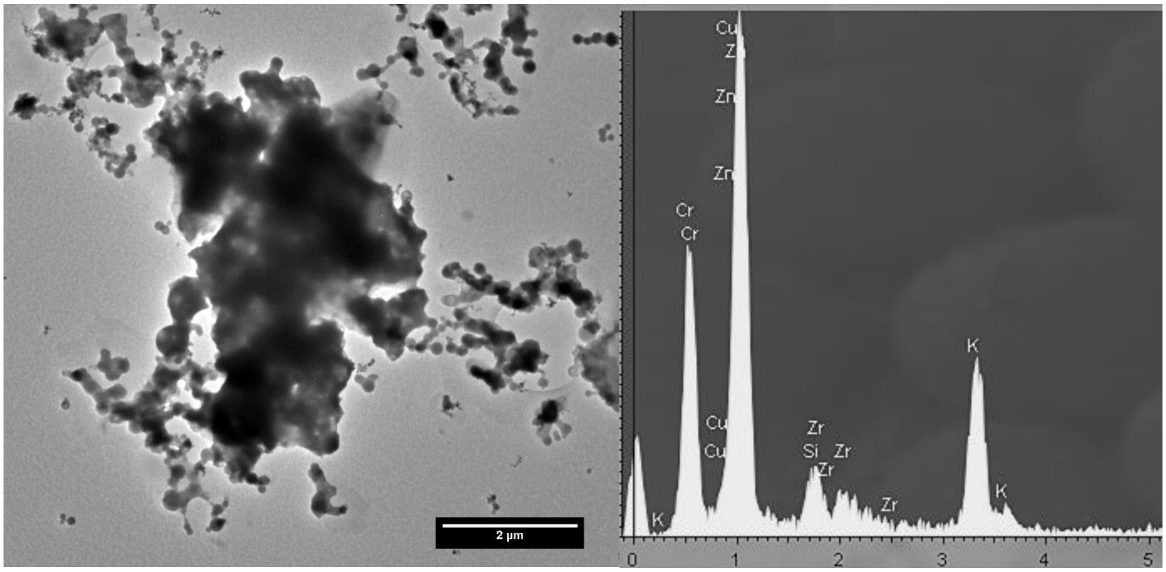

Figure S5. TEM image and EDX spectra of NPs emitted during GER ablation with the mid-IR laser.

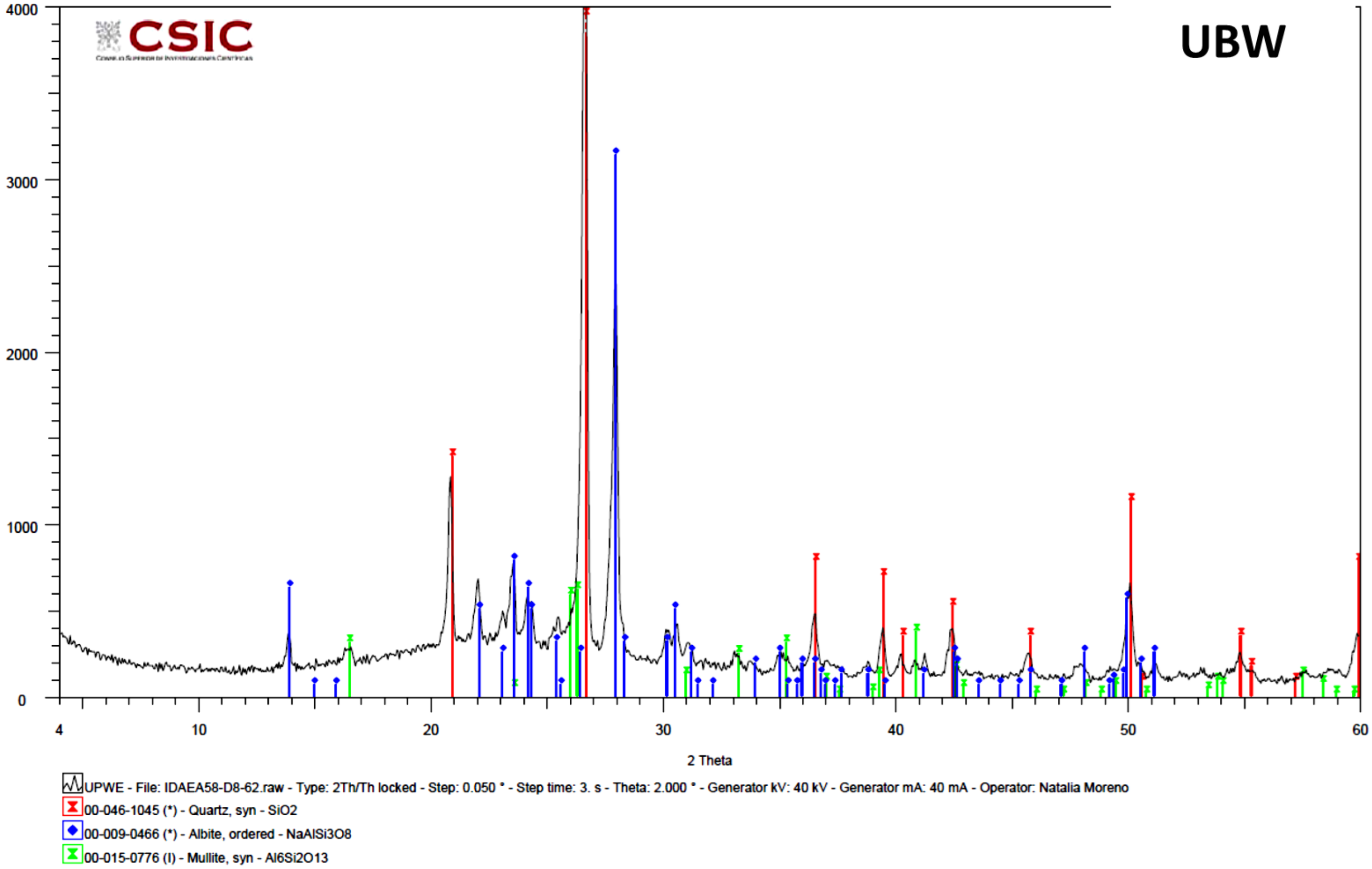
CSIC
UBW
4000
3000
2000
1000
0
4
10
20
30
40
50
60
2 Theta
UPWE - File: IDAEA58-D8-62.raw - Type: 2Th/Th locked - Step: 0.050 ° - Step time: 3. s - Theta: 2.000 ° - Generator kV: 40 kV - Generator mA: 40 mA - Operator: Natalia Moreno
00-046-1045 (*) - Quartz, syn - SiO2
00-009-0466 (*) - Albite, ordered - NaAlSi3O8
00-015-0776 (I) - Mullite, syn - Al6Si2O13

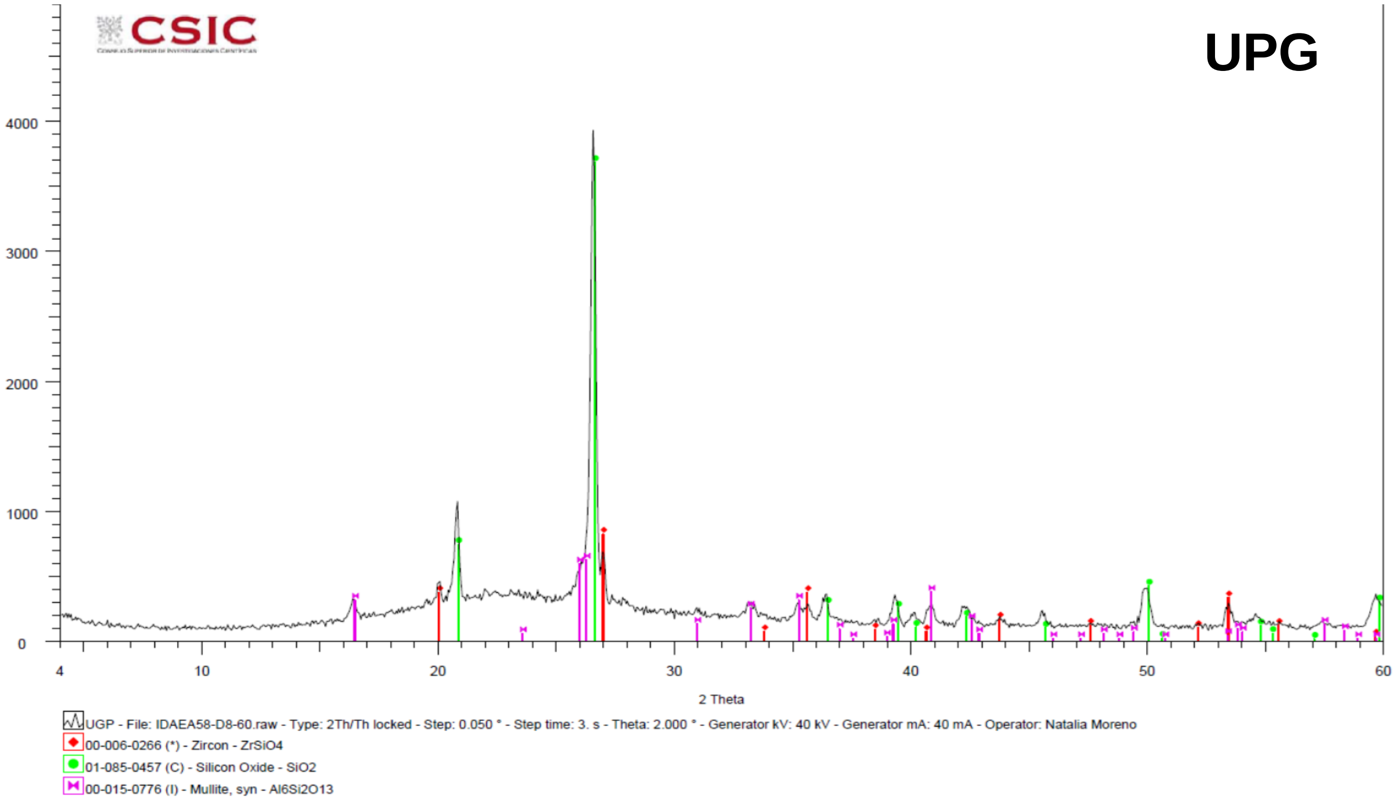
CSIC
UPG
4000
3000
2000
1000
0
4
10
20
30
40
50
60
2 Theta
UGP - File: IDAEA58-D8-60.raw - Type: 2Th/Th locked - Step: 0.050 ° - Step time: 3. s - Theta: 2.000 ° - Generator kV: 40 kV - Generator mA: 40 mA - Operator: Natalia Moreno
00-006-0266 (*) - Zircon - ZrSiO4
01-085-0457 (C) - Silicon Oxide - SiO2
00-015-0776 (I) - Mullite, syn - Al6Si2O13

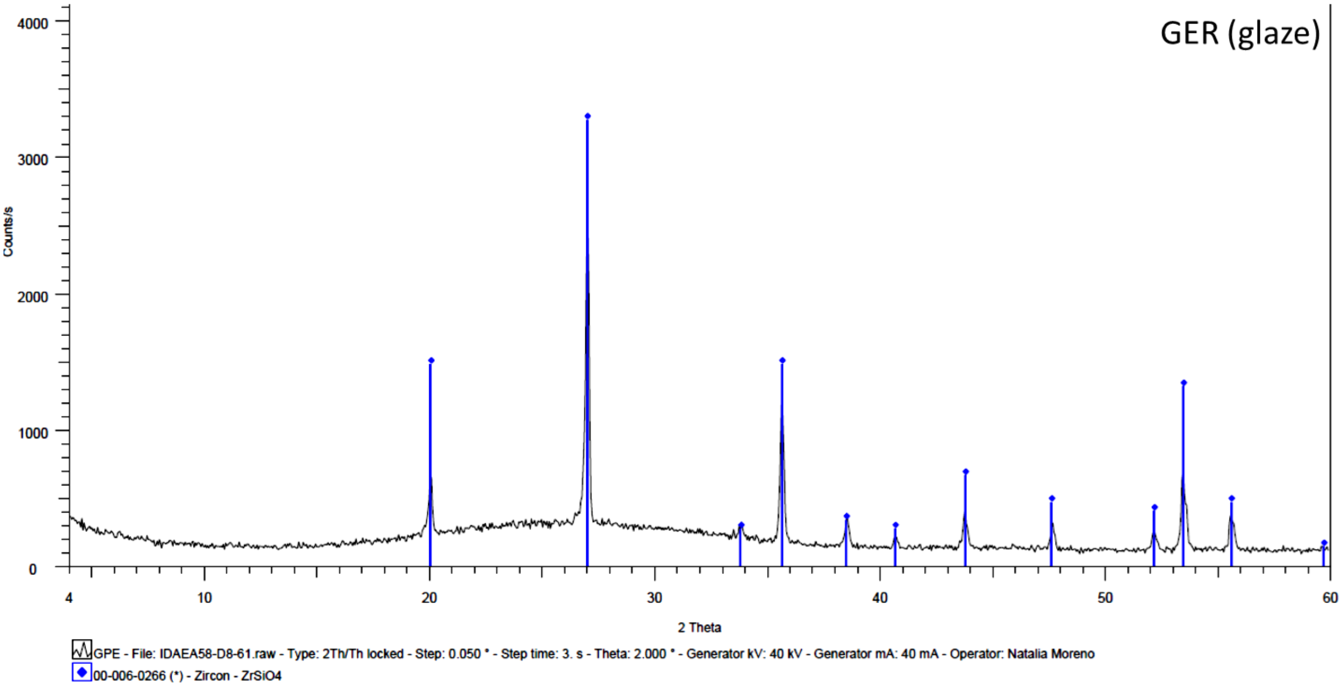

Figure S6. Mineralogical – crystal phase – analysis from the surface of the ceramic tiles (UBW, UPG, GER)

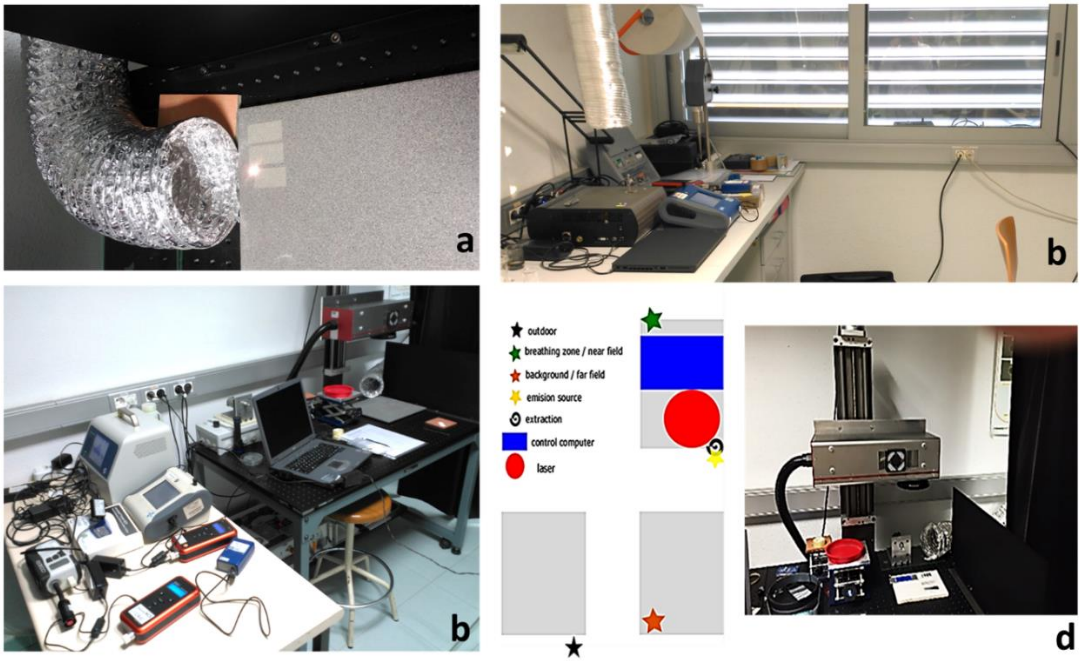

Figure S7. a) Incident laser beam during the PLA of UPG (3rd repetition), b) instruments in the far-field location, c) instruments in the near-field location (the laser was operated from the computer), d) layout of the monitoring location (left) and the emission source location (right)

4.2. Scientific publication 2

Workplace exposure to nanoparticles during thermal spraying of ceramic coatings

Salmatonidis A.[1,2], Ribalta C.[1,2], Sanfélix V.[3], Bezantakos S.[5], Biskos G.[6], Vulpoi A.[4], Simion S.[4], Monfort E.[3], Viana M.[1]

[1]*Institute of Environmental Assessment and Water Research (IDAEA-CSIC),08034 Barcelona, Spain*

[2] *University of Barcelona, Faculty of Chemistry, Department of Chemical Engineering and Analytical Chemistry, 08028, Barcelona, Spain.*

[3]*Institute of Ceramic Technology (ITC), Universitat Jaume I, 12006 Castellón, Spain*

[4]*Institute of Interdisciplinary Research in Bio-Nano-Sciences (ICI-BNS), Babeș-Bolyai University, 400000 Cluj-Napoca, Romania*

[5]*Université du Littoral Côte d'Opale, 59140 Dunkerque, France*

[6]*Energy Environment and Water Research Centre, The Cyprus Institute, 2121 Nicosia, Cyprus*

Published in: Annals of Work Exposures and Health, 2019, Volume 63, No. 1, Pages 91–106

DOI: 10.1093/annweh/wxy094

The following is a pre-print version, which was produced by the author, of an article published in Annals of Work Exposures and Health (Oxford University Press on behalf of the British Occupational Hygiene Society): Submitted on 5 June 2018; revised on 1 October 2018; accepted on 24 October 2018. Available online at:

https://doi.org/10.1093/annweh/wxy094

Workplace exposure to nanoparticles during thermal spraying of ceramic coatings

Salmatonidis A.[1,2]*, Ribalta C.[1,2], Sanfélix V.[3], Bezantakos S.[5], Biskos G.[6], Vulpoi A.[4], Simion S.[4], Monfort E.[3], Viana M.[1]

[1] *Institute of Environmental Assessment and Water Research (IDAEA-CSIC),08034 Barcelona, Spain*

[2] *University of Barcelona, Faculty of Chemistry, 08028 Barcelona, Spain*

[3] *Institute of Ceramic Technology (ITC), Universitat Jaume I, 12006 Castellón, Spain*

[4] *Institute of Interdisciplinary Research in Bio-Nano-Sciences (ICI-BNS), Babeș-Bolyai University, 400000 Cluj-Napoca, Romania*

[5] *Université du Littoral Côte d'Opale, 59140 Dunkerque, France*

[6] *Energy Environment and Water Research Centre, The Cyprus Institute, 2121 Nicosia, Cyprus*

**Author to whom correspondence should be addressed. e-mail: apostolos.salmatonidis@idaea.csic.es*

Abstract

Thermal spraying is widely used for industrial-scale application of ceramic coatings onto metallic surfaces. The particular process has implications for occupational health, as the high energy process generates high emissions of metal-bearing nanoparticles. Emissions and their impact on exposure were characterised during thermal spraying in a work environment, by monitoring size-resolved number and mass concentrations, lung-deposited surface area, particle morphology and chemical composition. Along with exposure quantification, the modal analysis of the emissions assisted in distinguishing particles from different sources, while an inhalation model provided evidence regarding the potential deposition of particulate matter on human respiratory system. High particle number ($>10^6$/cm^3; 30-40 nm) and mass (60-600 μgPM$_1$/m^3) concentrations were recorded inside the spraying booths, which impacted exposure in the worker area (10^4-10^5/cm^3, 40-65 nm; 44-87 μgPM$_1$/m^3). Irregularly-shaped, metal-containing particles (Ni, Cr, W) were sampled from the worker area, as single particles and aggregates (5-200 nm). Energy dispersive X-ray analysis confirmed the presence of particles originated from the coating material, establishing a direct link between the spraying activity and exposure. In particle number count, 90% of the particles were between 26-90 nm. Inhaled dose rates, calculated from the exposure levels, resulted in particle number rates ($\dot{n}$) between 353×10^6-1024×10^6/min, with 70% of deposition occurring in the alveolar region. The effectiveness of personal protective equipment (FPP3 masks) was tested under real working conditions. The proper sealing of the spraying booths was identified as a key element for exposure reduction. This study provides high time-resolved aerosol data which may be valuable for validating indoor aerosol models applied to risk assessment.

Keywords: nanoparticles; exposure assessment; inhalation exposure; inhalation model; occupational health; modal analysis; process-generated nanoparticles

Introduction

In numerous industrial sectors such as petroleum (Moskowitz 1993), naval (Baiamonte et al 2015), automobile (Gérard 2006), or aeronautical and space (Pawlowski 2008a, Strangman 1985), metal structures and mechanical parts are exposed to highly corrosive environments, and subject to mechanical and chemical abrasion. In these cases, protective ceramic coatings are widely used to prevent corrosion and wear, as well as to restore damaged surfaces (Lima and Marple 2006, Tan et al 1999, Toma et al 2010). Such coatings are frequently applied using thermal spraying techniques, where the feedstock (the coating material) is projected at high temperature and velocity onto the surface to be protected or repaired. Different types of spraying torches (electric arc, plasma, flame) define the types of thermal spraying techniques (Pawlowski 2008b).

This industrial process has been reported to generate high concentrations of nanoparticles (NP, with diameters < 100 nm) at pilot-plant scale (Viana et al 2017), which may result in occupational hazards (Hériaud-Kraemer et al 2003). Previous studies of thermal spraying emissions using offline measurements focused on the chemical characterisation of particles collected on filters (Huang et al 2016, Petsas et al 2007), showing also that these sources are associated with high particle mass concentrations. Furthermore, high NP number concentrations (> 10^9/cm^3) were monitored directly from electric arc guns (Bémer et al 2010). At pilot-plant scale, Viana et al. (2017) showed that NP released during atmospheric plasma spraying may impact worker exposure significantly. Despite the widespread industrial application of thermal spraying, emissions generated under real-world operating conditions are not well studied. Similarly to thermal spraying, the emissions of NP from other industrial processes and their impact on worker exposure is a growing topic of research (Ding et al 2017, Fonseca et al 2015, 2016, 2018, Fujitani et al 2008, Koivisto et al 2018, Koponen et al 2015, Kuhlbusch et al 2004, Losert et al 2014, Salmatonidis et al 2018, Viitanen et al 2017), and requires further investigations due to the large variety of processes and exposure scenarios. Awareness for nanomaterial release was raised (Maynard et al 2006, Poland et al 2008, Seaton et al 2010) since the use of manufactured nanomaterials (MNMs) in workplaces started. However, NP emissions can arise from multiple processes that neither produce nor use nanomaterials, which are referred as Process Generated Nanoparticles (PGNP) (Van Broekhuizen, et al 2012).

Pope et al (1995) associated air pollution with adverse health effects based on epidemiological evidence. Further epidemiological and toxicological studies showed that $PM_{2.5}$ (particles with diameter ≤2.5 µm) is a health hazardous pollutant (Gakidou et al 2017, Landrigan et al 2017, C Pope et al 2002, C. Pope and Dockery 2006, WHO 2017). More specifically, aerosol particles <100 nm (ultrafine) are linked to adverse health effects mainly due to exposure through inhalation (Araujo et al 2008, Hoek et al 2010, Ibald-Mulli et al 2002, Knibbs et al 2011, Landrigan et al 2017, Oberdörster 2001). In indoor air and more specifically in industrial settings, PGNPs pose an occupational risk, since they are unintentionally generated and released to the worker area, and they are potential health hazards (Koivisto et al., 2014). Health risks need to be dealt with by means of both technological and non-technological mitigation strategies (Ganser and Hewett 2017, Hallé et al 2015, Hewett and Ganser 2017, Shaffer and Rengasamy 2009).

The aim of this work was to assess NP emissions during thermal spraying of ceramic coatings onto metallic surfaces and their impact on inhalation exposure, under actual operating conditions in a real-world industrial setting. A near field (NF) / far field (FF) approach as used by Koivisto et al.(2015), among others, was applied. Workplace exposure monitoring strategies applied followed good practice as described by Asbach et al. (2015) and Brouwer et al. (2014), which were the base for internationally-recognised standard procedures (OECD.82, 2017). Modal analysis based on time-resolved particle number concentrations was used to quantitatively understand the size distribution and modal dependence of the aerosols generated during thermal spraying (Hussein et al 2005). Finally, a case study testing the effectiveness of mitigation strategies is presented.

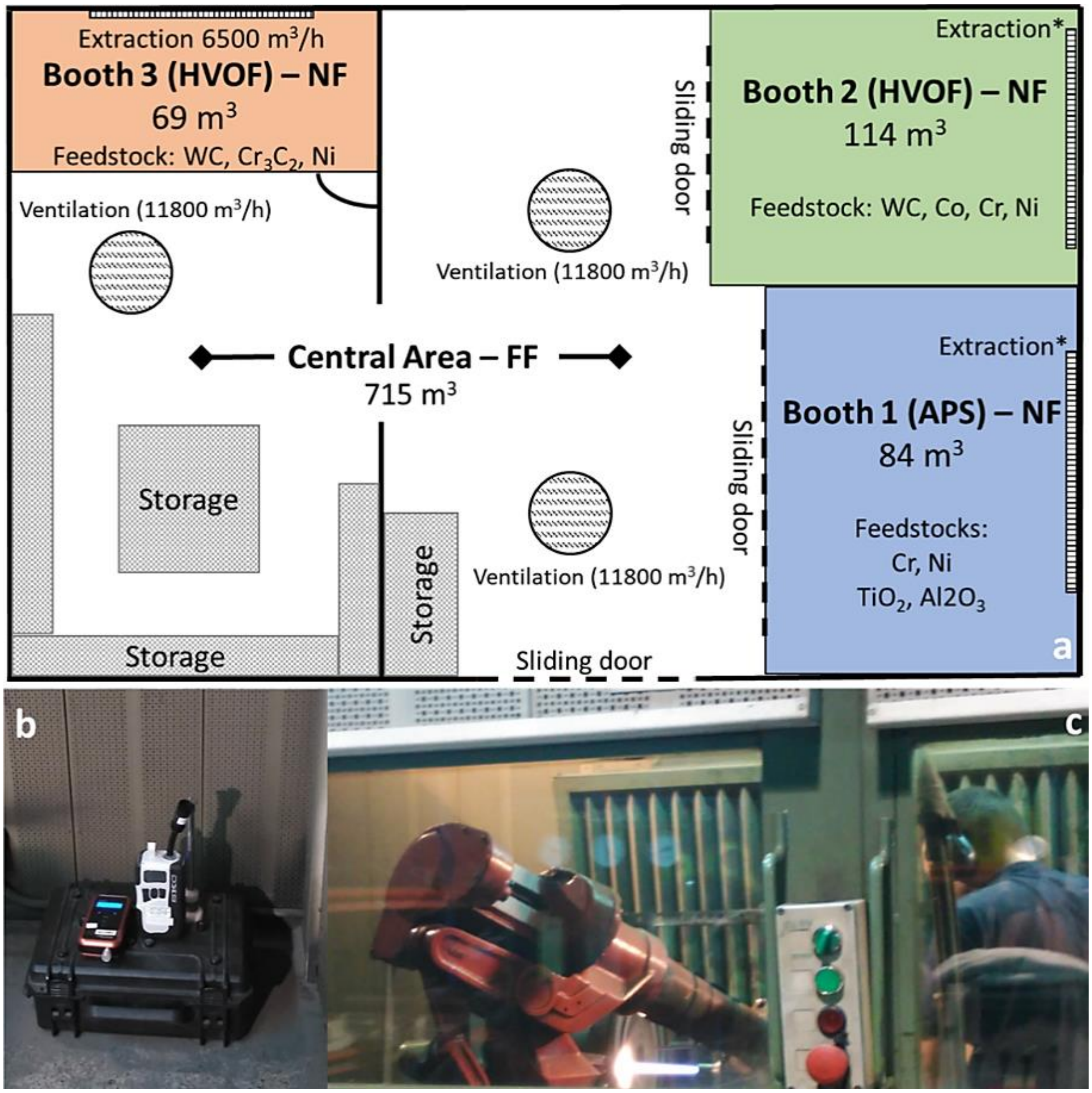

Figure 1. (a): Schematic representation of the thermal spraying section of the investigated facility (Extraction*: data not available). (b): instrument deployment in the near field location. (c): booth #3, showing the thermal spraying robot and the operator processing one of the work-pieces.

Methods and Materials

Work environment

Monitoring of thermal spraying was carried out at an industrial-scale precision engineering workshop (T.M. Comas) located in the vicinity of Barcelona, Spain. Measurements were carried out over a 5-day period in April 2017, and did not interfere with the usual operating conditions in the plant. The thermal spraying facilities are schematically depicted in Figure 1 (top). Three thermal spraying booths were located in an area of approximately 240 m^2 (14 m wide and 17 m in length), including also a storage and a central corridor. In all cases the operators of the thermal spraying equipment worked inside and outside the booths during spraying, and each booth had doors which were not always closed. Two small-scale sand blasting boxes for polishing the final pieces were located next to the spraying booths, but they were not operated simultaneously to the activities reported in this work. A general ventilation system operated constantly in the central area, with three extractors having a flow of 11800 m^3/h each (data provided by the company, not measured directly in this work). Additionally, in each of the plasma booths individual localised extraction systems were available (Figure 1a, Table 1). Information regarding the individual extraction air flowrates was only available for booth #3 (6500 m^3/h). The operational characteristics of each of the spraying activities and booths are summarised in Table 1. Because the duration of the individual spraying activities varied according to the parts to be coated, mean values of spraying duration and repetitions were different for each booth (Table 1).

Thermal spraying techniques and feedstock

Two different types of thermal spraying techniques were assessed:

- Atmospheric Plasma Spraying (APS), characterised by high temperatures (5000-20000 ºC) and projection velocities of 200-500 m/s. This technique was applied in plasma booth #1 (Figure 1). APS is generally used to project oxides and metals, which in this case of our measurements were a TiO_2-Al_2O_3 blend and a Cr-Ni blend (2 different feedstock materials that were applied separately).
- High Velocity Oxy-Fuel coating spraying (HVOF), characterised by high velocities (425-1500 m/s) and lower temperatures (2900 ºC). This type of spraying was applied in booths #2 and #3 (Figure 1b, bottom). Due to the lower temperatures compared to APS, HVOF is frequently used to project carbides and metals. During our measurements a WC-Co-Cr-Ni blend feedstock was used in booth #2, and a WC-CrC-Ni blend in booth #3.

Additional information about the feedstock powders is provided in Table S1 (Supplementary Data).

Table 1. Operational characteristics of each of the spraying booths and locations in the thermal spraying facility.

Characteristics	Booth #1	Booth #2	Booth #3	Central area
Thermal spraying technique	APS	HVOF	HVOF	None
Spraying duration	20-30 minutes	5-10 minutes	5-10 minutes	None
Nr. repetitions/half-day	3	2	7-9	None
Type of parts coated	Large, single part	Large, single part	Small, several parts	None
Door	Mostly closed	Open	Open/closed	None
Volume (ca.,m^3)	84	114	68	465
Local exhaust/ventilation flow	N.A.	N.A.	6500 m^3/h	3×11800 m^3/h
Personal protective equipment				
Respirators	Pressurised respirator hood, FPP3 mask	FPP3 mask	FPP3 mask	None
Cloths	Protective jacket	None	Protective jacket	None
Gloves	High temperature gloves	None	High temperature gloves	None

N.A.: not available. APS: Atmospheric Plasma Spraying. HVOF: High Velocity Oxy-Fuel coating spraying.

Particle monitoring and sampling

Particle number concentration (N), size-segregated mass concentrations (PM_x), size distribution, mean diameter (D_p) and lung-deposited surface area (LDSA) were monitored at near field (NF) and far field (FF) locations. The NF location was inside each of the spraying booths, while the FF was next to the storage area in the case of booth #3 and in the middle of the central area in the case of booths #2 and #3 (Figure 1a). The monitoring instruments in the FF and their inlets were located between 0.7 and 1.5 m above ground and were not placed directly inside the breathing zone (Ojima, 2012). The resulting measurements were considered representative of worker exposure, by assuming that the concentrations in the NF and FF were well-mixed. The online particle monitors deployed were:

- A Miniature diffusion size classifier “DiSCmini” (TESTO AG), that can measure particles having sizes from 10 to 700 nm, and can report total particle number (N), mean particle diameter (D_p) and lung deposited surface area (LDSA) with a 10 s time resolution. This instrument was deployed both in the NF and FF locations.
- A Mini Laser Aerosol Spectrometer “Mini-LAS 11-R” (GRIMM), that was used to measure particles in the size range 0.25-32 μm, and report total and size-segregated particle mass concentrations in 31 channels with a 6 s time resolution. This instrument was deployed both in the NF and FF locations.
- An Electrical mobility spectrometer “Nanoscan-SMPS” (TSI model 3910), covering particles in the size range 10-420 nm, that was used to measure the particle mobility size distributions in 13 channels with a 1-min time resolution. This instrument was deployed only in the FF location.
- A Mini Wide Range Aerosol Spectrometer “Mini-WRAS” (GRIMM), that can measure particles having sizes from 10 nm to 35 μm, for monitoring the particle mass concentrations across 41 channels. This instrument was also deployed in the FF location.

The mini-LAS units were operated enclosed in a protective case with a vertical stainless steel inlet (Figure 1b). Inlet extension tubes were not used for any of the other instruments. The default (manufacturer) impactor was used for the DiSCmini (cut-off diameter of 700 nm) and the default cyclone (cut-off diameter of 550 nm) was used for the Nanoscan. The DiscMini and MiniWRAS instruments were inter-compared prior to the measurements at an air quality monitoring station in Barcelona (Spain), using ambient air aerosols. The comparison resulted in R^2 coefficients >0.89, and as result the instruments were considered comparable for the purpose of our study (Table S2).

In addition to the online measurements described above, samples were collected on electron microscopy grids (Agar scientific Quantifoil 200 Mesh Au) for offline morphological and physicochemical particle characterisation. A Leland pump (SKC Inc.) with a flow of 5 L/min was connected to a cassette (SKC inlet diameter 1/8 inch and filter support pads that were 25 mm in diameter) to which the microscopy grid was attached. The morphology and primary particle size of the particles collected were analysed using Transmission Electron Microscopy (TEM; Jeol, JEM 1220, Tokyo, Japan) and TEM/HRTEM, FEI, Tecnai F20 (200 KV, Eindhoven, Netherlands) coupled with an Energy-Dispersive X-ray (EDX) spectrometer, following a similar method as Voliotis et al. (2014).

Modal analysis

While modal analysis has been applied to characterise the size distributions of atmospheric aerosols regarding the physicochemical processes they have been involved in (Hussein et al 2005), this type of analysis is seldom applied to indoor or, more specifically, industrially produced aerosols.

In the present study, NanoScan measurements were expressed as $dN/dLogdp$ distributions to apply modal analysis, because this method assumes that particle number concentrations are log-normally distributed across their size range. Their distribution can be analysed as three modes: $\text{Mode}_{10\text{-}25nm}$, $\text{Mode}_{26\text{-}90nm}$, and $\text{Mode}_{91\text{-}660nm}$ which includes mainly accumulation mode particles. The algorithm for modal analysis uses a non-linear least square fitting, based on the interior-reflective Newton method

(Coleman and Li 1994, 1996). The 3 lognormal fitted curves and their parameters (geometric standard deviation, GSDi; geometric mean diameter, GMDi; and mode number concentration, Ni) were calculated following the same assumptions and conditions as Hussein et al (2005). The modal analysis was performed exclusively on the size-distribution data obtained with NanoScan.

Inhalation model

The inhalation dose of deposited particles in the respiratory system was quantified by multiplying particle size concentrations on the worker area by the ICRP human respiratory tract model deposition probability (Cousins et al 2011). A respiratory volume of 25 L/min was used, which corresponds to male respiration during light exercise (Koivisto et al 2012). The regional dose was calculated for head airways, tracheobronchial and alveolar regions by using simplified deposition fraction equations for the ICRP model as described by Hinds et al.(1999). Particles were assumed to preserve their size during inhalation and the calculation was based on the mobility diameter. Background aerosol particles were assumed to be spherical and to have a density of 1.5 g/cm^3 (Martins et al 2015). The density of particles emitted during thermal spraying was set equal to the density of the feedstock material 4.3 g/cm^3, given that the particles released were found by EDX analysis to have similar composition with the feedstock (see next section). It should be noted that the use of the bulk density of the feedstock material probably overestimates the resulting particle concentrations, because particles may have vaporized and condensed to smaller particles. Results from the NanoScan and MiniWras instruments were combined to obtain a 10 nm-35 µm particle size distribution for the FF (Koivisto et al., 2014). NanoScan size bins between 11.5 - 86.6 nm were used, whereas bins ranging from 139 nm to 35 µm were taken from the MiniWras. Between 86.6 nm and 139 nm a combined channel (108.6 nm) was created.

The particle active surface area was calculated by applying particle size distribution obtained to the equation (1) described by Heitbrink et al. (2009) and Koivisto et al. (2012):

$$s = \frac{3\pi\lambda D_b}{C_c(D_b)\delta} \tag{1}$$

where λ is the mean free path for air, 0.066 µm, and δ is the scattering parameter for air, 0.905. D_b is the mobility diameter and C_c the slip correction factor for the corresponding aerodynamic or mobility particle size. This calculation refers to particles <700nm according to Heitbrink et al. (2009) and Keller et al. (2001). The particle mass was calculated by using mobility particle diameter and effective density (Koivisto et al 2012):

$$m = \rho_{eff}\ \frac{\pi}{6}\ D_b^3 \tag{2}$$

where ρ_{eff} is the effective density (DeCarlo et al 2004). The effective density used was 1.5 g/cm^3 for background particles and 4.3 g/cm^3 for PGNPs.

Results and Discussion

Particle emissions and impact on exposure

Activities in the thermal spraying facilities were planned by the company for half-day periods. While booth #1 was active during 2 half-days, booths #2 and #3 were operational for 4 half-days each. The data obtained were analysed considering two phases: a pre-process period (background) consisting of the 90-min lunch break when all activity ceased, and the activity periods when particle emissions were simultaneously monitored in the NF and in the FF location. The activity periods were different for each booth (Table 1): while spraying was longer and less repetitive in booth #1 (20-30 min, 3 repetitions/half-day), it had a shorter duration and higher frequency in booth #3 (5-10 min, 7-9 repetitions/half-day). In Booth#2 the spraying activity duration was highly variable (0.5-10 min) and, due to technical problems, there were deviations in the frequency of spraying applications. Hence, the dataset obtained was not representative of regular working days in Booth#2.

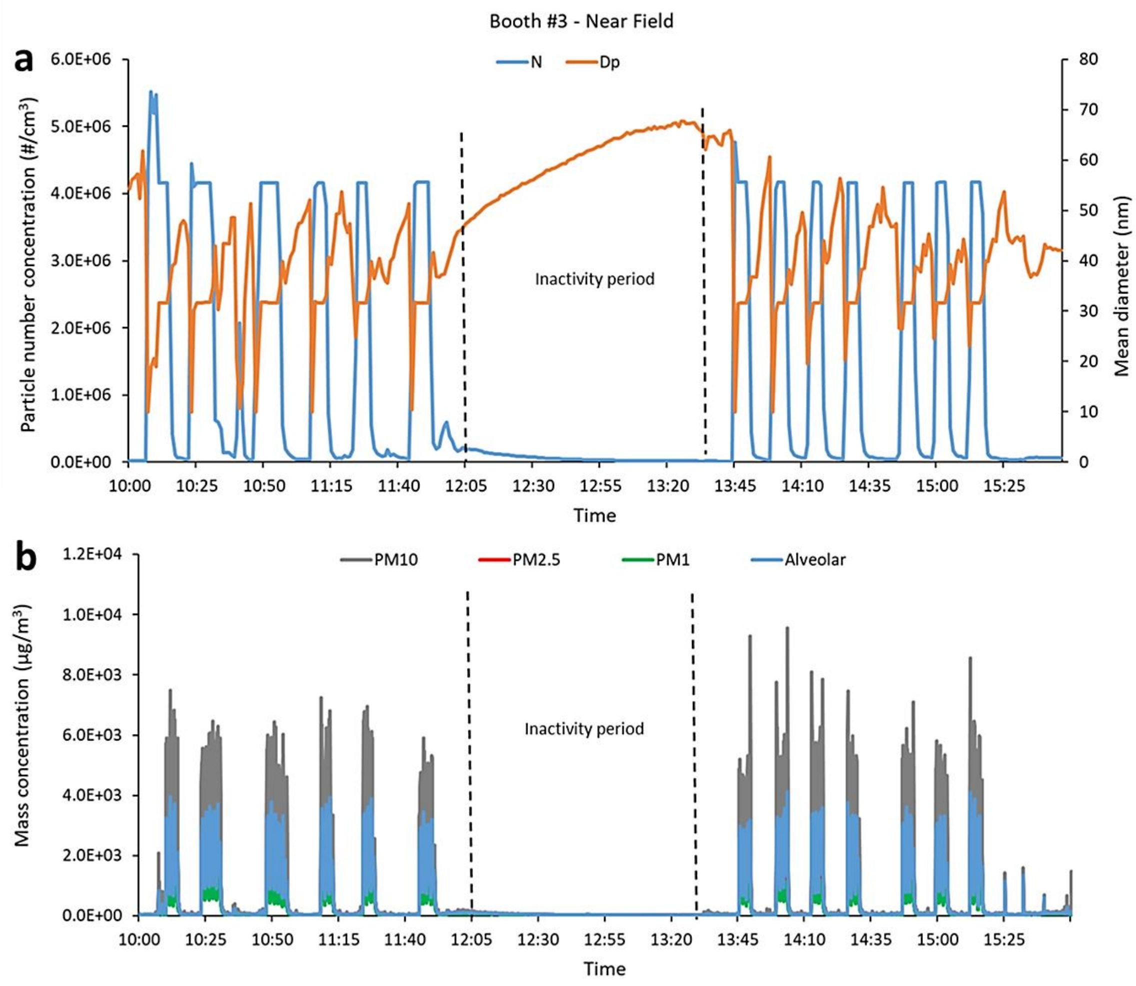

Figure 2. Particle concentrations monitored inside booth #3 (near field) on 26/04/2017 during spraying of feedstock WC/CrC/Ni: (a) particle number concentration and mean diameter; (b) size segregated particle mass concentrations.

In Table 2 average N, D_p, LDSA, and PM_1 values for each of the spraying activities and booths monitored are shown. A representative time series during the process in booth #3 is depicted in Figure 3 (NF) and Figure 4 (FF) during one of the days (26/04/2017), in to order to thoroughly analyse the emission patterns and impacts on exposure of the released NP. The time series for other days and booths are shown in Supplementary Data (Figures S1-S4). In the case of booth #3 each thermal spraying activity lasted for 5-10 minutes (Figure 2); subsequently the worker entered the booth and swapped the metal part which was coated with a new one. The process was repeated to 7-9 times/half-day.

In Figure 2 N, D_p, and size segregated mass concentrations (PM_1, $PM_{2.5}$, PM_{10}, alveolar) values monitored inside booth #3 (NF) are presented. The start of the spraying activity is evident by the rapid increase of N, which exceeded the instrument's (DiSCMini) monitoring range during all repetitions (maximum N = $4\times10^6/cm^3$). Particle number emissions were directly correlated with decreased D_p, which ranged between 30 and 35 nm during spraying and increased to 45-55 nm between repetitions. The patterns observed for the different spraying activities within each half-day showed good repeatability. N and D_p values during the process (3.8×10^6 /cm^3, 28.6 nm) were markedly different from background aerosols (N< $3.0\times10^4/cm^3$, D_p: 57.5-nm) monitored during the inactivity period on that day (Figure 2, Table 2). The same was true for particle mass concentrations (Figure 2b), which reached up to $4x10^3$ μg/m^3 for the alveolar size fraction (approximately similar to PM_4) while they remained < 30 μg/m^3 during the inactivity period. This result may be attributed to the release of fine and coarse particles (> 1 μm), in addition to NPs, during thermal spraying. The presence of fine and coarse particles was also confirmed by TEM analysis (Figure S5).

NP emitted during spraying in booth #3 were analysed by TEM (Figure 3), providing evidence that the particles in the collected samples were generated by different mechanisms. Particles collected exhibited a diversity of morphological characteristics, varying both in shape (e.g. spherical, fractal and star-like aggregates) and size (from ca. 5 to 500 nm). Possible emission mechanisms are: mechanical attrition as the feedstock particles crush onto the metal surface with high kinetic energy resulting in irregular-shaped particles, but also melting-evaporation-condensation of the feedstock material which would result in spherical particles (Fonseca et al 2015, Viana et al 2017). EDX analysis of the airborne particles collected on TEM grids confirmed that their chemical composition was similar to that of the feedstock (WC, CrC, Ni), demonstrating that particle release originated from the feedstock and not from other secondary or confounding sources. The thermal spraying processes investigated were not intended to produce nanoparticles. Hence, the NPs emitted from the micro-scaled feedstock (Table S1) were PGNP. In the case of fine and coarse particles, emissions probably resulted when the feedstock particles projected are in the outer plasma stream and do not reach high temperatures, they remain solid and are not deposited effectively on the metal surface.

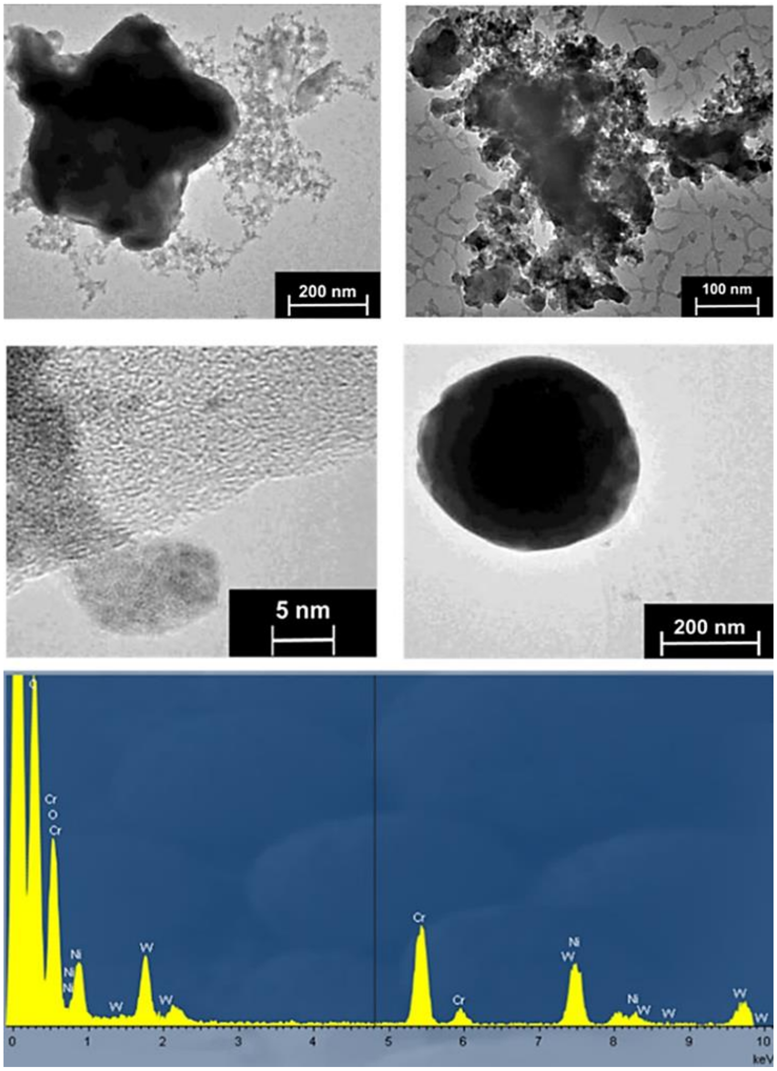

Figure 3. Particles released during spraying of W/CrC/Ni feedstock in booth #3 on 26/04/2017, analysed by TEM and showing similar chemical composition (WC, CrC, Ni) but different morphology and size. EDX spectrum confirming the origin of the particles (WC/CrC/Ni feedstock). The spectrum is representative of particles collected on other TEM grids.

In the FF location the impact of NP, fine and coarse particle emissions on exposure was assessed in terms of size-resolved N and PM_x (Figure 4). The same repetitive patterns which were monitored inside the spraying booth (Figure 3) were also detected in the worker area, indicating the representativeness of the results as well as clear impacts on exposure. The patterns were different in the morning and afternoon periods because the door of the booth was kept open while spraying during the morning, and closed in the afternoon. N values that reached up to $1.7\times10^6/cm^3$ (with the NanoScan instrument), were also outside this instrument's monitoring range and should be considered with high uncertainty. Size-resolved N values were highest in the range 20-85 nm (6×10^4 particles/cm^3) during the morning working session, providing evidence that the spraying activities substantially impacted worker exposure. The fact that the personal protective equipment (FPP3 mask) was frequently removed by the worker as soon as he exited the spraying booth (between repetitions) could further burden the workers' respiratory system. As in the case of the NF, particle concentrations in the FF location were markedly higher during activity than inactivity period. In addition, the effectiveness of keeping the booth door closed as a mitigation strategy was evident:

average *N* recorded in the worker area decreased by a factor of 0.31 in the afternoon when the door was closed, and LDSA concentrations were reduced by a factor of 0.38 (Table 2). Hence, the booth´s proper sealing during activity period demonstrated a much larger influence on exposure reduction than the total duration of the activity, or its repetition frequency. Similar findings on the importance of airtight booths had also been reported by Viana et al. (2017) during APS at pilot plant scale.

In terms of particle mass similar impacts and patterns were observed, although with two particle size modes: 50-500 nm and >3 µm. While the first mode corresponds to PGNP emissions, the second is attributed to direct feedstock release. Alveolar particle mass concentrations reached > 300 µg/m^3 (1-minute means) during the morning activity period, and 150 µg/m^3 in the afternoon.

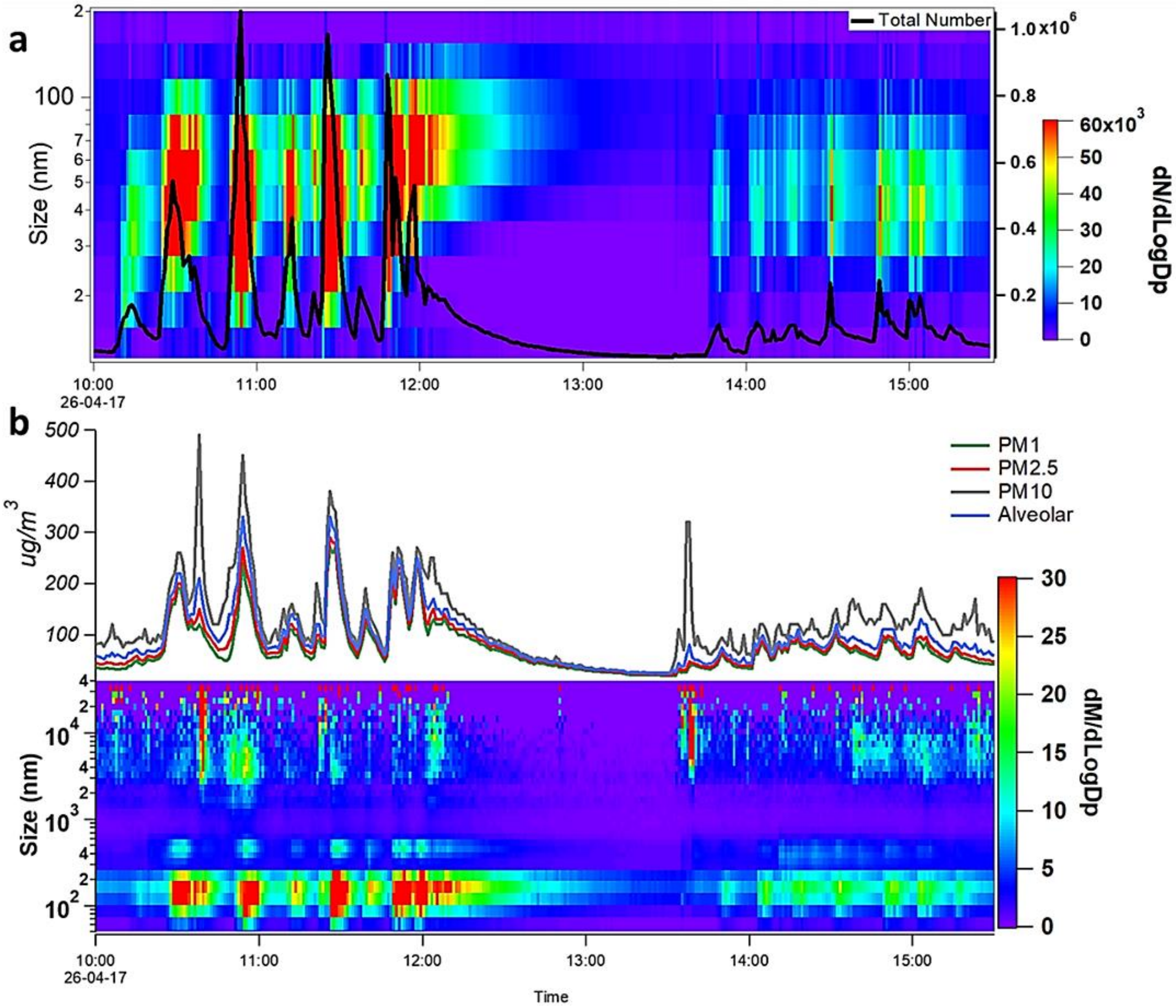

Figure 4. Size-resolved particle concentrations monitored in the worker area (far field) outside booth #3 on 26/04/2017 during spraying of feedstock WC/CrC/Ni: (a) particle number concentrations; (b) particle mass concentrations

As shown in Table 2, inside the NF concentrations ranged 1.8-3.4×10^6/cm^3 and had a clear impact on exposure at the FF location, where concentrations in the range of 5.8×10^4-2.0x10^5/cm^3 were monitored, and were significantly higher than the background concentrations (average 3.0×10^4). Concentrations in the FF were above the nano-reference values (NRV, non-regulatory reference values for nanomaterials, based on the precautionary approach) 4×10^4/cm^3 (Van Broekhuizen, et al 2012), and orders of magnitude higher inside the spraying booths (NF). This impact was considered statistically significant following the tiered approach established by Asbach et al. (2012), meaning that exposure concentrations were higher than the background plus 3 times the standard deviation of the background concentrations. The *N*, LDSA and PM values measured were comparable across the different booths, indicating that NP release is activity-dependent and not related to the specific feedstock powders applied. Although different spraying temperatures and velocities were applied in the different booths NP release was evident in all cases. This would indicate that NP emissions are independent of these parameters or that both of the thermal spraying techniques provide the necessary conditions for PGNP emissions.

Table 2. Mean particle number (N), particle diameter (Dp), lung deposition surface area (LDSA) from DiSCmini and mass (PM$_1$) concentrations during each of the activity periods monitored. Each half-day is labelled as (M) morning, (A) afternoon, or (cs) case study. N.A.: data not available. Statistical values: mean, standard deviation (SD), maximum (Max), minimum (Min) of each process calculated from non-normalized values for the total activity duration monitored during our studies (24-28/04/2017; DiSCmini).

		Near field (inside booths)				**Far field (worker area)**				**Inactivity**			
Date	**Feedstock**	**N (cm^{-3})**	**D_P (nm)**	**LDSA (μm^2/cm^3)**	**PM$_1$ (μg/m^3)**	**N (cm^{-3})**	**D_P (nm)**	**LDSA (μm^2/cm^3)**	**PM$_1$ (μg/m^3)**	**N (cm^{-3})**	**D_P (nm)**	**LDSA (μm^2/cm^3)**	**PM$_1$ (μg/m^3)**
Booth #1													
27/04–M	Cr/Ni,	2.0×10^{6}	31.5	4.0×10^{3}	5.3×10^{1}	N.A.	N.A.	N.A.	N.A.	2.3×10^{4}	51.6	6.6×10^{1}	2.8×10^{1}
27/04–A	Al_2O_3/TiO_2	1.6×10^{6}	36.8	3.1×10^{3}	6.9×10^{1}	5.8×10^{4}	40.0	1.2×10^{2}	4.4×10^{1}				
Mean		*1.8×10^{6}*	*34.2*	*3.6×10^{3}*	*6.1×10^{1}*	*5.8×10^{4}*	*40.0*	*1.2×10^{2}*	*4.4×10^{1}*	*2.3×10^{4}*	*51.6*	*6.6×10^{1}*	*2.8×10^{1}*
SD		*2.0×10^{5}*	*2.6*	*4.3×10^{2}*	*8.0×10^{0}*	*1.7×10^{4}*	*2.9*	*2.8×10^{1}*	*6.6×10^{0}*	*4.4×10^{3}*	*1.4*	*1.4×10^{1}*	*8.2×10^{0}*
Max		2.8×10^{6}	63.7	5.1×10^{3}	2.6×10^{2}	1.1×10^{5}	49.1	2.0×10^{2}	6.4×10^{1}	3.5×10^{4}	53.4	1.0×10^{2}	4.8×10^{1}
Min		5.2×10^{4}	12.1	4.6×10^{2}	3.0×10^{1}	3.4×10^{4}	33.2	8.5×10^{1}	3.2×10^{1}	1.7×10^{4}	49.2	4.9×10^{1}	1.9×10^{1}
Booth #2													
24/04–A	WC/Cr/Co/Ni	3.4×10^{6}	37.2	5.8×10^{3}	1.7×10^{2}	3.5×10^{4}	75.6	1.5×10^{2}	N.A.	7.0×10^{3}	86.1	4.0×10^{1}	2.0×10^{1}
25/04–M	WC/Cr/Co/Ni	5.3×10^{6}	28.3	7.6×10^{3}	1.0×10^{2}	5.4×10^{4}	54.3	1.7×10^{2}	8.3×10^{1}	6.3×10^{3}	123.3	4.9×10^{1}	2.9×10^{1}
26/04–M	WC/Cr/Co/Ni	6.0×10^{5}	55.7	1.9×10^{3}	3.8×10^{1}	N.A.	N.A.	N.A.	N.A.	3.7×10^{4}	56.8	6.7×10^{1}	2.9×10^{1}
27/04–cs	WC/Cr/Co/Ni	1.6×10^{6}	42.3	3.4×10^{3}	1.1×10^{2}	1.2×10^{5}	61.6	3.0×10^{2}	9.3×10^{1}	2.3×10^{4}	51.6	6.6×10^{1}	2.8×10^{1}
Mean		*2.7×10^{6}*	*40.9*	*4.7×10^{3}*	*1.0×10^{2}*	*6.9×10^{4}*	*63.8*	*2.1×10^{2}*	*6.5×10^{1}*	*1.8×10^{4}*	*79.5*	*5.6×10^{1}*	*2.5×10^{1}*
SD		*1.8×10^{6}*	*9.9*	*2.2×10^{3}*	*4.7×10^{1}*	*3.5×10^{4}*	*8.8*	*6.6×10^{1}*	*3.2×10^{1}*	*1.3×10^{4}*	*28.5*	*1.1×10^{1}*	*3.9×10^{0}*
Max		6.3×10^{6}	72.7	8.9×10^{3}	1.8×10^{3}	3.1×10^{5}	107.8	6.2×10^{2}	1.6×10^{2}	3.1×10^{5}	141.6	3.0×10^{2}	4.8×10^{1}
Min		7.6×10^{4}	19.8	2.1×10^{2}	3.3×10^{1}	9.3×10^{3}	45.7	4.3×10^{1}	4.1×10^{1}	2.8×10^{3}	50.5	2.1×10^{1}	1.9×10^{1}
Booth #3													
26/04–M	WC/CrC/Ni	3.8×10^{6}	28.6	5.7×10^{3}	7.0×10^{2}	3.6×10^{5}	33.2	5.6×10^{2}	1.0×10^{2}	3.0×10^{4}	57.5	1.1×10^{2}	2.9×10^{1}
26/04–A	WC/CrC/Ni	3.8×10^{6}	30.2	6.1×10^{3}	7.4×10^{2}	1.1×10^{5}	36.6	2.1×10^{2}	6.3×10^{1}				
28/04–M	WC/CrC/Ni	3.1×10^{6}	31.3	5.1×10^{3}	5.2×10^{2}	1.7×10^{5}	46.4	3.9×10^{2}	1.0×10^{2}	5.8×10^{4}	33.9	1.0×10^{2}	2.4×10^{1}
28/04–A	WC/CrC/Ni	2.9×10^{6}	32.1	4.8×10^{3}	5.8×10^{2}	1.5×10^{5}	42.1	3.2×10^{2}	8.4×10^{1}				
Mean		*3.4×10^{6}*	*30.6*	*5.4×10^{3}*	*6.4×10^{2}*	*2.0×10^{5}*	*39.6*	*3.7×10^{2}*	*8.7×10^{1}*	*4.4×10^{4}*	*45.7*	*1.1×10^{2}*	*2.7×10^{1}*
SD		*4.1×10^{5}*	*1.3*	*5.0×10^{2}*	*8.7×10^{1}*	*9.3×10^{4}*	*5.1*	*1.3×10^{2}*	*1.6×10^{1}*	*1.4×10^{4}*	*11.8*	*5.1×10^{0}*	*2.6×10^{0}*
Max		6.3×10^{6}	52.3	8.9×10^{3}	1.3×10^{3}	1.7×10^{6}	69.4	2.1×10^{3}	2.7×10^{2}	7.8×10^{4}	60.4	3.0×10^{2}	4.5×10^{1}
Min		1.9×10^{5}	10.0	2.2×10^{2}	2.1×10^{1}	3.3×10^{4}	18.4	8.6×10^{1}	1.8×10^{1}	1.5×10^{4}	29.4	5.0×10^{1}	2.0×10^{1}

However, differences in terms of PM_1 ranged from 61 μg/m^3 (booth #1) to 100 μg/m^3 (booth #2) and 640 μg/m^3 (booth #3). These can be attributed to the combination of different process parameters (spraying velocity, speed) of each spraying technique and the different feedstock materials (Cr/Ni and TiO_2/Al_2O_3, Table S1). In the case of booth #1, where two different feedstock powders were applied separately, clear differences were observed in terms of $PM_{2.5}$ (2×10^2 *vs.* 4×10^2 μg/m^3) but not for PM_1 (53 vs. 69 μg/m^3). The feedstock powders applied in booths #2 and #3 were similar (Table S1) resulted in higher PM_1 (100-640 μg/m^3) than in booth #1 (Table 2). These differences are probably associated with the physical-chemical properties of the feedstock materials rather than to the aggregate size, which as shown in Table S1 is larger for the lowest emitter. As a result, it may be concluded that PM_1emissions were independent of the feedstock and thermal spraying conditions applied, while emissions of coarse particles (>2.5 μm) were influenced by the feedstock. Further research would be necessary to interpret the different behaviour for micron-scaled particle emissions.

With regard to D_p for NP, similarities were detected across booths with particles ranging between 30-40nm in the NF and increasing during transport to 40-64 nm in the FF, where workers were exposed. Workers from other sectors of the facility frequently entered the central area without respiratory protection and were directly exposed to particle concentrations from the spraying booths. As expected, mean diameters during the inactivity period were larger and representative of urban background ultrafine (46-80 nm) aerosols (Reche et al 2015).

Modal distribution and analysis

The modal analysis was applied to the same results dataset as in Figure 4, in FF of booth #3. The time series of the modal particle number concentrations is plotted in Figure 5 for 3 periods: (a) morning activity, (b) midday inactivity period, and (c) afternoon activity. The relative contribution from each mode to total particle number concentrations is also shown for each period.

Modal analysis of particles in the worker area provides information on the size distribution as well as on the potential sources of particles. The $Mode_{26\text{-}90nm}$ was dominant throughout the day in the FF contributing 88-94% of particle number, with the time series of this mode highly resembling the one of total number concentration (Figure 4). New particle formation took place inside the booth (NF, Figure 2), and particles subsequently grew into the larger-sized mode ($Mode_{26\text{-}90nm}$) during their transport from the source towards the worker area (FF, Figure 4a). The relative contributions from the $Mode_{26\text{-}90nm}$ were similar during the morning (Figure 5a) and afternoon (Figure 5c) spraying activities, despite the differences in total particle number concentrations resulting from the open/closed doors scenarios (Figure 4). $Mode_{10\text{-}25nm}$ were minor contributors with 2-3% during both activity periods, while $Mode_{91\text{-}660nm}$ contributed with 4-9% of relative particle number concentrations. The lowest contribution of $Mode_{10\text{-}25nm}$ (which includes particles formed by nucleation) in terms of particle number release was recorded during the inactivity period (Figure 5b) as expected due to the absence of activities in the facility. $Mode_{91\text{-}660nm}$ showed the highest contribution during the morning activity (Figure 5a) due to the influence of the open door.

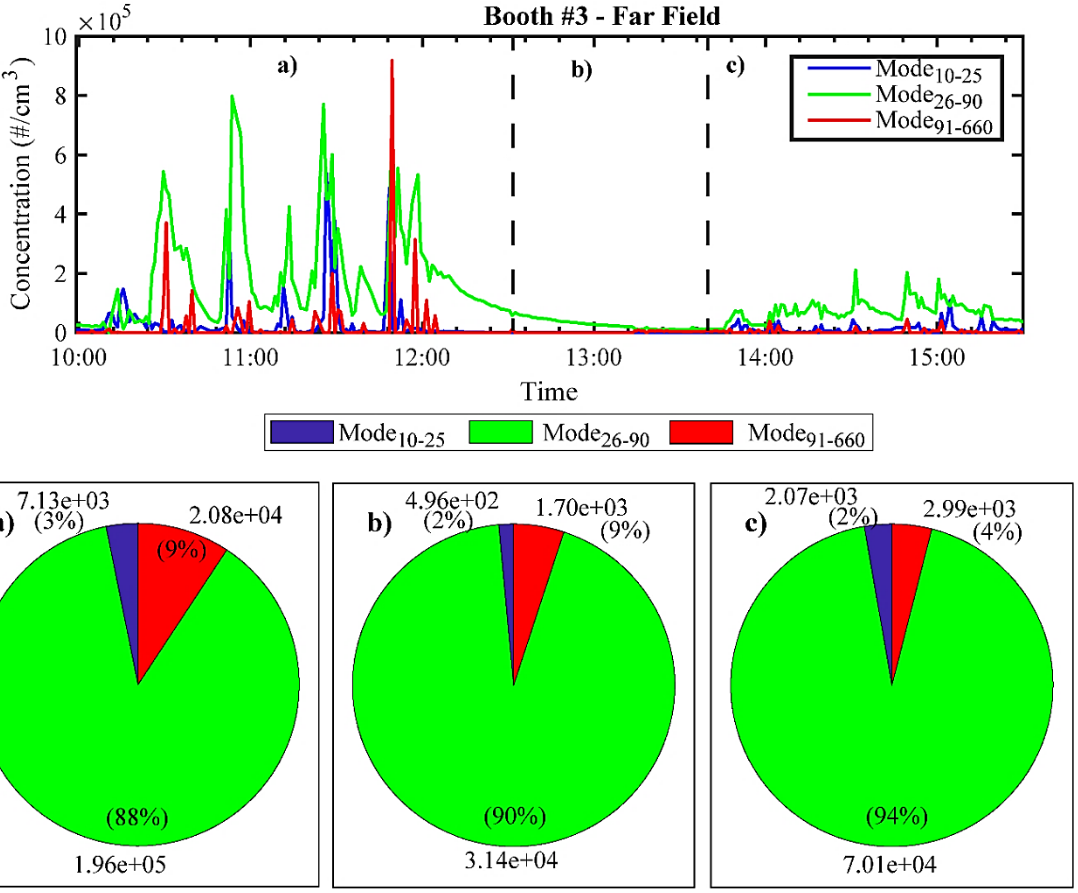

Figure 5. Particle number concentrations for particles in each of the modes identified by modal analysis (top) for booth #3 data for 26/04/2017. Absolute average number concentration and relative contribution (%) of each mode (bottom) for time intervals (a) morning, (b) inactivity period, and (c) afternoon.

Certain considerations should be taken into account in the application of modal analysis to the occupational dataset presented in this work Particles deriving from nucleation can have sizes from 1 nm, while very few instruments are able to measure particles in this size range. The instrumentation used in this work had a lower cutoff at 10 nm (NanoScan) which results in an underestimation of the $\text{Mode}_{10\text{-}25}$ contributions. The same is probably true for the $\text{Mode}_{91\text{-}660\text{nm}}$, given that the instruments had an upper cutoff size at 420 nm. The underestimation of the $\text{Mode}_{91\text{-}660\text{nm}}$ mode was probably lower since the number of particles in the range 420-660 nm emitted during thermal spraying is low.

Calculated deposited dose during inhalation

Inhalation dose rates for particle number, surface area and mass were estimated for booth #3 (26/04/2017 and 28/04/2017), for each half-day (morning and afternoon) and midday inactivity period for the FF location (Table 3), where workers carried out different tasks and the use of personal protection equipment was limited. Particle number dose rates ($\dot{n}$) were higher during activity

(353×10^6 to 1024×10^6/min) than during inactivity periods (138×10^6 to $374\text{x}10^6$/min). During the spraying activity, approximately 70% of the total inhaled particle number concentrations was deposited in the alveolar region, 12% in the trachea bronchi and 18% in the head airways. Hence, for workers in the FF location 82% of the total inhaled particles sourcing from thermal spraying were deposited in the deepest regions of the respiratory tract.

Table 3. Dose rates in particle number($\dot{n}$), surface area ($\dot{s}$), mass ($\dot{m}$),and regional deposition to head airways, trachea bronchi and alveolar regions, calculated based on particle size-resolved concentration data (measured with NanoScan combined with MiniWRAS).

Dose rates	26/04/2017-Booth #3			28/04/2017- Booth #3		
	Inactivity	Morning	Afternoon	Inactivity	Morning	Afternoon
Mean Size (nm)	76	47	49	51	57	54
Total: $\dot{n}, . 10^6$ [min $^{-1}$]	138	1024	353	374	535	483
Head airways: $\dot{n}, . 10^6$ [min $^{-1}$]	16.3	163	61.7	40.2	106	91.3
Trachea bronchi: $\dot{n}, . 10^6$ [min $^{-1}$]	20.2	130	43.3	65.7	61.6	56.8
Alveolar: $\dot{n}, . 10^6$ [min $^{-1}$]	102	730	248	268	367	335
Total: $\dot{s}, . 10^6$ [μm^2 min $^{-1}$]	1.8	6.3	3	1.8	5.7	4.4
Head airways: $\dot{s}, . 10^6$ [μm^2 min $^{-1}$]	0.3	2	1.1	0.2	2.2	1.6
Trachea bronchi: $\dot{s}, . 10^6$ [μm^2 min $^{-1}$]	0.2	0.54	0.3	0.3	0.4	0.3
Alveolar: $\dot{s}, . 10^6$ [μm^2 min $^{-1}$]	1.2	3.8	1.7	1.3	3.1	2.5
Total l $\dot{m}, .$ [ng min $^{-1}$] (inactivity ρ=1.5 g cm^{-3}; Process ρ = 4.3 g cm^{-3})	1	9.5	5.5	0.8	8.5	11.5
Head airways: $\dot{m}$, [ng min $^{-1}$]	0.9	8.8	5.1	0.7	7.7	11
Trachea bronchi: $\dot{m}$, [ng min $^{-1}$]	0.02	0.2	0.1	0.02	0.2	0.1
Alveolar: $\dot{m}$, [ng min $^{-1}$]	0.1	0.5	0.3	0.1	0.6	0.4

The same analysis was applied to the calculated active surface area concentrations of the particles deposited in the airways ($\dot{s}$) during activity periods (3.0 – 6.3×10^6 $\mu m^2/min^1$, Table 3): 60% was estimated to be deposited in the alveolar region, 9% in the trachea bronchi, and 31% in the head airways. Total surface area of the deposited particles during activity was higher than during inactivity (1.8×10^6 μm^2/min). The LDSA concentrations in this study (1.2-5.6 $\times10^3$ $\mu m^2/cm^3$, FF, Table 2) were mostly higher than others found in the literature, where LDSA concentrations were on average 21.6 $\mu m^2/cm^3$ during handling and loading of halloysite nanotubes (Koivisto et al., 2018), and <19 $\mu m^2/cm^3$during WC-Co fine powder production (Koivisto et al., 2016). Regarding the total deposited mass ($\dot{m}$), increases of 1-9.5 ng/min were calculated from inactivity to activity periods. These dose rates in terms of mass were higher than those reported by Koivisto et al. (2014) (0.03-0.53 ng/min) during a lab-scale exposure assessment to nanodiamonds.

Koivisto et al (2012), who found comparable results to those in the current work during a high energy process (Liquid Flame Spray), concluded that N was the most relevant metric for exposure assessment. However, biologically, the most relevant metric considering pulmonary inflammation is likely surface area (Schmid and Stoeger 2017).

Effectiveness of protective personal equipment

The effectiveness of a personal FPP3 respirator (Moldex Air Plus 3405, half-piece mask) was assessed on a case study basis by comparing measurements obtained simultaneously inside and outside the respirator, with two DiSCMini units, while the mask was worn by one volunteer-member of the research team. The respirator assigned protection factor (APF) was 10 as specified by the 29 CFR 1910.134 (Occupational Safety and Health Admin. 2006). Programme protection factors (PPFs) were studied by Koivisto et al (2015) for loose-fitting respirators. The measurements were carried out inside booth #2 (NF) and during two representative activity periods. The inlet of one of the instruments was held in the breathing zone (outside the mask), and the second was connected to the interior of the mask with Tygon conductive tubing (Asbach et al 2016).

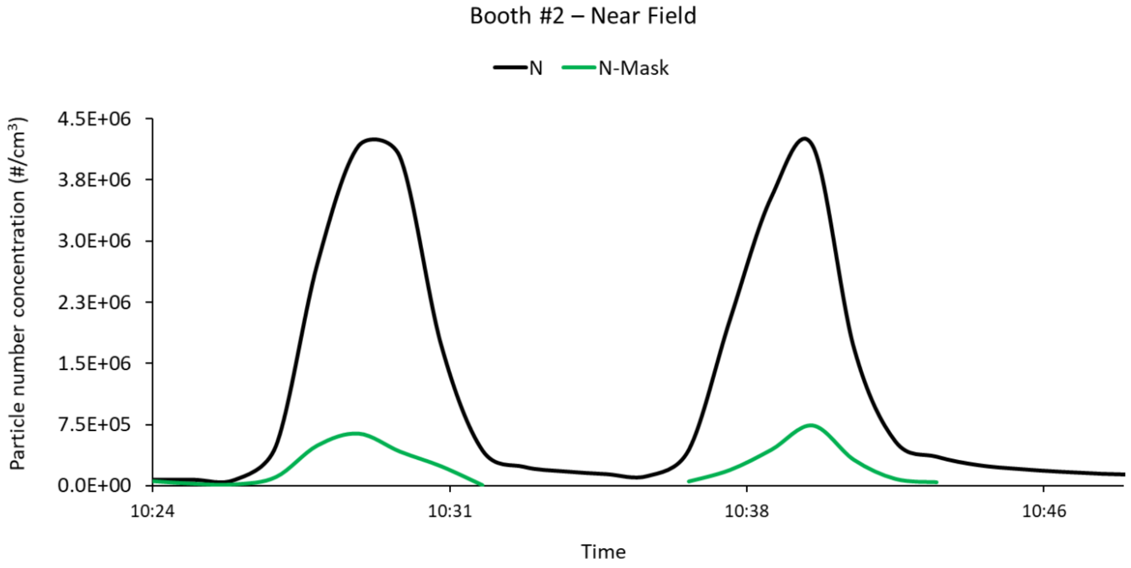

Figure 6. Particle number concentration and mean diameters measured with DiSCMini inside and outside an FPP3 personal mask worn by a volunteer-member of the research team. Measurements took place in the near field during two activity periods in booth #2 (27-04-2017).

The particle concentrations monitored (Figure 6) show that the mask achieved a reduction of worker exposure in terms of number concentration by 87% (from 3×10^6 to 4×10^5/cm^3) on average for both activity periods. This is likely a conservative estimate since the inlet of the instrument prevented from achieving a proper fit of the mask and it is highly probable that unfiltered air entered in the mask and interfered with the measurements.

Conclusions

Particle emissions and impacts on exposure were monitored for NPs and micron-scaled particles (fine and coarse) in terms of particle number and mass concentrations, LDSA, mean diameter and size distributions, during the application of ceramic coatings on metal surfaces by means of thermal spraying, at industrial scale. The results obtained are representative of the industrial facility under study, which has unique characteristics as most industrial facilities do, which highlights the need for additional studies with this kind of focus in the literature. Results may only be generalized once the body of literature regarding industrial thermal spraying emissions and the influence of different feedstock materials become available.

High particle number ($>10^6/cm^3$) and mass ($60-600\ \mu gPM_1/m^3$) concentrations were recorded inside the thermal spraying booths (NF), which were transported towards the worker area (FF) increasing the FF concentrations by one order of magnitude in terms of N ($10^4-10^5/cm^3$) and up to a factor of 4 in PM1 ($44-100\ \mu g/m^3$). NPs were generated through different mechanisms (mechanical, melting-condensation), resulting in diverse morphologies (irregular, spherical). NPs with small diameters were detected inside (31-41 nm) and outside (40-64 nm) the spraying booths. Worker exposure occurred both in the NF and FF locations, given that the workers operated equally inside and outside the spraying booths. The inhalation model applied showed that particles emitted during thermal spraying were mainly deposited in the alveolar region (70%).

The high correlation between particle concentrations in the NF and FF suggest that worker exposure was strongly impacted by NPs, fine and coarse particles emitted during thermal spraying. Whereas similar NP number concentrations were monitored irrespective of the spraying technique and feedstock material applied, coarser particle (>2.5 µm) mass concentrations showed differences as a function of the feedstock material. Additional research is necessary to understand the relationship between coarse particle emissions and feedstock physical-chemical properties.

The advantages and limitations of applying modal analysis to an occupational dataset were assessed. This analysis allowed for the identification of a dominant mode ($Mode_{26-90}$ particles, 89%), the increased contribution from $Mode_{10-25nm}$ (nucleation) particles during thermal spraying periods, and the influence of outdoor urban background aerosols during the inactivity period. In spite of the continuously working local extraction systems, the proper sealing of the spraying booths was identified as a key element for exposure reduction. Differences in exposure concentrations of one order of magnitude (from $10^5/cm^3$ to $10^4/cm^3$) were recorded when doors were open/closed. Optimising the production routine to prevent the opening of doors during the spraying activity as well as a delayed door-opening protocol could reduce NP transport from inside the booths and consequently minimise impacts on exposure in the adjacent worker areas. Furthermore, worker access in the central area should be restricted during spraying operation, or carried out with adequate personal protective equipment (PPE). Finally, the use of FPP3 masks (with APF 10) was also advised, given their high potential for reduction of particle number concentrations.

Acknowledgements

The current work was carried out in the framework of the CERASAFE project (www.cerasafe.eu), with the support of SIINN ERA-NET (project id: 16), and was funded by the Spanish MINECO (PCIN-2015-173-C02-01) and the Romanian UEFISCDI (PN-III-P4-ID-PCE-2016-0835). Partial funding from the "Generalitat de Catalunya" (project number: AGAUR 2017 SGR41) is also acknowledged. The authors kindly acknowledge TM COMAS (http://www.tmcomas.com) for their committed cooperation.

REFERENCES

Araujo JA, Barajas B, Kleinman M, Wang X, Bennett BJ, Gong KW, Navab M, Harkema J, Sioutas C, Lusis AJ and Nel AE (2008) Ambient particulate pollutants in the ultrafine range promote early atherosclerosis and systemic oxidative stress. *Circulation Research* 102(5): 589–596.

Asbach C, Kaminski H, Lamboy Y, Schneiderwind U, Fierz M and Todea AM (2016) Silicone sampling tubes can cause drastic artifacts in measurements with aerosol instrumentation based on unipolar diffusion charging. *Aerosol Science and Technology* 50(12): 1375–1384.

Asbach C, Kuhlbusch T a J, Kaminski H, Plitzko S, Götz U, Voetz M and Dahmann D (2012) *Authors : SOP-Tiered Approach Tiered Approach for the assessment of exposure to airborne nanoobjects in work- places.* .

Baiamonte L, Marra F, Gazzola S, Giovanetto P, Bartuli C, Valente T and Pulci G (2015) Thermal sprayed coatings for hot corrosion protection of exhaust valves in naval diesel engines. *Surface and Coatings Technology*. Elsevier B.V. 295: 78–87. Available at: http://dx.doi.org/10.1016/j.surfcoat.2015.10.072.

Bémer D, Régnier R, Subra I, Sutter B, Lecler MT and Morele Y (2010) Ultrafine Particles Emitted by Flame and Electric Arc Guns for Thermal Spraying of Metals. *The Annals of Occupational Hygiene* 54(6): 607–614.

Van Broekhuizen P, Van Veelen W, Streekstra WH, Schulte P and Reijnders L (2012) Exposure limits for nanoparticles: Report of an international workshop on nano reference values. *Annals of Occupational Hygiene* 56(5): 515–524.

Coleman TF and Li Y (1994) On the convergence of interior-reflective Newton methods for nonlinear minimization subject to bounds. *Mathematical Programming* 67(1–3): 189–224.

Coleman TF and Li Y (1996) An Interior Trust Region Approach for Nonlinear Minimization Subject to Bounds. *SIAM Journal on Optimization* 6(2): 418–445. Available at: https://doi.org/10.1137/0806023.

Cousins C, Boice Jr JD, Cooper UJR, Lee UJ and Lochard KJ (2011) Annals of the ICRP Published on behalf of the International Commission on Radiological Protection International Commission on Radiological Protection Members of the 2010–2013 Main Commission of ICRP. . Available at: http://www.icrp.org/docs/P.

DeCarlo PF, Slowik JG, Stainken K, Davidovits P, Williams LR, Jayne JT, Kolb CE, Worsnop DR, Rudich Y and Jimenez JL (2004) Particle morphology and density characterization by combined mobility and aerodynamic diameter measurements. Part 2: Application to combustion-generated soot aerosols as a function of fuel equivalence ratio. *Aerosol Science and Technology* 38(12): 1206–1222.

Ding Y, Kuhlbusch TAJ, Van Tongeren M, Jiménez AS, Tuinman I, Chen R, Alvarez IL, Mikolajczyk U, Nickel C, Meyer J, Kaminski H, Wohlleben W, Stahlmecke B, Clavaguera S and Riediker M (2017) Airborne engineered nanomaterials in the workplace—a review of release and worker exposure during nanomaterial production and handling processes. *Journal of Hazardous Materials* 322: 17–28.

Fonseca AS, Kuijpers E, Kling KI, Levin M, Koivisto AJ, Nielsen SH, Fransman W, Fedutik Y, Jensen KA and Koponen IK (2018) Particle release and control of worker exposure during laboratory-scale synthesis, handling and simulated spills of manufactured nanomaterials in fume hoods. *Journal of Nanoparticle Research*. Journal of Nanoparticle Research 20(2).

Fonseca AS, Maragkidou A, Viana M, Querol X, Hämeri K, de Francisco I, Estepa C, Borrell C, Lennikov V and de la Fuente GF (2016) Process-generated nanoparticles from ceramic tile sintering: Emissions, exposure and environmental release. *Science of the Total Environment* 565: 922–932.

Fonseca AS, Viana M, Querol X, Moreno N, de Francisco I, Estepa C and de la Fuente GF (2015) Ultrafine and nanoparticle formation and emission mechanisms during laser processing of ceramic materials. *Journal of Aerosol Science* 88: 48–57.

Fujitani Y, Kobayashi T, Arashidani K, Kunugita N and Suemura K (2008) Measurement of the physical properties of aerosols in a fullerene factory for inhalation exposure assessment. *Journal of Occupational and Environmental Hygiene* 5(6): 380–389.

Gakidou E, Afshin A, Abajobir AA, Abate KH, Abbafati C, Abbas KM, Abd-Allah F, Abdulle AM, Abera SF, Aboyans V, Abu-Raddad LJ, Abu-Rmeileh NME, Abyu GY, Adedeji IA, Adetokunboh O, Afarideh M, Agrawal A, Agrawal S, Ahmad Kiadaliri A, Ahmadieh H, Ahmed MB, Aichour AN, Aichour I, Aichour MTE, Akinyemi RO, Akseer N, Alahdab F, Al-Aly Z, Alam K, Alam N, Alam T, Alasfoor D, Alene KA, Ali K, Alizadeh-Navaei R, Alkerwi A, Alla F, Allebeck P, Al-Raddadi R, Alsharif U, Altirkawi KA, Alvis-Guzman N, Amare AT, Amini E, Ammar W, Amoako YA, Ansari H, Antó JM, Antonio CAT, Anwari P, Arian N, Ärnlöv J, Artaman A, Aryal KK, Asayesh H, Asgedom SW, Atey TM, Avila-Burgos L, Avokpaho EFGA, Awasthi A, Azzopardi P, Bacha U, Badawi A, Balakrishnan K, Ballew SH, Barac A, Barber RM, Barker-Collo SL, Bärnighausen T, Barquera S, Barregard L, Barrero LH, Batis C, Battle KE, Baune BT, Beardsley J, Bedi N, Beghi E, Bell ML, Bennett DA, Bennett JR, Bensenor IM, Berhane A, Berhe DF, Bernabé E, Betsu BD, Beuran M, Beyene AS, Bhansali A, Bhutta ZA, Bikbov B, Birungi C, Biryukov S, Blosser CD, Boneya DJ, Bou-Orm IR, Brauer M, Breitborde NJK, Brenner H, Brugha TS, Bulto LNB, Baumgarner BR, Butt ZA, Cahuana-Hurtado L, Cárdenas R, Carrero JJ, Castañeda-Orjuela CA, Catalá-López F, Cercy K, Chang HY, Charlson FJ, Chimed-Ochir O, Chisumpa VH, Chitheer AA, Christensen H, Christopher DJ, Cirillo M, Cohen AJ, Comfort H, Cooper C, Coresh J, Cornaby L, Cortesi PA, Criqui MH, Crump JA, Dandona L, Dandona R, Das Neves J, Davey G, Davitoiu D V., Davletov K, De Courten B, Degenhardt L, Deiparine S, Dellavalle RP, Deribe K, Deshpande A, Dharmaratne SD, Ding EL, Djalalinia S, Do HP, Dokova K, Doku DT, Dorsey ER, Driscoll TR, Dubey M, Duncan BB, Duncan S, Ebert N, Ebrahimi H, El-Khatib ZZ, Enayati A, Endries AY, Ermakov SP, Erskine HE, Eshrati B, Eskandarieh S, Esteghamati A, Estep K, Faraon EJA, Farinha CSES, Faro A, Farzadfar F, Fay K, Feigin VL, Fereshtehnejad SM, Fernandes JC, Ferrari AJ, Feyissa TR, Filip I, Fischer F, Fitzmaurice C, Flaxman AD, Foigt N, Foreman KJ, Frostad JJ, Fullman N, Fürst T, Furtado JM, Ganji M, Garcia-Basteiro AL, Gebrehiwot TT, Geleijnse JM, Geleto A, Gemechu BL, Gesesew HA, Gething PW, Ghajar A, Gibney KB, Gill PS, Gillum RF, Giref AZ, Gishu MD, Giussani G, Godwin WW, Gona PN, Goodridge A, Gopalani SV, Goryakin Y, Goulart AC, Graetz N, Gugnani HC, Guo J, Gupta R, Gupta T, Gupta V, Gutiérrez RA, Hachinski V, Hafezi-Nejad N, Hailu GB, Hamadeh RR, Hamidi S, Hammami M, Handal AJ, Hankey GJ, Harb HL, Hareri HA, Hassanvand MS, Havmoeller R, Hawley C, Hay SI, Hedayati MT, Hendrie D, Heredia-Pi IB, Hoek HW, Horita N, Hosgood HD, Hostiuc S, Hoy DG, Hsairi M, Hu G, Huang H, Huang JJ, Iburg KM, Ikeda C, Inoue M, Irvine CMS, Jackson MD, Jacobsen KH, Jahanmehr N, Jakovljevic MB, Jauregui A, Javanbakht M, Jeemon P, Johansson LRK, Johnson CO, Jonas JB, Jürisson M, Kabir Z, Kadel R, Kahsay A, Kamal R, Karch A, Karema CK, Kasaeian A, Kassebaum NJ, Kastor A, Katikireddi SV, Kawakami N, Keiyoro PN, Kelbore SG, Kemmer L, Kengne AP, Kesavachandran CN, Khader YS, Khalil IA, Khan EA, Khang YH, Khosravi A, Khubchandani J, Kieling C, Kim D, Kim JY, Kim YJ, Kimokoti RW, Kinfu Y, Kisa A, Kissimova-Skarbek KA, Kivimaki M, Knibbs LD, Knudsen AK, Kopec JA, Kosen S, Koul PA, Koyanagi A, Kravchenko M, Krohn KJ, Kromhout H, Kuate Defo B, Kucuk Bicer B, Kumar GA, Kutz M, Kyu HH, Lal DK, Lalloo R, Lallukka T, Lan Q, Lansingh VC, Larsson A, Lee A, Lee PH, Leigh J, Leung J, Levi M, Li Y, Li Y, Liang X, Liben ML, Linn S, Liu P, Lodha R, Logroscino G, Looker KJ, Lopez AD, Lorkowski S, Lotufo PA, Lozano R, Lunevicius R, Macarayan ERK, Magdy Abd El Razek H, Magdy Abd El Razek M, Majdan M, Majdzadeh R, Majeed A, Malekzadeh R, Malhotra R, Malta DC, Mamun AA, Manguerra H, Mantovani LG, Mapoma CC, Martin R V., Martinez-Raga J, Martins-Melo FR, Mathur MR, Matsushita K, Matzopoulos R, Mazidi M, McAlinden C, McGrath JJ, Mehata S, Mehndiratta MM, Meier

T, Melaku YA, Memiah P, Memish ZA, Mendoza W, Mengesha MM, Mensah GA, Mensink GBM, Mereta ST, Meretoja A, Meretoja TJ, Mezgebe HB, Micha R, Millear A, Miller TR, Minnig S, Mirarefin M, Mirrakhimov EM, Misganaw A, Mishra SR, Mohammad KA, Mohammed KE, Mohammed S, Mohamed Ibrahim N, Mohan MBV, Mokdad AH, Monasta L, Montañez Hernandez JC, Montico M, Moradi-Lakeh M, Moraga P, Morawska L, Morrison SD, Mountjoy-Venning C, Mueller UO, Mullany EC, Muller K, Murthy GVS, Musa KI, Naghavi M, Naheed A, Nangia V, Natarajan G, Negoi I, Negoi RI, Nguyen CT, Nguyen G, Nguyen M, Nguyen Q Le, Nguyen TH, Nichols E, Ningrum DNA, Nomura M, Nong VM, Norheim OF, Norrving B, Noubiap JJN, Obermeyer CM, Ogbo FA, Oh IH, Oladimeji O, Olagunju AT, Olagunju TO, Olivares PR, Olsen HE, Olusanya BO, Olusanya JO, Opio JN, Oren E, Ortiz A, Ota E, Owolabi MO, Pa M, Pacella RE, Pana A, Panda BK, Panda-Jonas S, Pandian JD, Papachristou C, Park EK, Parry CD, Patten SB, Patton GC, Pereira DM, Perico N, Pesudovs K, Petzold M, Phillips MR, Pillay JD, Piradov MA, Pishgar F, Plass D, Pletcher MA, Polinder S, Popova S, Poulton RG, Pourmalek F, Prasad N, Purcell C, Qorbani M, Radfar A, Rafay A, Rahimi-Movaghar A, Rahimi-Movaghar V, Rahman M, Rahman MHU, Rahman MA, Rai RK, Rajsic S, Ram U, Rawaf S, Rehm CD, Rehm J, Reiner RC, Reitsma MB, Reynales-Shigematsu LM, Remuzzi G, Renzaho AMN, Resnikoff S, Rezaei S, Ribeiro AL, Rivera JA, Roba KT, Rojas-Rueda D, Roman Y, Room R, Roshandel G, Roth GA, Rothenbacher D, Rubagotti E, Rushton L, Sadat N, Safdarian M, Safi S, Safiri S, Sahathevan R, Salama J, Salomon JA, Samy AM, Sanabria JR, Sanchez-Niño MD, Sánchez-Pimienta TG, Santomauro D, Santos IS, Santric Milicevic MM, Sartorius B, Satpathy M, Sawhney M, Saxena S, Schaeffner E, Schmidt MI, Schneider IJC, Schutte AE, Schwebel DC, Schwendicke F, Seedat S, Sepanlou SG, Serdar B, Servan-Mori EE, Shaddick G, Shaheen A, Shahraz S, Shaikh MA, Shamah Levy T, Shamsipour M, Shamsizadeh M, Shariful Islam SM, Sharma J, Sharma R, She J, Shen J, Shi P, Shibuya K, Shields C, Shiferaw MS, Shigematsu M, Shin MJ, Shiri R, Shirkoohi R, Shishani K, Shoman H, Shrime MG, Sigfusdottir ID, Silva DAS, Silva JP, Silveira DGA, Singh JA, Singh V, Sinha DN, Skiadaresi E, Slepak EL, Smith DL, Smith M, Sobaih BHA, Sobngwi E, Soneji S, Sorensen RJD, Sposato LA, Sreeramareddy CT, Srinivasan V, Steel N, Stein DJ, Steiner C, Steinke S, Stokes MA, Strub B, Subart M, Sufiyan MB, Suliankatchi RA, Sur PJ, Swaminathan S, Sykes BL, Szoeke CEI, Tabarés-Seisdedos R, Tadakamadla SK, Takahashi K, Takala JS, Tandon N, Tanner M, Tarekegn YL, Tavakkoli M, Tegegne TK, Tehrani-Banihashemi A, Terkawi AS, Tesssema B, Thakur JS, Thamsuwan O, Thankappan KR, Theis AM, Thomas ML, Thomson AJ, Thrift AG, Tillmann T, Tobe-Gai R, Tobollik M, Tollanes MC, Tonelli M, Topor-Madry R, Torre A, Tortajada M, Touvier M, Tran BX, Truelsen T, Tuem KB, Tuzcu EM, Tyrovolas S, Ukwaja KN, Uneke CJ, Updike R, Uthman OA, Van Boven JFM, Van Donkelaar A, Varughese S, Vasankari T, Veerman LJ, Venkateswaran V, Venketasubramanian N, Violante FS, Vladimirov SK, Vlassov VV, Vollset SE, Vos T, Wadilo F, Wakayo T, Wallin MT, Wang YP, Weichenthal S, Weiderpass E, Weintraub RG, Weiss DJ, Werdecker A, Westerman R, Whiteford HA, Wiysonge CS, Woldeyes BG, Wolfe CDA, Woodbrook R, Workicho A, Wulf Hanson S, Xavier D, Xu G, Yadgir S, Yakob B, Yan LL, Yaseri M, Yimam HH, Yip P, Yonemoto N, Yoon SJ, Yotebieng M, Younis MZ, Zaidi Z, El Sayed Zaki M, Zavala-Arciniega L, Zhang X, Zimsen SRM, Zipkin B, Zodpey S, Lim SS and Murray CJL (2017) Global, regional, and national comparative risk assessment of 84 behavioural, environmental and occupational, and metabolic risks or clusters of risks, 1990-2016: A systematic analysis for the Global Burden of Disease Study 2016. *The Lancet* 390(10100): 1345–1422.

Ganser GH and Hewett P (2017) Models for nearly every occasion: Part II - Two box models. *Journal of Occupational and Environmental Hygiene* 14: 58–71.

Gérard B (2006) Application of thermal spraying in the automobile industry. *Surface and Coatings Technology* 201(5): 2028–2031.

Hallé S, Nadeau S and Fatisson J (2015) Engineered containment and control of airborne nanoparticles: Current status. *International Journal of Safety and Security Engineering* 5(4): 336–351.

Heitbrink WA, Evans DE, Ku BK, Maynard AD, Slavin TJ and Peters TM (2009) Relationships among particle number, surface area, and respirable mass concentrations in automotive engine manufacturing. *Journal of*

Occupational and Environmental Hygiene 6(1): 19–31. Available at: http://www.tandfonline.com/doi/abs/10.1080/15459620802530096.

Hériaud-Kraemer H, Montavon G, Coddet C, Hertert S and Robin H (2003) Harmful risks for workers in thermal spraying: A review completed by a survey in a French company. *Journal of Thermal Spray Technology* 12(4): 542–554.

Hewett P and Ganser GH (2017) Models for nearly every occasion: Part I - One box models. *Journal of Occupational and Environmental Hygiene*. Taylor & Francis 14(1): 49–57.

Hinds WC (1999) *Aerosol technology: Properties, Behavior, and Measurement of Airborne Particles. Wiley-Interscience Publication*. Wiley. Available at: https://books.google.es/books/about/Aerosol_technology.html?id=ORxSAAAAMAAJ&redir_esc=y.

Hoek G, Boogaard H, Knol A, De Hartog J, Slottje P, Ayres JG, Borm P, Brunekreef B, Donaldson K, Forastiere F, Holgate S, Kreyling WG, Nemery B, Pekkanen J, Stone V, Wichmann HE and Van Der Sluijs J (2010) Concentration response functions for ultrafine particles and all-cause mortality and hospital admissions: Results of a European expert panel elicitation. *Environmental Science and Technology* 44(1): 476–482.

Huang H, Li H and Li X (2016) Physicochemical Characteristics of Dust Particles in HVOF Spraying and Occupational Hazards: Case Study in a Chinese Company. *Journal of Thermal Spray Technology*. Springer US 25(5): 971–981.

Hussein T, Hämeri K, Aalto PP, Paatero P and Kulmala M (2005) Modal structure and spatial-temporal variations of urban and suburban aerosols in Helsinki - Finland. *Atmospheric Environment* 39(9): 1655–1668.

Hussein T, Maso MD, Petäjä T, Koponen IK, Paatero P, Aalto PP, Hämeri K and Kulmala M (2005) Evaluation of an automatic algorithm for fitting the particle number size distributions. *Boreal Environment Research.* 10(October): 337–355.

Ibald-Mulli A, Wichmann H-E, Kreyling W and Peters A (2002) Epidemiological Evidence on Health Effects of Ultrafine Particles. *Journal of Aerosol Medicine* 15(2): 189–201. Available at: http://www.liebertonline.com/doi/abs/10.1089/089426802320282310.

Keller A, Fierz M, Siegmann K, Siegmann HC and Filippov A (2001) Surface science with nanosized particles in a carrier gas. *Journal of Vacuum Science & Technology A* 19(1): 1–8. Available at: https://doi.org/10.1116/1.1339832.

Knibbs LD, Cole-Hunter T and Morawska L (2011) A review of commuter exposure to ultrafine particles and its health effects. *Atmospheric Environment*. Elsevier Ltd 45(16): 2611–2622. Available at: http://dx.doi.org/10.1016/j.atmosenv.2011.02.065.

Koivisto AJ, Aromaa M, Koponen IK, Fransman W, Jensen KA, Mäkelä JM and Hämeri KJ (2015) Workplace performance of a loose-fitting powered air purifying respirator during nanoparticle synthesis. *Journal of Nanoparticle Research* 17(4).

Koivisto AJ, Aromaa M, Mäkelä JM, Pasanen P, Hussein T and Hämeri K (2012) Concept To Estimate Regional Inhalation Dose of Industrially Synthesized Nanoparticles. *ACSNano* 6: 1195–1203.

Koivisto AJ, Bluhme AB, Kling KI, Fonseca AS, Redant E, Andrade F, Hougaard KS, Krepker M, Prinz OS, Segal E, Holländer A, Jensen KA, Vogel U and Koponen IK (2018) Occupational exposure during handling and loading of halloysite nanotubes – A case study of counting nanofibers. *NanoImpact* 10(April): 153–160.

Koivisto AJ, Jensen ACØ, Levin M, Kling KI, Maso MD, Nielsen SH, Jensen KA and Koponen IK (2015) Testing the near field/far field model performance for prediction of particulate matter emissions in a paint factory. *Environmental Science: Processes & Impacts*. Royal Society of Chemistry 17(1): 62–73. Available at: http://xlink.rsc.org/?DOI=C4EM00532E.

Koivisto AJ, Kling KI, Levin M, Fransman W, Gosens I, Cassee FR and Jensen KA (2016) First order risk assessment for nanoparticle inhalation exposure during injection molding of polypropylene composites and production of tungsten-carbide-cobalt fine powder based upon pulmonary inflammation and surface area dose. *NanoImpact*. The Authors 6: 30–38. Available at: http://dx.doi.org/10.1016/j.impact.2016.11.002.

Koivisto AJ, Palomäki JE, Viitanen AK, Siivola KM, Koponen IK, Yu M, Kanerva TS, Norppa H, Alenius HT, Hussein T, Savolainen KM and Hämeri KJ (2014) Range-finding risk assessment of inhalation exposure to nanodiamonds in a laboratory environment. *International Journal of Environmental Research and Public Health* 11(5): 5382–5402.

Koponen IK, Koivisto AJ and Jensen KA (2015) Worker exposure and high time-resolution analyses of process-related submicrometre particle concentrations at mixing stations in two paint factories. *Annals of Occupational Hygiene* 59(6): 749–763.

Kuhlbusch TAJ, Neumann S and Fissan H (2004) Number Size Distribution, Mass Concentration, and Particle Composition of PM $_1$, PM $_{2.5}$, and PM $_{10}$ in Bag Filling Areas of Carbon Black Production. *Journal of Occupational and Environmental Hygiene* 1(10): 660–671. Available at: http://www.tandfonline.com/doi/abs/10.1080/15459620490502242.

Landrigan PJ, Fuller R, Acosta NJR, Adeyi O, Arnold R, Basu N, Baldé AB, Bertollini R, Bose-O'Reilly S, Boufford JI, Breysse PN, Chiles T, Mahidol C, Coll-Seck AM, Cropper ML, Fobil J, Fuster V, Greenstone M, Haines A, Hanrahan D, Hunter D, Khare M, Krupnick A, Lanphear B, Lohani B, Martin K, Mathiasen K V., McTeer MA, Murray CJL, Ndahimananjara JD, Perera F, Potočnik J, Preker AS, Ramesh J, Rockström J, Salinas C, Samson LD, Sandilya K, Sly PD, Smith KR, Steiner A, Stewart RB, Suk WA, van Schayck OCP, Yadama GN, Yumkella K and Zhong M (2017) The Lancet Commission on pollution and health. *The Lancet* 391.

Lima RS and Marple BR (2006) From APS to HVOF spraying of conventional and nanostructured titania feedstock powders: A study on the enhancement of the mechanical properties. *Surface and Coatings Technology* 200(11): 3428–3437.

Losert S, von Goetz N, Bekker C, Fransman W, Wijnhoven SWP, Delmaar C, Hungerbuhler K and Ulrich A (2014) Human Exposure to Conventional and Nanoparticle-Containing Sprays—A Critical Review. *Environmental Science & Technology*. American Chemical Society 48(10): 5366–5378.

Martins V, Cruz Minguillón M, Moreno T, Querol X, de Miguel E, Capdevila M, Centelles S and Lazaridis M (2015) Deposition of aerosol particles from a subway microenvironment in the human respiratory tract. *Journal of Aerosol Science*. Elsevier 90: 103–113. Available at: http://dx.doi.org/10.1016/j.jaerosci.2015.08.008.

Maynard AD, Aitken RJ, Butz T, Colvin V, Donaldson K, Oberdörster G, Philbert MA, Ryan J, Seaton A, Stone V, Tinkle SS, Tran L, Walker NJ and Warheit DB (2006) Safe handling of nanotechnology. *Nature*. Nature Publishing Group 444: 267. Available at: http://dx.doi.org/10.1038/444267a.

Moskowitz LN (1993) Application of HVOF thermal spraying to solve corrosion problems in the petroleum industry-an industrial note. *Journal of Thermal Spray Technology* 2(1): 21–29.

Oberdörster G (2001) Pulmonary effects of inhaled ultrafine particles. *International Archives of Occupational and Environmental Health* 74(1): 1–8. Available at:

http://www.springerlink.com/index/FVM951M11WWCV5JT.pdf%5Cnhttp://www.springerlink.com/openurl.asp?genre=article&id=doi:10.1007/s004200000185.

Occupational Safety and Health Admin. L (2006) 29 CFR 1910.134. Code of Federal Regulations, 427–451. Available at: https://www.osha.gov/pls/oshaweb/owadisp.show_document?p_table=standards&p_id=12716.

OJIMA J (2012) Gaseous Contaminant Distribution in the Breathing Zone. *Industrial Health* 50(3): 236–238. Available at: https://www.jstage.jst.go.jp/article/indhealth/50/3/50_MS1314/_article.

Pawlowski L (2008a) *The Science and Engineering of Thermal Spray Coatings*. *The Science and Engineering of Thermal Spray Coatings: Second Edition*. Available at: http://doi.wiley.com/10.1002/9780470754085.

Pawlowski L (2008b) *The Science and Engineering of Thermal Spray Coatings*. *The Science and Engineering of Thermal Spray Coatings: Second Edition*.

Petsas N, Kouzilos G, Papapanos G, Vardavoulias M and Moutsatsou A (2007) Worker Exposure Monitoring of Suspended Particles in a Thermal Spray Industry. *Journal of Thermal Spray Technology* 16(2): 214–219. Available at: http://link.springer.com/10.1007/s11666-007-9027-6.

Poland CA, Duffin R, Kinloch I, Maynard A, Wallace WAH, Seaton A, Stone V, Brown S, MacNee W and Donaldson K (2008) Carbon nanotubes introduced into the abdominal cavity of mice show asbestos-like pathogenicity in a pilot study. *Nature Nanotechnology*. Nature Publishing Group 3: 423. Available at: http://dx.doi.org/10.1038/nnano.2008.111.

Pope C and Dockery DW (2006) Health effects of fine particulate air pollution: Lines that connect. *Journal of the Air and Waste Management Association* 56(6): 709–742.

Pope C, RT B, MJ T and Al E (2002) Lung cancer, cardiopulmonary mortality, and long-term exposure to fine particulate air pollution. *JAMA* 287(9): 1132–1141. Available at: http://dx.doi.org/10.1001/jama.287.9.1132.

Pope CA, Dockery DW and Schwartz J (1995) Review of Epidemiological Evidence of Health Effects of Particulate Air Pollution. *Inhalation Toxicology* 7(1): 1–18.

Reche C, Viana M, Karanasiou A, Cusack M, Alastuey A, Artiñano B, Revuelta MA, López-Mahía P, Blanco-Heras G, Rodríguez S, Sánchez de la Campa AM, Fernández-Camacho R, González-Castanedo Y, Mantilla E, Tang YS and Querol X (2015) Urban NH3levels and sources in six major Spanish cities. *Chemosphere*. Elsevier Ltd 119: 769–777. Available at: http://dx.doi.org/10.1016/j.chemosphere.2014.07.097.

Salmatonidis A, Viana M, Pérez N, Alastuey A, de la Fuente GF, Angurel LA, Sanfélix V and Monfort E (2018) Nanoparticle formation and emission during laser ablation of ceramic tiles. *Journal of Aerosol Science*. Elsevier Ltd 126(September): 152–168. Available at: https://linkinghub.elsevier.com/retrieve/pii/S0021850218301897.

Schmid O and Stoeger T (2017) Surface area is the biologically most effective dose metric for acute nanoparticle toxicity in the lung. *Journal of Aerosol Science*. Elsevier 113: 276. Available at: http://dx.doi.org/10.1016/j.jaerosci.2015.12.006.

Seaton A, Tran L, Aitken R and Donaldson K (2010) Nanoparticles, human health hazard and regulation. *Journal of The Royal Society Interface* 7(Suppl_1): S119–S129. Available at: http://rsif.royalsocietypublishing.org/cgi/doi/10.1098/rsif.2009.0252.focus.

Shaffer RE and Rengasamy S (2009) Respiratory protection against airborne nanoparticles: A review. *Journal of Nanoparticle Research* 11(7): 1661–1672.

Strangman TE (1985) Thermal barrier coatings for turbine airfoils. *Thin Solid Films* 127(1–2): 93–106.

Tan JC, Looney L and Hashmi MSJ (1999) Component repair using HVOF thermal spraying. *Journal of Materials Processing Technology* 92–93: 203–208.

Toma FL, Stahr CC, Berger LM, Saaro S, Herrmann M, Deska D and Michael G (2010) Corrosion resistance of APS- and HVOF-sprayed coatings in the Al2O3-TiO2system. *Journal of Thermal Spray Technology* 19(1–2): 137–147.

Viana M, Fonseca AS, Querol X, López-Lilao A, Carpio P, Salmatonidis A and Monfort E (2017) Workplace exposure and release of ultrafine particles during atmospheric plasma spraying in the ceramic industry. *Science of the Total Environment* 599–600: 2065–2073.

Viitanen AK, Uuksulainen S, Koivisto AJ, Hämeri K and Kauppinen T (2017) Workplace measurements of ultrafine particles-A literature review. *Annals of Work Exposures and Health* 61(7): 749–758.

Voliotis A, Bezantakos S, Giamarelou M, Valenti M, Kumar P and Biskos G (2014) Nanoparticle emissions from traditional pottery manufacturing. *Environ. Sci.: Processes Impacts* 16(6): 1489–1494. Available at: http://xlink.rsc.org/?DOI=C3EM00709J.

WHO WHO (2017) *WHO Guidelines on Protecting Workers from Potential Risks of Manufactured Nanomaterials*. World Health Organization.

Supplementary Data

Workplace exposure to nanoparticles during thermal spraying of ceramic coatings

Salmatonidis A., Ribalta C., Sanfélix V., Bezantakos S., Biskos G., Vulpoi A., Simion S., Monfort E., Viana M.

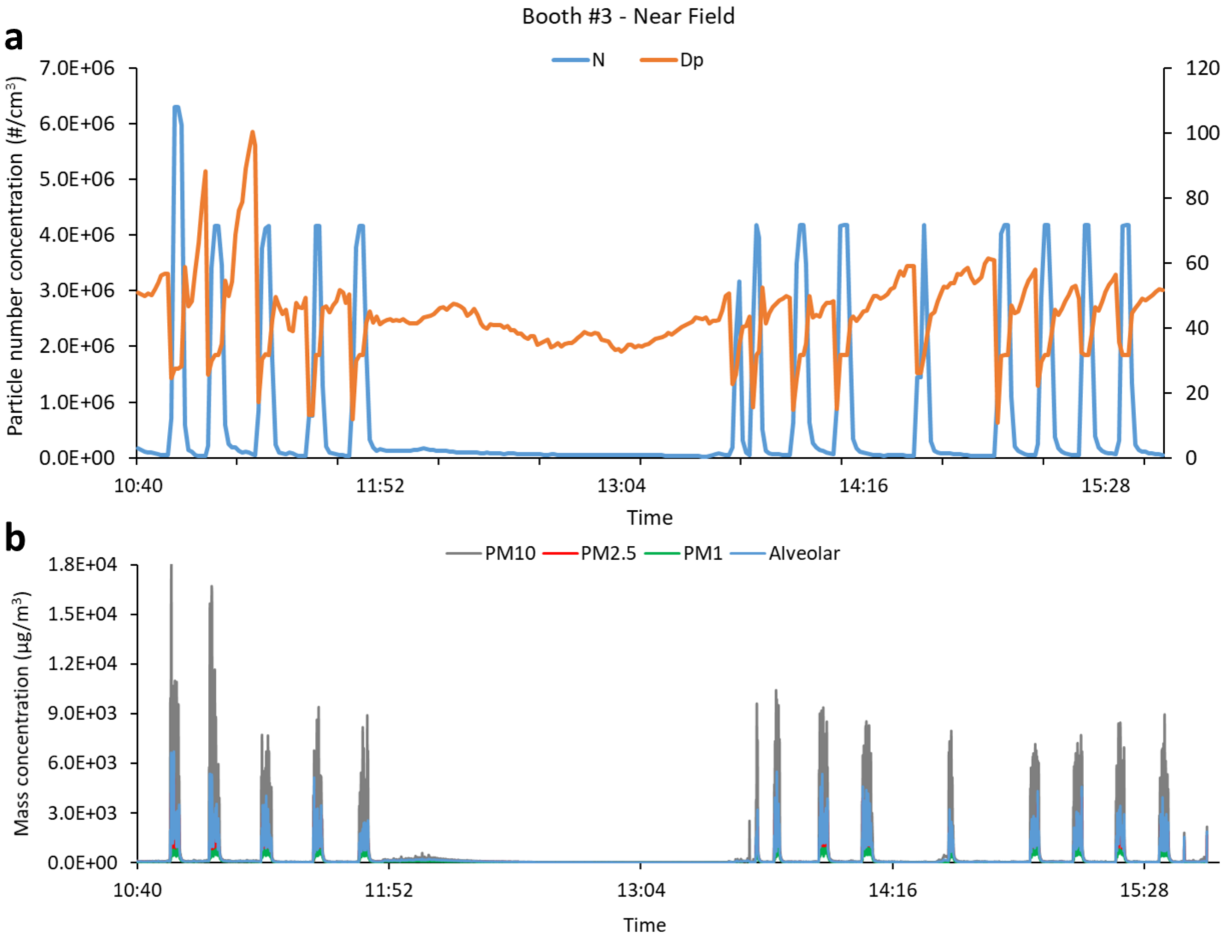

Figure S1. (a) Particle number concentration and mean diameter and (b) size segregated particle mass concentrations, in the near field location for booth #3 (28-04-2017).

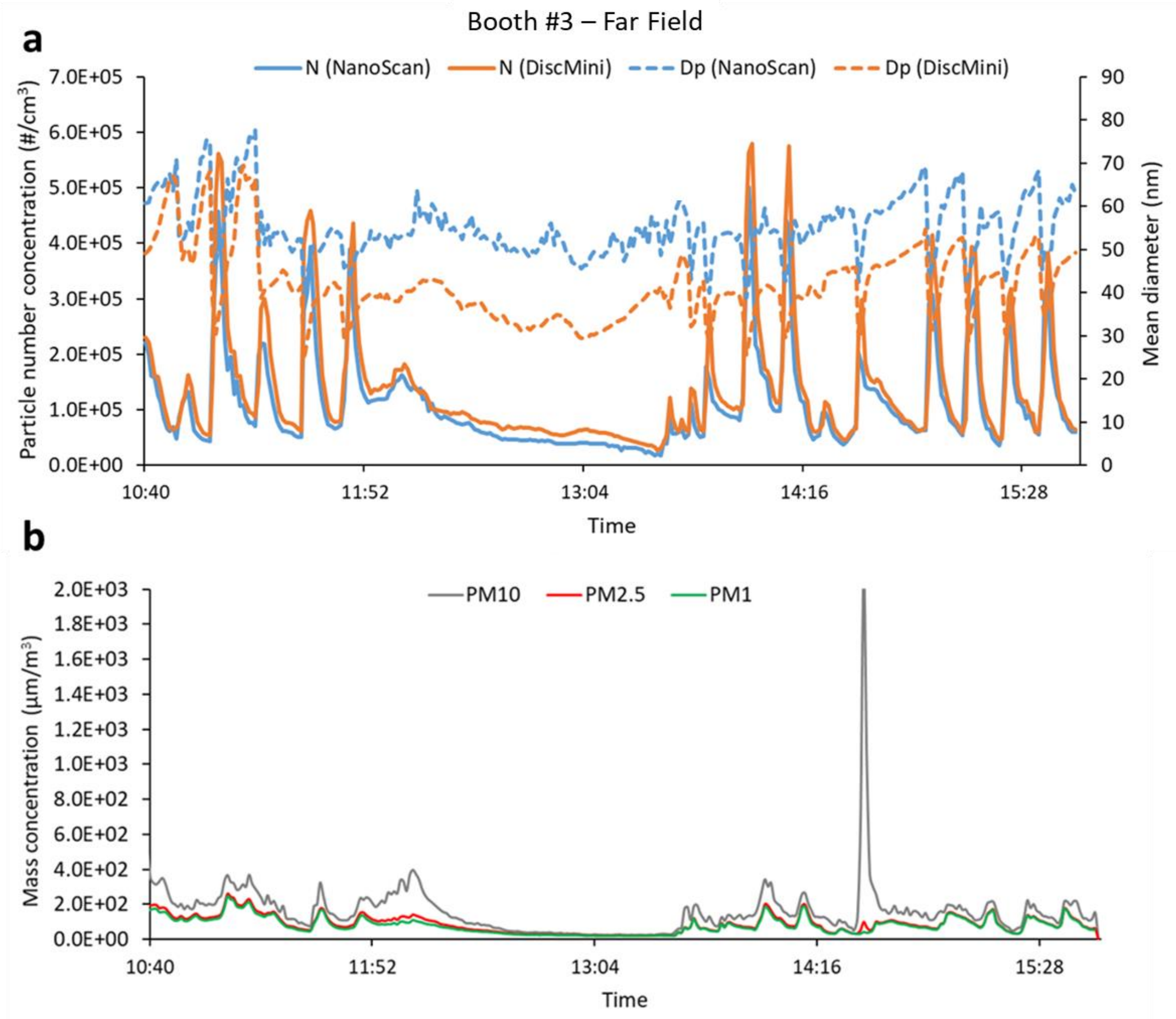

Figure S2. (a) Particle number concentration and mean diameter and (b) size segregated particle mass concentrations, in the far field location for booth #3 (28-04-2017)

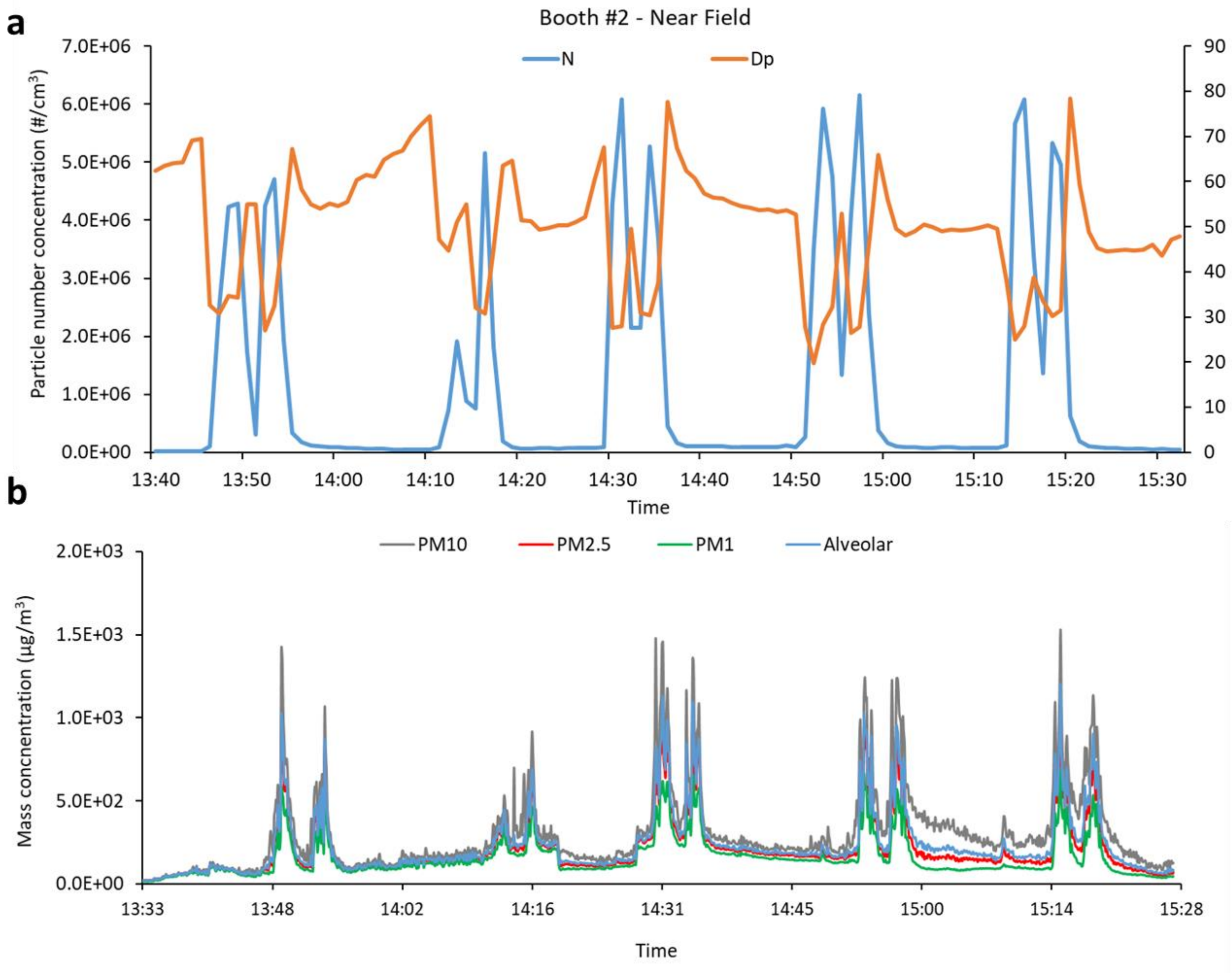

Figure S3 Particle number concentration and mean diameter and (b) size segregated particle mass concentrations, in the near field location for booth #2 (24-04-2017).

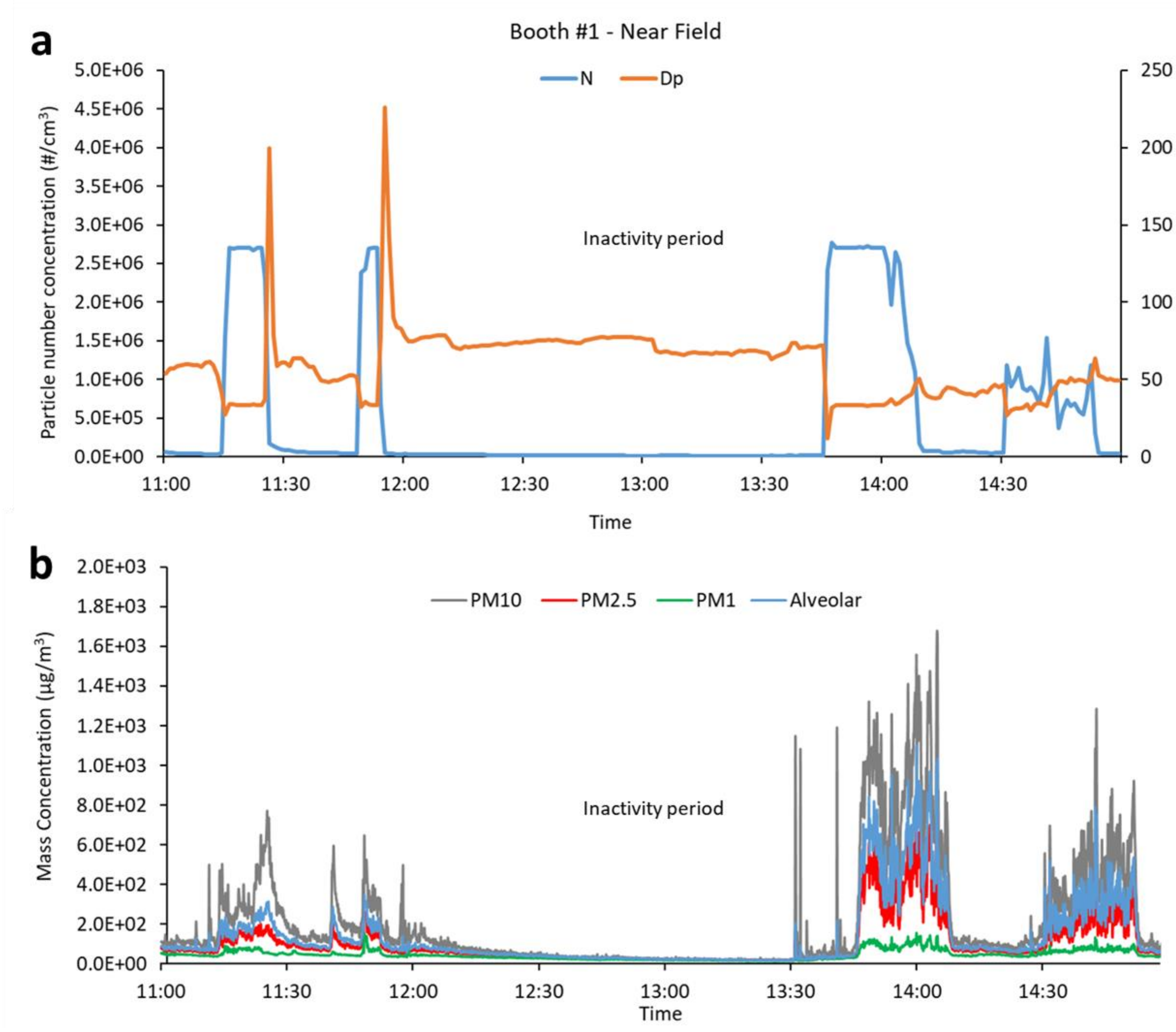

Figure S4 Particle number concentration and mean diameter and (b) size segregated particle mass concentrations, in the near field location for booth #1 (27-04-2017).

Table S1. Feedstock material characterisation. Material composition as provided by the manufacturer, and aggregate size measured by laser diffraction (Mastersizer-Malvern).

Booth	Feedstock	Material Composition (Blend)	Aggregate Size (µm)
Booth #1	ANVAL 50/50	Cr, Ni	76.5
Booth #1	Amdry 6228	TiO_2, Al_2O_3	36.0
Booth #2	Woka 3604	WC, Co, Cr, Ni	29.2
Booth #3	Woka 3702-1	WC, Cr_3C_2, Ni	34.3

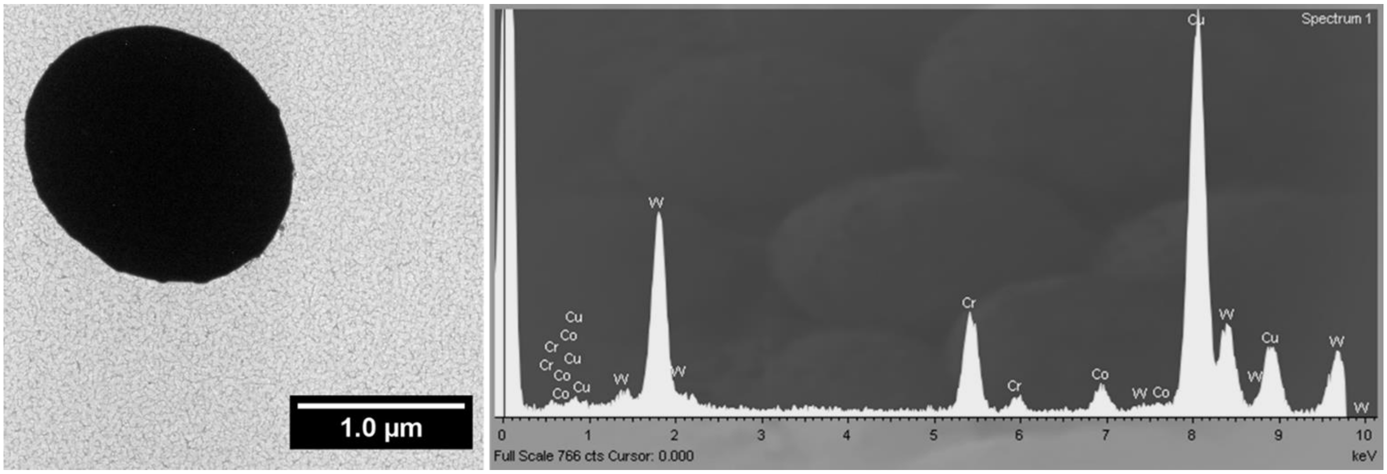

Figure S5. Particle > 1 µm emitted from Booth #3 (HVOF) having similar composition as the feedstock. Cu signal due to TEM grid.

Table S2. Instrument intercomparison results in terms of R^2 coefficients

Instrument	DiSCmini-UB	DiSCmini-ITC	DiSCmini-Impact	miniWRAS
DiSCmini-UB	-	$R^2 = 0.9978$	$R^2 = 0.9966$	-
DiSCmini-ITC	$R^2 = 0.9978$	-	$R^2 = 0.9981$	-
DiSCmini-Impact	$R^2 = 0.9966$	$R^2 = 0.9981$	-	-
CPC	$R^2 = 0.9461$	$R^2 = 0.9557$	$R^2 = 0.9503$	$R^2 = 0.8969$

4.3. Scientific publication 3

Hygroscopic measurements and derived structural properties of ultrafine particles emitted during thermal spraying

A. Salmatonidis[1,2], M. Viana[1], G. Biskos[3,4], S. Bezantakos[3,5]

[1]*Institute of Environmental Assessment and Water Research (IDAEA-CSIC), Barcelona, Spain*

[2]*Department of Chemical Engineering and Analytical Chemistry, Faculty of Chemistry, University of Barcelona, Barcelona, Spain*

[3]*Energy Environment and Water Research Centre, The Cyprus Institute, Nicosia, Cyprus*

[4]*Faculty of Civil Engineering and Geosciences, Delft University of Technology, Delft, The Netherlands*

[5]*Université du Littoral Côte d' 'Opale, Dunkerque, France*

Submitted to: Journal of Aerosol Science, under review

The following is the manuscript version, which was produced by the author, and submitted for publication in the Journal of Aerosol Science (Elsevier): Submitted on 15 February 2019.

Hygroscopic measurements and derived structural properties of ultrafine particles emitted during thermal spraying

A. Salmatonidis[1,2], M. Viana[1], G. Biskos[3,4], S. Bezantakos[3,5]*

[1]Institute of Environmental Assessment and Water Research (IDAEA-CSIC), Barcelona, Spain

[2]Department of Chemical Engineering and Analytical Chemistry, Faculty of Chemistry, University of Barcelona, Barcelona, Spain

[3]Energy Environment and Water Research Centre, The Cyprus Institute, Nicosia, Cyprus

[4]Faculty of Civil Engineering and Geosciences, Delft University of Technology, Delft, The Netherlands

[5]Université du Littoral Côte d' 'Opale, Dunkerque, France

**Corresponding author: Spyridon Bezantakos*

Abstract

In this work we report measurements of the size, concentration, and hygroscopicity of ultrafine particles (UFPs) emitted during thermal spraying of ceramic coatings in an industrial setting. High emissions of agglomerated/aggregated UFPs (exhibiting concentrations higher than 10^6 cm^{-3}) were measured inside the spraying booths of the facilities, whereas modal analysis of the recorded size distributions indicated that the particles had often diameters in the range of 26-90 nm. The emitted UFPs were found to take up moderate amounts of water when exposed to elevated relative humidity (87% RH), with their hygroscopicity being distinguishably lower compared to that of the atmospheric background aerosol particles present in the breathing air. The hygroscopicity measurements were further used to derive structural information of the aerosol particles emitted during the thermal spraying process. More specifically, the primary particle number and size of the emitted agglomerated/aggregated UFPs were derived based on the hygroscopic behaviour of the sampled particles when exposed to 87% RH. Discrepancies between the primary particle sizes of the agglomerated/aggregated UFPs estimated by the hygroscopicity measurements and those observed by electron microscopy were attributed to their incomplete restructuring inside the HTDMA.

Keywords: exposure assessment; health risk; real-time characterization; particle growth; ceramic nanoparticles.

1. Introduction

Release of airborne particles in the workplace air has become an issue of growing concern with regard to worker exposure (Pietroiusti et al., 2018; Viitanen et al., 2017), mainly due to the well-established adverse respiratory and cardiovascular impacts of ultrafine, fine and coarse particles (Oberdörster, 2001; World Health Organization, 2016; Gakidou et al., 2017; Landrigan, 2017). Ultrafine particles (UFPs) may be unintentionally emitted during different industrial processes such as welding (Zhang et al., 2013), ceramic tile sintering (Fonseca et al., 2016), atmospheric plasma spraying (Salmatonidis et al., 2019), laser ablation (Salmatonidis et al., 2018), or iron casting (van Broekhuizen, 2017). Thermal spraying processes, such as atmospheric plasma spraying (APS) and High Velocity Oxy-fuel (HVOF) have been associated with high UFP emissions (Salmatonidis et al., 2019). Unintentional release of UFPs in industrial settings frequently results in high exposure concentrations, which contrast with relatively low background particle concentrations (Fonseca et al., 2015; Dahmann, 2016; van Broekhuizen, 2017). Nevertheless, distinguishing between the two particle populations based on their intrinsic properties, is of primary importance for assessing their potential toxicological and health effects (Ganguly et al., 2018; Limbach et al., 2007; Song et al., 2009).

Discriminating unintentionally-released UFPs (also referred to as process-generated or incidental particles) from background aerosol particles using strategies based on spatially or temporally distributed data are already reported in the literature (Kuhlbusch et al., 2011, 2009; Schill and Chosewood, 2013; OECD, 2015; Asbach et al., 2016; Dahmann, 2016). Most of the studies applying similar approaches quantify background and UFP sources in terms of aerosol metrics such as particle number or mass concentrations (Ono-Ogasawara et al., 2009; Peters et al., 2009; Asbach et al., 2012), but not based on intrinsic particle properties. This is mainly due to the fact that most of the instruments available for exposure monitoring use these metrics (Asbach et al., 2016), posing a challenge for source identification and distinction of process-generated from background aerosol particles; something that state-of-the-art aerosol instrumentation can achieve (Kalantzi and Biskos, 2014).

In this work we provide measurements of the size and concentration of aerosol particles in the breathing air at a thermal spraying facility where UFPs were emitted under real-world operating conditions. A Hygroscopic Tandem Differential Mobility Analyzer (HTDMA; Rader and McMurry, 1986) was also utilized to probe the hygroscopicity of the UFPs (i.e., their ability to take up water upon exposure to elevated water vapor concentrations) as well as the mixing state of the sampled aerosol. These are two intrinsic aerosol properties that define the deposition behavior of inhaled aerosol particles in the human respiratory system (Löndahl et al., 2007; Ching and Kajino, 2018) and consequently the associated health effects.

Another application of the HTDMA measurements carried out in this work involves the identification of particles with irregular morphology (aggregates or/and agglomerates) as their shape can change to that of more compact structures at elevated relative humidity (RH) conditions during the measurement. This phenomenon is manifested as an apparent shrinking of the particles when exposed to elevated RH. Such observations have been reported for non-spherical but hygroscopic particles (e.g., sodium chloride particles; Krämer et al., 2000; Biskos et al., 2006), as well as for hydrophobic non-spherical aggregates (e.g., soot particles; Weingartner et al., 1995; Tritscher et al., 2011). In this work, we connect apparent shrinking (i.e., measured by the HTDMA) of the aggregated/agglomerated particles emitted by thermal spraying, with the primary particle number and diameter of the aggregates, and qualitatively compare the results with measurements by Transmission Electron Microscopy (TEM).

2. Experimental

Particle concentrations were monitored during thermal spraying at an industrial-scale precision engineering workshop (T.M. Comas, Blanes, Spain). The measurements were carried out over a 4-day period, and were representative of the usual operating conditions in the plant. The facility had three thermal spraying booths located in an area of approximately 240 m^2 (14 m wide and 17 m in length) that includes also a storage and a central area (cf. Figure S1 in the Electronic Supplementary Information; ESI). Different spraying techniques were used in each of the booths (cf. Figure S1). Booth #1 housed an Atmospheric Plasma Spraying (APS) system, characterised by high temperatures (5-20×10^3 ºC) and relatively low projection velocities (200-500 m/s), that was used to spray TiO_2-Al_2O_3 or Cr-Ni powder blends having mean grain diameters of 36.0 and 76.5 µm, respectively. At the very high temperatures that are developed during APS, the feedstock is melted and driven through the formed jet towards the workpiece, i.e., the surface being coated (Pawlowski, 2008). Between the plasma gun and the workpiece, metal vapors are oxidized by entrained air and condense in the cold zone of the jet (Fauchais et al., 2001; Mauer et al., 2011; Planche et al., 2003), a mechanism that results in nanoparticle formation (cf. Figure S8a in the ESI). According to this mechanism, the primary nanoparticles emitted by APS should principally have spherical shapes as they mainly originate from condensation of gaseous or liquid precursors.

The other spraying booth (located in booth #3; cf. Figure S8b in the ESI) housed a High Velocity Oxy-Fuel coating spraying (HVOF) system, characterised by high velocities (425-1500 m/s) and lower temperatures (2.9×10^3 ºC), in which a WC-Cr_3C_2-Ni powder blend (mean grain diameter of 34 µm) was used as feedstock. During HVOF, feedstock particles with high kinetic energies are sprayed onto the metal surface of the workpiece. In this case the feedstock material is not entirely melted as the temperatures are relatively lower, and it is driven with supersonic speeds towards the workpiece (Pawlowski, 2008). Microscaled particles are in a solid-liquid two-phase droplet state when impacting on their target, and thus are flattened during deposition (Li et al., 2004). Consequently, particles from the HVOF mechanism are expected to have irregular shapes. An additional emission route could be the fugitive emission of submicron particles, which would not be deposited on the substrate as they would simply disperse inside the booth (Li and Christofides, 2006). We should note here that booth #2 was not fully operational and its processes were not studied.

2.1. Monitoring locations and instrumentation

Particle concentrations were monitored inside two spraying booths (#1 and #3) where workers used personal protective equipment (PPE). The following particle monitoring instrumentation was deployed:

- A custom-made HTDMA (cf. Figure S2 in the ESI) system was used to measure the hygroscopicity of the sampled particles. The instrument consisted of two custom-made Differential Mobility Analyzers (DMAs; Knutson and Whitby, 1975) and a Condensation Particle Counter (CPC; TSI 3010 CPC; Agarwal and Sem, 1980). The first DMA (DMA-1) of the system was used for selecting nearly monodisperse dried particles, which were then exposed to elevated RH conditions, before their size distribution was measured by the second DMA (DMA-2) and the CPC (cf. more details in ESI). The system was operated with sheath and aerosol flow rates of 3.0 and 0.3 L/min, respectively, and for both of them the RH was controlled to 87% in order to avoid RH non-uniformities through the systems that can lead to experimental artefacts (cf. ESI; Biskos et al., 2006; Bezantakos et al., 2016). The sampling time of the instrument was 180 s, and the voltage of DMA-1 was changed every 6 minutes (i.e., every two sampling periods) in order to sequentially select particles having dry electrical mobility diameters of either 30 or 90 nm. These sizes were selected as they are representative of the particles produced by the plasma spraying processes (Salmatonidis et al., 2019). The instrument was deployed in the worker area, sampling directly from spraying booths #1 and #3, except from a short period of ca. 2 hours before the end of the campaign during which it sampled from the storage area outside booth #3.
- A NanoScan Scanning Mobility Particle Sizer (NanoScan-SMPS; TSI Model 3910), was used to measure the particle size distribution (10-420 nm) in 13 channels with a 1-min time resolution. Similarly to the HTDMA, the NanoScan-SMPS was in the worker area but was sampling inside the spraying booths through 3-m long conductive tubing inlets. The NanoScan-SMPS data were converted to particle size distributions, based on mobility diameters.
- A particle sampling system cassette (SKC, inlet diameter 1/8 inch), which housed transmission electron microscope (TEM) grids attached on filter support pads (25 mm in diameter), was used to collect particles for offline characterisation. The system employed an SKC Leland pump that was operated at a flow of 5 L/min. The grids (Agar Scientific Quantifoil 200 Mesh Au) were analysed offline for morphological and physicochemical particle characterisation using a TEM (Jeol, JEM 1220, Tokyo, Japan) coupled with an Energy-Dispersive X-ray (EDX; Oxford Instruments) spectrometer, following a similar procedure as described elsewhere (Voliotis et al., 2014). Samples were collected inside all the spraying booths, while TEM images were processed by the “ImageJ” software, version 1.52f.

2.2. Deriving the number and size of primary particles from the HTDMA measurements

The hygroscopic behavior of aerosol particles sampled by the HTDMA and exposed to high RH conditions can be expressedby their hygroscopic factor given by:

$$g(\mathrm{RH})=\frac{d_m(\mathrm{RH})}{d_{m,dry}}\ , \tag{1}$$

where d_m(RH) and $d_{m,dry}$ are the geometric mean mobility diameters of the sampled particles at the elevated RH (87%), measured by DMA-2 and the CPC, and at the dry state, measured as the mobility diameter selected by DMA-1, respectively (cf. ESI for more details). Dried internally mixed particles sampled by the HTDMA and exposed to the elevated RH conditions in the humidifier of the system grow (or apparently shrink) to the same sizes as a result of water uptake, exhibiting a unimodal size distribution when measured by DMA-2 and the CPC of the HTDMA. Externally mixed particles sampled by the system, on the other hand, may grow (or apparently shrink) to different sizes exhibiting either a wider unimodal or a bimodal size distribution in the measurements. To distinguish between internally and externally mixed aerosol particles sampled by the HTDMA we employed the "TDMAfit" algorithm (Bezantakos et al., 2013; McMurry and Stolzenburg, 1989; cf. Figure S3 in the ESI).

The factor g is greater than unity when the particles grow upon exposure to the elevated RH conditions, or less than unity when they exhibit apparent shrinking. Irregularly-shaped and hydrophobic particles exposed to elevated RH (87%) in the HTDMA will most likely appear to shrink, having $g(\mathrm{RH}) < 1$ exhibiting an apparent shrinking (cf. Figure S4 in the ESI). The reason for this behavior is that in the calculation of $g(\mathrm{RH})$, the two electrical mobility diameters (i.e., $d_{\mathrm{m}}(\mathrm{RH})$ and $d_{\mathrm{m,dry}}$) correspond to spherical particles (cf. Equations S1-S3 in the ESI). However, the drag force acting upon a moving irregularly-shaped particle during classification in the DMA is higher than that of a spherical particle having the same volume.

Irregurarly-shaped particles produced by high-temperature processes in the gas phase are typically aggregates or agglomerates of smaller (primary) particles. Here the term primary particle refers to the smaller particulate component (building block) that forms an aggregate/agglomerate. While both aggregate and agglomerate are interchangeably used in the literature we adopt the terminology followed by Eggersdorfer et al., (2012b) depending on the nature of the forces that bind together the primary particles. Thus an aggregate consists of primary particles that are held together by chemical forces, while in an agglomerate these forces are of physical nature.

A number of models is available in the literature for relating the electrical mobility (i.e., the properties of the particles measured at dry and humidified conditions by the HTDMA) of non-spherical, fractal-like aggregates/agglomerates with their structural properties (i.e., number and size of the primary particles they consist of; Sorensen, 2011). More established models are available for the free molecular regime (Chan and Dahneke, 1981; Rogak and Flagan, 1993 Lall and Friedlander, 2006; Eggersdorfer et al., 2012b), which is defined by the Knudsen number (i.e., ratio between the gas mean free path to the radius of the primary particles; cf. ESI). Since however, DMAs, which are commonly used for measuring the electrical mobility of particles operate in the transition regime, the above mentioned methods most likely will not give accurate results (Thajudeen et al., 2015).

Attempts to develop models for relating the structural properties of fractal-like particles with their electrical mobility (e.g., Melas et al., 2014; Corson et al., 2017), which were based on the adjusted sphere method (Dahneke ,1973; Zhang et al., 2012), were introduced in order to cover their behavior in the transition regime. Among these models, we found more suitable the one proposed by Corson et al. (2017), the results of which compare well with the adjusted sphere method for a wide range of primary particle sizes and number (cf. Corson et al., 2017 for more details).

In this analytical equation the friction coefficient of an aggregate/agglomerate (ζ_{agg}) is related to the number of primary particles (N) and the size of the primary particles via:

$$\zeta_{\mathrm{agg}} = 3\pi\mu d_{\mathrm{p}} \frac{1+1.612Kn}{C_c(Kn)} \left\{ [0.852N^{0.535} + 0.148]^{-1} + 1.612Kn\left[[0.843N^{0.939} + 0.157]\right]^{-1} \right\}^{-1}. \quad (2)$$

Here, μ is the dynamic viscosity of air, Kn is the Knudsen number of the primary particles (calculated as $\mathrm{Kn} = 2\lambda/d_{\mathrm{p}}$, where λ is the gas mean free path and r_{p} or d_{p} the radius and the diameter of the primary particles, respectively), and $C_{\mathrm{c}}(Kn)$ is the Cunningham slip correction factor corresponding to the primary particles. The drag force coefficient of the aggregates/agglomerates, selected by DMA-1 can be obtained from their electrical mobility assuming that they carry a single charge as:

$$Z_{\mathrm{agg}} = Z_{\mathrm{DMA-1}} = \frac{(Qs+Qa)\ln(\frac{R2}{R1})}{3\pi VL} = \frac{e}{\zeta_{\mathrm{agg}}}. \quad (3)$$

Here, Z_{agg}, $Z_{\mathrm{DMA\text{-}1}}$, denote the electrical mobility of the agglomerate/aggregate and the electrical mobility classified by the first DMA (i.e., DMA-1) of the HTDMA system. The latter is related with the geometrical characteristics of the DMA (i.e., inner radius: $R1$, outer radius: $R2$; effective classification length: L) and its operating conditions (i.e., voltage: V; sheath in/out flow rates: Q_{s} and Q_{a}, respectively). Therefore, assuming that each particle carries a single elementary charge, its drag force coefficient (i.e., ζ_{agg}) can be directly related to the operating conditions of DMA-1 of the HTDMA, which was used for classifying particles (i.e., its voltage, as the sheath flow rate was maintained constant throughout the measurements).

Equation 2 has two unknown values, namely the primary particle diameter (i.e., d_{p}) and number (i.e., N) and thus its solution requires the determination of either one of these values. Assuming that the sampled particles are hydrophobic (i.e., they do not take up any water) and undergo a shape change towards more compacted/spherical-like structures, we can estimate the number of the primary particles forming the fractal-like particles by using two approaches and the measurements of the size of the restructured particles from DMA-2 of the HTDMA system. In the first approach we determine the shape factor of the particles by comparing the mobility diameter of the agglomerates selected by DMA-1 to that of the restructured particles determined by DMA-2 as follows:

$$\chi = \frac{C_c(d_{\mathrm{m}}(RH))}{g(RH)C_c(\, d_{m,dry})}. \quad (4)$$

The dynamic shape factor (determined by Equation 4) is related to the number of primary particles forming Diffussion Limited Cluster Aggregates (DLCA) fractal-like particles for a wide range of Kn (Baron and Willeke, 2001):

$$\chi = N^{0.11} \text{ , for } N \leq 60, \text{and} \quad (5)$$

$$\chi = 0.6N^{0.24} \text{ , for } N \geq 60. \quad (6)$$

The second approach on the number of the primary particles that form an aggregate/agglomerate can be made using the volume of the assumed reshaped, spherical-like particle (i.e., measured by DMA-2). Following the consideration of Kruis et al. (1993), that the volume of a fractal-like particle that forms from collisions of identical primary spherical particles is the sum of the volume of its individual primary particles and it is also maintained when these fractal-like particles restructure to more compact, spherical-like particles, through sintering.

The number of primary particles (N) that form an aggregate/agglomerate is determined according to Kruis et al. (1993) as:

$$N = \frac{6v}{\pi d_{\mathrm{va}}^3}, \tag{7}$$

where v is the volume of the aggregate/agglomerate and d_{va} is the Sauter diameter, or surface area mean primary particle diameter. The latter can be estimated by (Eggersdorfer et al., 2012b):

$$d_{\mathrm{va}} = \left(\frac{\pi k_{\mathrm{a}}}{6v}\left(d_{\mathrm{m,dry}}\right)^{2D_a}\right)^{1/(2D_a-3)}. \tag{8}$$

Here $d_{\mathrm{m,dry}}$ is the electrical mobility diameter (i.e., selected at dry conditions) of the aggregates/agglomerates, while k_{a} and D_{a} are constants having values of 1.1 and 1.08, respectively for agglomerates, or 1.0 and 1.07, respectively, for aggregates(Eggersdorfer et al., 2012a). It should be noted that the approach based on Kruis et al. (1993) and Eggersdorfer et al., (2012b) applies to fractal-like particles in the free molecular regime. However, since the pre-factor k_{a} and projected area exponent D_{a} depend only on whether a fractal-like particle is an agglomerate or an aggregate, this approach can be used as a first approximation on the number of their primary particles, without further knowledge on other fractal descriptors (e.g., radius of gyration, fractal dimension).

Assuming that the sampled particles are hydrophobic and that they only undergo a shape change at elevated RH conditions to become nearly spherical, their volume (used in Equations. 7 and 8) can be estimated based on the diameter measured by DMA-2 as:

$$v = \frac{\pi}{6} d_{\mathrm{m}}(\mathrm{RH} = 87\%)^3, \tag{9}$$

where d_m(RH = 87%) is the electrical mobility diameter of the spherical particles at 87% RH.

3. Results and discussion

3.1. Nanoparticle emissions: particle number concentration and mean diameters

Figures 1 and 2 show time series of particle number concentrations and size distributions measured inside booths #1 and #3, respectively. The observed patterns reflect the particle emissions during the morning shift, a break for lunch, and finally the afternoon shift. Particle number concentrations showed a high temporal variability and reached concentrations larger than 10^6 cm^{-3} as measured by the NanoScan-SMPS. These high concentrations can cause an underestimation of the particle number concentration and size as a result of ion depletion by the sampled particles in the corona charger. This underestimation, however, is negligible as indicated by the very similar particle sizes measured with the NanoScan-SMPS when sampling outside the spraying booths where the number concentration was at least an order of magnitude lower (i.e., 10^5 cm^{-3}; Salmatonidis et al., 2019). In all cases, emissions from the spraying processes yielded particles number concentrations that were significantly higher compared to those in the background air, which was in the order of 10^4 cm^{-3}. The variability in particle concentrations and sizes is the result of numerous factors such as fluctuations in the process (different spraying conditions, variations of the feedstock, etc.), opening/closing of doors (effecting air exchange inside the booths and consequently the physical mechanisms leading to particle growth), and worker movement inside the booth (also impacting air flows), among others.

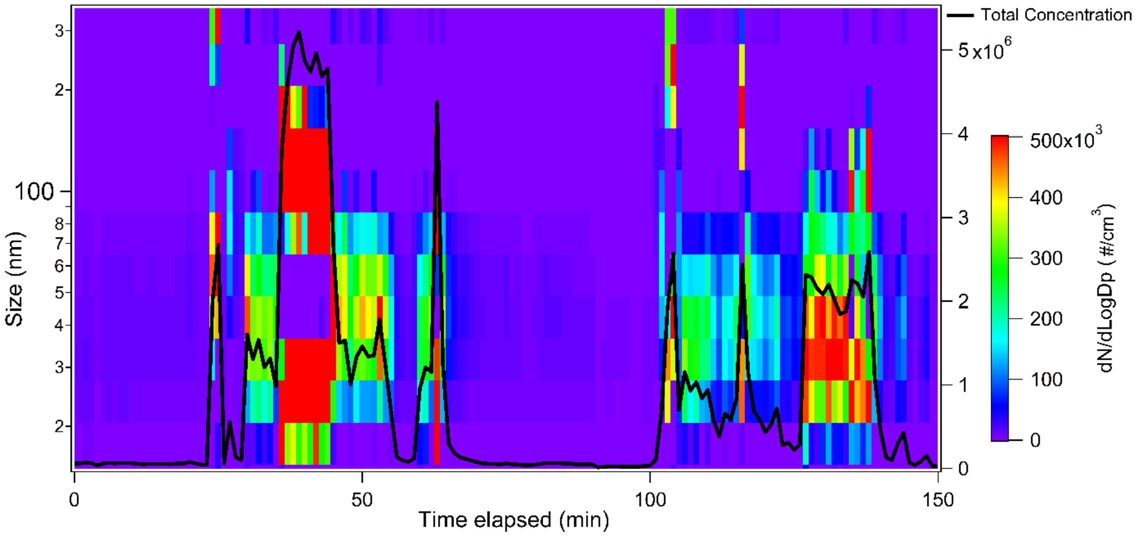

Figure 1. Evolution of the particle number size distributions inside booth #1: Total particle number concentration (black curve) and the corresponding size distribution (NanoScan-SMPS).

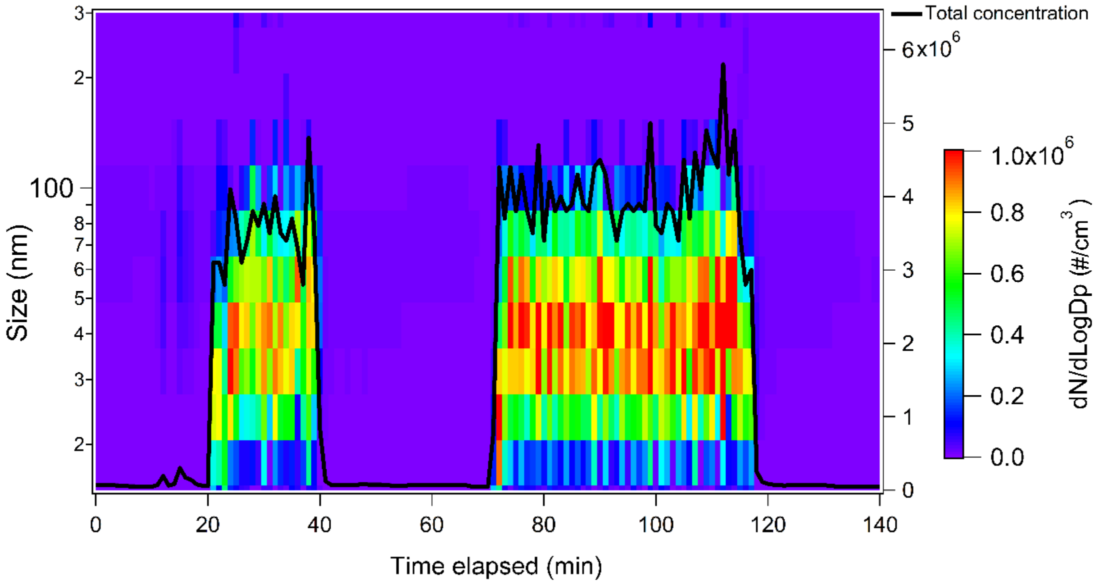

Figure 2. Evolution of the particle number size distributions inside booth #3: Total particle number concentration (black curve) and the corresponding size distribution (NanoScan-SMPS).

The emission patterns were relatively comparable across the different repetitions of the spraying process, especially in booth #3. The size distribution patterns were moderately irregular in booth #1 (cf. Figure 1), with three peaks (one between 30 and 40 nm, one between 25 and 100 nm, and one from 100 to 200 nm) and total concentrations up to 5×10^{6} cm^{-3} being observed during the first spraying operation (Figure 1, left). During the second repetition, the total particle concentration was lower (ca. 2.5×10^{6} cm^{-3}), while the mean particle diameter ranged between 40 and 100 nm. In booth #3, total particle number concentrations reached ca. 5×10^{6} cm^{-3} in each repetition, with their diameters being in the range of 40-80 nm (cf. Figure 2). Variation of the emissions patterns observed during spraying in booth #1 were attributed to the sequence of the activities followed in this process (Salmatonidis et al., 2019), where different feedstock materials were used to create different layers of coatings on the same workpiece. Process parameters and feedstock used during spraying in booth #3 were undifferentiated over the repetitions, resulting in more uniform emission patterns.

3.2. Modal analysis of particle emissions

Modal analysis was applied to data obtained directly from the nanoparticle emission source during thermal spraying. Particle size distribution measurements were split in three modes, representing the ambient modes nucleation (i.e., particles having diameters from 10 to 25 nm; $Mode_{10\text{-}25nm}$), Aitken (i.e., particles from 26 to 90 nm; $Mode_{26\text{-}90nm}$) and accumulation (i.e., particles from 91 to 660 nm; $Mode_{91\text{-}660nm}$), following the approach applied elsewhere (Salmatonidis et al., 2019). The algorithm for modal analysis uses a non-linear least square fitting, based on the interior-reflective Newton method (Coleman and Li, 1996, 1994). The three fitted lognormal curves and their parameters were calculated following the same assumptions and conditions suggested by Hussein et al. (2005). The NanoScan-SMPS measurements were expressed as dN/dLogdp distributions before applying the modal analysis.

Figure 3a-c shows the modal analysis results for particles emitted inside booth #1. During the morning session (Figure 3a), $Mode_{26\text{-}90nm}$ was slightly more dominant compared to $Mode_{91\text{-}660nm}$, and together they constituted the majority of the emitted particles (94%). $Mode_{26\text{-}90nm}$ was dominant, accounting for 70% of the total particle number concentration, during the afternoon session (Figure 3c), while $Mode_{91\text{-}660nm}$ accounted for only 27% of the total particle number concentration. Their combined contribution still included the vast majority of the particles (97%), similarly to the morning session. The differences in the particle distributions recorded in the morning and in the afternoon sessions can be attributed to the different feedstock materials that were used in each case. In booth #3 (HVOF) the modal contributions are similar for the two different repetitions of the process (Figure 3d-e). $Mode_{26\text{-}90nm}$ was dominant accounting for 76 to 84% of the total particle number concentration, while the contribution of $Mode_{91\text{-}660nm}$ ranged from 17 to 13%. The contribution of $Mode_{10\text{-}25nm}$ (which includes particles formed by nucleation) was the lowest for all of the cases in terms of particle number emissions.

$Mode_{26\text{-}90nm}$ was dominant in both processes for particles inside the spraying booths. Similar results were obtained in a previous work for particles transported from the booths to the worker area (Salmatonidis et al., 2019). These similarities are especially relevant from an exposure perspective, and show that the workers outside the booths (wearing no PPE) were exposed to particles of similar sizes and chemical compositions as those operating inside the booths (where PPE was used).

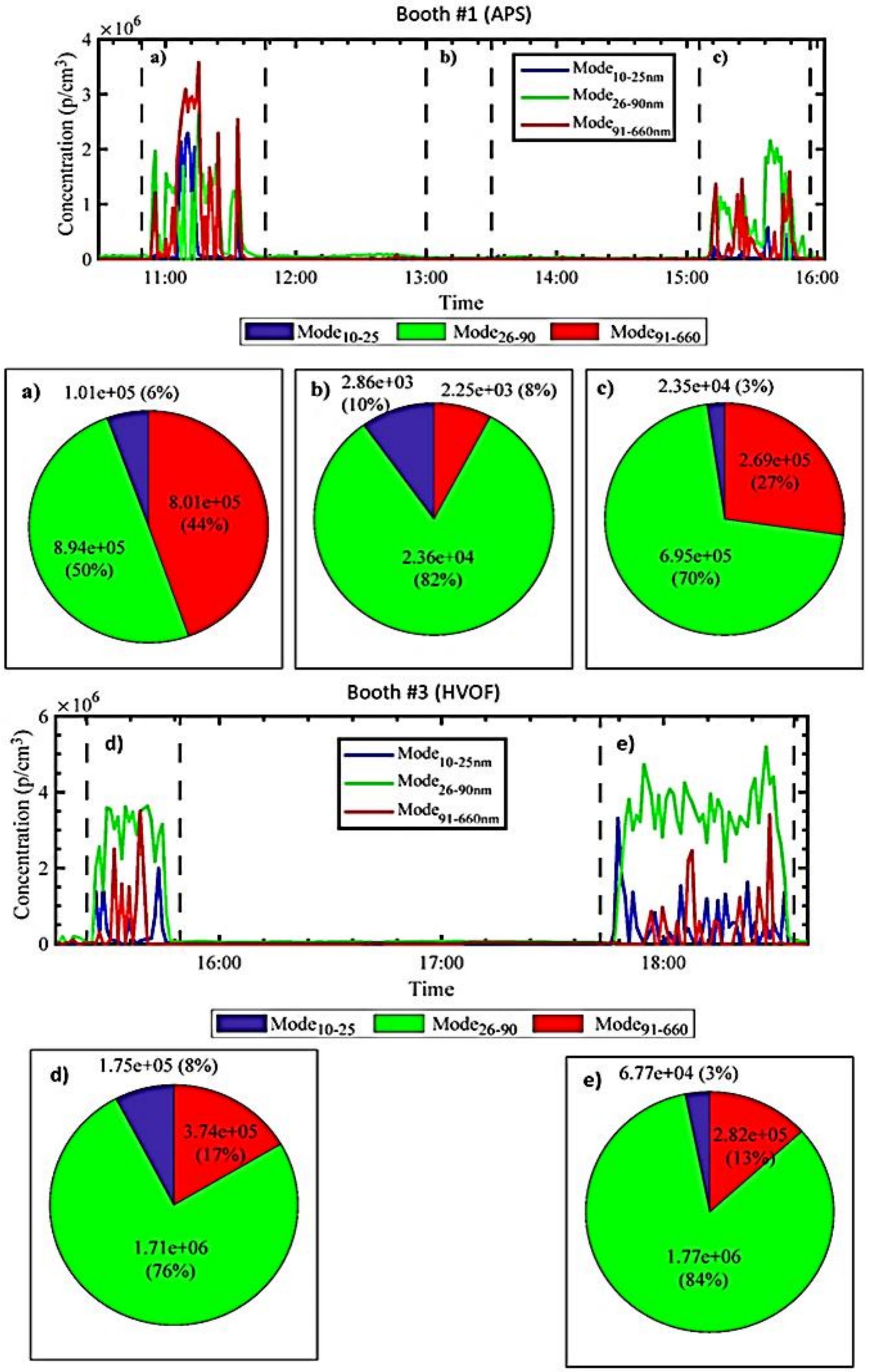

Figure 3. Modal analysis results for particles emitted inside booth #1 (a,b,c) and inside booth #3 (d,e). The different time intervals represent different repetitions of each process.

3.3. Particle hygroscopicity and mixing state

Figures 4 and 5 show the measured hygroscopic factors of particles with dry electrical mobility diameters of 30 and 90 nm, which can be classified as hydrophobic/less hygroscopic (HP) having $g(87\%) \leq 1.15$, or as hygroscopic/more hygroscopic (HS) having $g(87\%) > 1.15$. It should be noted here that the threshold value of 1.15 is used arbitrarily, following studies reported hygroscopicity measurements from field observations (Swietlicki et al., 2008). The relative fractions of HP or HS particles is reflected by the size of the circles in Figures 4 and 5, which is proportional to the number fraction of each mode (i.e., HP or HS). The hygroscopic factors $g(87\%)$ of the 90-nm particles during non-activity hours (i.e., background aerosol; cf. Figure S5) are clustered between 1.07 and 1.13 for the HP mode and at approximately 1.23 for the HS mode, being representative of urban background measurements (Swietlicki et al., 2008). During these hours, the sampled aerosol is externally mixed with HP particles being much more dominant, which is indicative of an area affected mainly by both nearby and distant aerosol sources. The combination of the low concentrations of 30-nm particles during non-working hours (Figure S6), together with the relatively increased particle losses inside the HTDMA, is responsible for the absence of the respective results during these hours (Figure S5). In contrast, during working hours, the signal of the HTDMA becomes strong when sampling 30-nm aerosols (cf. Figures 4 and 5), indicating a higher fraction of locally produced nano-scaled aerosols.

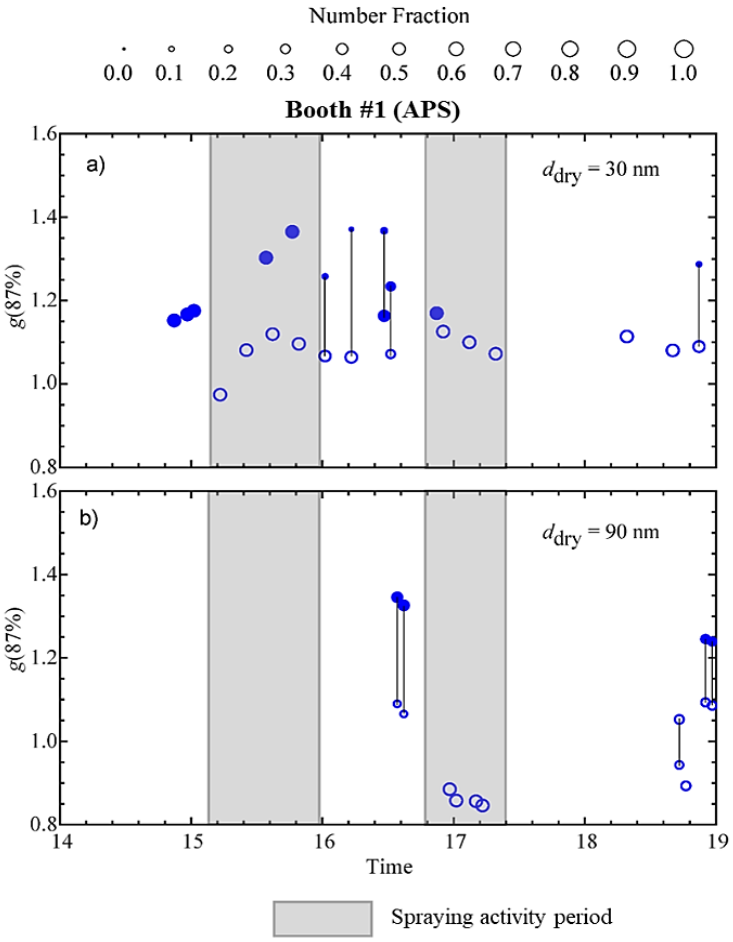

Figure 4. HTDMA measurements of particles having dry mobility diameters of 30 nm (**a**) and 90 nm (**b**), sampled from within spraying booth #1 (APS). The size of the circles is proportional to the number fraction of each hygroscopic mode. Particles having hygroscopic factors below 1.15 (hydrophobic/less hygroscopic; HP) are denoted with open circles, while closed circles denote particles with hygroscopic factors above 1.15 (hygroscopic). Vertical lines, added for clarification reasons, denote externally mixed samples, while the shaded areas mark time intervals during activity periods.

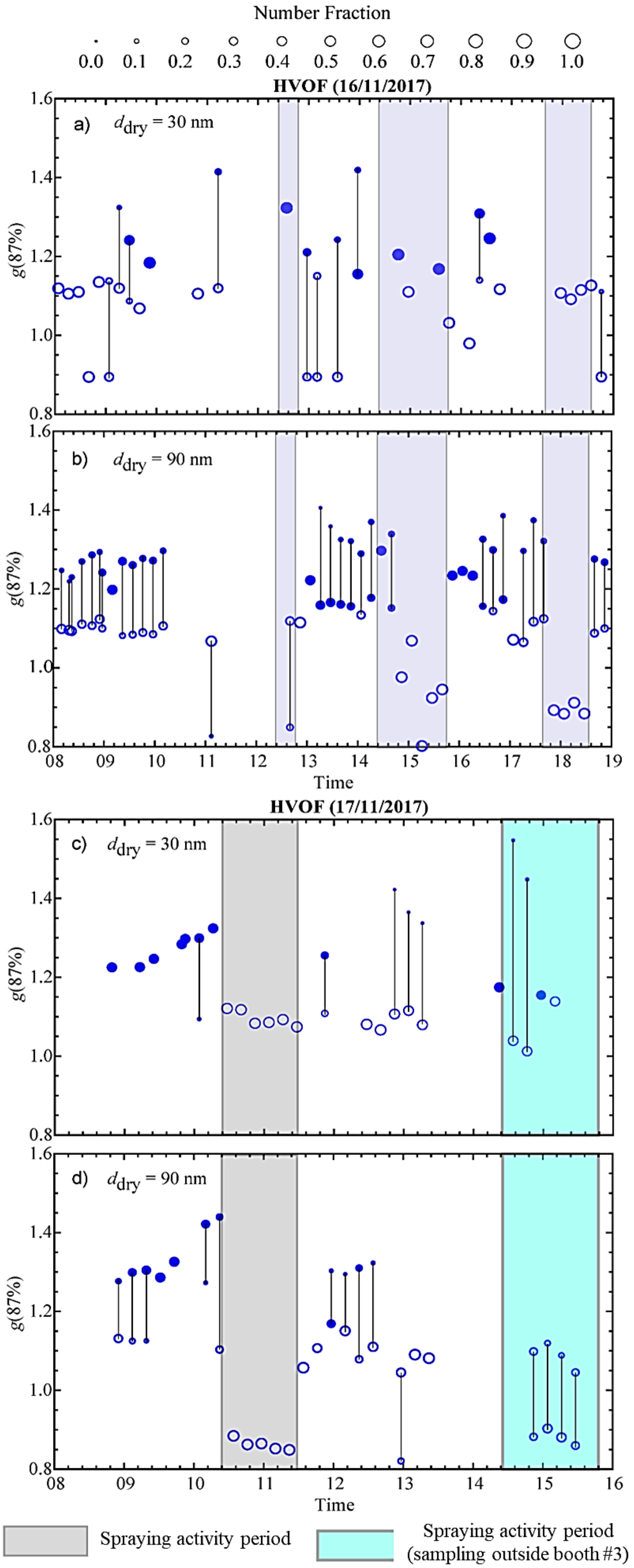

Figure 5. HTDMA measurements of particles having dry mobility diameters of 30- (**a, c**) and 90- (**b, d**) nm, sampled from within booth #3 (HVOF) on 16 and 17 Nov. 2017. The size of the symbols (i.e., the size of the circles) is proportional to the number fraction of each hygroscopic mode. Particles which exhibited hygroscopic factor below 1.15 (hydrophobic/less hygroscopic; HP) are denoted with different symbols (i.e. open circles), than the more hygroscopic ones (i.e., hygroscopic factor > 1.15; HS). Vertical lines, added for clarification reasons, denote externally mixed samples, while the shaded areas mark time intervals during activity periods and the period when the HTDMA was sampling from the storage area, outside booth #3, while it was active.

During working hours, but without spraying activity (unshaded areas in Figures 4, 5), we observed an externally mixed aerosol for ca. 45% of the cases for the 30-nm particles and ca. 76% for the 90-nm particles. The lower occurrence of the externally mixed samples with 30-nm dry particles can be attributed to the fact that those are produced locally (i.e., in the workshop) and as expected for freshly emitted particles, they exhibited almost common hygroscopicities. During periods of spraying activities (shaded areas in Figures 4 and 5) both the 30- and 90-nm particles exhibited a behavior indicating internally mixed particles. These cases should not be interpreted as a total absence of background aerosols but as a result of the significantly high process-generated nanoparticle emissions, which were up to 3 orders of magnitude higher than those of the background and dominated the sample.

The most striking observation during the spraying activity periods was that the hygroscopic factor of sampled aerosol particles was in many cases lower than unity, indicating that the particles undergo shape transformation within the HTDMA upon humidification (Tritscher et al., 2011; Weingartner et al., 1995). This observation is much more pronounced for the 90-nm dry particles sampled by the HTDMA, indicating that their shape departs much more from that of a compact/spherical shape compared to the 30-nm particles. Towards the end of the measurements, when the HTDMA was sampling outside booth #3 and the spraying system in that booth was operational (cf. data in Figure 5 after 14:30), the sampled aerosol was externally mixed, as the influence of the background aerosols increased. This was more pronounced for the 90-nm particles, which in all samples exhibited two hygroscopic modes, with the first having $g(87\%)$ values < 1.0 (i.e., indicative of particles originating from the HVOF process), comprising ca. 60% of the total population. Aggregated results of $g(87\%)$ values for both 30- and 90-nm particles, together with the associated number fraction of particles residing in the HP and HS hygroscopic modes are provided in Table S1.

3.4. Estimation of primary particle number and size

Equations 2 to 9 are used to estimate the number of primary particles that form the aggregate/agglomerated sample aerosol particles from their dynamic shape factor, or from their volume. In these equations, we assumed that the aggregates/agglomerates restructure to nearly spherical particles upon humidification, thus their dynamic shape factor (Equation 4) and volume (Equation 9) can be approximated by their measured diameters in DMA-2 of the HTDMA. Subsequently, Equation 2 is used to estimate the size of the primary particles involved in the formation of the sampled aggregates/agglomerates. Calculated values of the dynamic shape factors of these irregularly shaped particles, together with the number and the size of the primary particles forming them are provided in Table 1. It should be noted that the calculations correspond to particles that exhibit a dominant fraction having $g(87\%)$ < 1.0, which is more often and more distinctively observed for the 90-nm particles.

As shown in Table 1, the number of particles estimated by the dynamic shape factor of the irregularly shaped particles (i.e., through Equations 5 and 6 using the first approach described in Section 2.2) was always higher than that estimated by the second approach that uses the measured volume of the restructure particles (Equations 7 to 9).

Irregularly shaped particles produced in booth #1 and having dry electrical mobility diameters of 90 nm exhibited on average a dynamic shape factor of 1.38. The number of primary particles forming the observed aggregates/agglomerates is estimated on average to be 6, using approach of Eggersdorfer et al. (2012b) and 23 based on approach using the estimated dynamic shape factors (Baron and Willeke, 2001). This difference resulted in estimated mean size of these primary particles of ca. 41 and 27 nm with the first and later approach, respectively. Only one sample of particles with dry electrical mobility diameters of 30 nm was found to have irregular shape, exhibiting a dynamic shape factor of 1.05, consisting of 2 primary particles with sizes of ca. 21 nm (i.e., estimated by both approaches). When the process in booth #1 was active, the majority of the 30-nm particles samples (6 out of 7) exhibited $g(87\%)$ values very close to 1. The latter suggests that 30-nm particles from booth #1 comprise a low number of primary particles, and have a more compact/spherical shape at dry conditions. As a result, they do not undergo significant restructuring upon humidification, in contrast to their 90-nm counterparts.

Table 1. Results showing the average and standard deviation of the estimated dynamic shape factor χ of the irregularly shaped particles, together with the number N of the primary particles they consist of, derived from the two approaches described in section 2.2. The primary particle size is then derived using the above estimated primary particle numbers and the drag force coefficient of the irregular shape aerosols for the transition regime (Equation 2).

				Appr. 1	*Appr. 2*	*Appr. 1*	*Appr. 2*
	Booth	$d_{\mathrm{m,dry}}$ (nm)	χ	N	N	d_{p}	d_{p}
Agglomerates	#1	30	1.05 ± 0.00	2 ± 0	2 ± 0	21.2±0.0	21.2±0.0
	#1	90	1.38 ± 0.16	23 ± 25	6 ± 3	26.8±8.6	41.0±7.0
	#3	30	1.20 ± 0.08	6 ± 2	3 ± 1	13.8±3.2	18.2±1.4
	#3	90	1.28 ± 0.12	13 ± 14	5 ± 2	34.6±12.0	47.4±8.4
Aggregates	#1	30	1.05 ± 0.00	2 ± 0	1 ± 0	21.2±0.0	28.0±0.0
	#1	90	1.38 ± 0.16	23 ± 25	4 ± 2	26.4±8.6	48.6±8.2
	#3	30	1.20 ± 0.08	6 ± 2	2 ± 1	13.8±3.6	22.2±2.8
	#3	90	1.28 ± 0.13	13 ± 14	3 ± 1	34.6±12.0	56.2±9.8

In booth #3, where the HTDMA sampled for more time, irregularly shaped particles having a dry diameter of 90 nm exhibited an average dynamic shape factor of 1.28. The estimated number of primary particles comprising these aggregates/agglomerates is estimated to be 5 and 13 on average, depending on which approach is used. The respective estimated mean diameter of the primary particles was ca. 47 and 35 nm. The detection frequency of irregularly shaped particles having dry electrical mobility diameters of 30 nm, was also lower compared to that of the 90-nm particles when the spraying process in booth #3 was active. However, the 30-nm aggregates/agglomerates were detected more frequently in this case compared to when the spraying process in booth #1 was active during working hours, exhibiting an average dynamic shape factor of 1.20. This yields that on average the aggregates/agglomerates consist of 6 primary particles, with a mean size of ca. 14 nm, when the first approach (based on the estimated dynamic shape factors) is used, or of ca. 3 primary particles with an average size of ca. 18 nm when the second approach (based on the measured volume of the restructured particles) is employed.

3.5 TEM analysis and comparison with HTDMA results

TEM images of particles collected inside booth #1 are shown in Figure 6a-b. Chain-like agglomerates were observed across the TEM grid with different sizes and numbers of primary particles. It should be noted that agglomerates may form on the grid during collection, and thus constitute a sampling artefact. As a result, comparison of the structural properties of the sampled particles determined by the TEM images and the HTDMA measurements can only be made in terms of the size of the primary particles forming the aggregates/agglomerates, and not for the number of primary particles they consist of.

Spherical or spheroid shape of primary particles, ranging from 5 to 20 nm, can be observed in the TEM images of aggregates produced in booth #1 (Figure 6a-b), and their composition was found to be similar to the feedstock material (cf. Figure S9). Compared to the calculations discussed in Section 3.4, the TEM images suggest that the size of primary particles comprising the 90-nm dry agglomerates/aggregates was overestimated by the HTDMA measurements. Better agreement between the TEM observations and the estimations of the primary particle size derived by the HTDMA measurements is achieved when the first approach (based on the estimation of the shape factor of the particles) is used. For the 30-nm particles, the estimated primary particle diameters derived from the HTDMA data was similar to the ones observed by the TEM (ca. 20 nm). It should be noted here, however, that the TEM images show polydisperse (i.e., not size selected) aggregated/agglomerated particles collected during the spraying process, and thus making a direct comparison for the case of the 30- and 90-nm particles analyzed by the HTDMA is impossible. Nevertheless, the information of the size of the primary particles obtained by the two methods is qualitatively comparable assuming that this does not differ much with the size of the aggregates/agglomerates.

TEM images of particles sampled inside booth #3 during spraying are shown in Figure 6c-f. Irregularly-shaped primary particles appear to be strongly aggregated, resembling nanoparticles which have undergone mild sintering, and therefore it becomes challenging to distinguish them even in the higher TEM magnification (Figure 6d). This could also be an indication that the particles were directly emitted as aggregates, formed by high energy collisions, and not as single primary particles which agglomerated/aggregated after released in the air. The chemical composition of the particles emitted was similar to that if the micron-sized feedstock used (Figure S9), confirming thermal spraying was the source of the sampled particles.

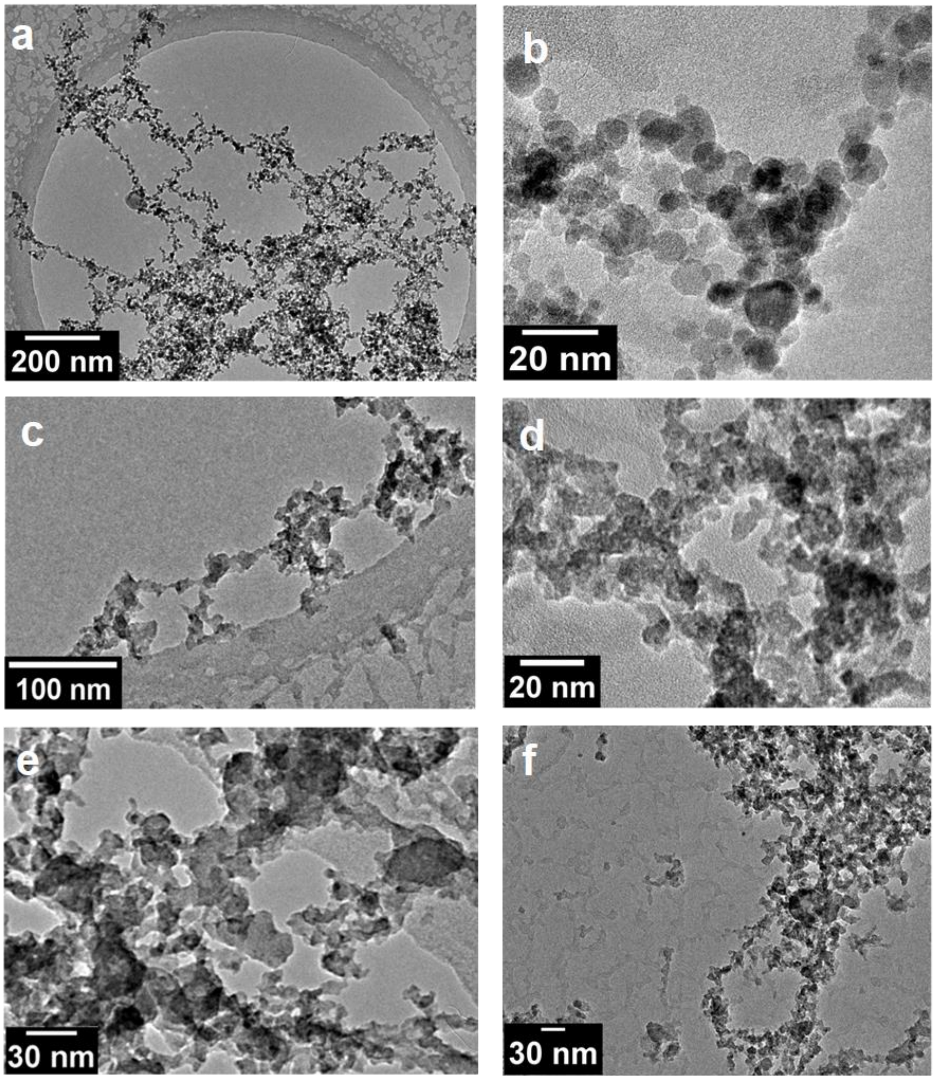

Figure 6. TEM images of the particles emitted during APS in booth #1 (a, b), and during HVOF in booth #3 (c-f).

By comparing the size of the primary particles observed with the TEM (i.e., ca. 20 nm) and that derived by the HTDMA measurements (i.e., ca. 35 nm), it is evident that the latter overestimate 90-nm agglomerates by 73%, even when their primary particle number was derived by their shape factor (i.e., first approach; cf. Table 1). In contrast, in the case of the 30-nm aggregates/agglomerates, the primary particle size was estimated (i.e., from the HTDMA measurements) to be ca. 18 or 14 nm, depending on the approach for estimating the primary particle number, which is in good agreement with the TEM observations.

In the analysis for the estimation of the number and size of primary particles that make up the aggregates/agglomerates it was assumed that the hydrophobic nanoparticles were restructured to more compact, spherical-like particles upon humidification in the HTDMA. However, in the case that these irregular-shaped particles do not restructure completely into perfect spheres upon humidification in the HTDMA, their dynamic shape factors would be even higher than the ones calculated by Equation 4.

3.6 Sensitivity analysis of the primary particle number and size derived by the HTDMA measurements

In view of the comparison of the results from the TEM analysis and the HTDMA measurements here we take a more critical view of the number and size of primary particles derived from the hygroscopicity measurements. To assess the effect that the sampled aggregates/agglomerates do not undergo full restructuring at the elevated RH within the HTDMA would have in the interpretation of our results, we carry out a sensitivity analysis showing that an increase in the dynamic shape factor of the particles will result in an increase of the number and a decrease of the size of primary particles that form an aggregate/agglomerate. The effects of the dynamic shape factor on both the number and size of primary particles for agglomerates are provided in the ESI (cf. Figure S7). For the irregularly-shaped particles observed during the process taking place in booth #1, an increase of the dynamic shape factor by 0.05 in the calculated average dynamic shape factors (1.10 and 1.43 for the 30- and 90-nm particles, respectively) would result in an estimated primary particle size of 20 nm. This value is ca. 5% lower compared to that determined from the measurements in section 3.4, and would be in agreement, within experimental uncertainty, with the TEM analysis. Regarding the 90-nm irregularly shaped particles observed in booth #3, an absolute increase of 0.15 on their shape factor (i.e., from ca. 1.28 to 1.43) would be needed in order that the estimate primary particle size to be ca. 20 nm. This suggests that the assumption that the 90-nm particles were completely restructured to form spherical particles upon exposure to 87% RH may not be absolutely valid in this particular case. Based on the above sensitivity analysis it is evident that an incomplete restructuring of the irregular particles upon humidification in the HTDMA can significantly influence the estimated number and size of primary particles that form the aggregates/agglomerates. Based on experimental observations, it has been suggested that for complete restructuring of agglomerated nanoparticles into compact spherical-like structures, supersaturated conditions (RH > 100%) are necessary (Kelesidis et al., 2018). The HTDMA, however, cannot operate at such high concentrations of water vapour, as its main function is to measure the hygroscopicity of particles at certain RH conditions. Therefore, incomplete restructuring of the irregular particles upon humidification is the most probable cause for the discrepancies between the observed (TEM) and the estimated (from the HTDMA measurements) numbers and sizes of the primary particles forming the aggregates/agglomerates.

3.7 Significance of hygroscopicity as a human health-related particle property

This intrinsic property of aerosols is relevant given that inhaled particles are exposed to relative humidity (RH) levels close to 99% in the human respiratory system (Anselm et al., 1990; Ferron et al., 1988), thus any changes in particle size (i.e., due to their hygroscopicity) can change their deposition patterns (Löndahl et al., 2007). The mixing state of particles plays also a role on their deposition behavior in the human respiratory system, and consequently on their associated health effects: in externally mixed aerosols, particles having the same size at dry conditions but are of different composition, will grow to different sizes, and therefore exhibit different deposition efficiencies, upon inhalation. Along these lines, it has been shown that the deposition of externally mixed fresh soot particles (i.e., hydrophobic; found in urban plumes) in the alveolar region can be underestimated by 5 to 20% if treated as internally mixed with more hygroscopic background aerosols (Ching and Kajino, 2018).

The hygroscopicity measurements in this work showed that UFPs produced by both the APS and HVOF plasma processes, having dry electrical mobility diameters of 30 nm, exhibited some water uptake when exposed to 87% RH (i.e., less hygroscopic), while having a compact shape, close to that of a sphere. Upon inhalation, these particles will grow, due to the high RH in the human respiratory system by ca. 28%, reaching sizes of approx. 38.5 nm (cf. ESI). On the other hand, their 90-nm counterparts were characterized as hydrophobic, clearly exhibited irregular shapes and restructuring upon humidification (i.e., exhibiting hygroscopic factors less than unity). Due to these characteristic properties they can be easily distinguished, on a real-time basis with the HTDMA, from other aerosols of the same electrical mobility. While a incomplete restructuring of these particles at 87% RH may very well be the main reason explaining the differences with TEM observations (cf. sections 3.4, 3.5 and 3.6), we cannot completely exclude this from happening upon inhalation (i.e., 99% RH inside the human respiratory system). Our sensitivity analysis indicates that in this case, these 90-nm electrical mobility diameter UFPs will exhibit aerodynamic diameters of approx. 70 nm (i.e., having shape factors of 1.43 or more; cf. section 3.6).

It is expected that the deposition behavior of these UFPs inside the human respiratory tract will differ from those estimated if their hygroscopic properties are not taken into account. This is, however, beyond the scope of this paper, but warranties further investigation. In addition, other size/shape related metrics such as their Lung Deposition Surface Area (LDSA) are expected to differ compared to those of the particles measured/calculated at dry conditions, as they are only valid for spherical particles which do not grow when exposed to elevated RH conditions (Asbach et al., 2017). Therefore, in exposure studies the HTDMA provides important additional information which is complementary to other aerosol parameters (e.g., number concentration, size distribution) in order to better understand the behavior and health impacts of UFPs. Additionally, despite lacking the accuracy of off-line methods (e.g., TEM) in determining the morphology and the size of the primary particles, the HTDMA can be used to identify particles of irregular shape in almost real time, thus allowing fast identification of particle emission hotspots or accidental releases. This would contribute to streamlining and tailoring particle exposure assessments in workplace scenarios.

4. Conclusions

High concentrations of process-generated ultrafine particles (UFPs), which were often higher than 10^6 cm^{-3}, were monitored at an industrial workplace setting during thermal spraying, inside the spraying booths of the facility. Emission patterns were irregular in the case of the process taking place in booth #1 (Atmospheric Plasma Spraying; APS) and more uniform during spraying in booth #3 (High Velocity Oxy-Fuel; HVOF). Modal analysis of the emissions showed that the majority of the emitted UFPs were in the size range of 26 to 90 nm, regardless of the process and the operating conditions. Particles were emitted inside the spraying booths where workers were equipped with personal protective equipment, but they also impacted the area where workers were not equipped with personal protective equipment.

Measurements were also conducted for providing complementary information on UFP hygroscopicity and mixing state, as a means to distinguish between process-generated and background particles, as well as for estimating their structural properties (i.e., the number and size of primary particles comprising the emitted agglomerates/aggregates). In these measurements we observed that 30-nm (electrical mobility diameter) particles originating from the plasma processes exhibited hygroscopicities which did not differ significantly from other aerosols sampled when thermal spraying was not operational. However, taking into account that 30-nm particles were observed by the HTDMA only during working hours, their presence has to be attributed to processes taking place inside the workshop. The shape of these particles was closer to that of a sphere, while based on their measured hygroscopicities they are expected to grow in size by ca. 28% upon inhalation (i.e., at 99% RH). The 90-nm particles, on the other hand, were hydrophobic at 87% RH and underwent a shape change upon humidification (i.e., $g(87\%) < 1.0$). This allowed to clearly distinguish them from other aerosols of the same dry size that were present in the workplace.

TEM/EDX analysis confirmed that process-generated particles had the same composition as the feedstock material, verifying that thermal spraying (APS, HVOF) was the dominant UFP source in the breathing air in the facility. Agglomerates were dominant on the sample grids collected from both booths, but exhibited different levels of aggregation, shapes and sizes. A qualitative comparison of the HTDMA measurements and the TEM analysis, showed that the size of spherical particles which formed chain-like agglomerates was overestimated, while their number was probably underestimated with the former technique. For the 90-nm agglomerates that exhibited a clear restructuring, in order for the calculated primary particle size determined using the HTDMA measurements to match the TEM observations the dynamic shape factors of these particles had to be ca. 5-10% higher than the measured ones. The latter suggests that the sampled aggregates/agglomerates do not fully restructure to form perfect spheres when exposed to sub-saturated conditions of 87% RH. Despite that, it is evident that the aerodynamic diameters of these particles will be significantly smaller than their electrical mobility diameters (i.e., 90 nm, measured at dry conditions) as they approach the shape of a sphere when exposed to elevated RH conditions upon inhalation (i.e., ca. 70 nm if completely restructured at 99% RH). In addition, this information is obtainable in almost real time by the HTDMA, providing a competitive advantage compared to other offline techniques.

The additional information provided by the HTDMA can complement existing methods used for an accurate assessment of the health effect associated to process-generated UFPs, as any changes in their size/shape upon inhalation can impact on other properties, such as their LDSA, while changing their deposition patterns inside the human respiratory system.

Acknowledgements

The authors kindly acknowledge TM COMAS (http://www.tmcomas.com) for their committed cooperation. The current work was carried out in the framework of the CERASAFE project (www.cerasafe.eu), with the support of SIINN ERA-NET (project id: 16), and was funded by the Spanish MINECO (PCIN-2015-173-C02-01) and the respective French agency (Region Hauts de France). Partial funding from the "Generalitat de Catalunya" (project number: AGAUR 2017 SGR41) is also acknowledged.

References

Agarwal, J.K., Sem, G.J., 1980. Continuous flow, single-particle-counting condensation nucleus counter. J. Aerosol Sci. 11, 343–357. https://doi.org/https://doi.org/10.1016/0021-8502(80)90042-7

Anselm, A., Heibel, T., Gebhart, J., Ferron, G., Inhalation, P., 1990. of Sodium Chria3Ride Particles in the Human Respiratory Tract. Growth Factors 21, 427–430.

Asbach, C., Alexander, C., Clavaguera, S., Dahmann, D., Dozol, H., Faure, B., Fierz, M., Fontana, L., Iavicoli, I., Kaminski, H., MacCalman, L., Meyer-Plath, A., Simonow, B., van Tongeren, M., Todea, A.M., 2017. Review of measurement techniques and methods for assessing personal exposure to airborne nanomaterials in workplaces. Sci. Total Environ. 603–604, 793–806. https://doi.org/10.1016/j.scitotenv.2017.03.049

Asbach, C., Clavaguera, S., Todea, A.M., 2016. Measurement Methods for Nanoparticles in Indoor and Outdoor Air, in: Viana, M. (Ed.), Indoor and Outdoor Nanoparticles: Determinants of Release and Exposure Scenarios. Springer International Publishing, Cham, pp. 19–49. https://doi.org/10.1007/698_2015_423

Asbach, C., Kuhlbusch, T. a J., Kaminski, H., Plitzko, S., Götz, U., Voetz, M., Dahmann, D., 2012. Authors : SOP-Tiered Approach Tiered Approach for the assessment of exposure to airborne nanoobjects in work- places.

Baron P. A and Willeke,K. *Aerosol Measurement: Principles, Techniques and Applications.* Second Edition, Willey-InterScience, Inc., 2001.

Bezantakos, S., Barmpounis, K., Giamarelou, M., Bossioli, E., Tombrou, M., Mihalopoulos, N., Eleftheriadis, K., Kalogiros, J., Allan, J.D., Bacak, A., Percival, C.J., Coe, H., Biskos, G., 2013. Chemical composition and hygroscopic properties of aerosol particles over the Aegean Sea. Atmos. Chem. Phys. 13, 11595–11608. https://doi.org/10.5194/acp-13-11595-2013

Bezantakos, S., Huang, L., Barmpounis, K., Martin, S. T. and Biskos G., 2016. Relative humidity non-uniformities in hygroscopic tandem differential mobility analyzer measurements. J. Aerosol Sci., 101, 1-9.

Biskos, G., Russell, L.M., Buseck, P.R., Martin, S.T., 2006a. Nanosize effect on the hygroscopic growth factor of aerosol particles. Geophys. Res. Lett. 33, 2–5. https://doi.org/10.1029/2005GL025199

Biskos, G., Russell, L. M., Buseck, P. R. and Martin S. T., 2006b. Prompt deliquescence and efflorecence of aerosol nanoparticles. Atmos. Chem. Phys., 6, 4633-4642

Chan, P., Dahneke, B., 1981. Free-molecule drag on straight chains of uniform spheres. J. Appl. Phys. 52, 3106–3110. https://doi.org/10.1063/1.329173

Ching, J., Kajino, M., 2018. Aerosol mixing state matters for particles deposition in human respiratory system. Sci. Rep. 8, 8864. https://doi.org/10.1038/s41598-018-27156-z

Coleman, T.F., Li, Y., 1996. An Interior Trust Region Approach for Nonlinear Minimization Subject to Bounds. SIAM J. Optim. 6, 418–445. https://doi.org/10.1137/0806023

Coleman, T.F., Li, Y., 1994. On the convergence of interior-reflective Newton methods for nonlinear minimization subject to bounds. Math. Program. 67, 189–224. https://doi.org/10.1007/BF01582221

Corson, J., Mulholland, G. W. and Zachariah, M. R., 2017. Analytical expression for the friction coefficient of DLCA aggregates based on extended Kirkwood–Riseman theory. Aerosol Sci. Technol., 51:6, 766-777. https://doi.org/10.1080/02786826.2017.1300635

Dahmann, D., 2016. Exposure Assessment: Methods, in: Viana, M. (Ed.), Indoor and Outdoor Nanoparticles: Determinants of Release and Exposure Scenarios. Springer International Publishing, Cham, pp. 51–72. https://doi.org/10.1007/698_2015_436

Dahneke, B. E. 1973c. Slip Correction Factors for Nonspherical Bodies - III: The Form of the General Law. *J. Aerosol Sci.*, 4:163–170.

Eggersdorfer, M.L., Gröhn, A.J., Sorensen, C.M., McMurry, P.H., Pratsinis, S.E., 2012b. Mass-mobility characterization of flame-made ZrO 2 aerosols: Primary particle diameter and extent of aggregation. J. Colloid Interface Sci. 387, 12–23. https://doi.org/10.1016/j.jcis.2012.07.078

Eggersdorfer, M.L., Kadau, D., Herrmann, H.J., Pratsinis, S.E., 2012a. Aggregate morphology evolution by sintering: Number and diameter of primary particles. J. Aerosol Sci. 46, 7–19. https://doi.org/10.1016/j.jaerosci.2011.11.005

Fauchais, P., Vardelle, A., Dussoubs, B., 2001. Quo Vadis thermal spraying? J. Therm. Spray Technol. 10, 44–66. https://doi.org/10.1361/105996301770349510

Ferron, G.A., Kreyling, W.G., Haider, B., 1988. AND DEPOSITION IN THE H U M A N RESPIRATORY TRACT * Ioo [19, 611–631.

Fonseca, A.S., Maragkidou, A., Viana, M., Querol, X., Hämeri, K., de Francisco, I., Estepa, C., Borrell, C., Lennikov, V., de la Fuente, G.F., 2016. Process-generated nanoparticles from ceramic tile sintering: Emissions, exposure and environmental release. Sci. Total Environ. 565, 922–932. https://doi.org/10.1016/j.scitotenv.2016.01.106

Fonseca, A.S., Viana, M., Querol, X., Moreno, N., de Francisco, I., Estepa, C., de la Fuente, G.F., 2015. Ultrafine and nanoparticle formation and emission mechanisms during laser processing of ceramic materials. J. Aerosol Sci. 88, 48–57. https://doi.org/10.1016/j.jaerosci.2015.05.013

Gakidou, E., Afshin, A., Abajobir, A.A., et Al., A., 2017. Global, regional, and national comparative risk assessment of 84 behavioural, environmental and occupational, and metabolic risks or clusters of risks, 1990–2016: a systematic analysis for the Global Burden of Disease Study 2016. Lancet 390, 1345–1422. https://doi.org/10.1016/S0140-6736(17)32366-8

Ganguly, P., Breen, A., Pillai, S.C., 2018. Toxicity of Nanomaterials: Exposure, Pathways, Assessment, and Recent Advances. ACS Biomater. Sci. Eng. acsbiomaterials.8b00068. https://doi.org/10.1021/acsbiomaterials.8b00068

Hussein, T., Maso, M., Petäjä, T., Koponen, I., Paatero, P., Aalto, P., Hämeri, K., Kulmala, M., 2005. Evaluation of an automatic algorithm for fitting the particle number size distributions. Boreal Environ. Res. 10, 337–355.

Kalantzi, O., Biskos G., 2014. Methods for assessing basic particle properties and cytotoxicity of engineered nanaparticles. Toxics 2 (1), 79-91.

Kelesidis, G.A., Furrer, F.M., Wegner, K., Pratsinis, S.E., 2018. Impact of Humidity on Silica Nanoparticle Agglomerate Morphology and Size Distribution. Langmuir 34, 8532–8541. https://doi.org/10.1021/acs.langmuir.8b00576

Knutson, E.O., Whitby, K.T., 1975. Aerosol classification by electric mobility: apparatus, theory, and applications. J. Aerosol Sci. 6, 443–451. https://doi.org/10.1016/0021-8502(75)90060-9

Krämer, L., Pöschl, U., Niessner, R., 2000. Microstructural rearrangement of sodium chloride condensation aerosol particles on interaction with water vapor. J. Aerosol Sci. 31, 673–685. https://doi.org/10.1016/S0021-8502(99)00551-0

Kruis, F.E., Kusters, K.A., Pratsinis, S.E., Scarlett, B., 1993. A Simple Model for the Evolution of the Characteristics of Aggregate Particles Undergoing Coagulation and Sintering. Aerosol Sci. Technol. 19, 514–526. https://doi.org/10.1080/02786829308959656

Kuhlbusch, T.A.J., Asbach, C., Fissan, H., Göhler, D., Stintz, M., 2011. Nanoparticle exposure at nanotechnology workplaces: A review. Part. Fibre Toxicol. 8, 1–18. https://doi.org/10.1186/1743-8977-8-22

Kuhlbusch, T.A.J., John, A.C., Quass, U., 2009. Sources and source contributions to fine particles. Biomarkers 14, 23–28. https://doi.org/10.1080/13547500902965377

Landrigan, P.J., 2017. Air pollution and health. Lancet Public Heal. 2, e4–e5. https://doi.org/10.1016/S2468-2667(16)30023-8

Lall. A. A. and Friedlander, S.K., 2006. On-line measurement of ultrafine aggregate surface area and volume distributions by electrical mobility analysis: I. Theoretical analysis. J. Aerosol Sci., 37, 260-271.

Li, C.-J., Wang, Y.-Y., Yang, G.-J., Ohmori, A., Khor, K.A., 2004. Effect of solid carbide particle size on deposition behaviour, microstructure and wear performance of HVOF cermet coatings. Mater. Sci. Technol. 20, 1087–1096. https://doi.org/10.1179/026708304225019722

Li, M., Christofides, P.D., 2006. Computational study of particle in-flight behavior in the HVOF thermal spray process. Chem. Eng. Sci. 61, 6540–6552. https://doi.org/10.1016/j.ces.2006.05.050

Limbach, L.K., Wick, P., Manser, P., Grass, R.N., Bruinink, A., Stark, W.J., 2007. Exposure of Engineered Nanoparticles to Human Lung Epithelial Cells: Influence of Chemical Composition and Catalytic Activity on Oxidative Stress. Environ. Sci. Technol. 41, 4158–4163. https://doi.org/10.1021/es062629t

Löndahl, J., Massling, A., Pagels, J., Swietlicki, E., Vaclavik, E., Loft, S., 2007. Size-Resolved Respiratory-Tract Deposition of Fine and Ultrafine Hydrophobic and Hygroscopic Aerosol Particles During Rest and Exercise. Inhal. Toxicol. 19, 109–116. https://doi.org/10.1080/08958370601051677

Mauer, G., Vaen, R., Stöver, D., 2011. Plasma and particle temperature measurements in thermal spray: Approaches and applications. J. Therm. Spray Technol. 20, 391–406. https://doi.org/10.1007/s11666-010-9603-z

McMurry, P.H., Stolzenburg, M.R., 1989. On the sensitivity of particle size to relative humidity for Los Angeles aerosols. Atmos. Environ. 23, 497–507. https://doi.org/10.1016/0004-6981(89)90593-3

Melas D. A., Isella, L., Konstadopoulos, A. G., Drossinos, Y., 2014. Friction coefficient and mobility radius of fractal-like aggregates in the transition regime. Aerosol Sci. Technol., 48, 1320-1331, https://doi.org/10.1080/02786826.2014.985781.

Oberdörster, G., 2001. Pulmonary effects of inhaled ultrafine particles. Int. Arch. Occup. Environ. Health 74, 1–8. https://doi.org/10.1007/s004200000185

OECD, 2015. Harmonized Tiered Approach to Measure and Assess the Potential Exposure to Airborne Emissions of Engineered Nano-Objects and their Agglomerates and Aggregates at Workplaces. Ser. Saf. Manuf. Nanomater. No.55 55, JT03378848-JT03378848.

Ono-Ogasawara, M., Serita, F., Takaya, M., 2009. Distinguishing nanomaterial particles from background airborne particulate matter for quantitative exposure assessment. J. Nanoparticle Res. 11, 1651–1659. https://doi.org/10.1007/s11051-009-9703-1

Pawlowski, L., 2008. The Science and Engineering of Thermal Spray Coatings, The Science and Engineering of Thermal Spray Coatings: Second Edition. https://doi.org/10.1002/9780470754085

Peters, T.M., Elzey, S., Johnson, R., Park, H., Grassian, V.H., Maher, T., O'Shaughnessy, P., 2009. Airborne monitoring to distinguish engineered nanomaterials from incidental particles for environmental health and safety. J. Occup. Environ. Hyg. 6, 73–81. https://doi.org/10.1080/15459620802590058

Pietroiusti, A., Stockmann-Juvala, H., Lucaroni, F., Savolainen, K., 2018. Nanomaterial exposure, toxicity, and impact on human health. Wiley Interdiscip. Rev. Nanomedicine Nanobiotechnology 1–21. https://doi.org/10.1002/wnan.1513

Planche, M.P., Bolot, R., Coddet, C., 2003. In-Flight Characteristics of Plasma Sprayed Alumina Particles : Measurements , Modeling , and Comparison 12, 101–111.

Rader, D.J., McMurry, P.H., 1986. Application of the tandem differential mobility analyzer to studies of droplet growth or evaporation. J. Aerosol Sci. 17, 771–787. https://doi.org/10.1016/0021-8502(86)90031-5

Rogak, S. N., Flagan, R. C., and Nguyen, H. V., 1993. The mobility and structure of aerosol agglomerates, *Aerosol Sci. Technol.* 18:25–47.

Salmatonidis, A., Ribalta, C., Sanfélix, V., Bezantakos, S., Biskos, G., Vulpoi, A., Simion, S., Monfort, E., Viana, M., 2019. Workplace Exposure to Nanoparticles during Thermal Spraying of Ceramic Coatings. Ann. Work Expo. Heal. 63, 91–106. https://doi.org/10.1093/annweh/wxy094

Salmatonidis, A., Viana, M., Pérez, N., Alastuey, A., de la Fuente, G.F., Angurel, L.A., Sanfélix, V., Monfort, E., 2018. Nanoparticle formation and emission during laser ablation of ceramic tiles. J. Aerosol Sci. 126, 152–168. https://doi.org/10.1016/j.jaerosci.2018.09.006

Schill, A.L., Chosewood, L.C., 2013. The NIOSH total worker health program: An overview. J. Occup. Environ. Med. 55, 10–13. https://doi.org/10.1097/JOM.0000000000000037

Song, Y., Li, X., Du, X., 2009. Exposure to nanoparticles is related to pleural effusion, pulmonary fibrosis and granuloma. Eur. Respir. J. 34, 559–567. https://doi.org/10.1183/09031936.00178308

Sorensen, C.M., 2011. The Mobility of Fractal Aggregates: A Review. Aerosol Sci. Technol. 45, 765–779. https://doi.org/10.1080/02786826.2011.560909

Swietlicki, E., Hansson, H.C., Hämeri, K., Svenningsson, B., Massling, A., Mcfiggans, G., Mcmurry, P.H., Petäjä, T., Tunved, P., Gysel, M., Topping, D., Weingartner, E., Baltensperger, U., Rissler, J., Wiedensohler, A., Kulmala, M., 2008. Hygroscopic properties of submicrometer atmospheric aerosol particles measured with H-TDMA instruments in various environments - A review. Tellus, Ser. B Chem. Phys. Meteorol. 60 B, 432–469. https://doi.org/10.1111/j.1600-0889.2008.00350.x

Thajudeen, T., Jeon, S., Hogan Jr. C. J., 2015. The mobilities of flame synthesized aggregates/agglomerates in the transition regime. J. Aerosol Sci., 80, 45-57.

Tritscher, T., Jurnyi, Z., Martin, M., Chirico, R., Gysel, M., Heringa, M.F., Decarlo, P.F., Sierau, B., Prévt, A.S.H., Weingartner, E., Baltensperger, U., 2011. Changes of hygroscopicity and morphology during ageing of diesel soot. Environ. Res. Lett. 6. https://doi.org/10.1088/1748-9326/6/3/034026

van Broekhuizen, P., 2017. Applicability of provisional NRVs to PGNPs and FCNPs Applicability of provisional NRVs to PGNPs and FCNPs. Amsterdam. https://doi.org/10.13140/RG.2.2.18241.25445

Voliotis, A., Bezantakos, S., Giamarelou, M., Valenti, M., Kumar, P., Biskos, G., 2014. Nanoparticle emissions from traditional pottery manufacturing. Environ. Sci. Process. Impacts 16, 1489–1494. https://doi.org/10.1039/C3EM00709J

Weingartner, E., Baltensperger, U., Burtscher, H., 1995. Growth and Structural Change of Combustion Aerosols at High Relative Humidity. Environ. Sci. Technol. 29, 2982–2986. https://doi.org/10.1021/es00012a014

World Health Organization, 2016. Ambient Air Pollution: A global assessment of exposure and burden of disease. World Heal. Organ. 1–131. https://doi.org/9789241511353

Zhang, C., Thajudeen, T., Larriba, C., Schwartzentruber, T. E., and Hogan, Jr, C. J. 2012. Determination of the Scalar Friction Factor for Nonspherical Particles and Aggregates Across the Entire Knudsen Number Range by Direct Simulation Monte Carlo (DSMC). *Aerosol Sci. Technol.*, 46:1065–1078.

Zhang, M., Jian, L., Bin, P., Xing, M., Lou, J., Cong, L., Zou, H., 2013. Workplace exposure to nanoparticles from gas metal arc welding process. J. Nanoparticle Res. 15. https://doi.org/10.1007/s11051-013-2016-4

Supplementary material

Hygroscopic measurements and derived structural properties of ultrafine particles emitted during thermal spraying

A. Salmatonidis, M. Viana, G. Biskos, S. Bezantakos

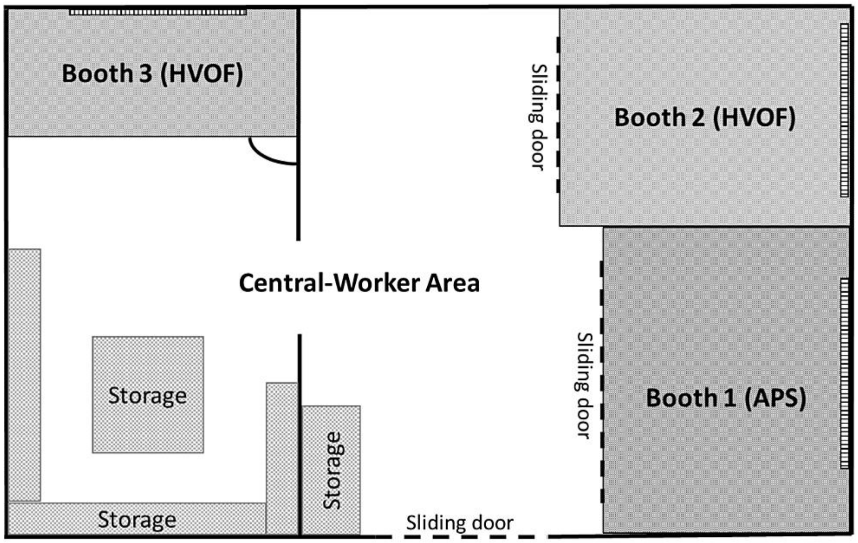

Figure S1. Schematic illustration or the facility investigated

Sampled particles were initially dried through a silica gel diffusion drier, brought to a charge equilibrium by passing through a soft X-ray aerosol neutralizer (TSI Model 3088) before entering the first DMA of the system (DMA-1). The quasi-monodisperse particles downstream DMA-1 are then exposed to elevated RH conditions by passing through a nafion membrane humidity exchanger (Permapure Model MD-700-06S-1), before their size distribution is measured by the second DMA (DMA-2) of the system that is coupled to a CPC (TSI 3010). Both DMAs employ closed loop sheath flows, while an additional humidification system, consisting of a second nafion humidifier (Permapure PD-50T-MPR) is added to the sheath flow of DMA-2 in order to maintain it at the same RH level with that of the sample flow. Two RH and temperature sensors (Rotronic HC02-05), together with a software closed loop control (National Instruments Labview 2014), are utilized for measuring and controlling the stability of the RHs in the system. The system was operated at a constant 87±2% RH, as this is above the deliquescence RH (i.e., RH above which a solid particle will form a droplet) of ammonium sulfate (i.e., one of the most abundant, hygroscopic, inorganic species in the atmosphere), while being low enough to prevent accidental forming of supersaturated conditions in parts of the HTDMA.

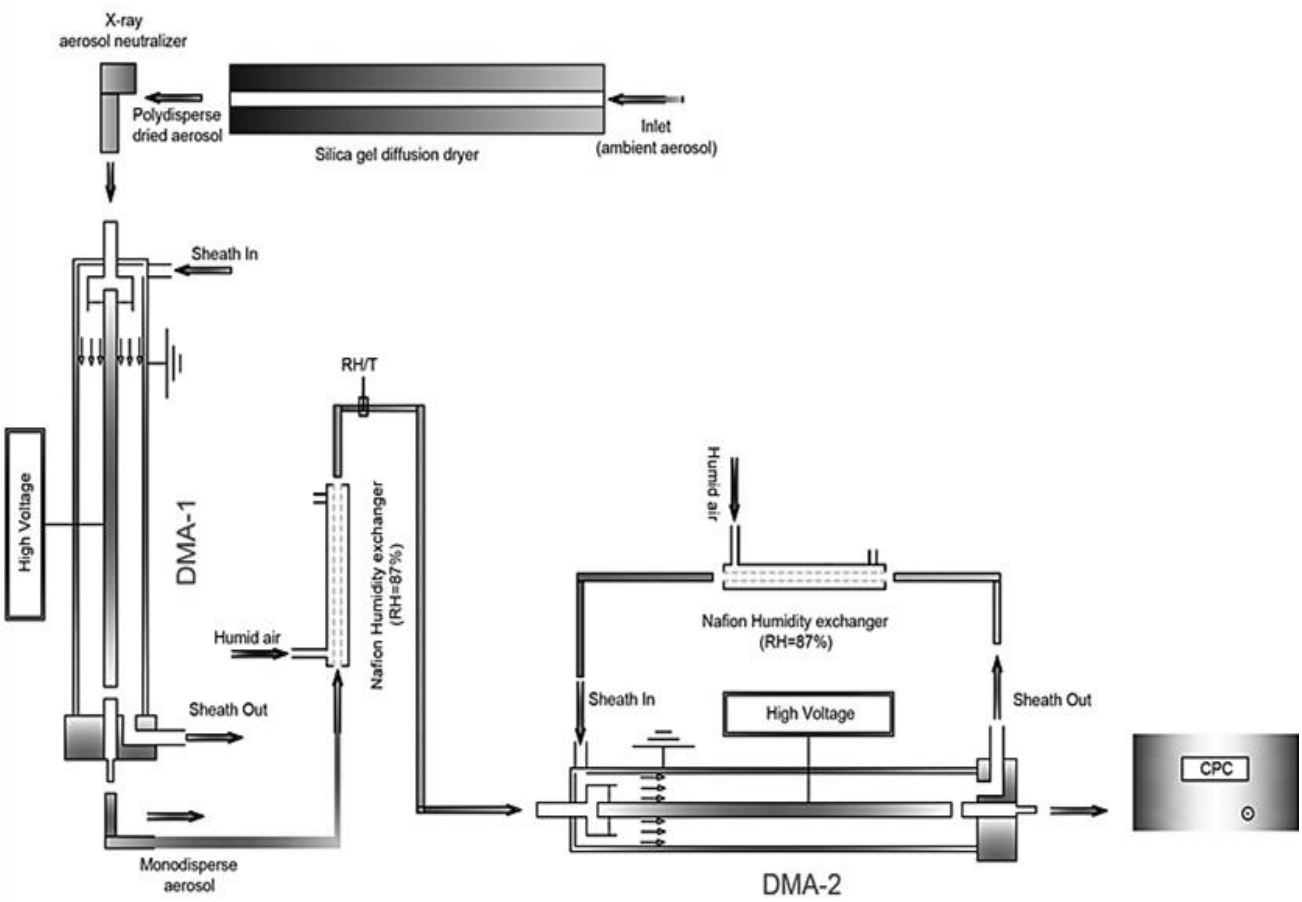

Figure S2. Major parts of the HTDMA system assembled for the characterization of PGNPs hygroscopicity and mixing state.

Deriving hygroscopic factor from the HTDMA.

In the HTDMA the first DMA (DMA-1) operates at a steady voltage during each sample, thus constantly classifying particles having a quasi-monodisperse electrical mobility (Z), while the voltage of DMA-2 is scanned, allowing the classification of particles having different electrical mobilities, which are then detected by the CPC. In general, the electrical mobility Z of the particles that are classified in a cylindrical DMA (i.e., like the ones used in the HTDMA) is related with its geometrical features and operating conditions (Baron and Willeke, 2001) as:

$$Z = \frac{(Q_{\mathrm{sh}}+Q_{\mathrm{e}})\ln\frac{R_2}{R_1}}{4\pi V L}. \tag{S1}$$

Here, R_1, R_2 are respectively the inner and outer radii of the DMA, L is characteristic classification length, Q_{sh} the sheath flow rate, Q_{e} the excess flow rate and V the applied potential in its inner electrode.

In the case of spherical particles, Z is related to particle diameter (d) using Hinds (1999):

$$Z = \frac{neCc}{3\pi\mu d}, \tag{S2}$$

where n is the number of elementary charges, e the electron charge (1.6e-19 Cb), μ the air viscosity (1.81e-5 Pa S, at 20 °C) and Cc the Cunningham slip correction factor.

The Cunningham slip correction factor, Cc, can be calculated via the empirical formula (Allen and Raabe, 1985) as:

$$Cc(Kn) = 1 + Kn\left[a + b\exp\left(-\frac{c}{Kn}\right)\right]. \tag{S3}$$

Here Kn is the Knudsen number, which is the ratio of the gas mean free path (λ) to the radius of the spherical particle (r), while a= 1.257, b=0.4, c=1.1, are fitted parameters (Davies, 1945). Note that the Kn number is used for defining the behavior of a particle while moving inside its surrounding gas molecules (i.e., its flow regime). For example, a particle much bigger than the gas mean free path (i.e, Kn<<0) will be subjected to a number of gas molecules collisions while a particle, much smaller than the gas mean free path (i.e., Kn>>1) will be subjected to significantly lower collisions by the surrounding gas molecules (i.e., resulting in a reduction in its drag).

Assuming particles of spherical shape, carrying one elementary charge, equations S1 to S3 are used for inverting the HTDMA measurements and for calculating the geometric mean electrical mobility diameters of particles selected by DMA-1 and measured by DMA-2 and the CPC, thus deriving their hygroscopic factor.

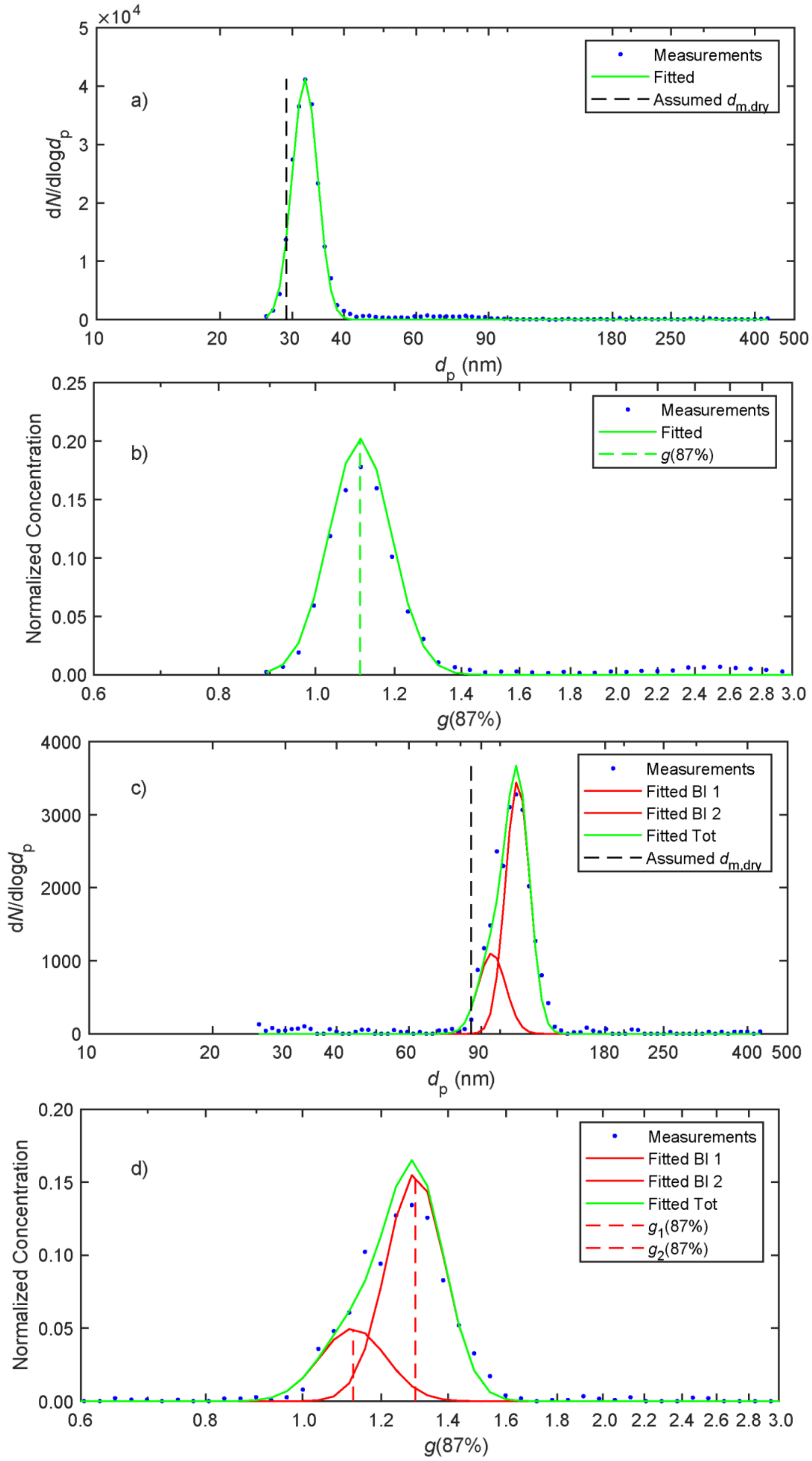

Figure S3. Example of inverted HTDMA measurements of particles having dry electrical mobility diameters of 30 (**a**) and 90 (**c**) nm and their corresponding distributions, expressed as hygroscopic factor distributions at 87% RH (**b, d**), respectively. Note that in this example the 30-nm particles exhibited internally mixed behavior (i.e., unimodal distribution when exposed to 87% RH), while in contrast their 90-nm counterparts exhibited a wider distribution upon humidification, which can be analyzed in two separate modes (i.e., externally mixed), thus having two hygroscopic factors (i.e., g_1 and g_2, respectively).

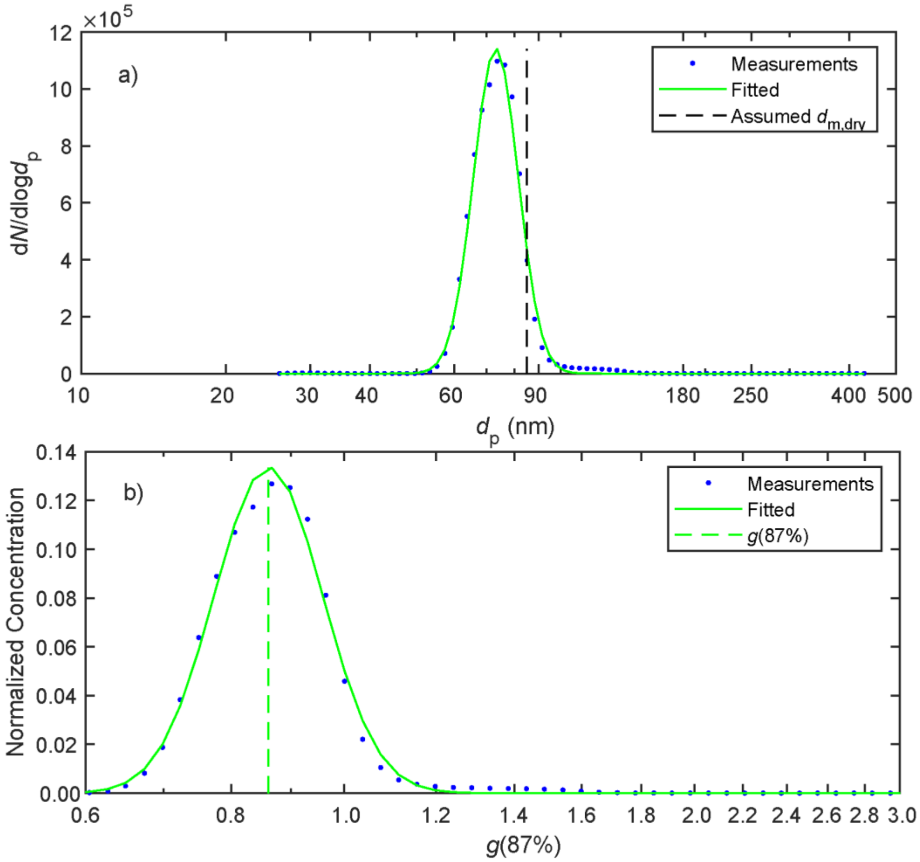

Figure S4. Example of inverted HTDMA measurements of particles having an assumed (i.e., if they were spherical) dry electrical mobility diameter of 90 nm (**a**) and the corresponding distribution, expressed as hygroscopic factor distribution at 87% RH (**b**). Note that in this example the assumed 90-nm particles (i.e., based on the operational settings of DMA-1, corresponding for spherical particles) exhibited a unimodal distribution (i.e., internally mixed) when exposed to 87% RH, with a hygroscopic factor < 1.0. The latter is a clear indication of hydrophobic particles with irregular shape, that undergo restructuring upon humidification after exposed to 87% RH.

Calculating particle hygroscopic factor on different than 87% RH.

The water affinity of soluble particulate matter can be represented by the single hygroscopic parameter κ (Petters and Kreidenweis, 2007), which can be also used for calculating its water uptake characteristics at various RHs. The value of κ can be calculated from the measured (i.e., by the HTDMA) hygroscopic factor (Kreidenweis et al., 2008):

$$\kappa_{HTDMA} = \frac{\left(g(87\%)^3 - 1\right)}{a_w/(1-a_w)}, \tag{S4}$$

where $g(87\%)$ is the measured hygroscopic factor (i.e., at 87% RH in our measurements) and a_w is the water activity of the solution droplet, which can be calculated by:

$$a_{\mathrm{w}} \approx \frac{\mathrm{RH}}{100}\left(exp\left(\frac{4\sigma_{s/\alpha}\ M_w}{RT\rho_w d_m(\mathrm{RH})}\right)\right)^{-1}. \tag{S5}$$

Here $\sigma_{s/a}$ and M_w are the surface tension and molecular weight of pure water (0.072 J m^{-2} and 18^{-3} kg/mol, respectively), R is the universal gas constant, T is the absolute temperature, ρ_{w} is the density of water and d_m is the diameter of the particles at 87% RH.

The single hygroscopic parameter κ (i.e., calculated using the Eqs. S4 and S5) can be used for predicting the hygroscopic factor of the same particles at 99% RH (i.e., similar to that inside the human respiratory system) as follows:

$$g\ (99\%) = \left(1 + \kappa_{\mathrm{HTDMA}}\left(\frac{a_w}{1-a_w}\right)\right)^{1/3}. \tag{S6}$$

In Eq. S6, the water activity of the solution droplet (a_{w}) is calculated iteratively for 99% RH using Eq. S5.

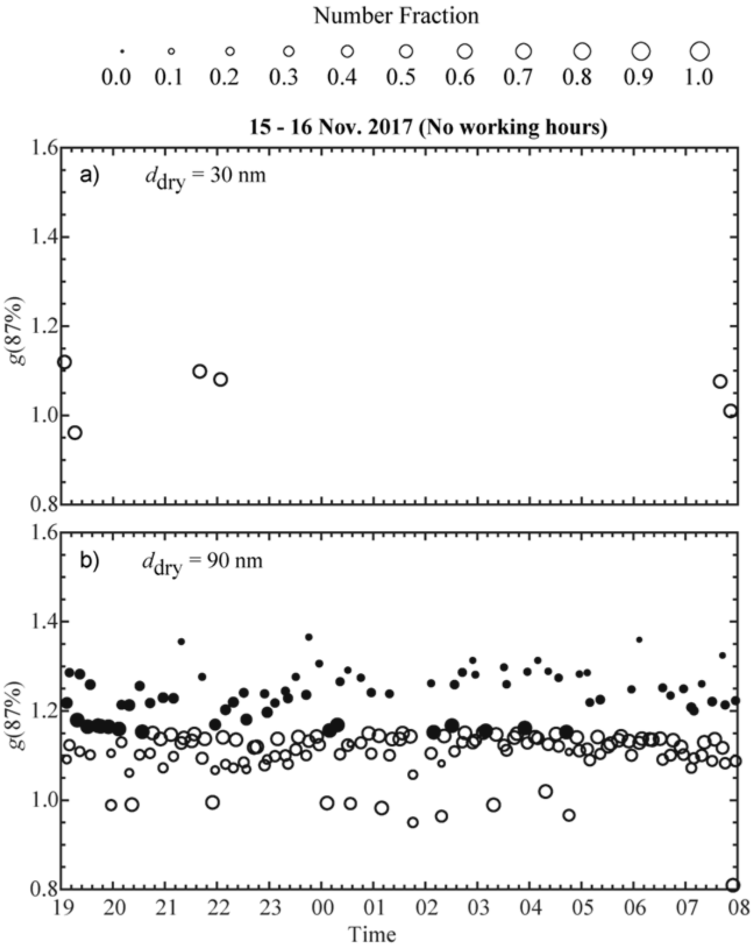

Figure S5. HTDMA measurements of particles having dry mobility diameters of 30- (**a**) and 90- (**b**) nm, sampled from during the non-working hours on 15-16 Nov. 2017. The size of the symbols (i.e., the size of the circles) is proportional to the number fraction of each hygroscopic mode. Particles which exhibited hygroscopic factor below 1.15 (hydrophobic/less hygroscopic; HP) are denoted with different symbols (i.e. open circles), than the more hygroscopic ones (i.e., hygroscopic factor > 1.15; HS).

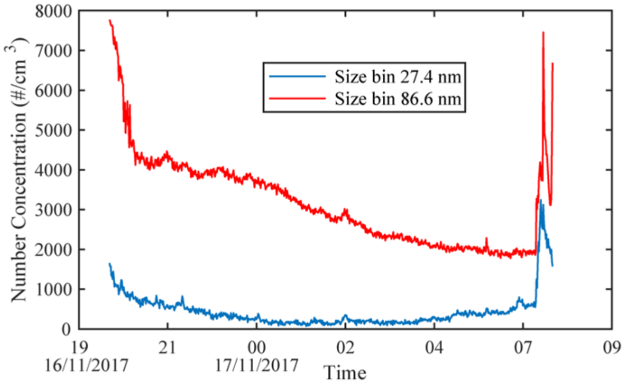

Figure S6. Number concentrations of particles classified by the NanoScan-SMPS as having midpoint electrical mobility diameters of 27.4 and 86.6 nm, measured during the non-working hours between 16 and 17 Nov. 2017. These size bins were selected due to their proximity to dry electrical mobility diameters selected by the HTDMA (i.e., 30 and 90 nm, respectively).

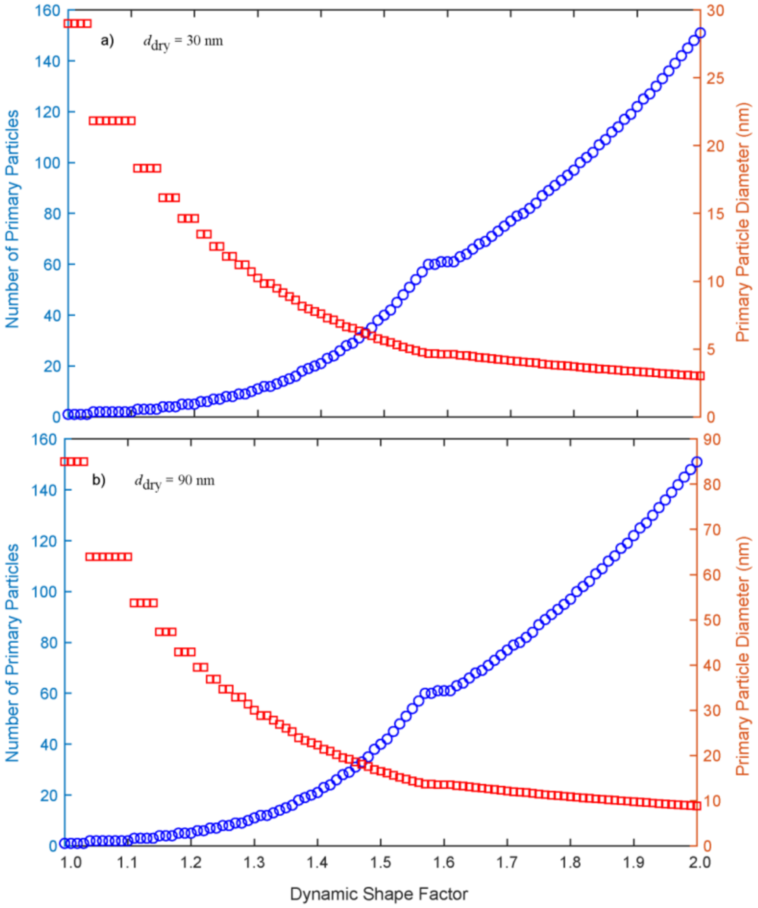

Figure S7. Number and size of primary particles forming aggregate/agglomerate particles with dry electrical mobility diameters of 30 (**a**) and 90 (**b**) nm as a function of their dynamic shape factor χ. The results, especially for $\chi < 1.2$, appear to have the same values for a range of χ, due to rounding the number of primary particles, which has to be integer.

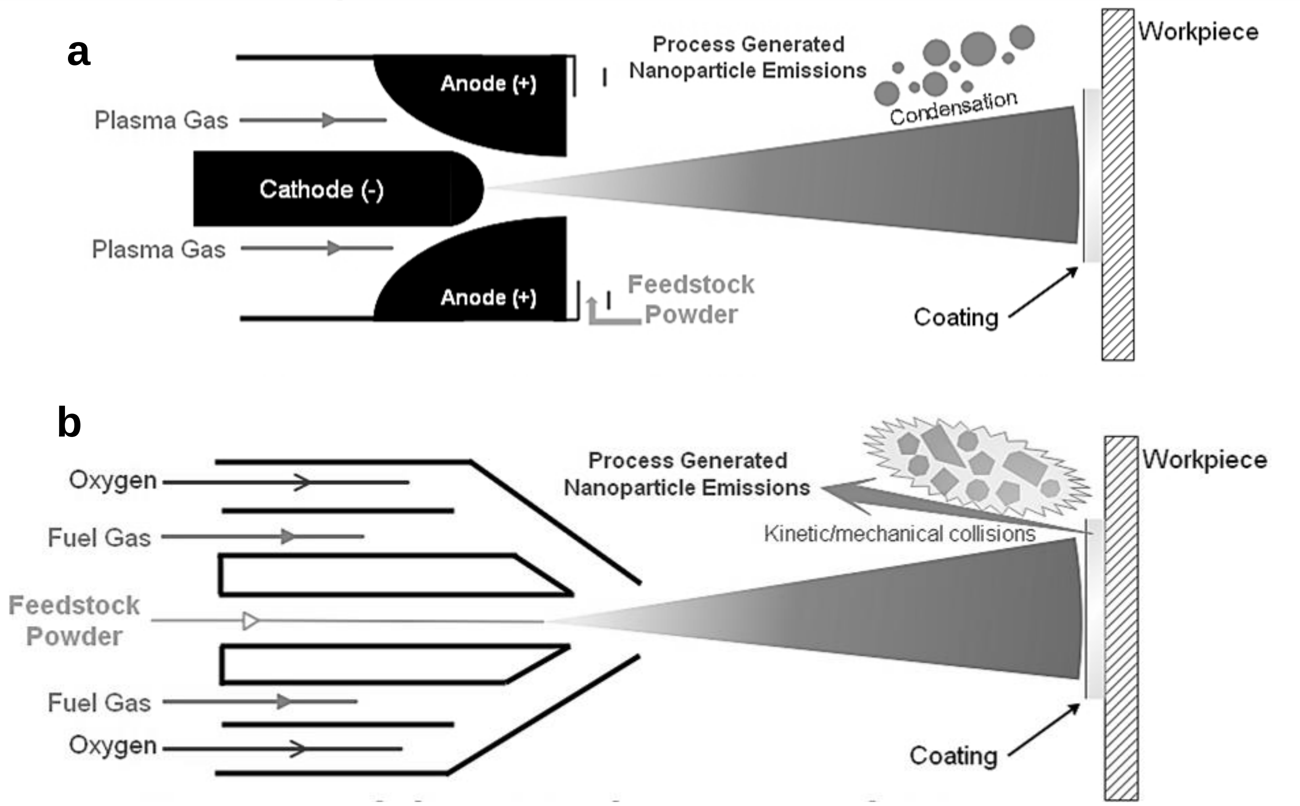

Figure S8. Schematic illustration of the thermal spraying techniques, (a) APS and (b) HVOF and their potential particle emission mechanisms.

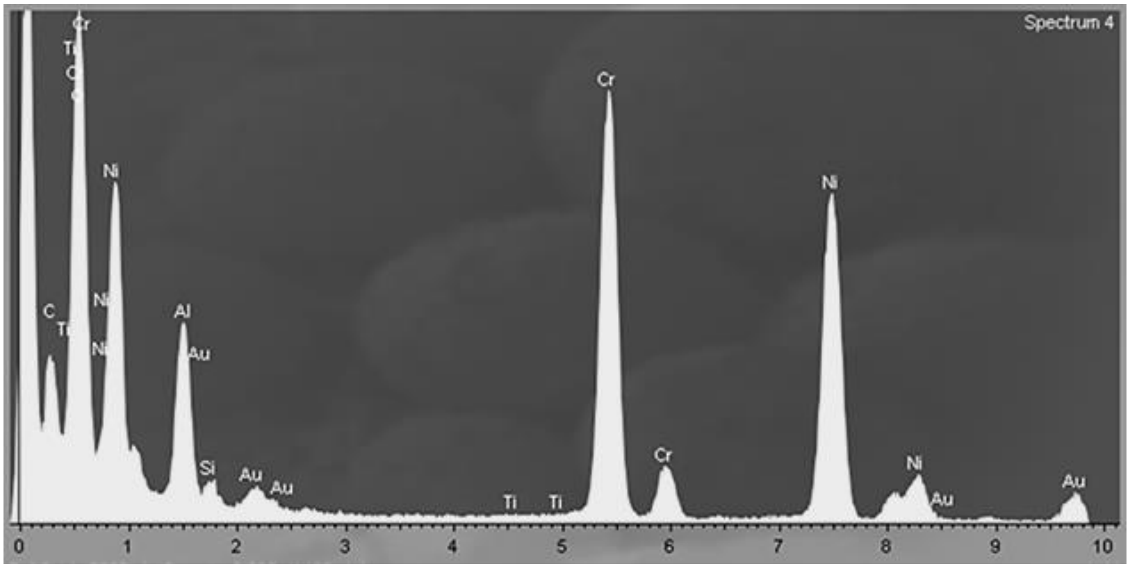

Figure S9. EDX analysis from the respective TEM samples of emitted UFP from (a) APS and (b) HVOF

Table S1. Average hygroscopic factors together with their respective number fractions for different time intervals during the measuring period. Here $d_{m,dry}$ stands for the electrical mobility diameter of particles selected by DMA-1 of the HTDMA. The average hygroscopic factors g_1, g_2 and their respective average number fractions, FR$_1$, FR$_2$ are obtained for two different hygroscopic modes (i.e., externally mixed samples). If during a time interval, only one mode is present (i.e., internally mixed particles), then the g value of the second mode is assigned with "NaN" while its respective FR is assigned with 0. The starting and ending times of the time intervals are denoted with "date S" and "date E", respectively. These time intervals of interest are based upon different activities (cf. table legend). Finally, the symbol "#" denotes in which booth (i.e., 1,2,3) the inlet of the HTDMA was located. During the end of the measuring campaign the HTDMA was sampling from the area, outside booth #3 and these time intervals are denoted with the letter "C" in the same column.

Booth #1	Booth #3	No working hours	Launch break
🟧	▨	🟩	🟩

$d_{m,dry}$	g_1	g_2	FR$_1$	FR$_2$	date S	date E	#
30	NaN	1.16	0.00	1.00	15/11/2017 14:40	15/11/2017 15:00	1
30	1.07	1.27	0.60	0.40	15/11/2017 15:00	15/11/2017 16:00	1
30	1.12	1.30	0.64	0.36	15/11/2017 16:15	15/11/2017 16:45	1
30	1.10	1.17	0.75	0.25	15/11/2017 16:45	15/11/2017 17:25	1

30	1.07	1.29	0.98	0.02	15/11/2017 18:00	16/11/2017 8:00	3
30	1.07	1.26	0.79	0.21	16/11/2017 8:00	16/11/2017 12:25	3
30	NaN	1.32	0.00	1.00	16/11/2017 12:25	16/11/2017 12:35	3
30	0.89	1.21	0.57	0.43	16/11/2017 12:45	16/11/2017 13:00	3
30	0.98	1.27	0.71	0.29	16/11/2017 13:00	16/11/2017 14:30	3
30	1.11	1.20	0.50	0.50	16/11/2017 14:30	16/11/2017 15:10	3
30	1.03	1.17	0.50	0.50	16/11/2017 15:10	16/11/2017 15:50	3
30	1.08	1.28	0.57	0.43	16/11/2017 15:50	16/11/2017 17:00	3
30	1.10	NaN	1.00	0.00	16/11/2017 17:45	16/11/2017 18:30	3
30	1.01	1.11	0.93	0.07	16/11/2017 18:30	16/11/2017 20:00	3
30	0.91	1.16	0.89	0.11	16/11/2017 20:00	16/11/2017 22:20	3
30	1.09	1.27	0.01	0.99	17/11/2017 8:50	17/11/2017 10:20	3
30	1.10	NaN	1.00	0.00	17/11/2017 10:20	17/11/2017 11:20	3
30	1.09	1.25	0.69	0.31	17/11/2017 11:20	17/11/2017 12:20	3
30	1.08	1.42	0.97	0.03	17/11/2017 12:20	17/11/2017 13:00	C
30	1.10	1.29	0.58	0.42	17/11/2017 13:00	17/11/2017 14:30	C
30	1.02	1.50	0.83	0.17	17/11/2017 14:30	17/11/2017 14:50	C
30	1.15	NaN	1.00	0.00	17/11/2017 14:50	17/11/2017 15:30	C

$d_{m,dry}$	g_1	g_2	FR_1	FR_2	date S	date E	#
90	1.08	1.33	0.32	0.68	15/11/2017 16:15	15/11/2017 16:45	1
90	0.84	NaN	1.00	0.00	15/11/2017 16:45	15/11/2017 17:25	1
90	1.10	1.22	0.72	0.28	15/11/2017 18:00	16/11/2017 8:00	3
90	1.08	1.24	0.47	0.53	16/11/2017 8:00	16/11/2017 12:25	3
90	0.85	1.12	0.38	0.62	16/11/2017 12:35	16/11/2017 12:45	3
90	1.11	NaN	1.00	0.00	16/11/2017 12:45	16/11/2017 13:00	3
90	1.16	1.32	0.54	0.46	16/11/2017 13:00	16/11/2017 14:30	3

90	1.06	1.34	0.85	0.15	16/11/2017 14:30	16/11/2017 15:10	3
90	0.89	NaN	1.00	0.00	16/11/2017 15:10	16/11/2017 15:50	3
90	1.16	1.29	0.28	0.72	16/11/2017 15:50	16/11/2017 17:00	3
90	1.09	1.33	0.71	0.29	16/11/2017 17:00	16/11/2017 17:45	3
90	0.89	NaN	1.00	0.00	16/11/2017 17:45	16/11/2017 18:30	3
90	1.07	1.23	0.48	0.52	16/11/2017 18:30	16/11/2017 20:00	3
90	1.13	NaN	1.00	0.00	16/11/2017 20:00	16/11/2017 22:20	3
90	1.15	1.34	0.24	0.76	17/11/2017 8:50	17/11/2017 10:20	3
90	0.90	1.44	0.91	0.09	17/11/2017 10:20	17/11/2017 11:20	3
90	1.01	1.25	0.73	0.27	17/11/2017 11:20	17/11/2017 12:20	3
90	1.00	1.22	0.51	0.49	17/11/2017 12:20	17/11/2017 13:00	C
90	1.08	NaN	1.00	0.00	17/11/2017 13:00	17/11/2017 14:30	C
90	0.88	1.09	0.62	0.38	17/11/2017 14:50	17/11/2017 15:30	C

Sources of uncertainty when exceeding the nominal maximum number concentration of the NanoScan-SMPS.

During plasma spraying activities in both booth #1 and #3 the Nanoscan-SMPS often reported total concentration values >10^6 cm^{-3}, reaching in some cases 5 x 10^6 cm^{-3}, thus exceeding the nominal maximum total number concentration limit of the instrument (as stated by the manufacturer; TSI). While the instrument manufacturer does not recommend its use, under these high concentrations, these measurements can still be valid, although with slightly increased uncertainties, if all the individual parts of the Nanoscan-SMPS operate within (or slightly above) their designed limits (personal communication with TSI). A major concern with SMPS measurements under very high number concentrations is the response of the particle detector (i.e., most usually a CPC downstream the DMA), which could reach its maximum counting ability, thus reporting the same (i.e., the maximum) number of particles through a wide number of size bins (or even at all of them). This has a major impact in both the number concentration but also in the size that the instrument reports. Such behavior however, was never encountered in our measurements (cf. Figs 1 and 2). Another part of concern under very high particle concentrations is the DMA of an SMPS system, as the motion of charged particles inside the DMA is not only dictated by the DMA's electric field but it can be distorted as they electrically interact between each other. However, such a behavior has been observed mainly for small nanoparticles (ca. 10 nm), which require low classification voltages, in DMAs operating with > 10^8 cm^{-3} (Camata et al., 2001). Another part that can be affected by very high particle number concentrations of particles is the charger of an SMPS system, as its efficiency can by reduced. The NanoScan-SMPS carries a corona charger and its ion current is constantly monitored and regulated, within some limits, by the instrument itself. In extreme cases (i.e., when the number concentration of particles exceeds by far the design characteristics of the charger) the ion current drops significantly and the instrument reports an error. In less extreme conditions, (i.e., the instrument's charger operates at reduced efficiency but without reporting ion current error), deviations in particle size and number concentration may appear (i.e., the instrument will report reduced particle size and number concentration than the actual one). In our measurements a current error was never encountered, indicating that the NanoScan-SMPS charger was operating within its (ion current) design limits. In addition, previously published measurements, obtained with the same instrument, the same technique, outside (i.e., far field) of the spray booths, at the same workplace, where the total number concentration of particles was $<10^5$ cm^{-3} (i.e., well within the instruments concentration limit), reported similar sizes of particles as the ones measured in this campaign, during thermal spraying activities (cf. Salmatonidis et al., 2019). This is a strong indication that the performance of the instrument was not demoted by the $>10^6$ cm^{-3} particle number concentrations, encountered within the spraying booths in this campaign.

REFERENCES:

Allen, M. D and Raabe O. G. Slip correction measurements of spherical solid aerosol particles in an improved Millikan apparatus. Aerosol Sci. Technol., 4:269-286, 1985.

Baron P. A and Willeke,K. Aerosol Measurement: Principles, Techniques and Applications. Second Edition, Willey-InterScience, Inc., 2001.

Camata, R.P., Atwater, H. A., Flagan, R. C., Space-charge effects in nanoparticle processing using the differential mobility analyzer. Aerosol Science 32, 583-599, 2001.

Davies, C. N. Definitive Equations for the Fluid Resistance of Spheres. *Proc. Phys. Soc.*, 57:259–270, 1945.

Hinds, W.C. *Aerosol Technology.* New York: John Willey and Sons, 1999.

Kreidenweis, S.M., Petters, M.D., DeMott, P.J.: Single parameter estimates of aerosol water content, Environ. Res. Lett., 3, 035002, 2008.

Petters, M.D. & Kreidenweis S.M.: A single parameter representation of hygroscopic growth and cloud condensation nucleus activity, Atmos. Chem. Phys., 7, 1961-1971, 2007.

Salmatonidis, A., Ribalta, C., Sanfélix, V., Bezantakos, S., Biskos, G., Vulpoi, A. Simion, S., Monfort, E. and Viana, M. *Ann. Work Expo. Heal.*, 2019, **63**, 91–106.

4.4. Scientific publication 4

Effectiveness of nanoparticle exposure mitigation measures in industrial settings

Salmatonidis A.[a,b] *, Sanfélix V.[c], Carpio P.[c,d], Pawłowski L.[e], Viana M.[a], Monfort E.[c]

[a]*Institute of Environmental Assessment and Water Research (IDAEA-CSIC),08034 Barcelona, Spain*

[b]*University of Barcelona, Faculty of Chemistry, 08028 Barcelona, Spain*

[c]*Institute of Ceramic Technology (ITC), Universitat Jaume I, 12006 Castellón, Spain*

[d]*Polytechnic University of Valencia, 46022 Valencia, Spain*

[e]*Institute of Research on Ceramics (IRCER), UMR CNRS 7315, 97068 Limoges, France*

Published in: International Journal of Hygiene and Environmental Health, 2018, Volume 222, Pages 926–935

DOI: 10.1016/j.ijheh.2019.06.009

The following is a pre-print version, which was produced by the author, of an article submitted to International Journal of Hygiene and Environmental Health (Elsevier): Submitted on 21 February 2019; revised on 27 May 2019; accepted on 24 June 2019. Available online at:

https://doi.org/10.1016/j.ijheh.2019.06.009

Effectiveness of nanoparticle exposure mitigation measures in industrial settings

*Salmatonidis A.[a,b] *, Sanfélix V.[c], Carpio P.[c, d], Pawłowski L.[e], Viana M.[a], Monfort E.[c]*

[a]Institute of Environmental Assessment and Water Research (IDAEA-CSIC),08034 Barcelona, Spain

[b]University of Barcelona, Faculty of Chemistry, 08028 Barcelona, Spain

[c]Institute of Ceramic Technology (ITC), Universitat Jaume I, 12006 Castellón, Spain

[d]Polytechnic University of Valencia, 46022 Valencia, Spain

[e]Institute of Research on Ceramics (IRCER), UMR CNRS 7315, 97068 Limoges, France

** Corresponding author: A. Salmatonidis; Present address: Jordi Girona 18, 08034 Barcelona, Spain; email: apostolos.salmatonidis@idaea.cisic.es*

Abstract

Inhalation of airborne nanoparticles is a well-known source of potentially health-hazardous occupational exposures. Effective mitigation measures are necessary to reduce exposure, but also challenging to implement due to the different characteristics of each individual emission source and industrial scenario. The present paper describes four different exposure case studies in the ceramic industry and quantifies the effectiveness of mitigation strategies implemented during: ceramic tile processing by thermal spraying, laser ablation, the use of diesel engines, and tile firing. The mitigation measures for exposure reduction were tailored to each industrial scenario. The NP removal efficiency of source enclosure (partial/full) combined with local exhaust ventilation (LEV) were quantified to range between 65-85% when the enclosure was partial. The efficiency reached 99% with full enclosure and vigorous ventilation (Air Change per Hour; ACH =132 h^{-1}). The elimination of the source was the optimal strategy to minimize exposure in the case of diesel forklifts use. The conventional ceramic kilns used intensively (>10 years) generated high NP exposure concentrations ($>10^6$ /cm^3). Appropriate maintenance and enhanced sealing enabled the reduction of exposure down to 52% of the initial value. It must be added that technologically advanced kilns, enabled even greater NP reductions (down to 84%), compared to the conventional ones. This proves technological improvements can lead to significant reduction of work exposures. This work evidences the need for tailored mitigation measures due to the broad variety of potential sources and activities in industrial scenarios. The quantitative efficiency rates reported here may be valuable for the adequate parametrization of exposure prediction and risk assessment models.

Keywords: risk assessment; worker health; hygiene and safety; non-engineered nanoparticles; ceramic industry; thermal processes

1. Introduction

The adverse effects of exposure to fine and coarse particles are well described in the literature (Pope et al., 1995; Pope and Dockery, 2006). Exposure to nanoparticles (<100 nm; NPs) in workplaces has been an issue of concern for the last decades, and the subject of numerous research studies (Brouwer, 2010; Brouwer et al., 2009, 2004; Hämeri et al., 2009; Seaton et al., 2010; Wiesner et al., 2006). The health impacts deriving from inhalation of NPs results from their capacity to penetrate into the deeper sections of the respiratory tract due to their small size has been established (Oberdorster, 2000; Oberdorster et al., 1992). NPs are also able to translocate to other body organs through the blood stream (Donaldson et al., 2005; Oberdörster et al., 2004). Other health hazardous factors are their surface area and chemical composition, which determine toxicological responses and interactions with biological molecules (Schmid and Stoeger, 2017).

Nanoparticles found in industrial workplaces and impacting exposure originate generally from two sources: (i) emission resulting from industrial activities and (ii) background aerosols. Nanoparticles in ambient background air, frequently referred to as ultrafine particles (UFPs), result from anthropogenic emissions (e.g. combustion products from vehicles) and from new particle formation (e.g., atmospheric nucleation) among other sources (Brines et al., 2015; Kulmala et al., 2014; Pey et al., 2009). The NPs emitted by industrial activities may be engineered and used as input/output in the manufacturing process, or non-engineered and formed unintentionally as a result of a given industrial activity. The latter are also referred to as process-generated (PGNPs; Van Broekhuizen et al., 2012) and incidental NPs (Viitanen et al., 2017) are the subject of the present study which is focused on ceramic industry.

A recent literature review, which assessed publications reporting industrial sources of UFPs particles and exposure concentrations in workplaces (Viitanen et al., 2017) concluded that real exposures (e.g. in welding and metal industry) were more than hundred times greater than those resulting from background aerosols. The obtained results of measurements were not conclusive enough to draw general conclusions with regard to exposure. In particular, NP release in the ceramic industry resulting in worker exposures can be found in traditional pottery (Voliotis et al., 2014), in ceramic tiles sintering (Fonseca et al., 2016) and in innovative processes (Fonseca et al., 2015; Salmatonidis et al., 2018) such as high energy ones (e.g. thermal spraying; Salmatonidis et al., 2019; Viana et al., 2017). Hence, there is sufficient evidence to conclude that unintentional NP release generates statistically significant impacts on worker exposure in the ceramic industry.

Consequently, efficient exposure mitigation strategies must be implemented. Certain measures are based on industrial practices and on the hierarchy of control methods (Conti et al., 2008; E.U., 2014; Gerritzen et al., 2006; Schulte et al., 2008). The European Council Directive 98/24/EC (E.U., 2014) recommends the elimination or isolation of sources as methods to minimize exposures to hazardous substances in workplaces. If these measures are not applicable, engineering controls should be applied (e.g. dilution and local exhaust ventilation) and finally personal protective equipment (PPE), such as respirators or masks are recommended. A recent review that quantified the efficiency of PPE and engineering controls (Goede et al., 2018), especially for engineered NPs in controlled scenarios such as laboratories, reported that the available data are inconclusive. Previous studies discussed the efficiency of PPE such as protective gloves, clothes, filtering facepieces respirators and half mask respirators (Kim et al., 2006, 2007; Lee et al., 2007; Myojo et al., 2017; Tsai et al., 2010). A review of this literature, based on search terms “nanoparticles”, “protective equipment” “ventilation”, “extraction”,” safety”, “mitigation”, evidenced that: (i) studies for incidentally-released NPs are less frequent than for engineered ones; (ii) in spite of a great number of studies on PPE efficiency, less information can be found about the effectiveness of applied technical measures, and they refer mostly to laboratory-scale; (iii) the results obtained cannot be easily generalized beyond the specific cases; and (iv) experimental studies at industrial scale constitute a clear research gap. The diversity of industrial processes poses a major challenge when assessing the effectiveness of exposure mitigation measures. The literature shows that data regarding the efficiency of NP exposure mitigation measures in real world facilities, at an industrial scale, are scarce and not standardized. This is not the case for coarse and fine particles, for which the Exposure Control Efficacy Library (ECEL) provides information on the efficacy of control methods for inhalation exposure (Fransman et al., 2008), mainly focusing on particle mass concentration as main metric (as opposed to particle number concentration, used for NPs). It should be added that the quantitative data on exposure reduction for specific technological measures are also a key input for exposure prediction models applied to indoor settings in the framework of risk assessment (e.g., one- and two-box models; Hewett and Ganser, 2017; Hussein and Kulmala, 2008; Nazaroff, 2004; Ribalta et al., 2019).

The present work aims to quantify the efficiency of measures for NP exposure reduction implemented under real-world operating conditions in the ceramic industry. These measures include: (i) ventilation (extraction and dilution); (ii) source enclosure; (iii) source substitution; and (iv) periodical source isolation. The efficiency of the measures was assessed by a case study approach. The approach presented consists of characterization of NP exposure before and after the implementation of mitigation measures. The exposure reductions are characterized by the measurements of particle number concentrations. It should be noted that this study does not aim to discuss the measured exposure concentrations from a regulatory compliance perspective. Thus, this work aims to expand the current literature on exposure mitigation strategies by contributing with quantitative assessments of effectiveness of specific technical measures. The data obtained will make a valuable contribution for the adequate parametrization of exposure prediction and risk assessment models.

2. Materials and methods

2.1 Particle emission scenarios

Four particle emission scenarios were evaluated:

(A) *Thermal spraying deposition of coatings*

Particle monitoring was carried out during processing using atmospheric plasma spraying (APS) in a semi-industrial pilot plant. Details on this industrial technique and on the NPs generated may be found elsewhere (Salmatonidis et al., 2019; Viana et al., 2017). The APS installation was located inside the spraying room with a torch installed on a robot. The pilot plant included three compartments like the one in Figure 1. The spraying room and the worker's room were connected by an interior door

(Figure 1), which may remain either closed or open (binary condition) during processing. The door remains closed in routine processing (source enclosure). Sometimes, the operator should intervene manually and the door was open (source partial enclosure). The APS area was equipped in with a local exhaust ventilation (LEV) system. The particle monitoring locations were: (i) the spraying room (emission source); (ii) the worker´s room (exposure area); and (iii) outdoor background (located in the corridor outside of the worker´s room; Figure 1). The monitoring instruments were placed on a desk, next to the operator at breathing height but not directly at the worker breathing zone. The mitigation variables modified were door configuration (closed or open) and extraction flow rate in the studied APS rooms, these two variables can be expressed in a single parameter: air changes per hour (ACH).

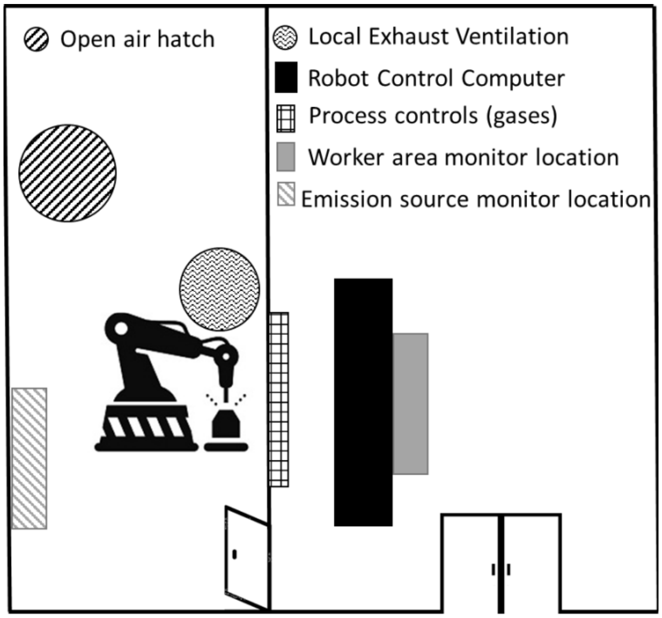

Figure 1. Schematic illustration of the APS facility (scenario A), spraying room (left) and worker room (right).

(B) Laser ablation of ceramic tiles

The use of this technology in ceramic tile treatment and NP release mechanisms were studied previously in laboratory (Salmatonidis et al., 2018) and in pilot-plant scales (Fonseca et al., 2015). In this case study, the NP emissions associated to laser ablation of fired ceramic tiles was studied in an industrial facility, in which the laser source was located in a partially closed chamber having volume of 5.6 m^3 equipped with a LEV system having ventilation capacity of about ca. 2000 /m^3. The laser processing was carried out discontinuously, with laser working cycle duration of ca. 2 minutes. The measurements were performed at a distance of ca. 0.5 m from the emission source what is, representative of the worker exposure area (Figure 2). The efficiency of NP reduction was measured at: (i) laser inactivity (background); (ii) laser ablation with LEV; and (iii) laser ablation without LEV.

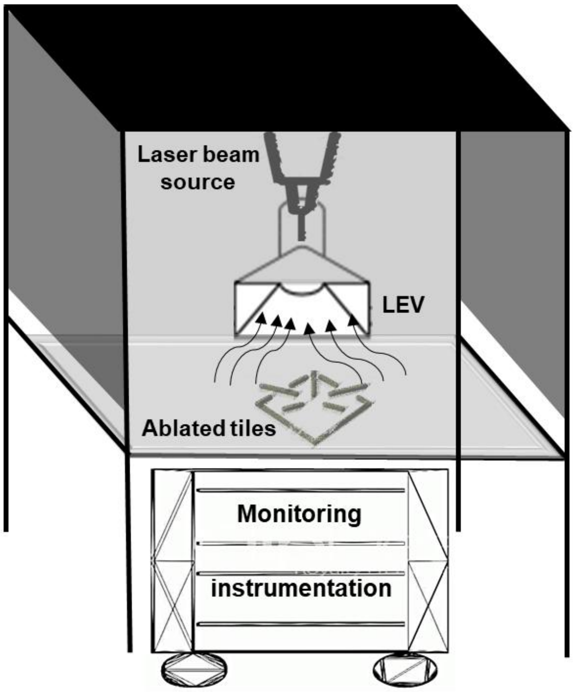

Figure 2. Schematic illustration of the measurement set-up during laser ablation of tiles (scenario B).

(C) Diesel engines emissions

The machines powered by diesel engines are widely used in indoor industrial facilities (Gaines et al., 2008). The use should be reduced to comply with the upcoming indoor air exposure limit values for carcinogen contaminants such as diesel soot measured as elemental carbon set by the European Council Directive 2019/130 (EU, 2019). The directive sets the concentration limits equal to 0.05 mg/m^3 after the year 2023., The impacts of the use of two Toyota 2z forklifts having power of 42 kW (EU stage II clear) was studied inside an industrial workplace. The forklifts were continuously operating inside the plant performing loading and unloading of material pallets. In this experiment it was not possible to isolate the source from any secondary ones because of their continuous movement. However, it could be assumed that diesel forklifts were the main NPs source in the worker´s breathing zone. The particle concentration monitoring was performed in a stationary location in the loading and unloading area (worker area). Moreover, a personal monitor was worn by the forklift operator (breathing zone), working in an open cabin. The mitigation measure studied was source substitution based on the use of electrically powered forklifts instead of the diesel ones.

(D) Ceramic tile firing in a roller hearth kiln

The study was carried out in an industrial plant for production of ceramic tiles (glazed white-body earthenware wall tiles) under real operating conditions (peak temperatures around 1150ºC; Ferrer et al., 2015). The activity included the use of a roller kiln (120 m-long), which is the most frequently-used technology for firing ceramic tiles (Mezquita et al., 2014). The experimental measures were performed outside the roller kiln at 1.5m in height and 2m aside from its external walls, every 10 m along the kiln. The monitoring of NPs was performed in three areas which correspond to the firing cycle: heating, firing and cooling. Three particle monitoring campaigns were carried out in the industrial plant. The first campaign monitored a conventional kiln being in an intensive service for ca. 10 years. The second campaign at the former kiln after having done maintenance works in the refractory walls. The third campaign was carried out in a new and technologically advanced kiln with optimized refractory conditions (being less than 2 years in service).

2.2 Mitigation strategies implemented and assessed

The case studies were performed to allow the assessment of three different mitigation strategies. The strategies were classified following the hierarchy approach (E.U., 2014; Schulte et al., 2008) as:

- **source substitution/elimination,** tested in particle emission scenario (C) in which the diesel forklifts were substituted by the electric ones.
- **source isolation,** tested in particle emission scenario (D) which comprised maintenance and sealing improvement for enhancing source enclosure, during the operation of a roller kiln firing ceramic tiles.
- **engineering controls,** tested in the particle emission scenarios (A) and (B) (thermal spraying and laser ablation, respectively) in which ventilation and LEV system were combined with source enclosure.

The particle emission scenarios and the mitigation measures are shown in Table 1. All data were obtained under real industrial operating conditions. The conditions include the production scale (from kgs to tons), facility surface area (from tens to thousands m^2), the number of workers (from two to hundreds). The efficiency of mitigations measures was quantitatively determined, but some practical limitations must be mentioned. Namely, the different mitigation measures overlapped in some scenarios (e.g., LEV and partial source enclosure were operating in parallel in the APS facility) or potential influence of external sources resulting from inadequate isolation of studied areas B, C and D.

Table 1. Particle emission scenarios and applied mitigation measures.

Case study	Activity-Source	Scale of facility	Mitigation measure
A	Atmospheric plasma spraying	Semi-industrial	Engineering controls: LEV & partial/full enclosure
B	Laser ablation	Industrial	Engineering controls: LEV & partial enclosure
C	Diesel forklifts	Industrial	Source substitution
D	Ceramic tile firing	Industrial	Source isolation: refurbishment & technology upgrade

2.3 Particle monitoring instrumentation

Workplace exposure assessments were carried out by monitoring particle number concentration and their mean diameter, using online instrumentation (Table 2). The monitors measured particle diameters range from 4nm to 32µm. Particle number concentrations were monitored with fixed and portable instrumentation (TSI CPC 3775; DiSCmini, TESTO) and size distributions were measured using NanoScan-SMPS (TSI 3910) and a laser spectrometer (Mini WRAS 1371, GRIMM). All instruments were intercompared prior to the measurements for quality assurance purposes. The performance of the DiscMini and NanoScan monitors and the intercomparison methodology were recommended elsewhere (Fonseca et al., 2016; Viana et al., 2015).

Table 2. Instrumentation used for particle monitoring.

Instruments	**Size range (nm)**	**Data recorded**	**Sampling locations**
NanoScan-SMPS (TSI 3910)	10-420	Size resolved particle number concentration (#/cm^3)	Emission source Worker area
Condensation Particle Counter (CPC, TSI 3775)	4-3000	Total particle number concentration (#/cm^3)	Emission source Worker area
Diffusion Size Classifier miniature (DiSCmini, TESTO)	10-700	Particle number concentration (#/cm^3), mean diameter (D_p, nm)	Emission source Indoor background Outdoor background
Mini Laser Aerosol Spectrometer (Mini-LAS 11R, GRIMM)	250-32000	Size segregated mass concentration (µg/m^3)	Emission source Indoor background Outdoor background
Mini Wide Range Aerosol Spectrometer (Mini WRAS 1371, GRIMM)	10-32000	Size resolved particle number concentration (#/cm^3), Size segregated mass concentration (µg/m^3)	Indoor background Outdoor background

Particle number concentrations were monitored at the emission source, in the worker area or in the breathing zone (depending on the scenario) in indoor and outdoor locations (OECD, 2015; Ramachandran et al., 2011). The indoor (background) location was located at a distance greater than 2 m from the emission source in each case to avoid potential interferences. The outdoor location was to evaluate the possible contribution of outdoor sources (e.g., road traffic).

The effectiveness of the exposure mitigation measures (E_{EMM}) was quantified according to Eq. 1:

$$E_{EMM} = (1 - \frac{C_{EMM}}{C_0}) \times 100 \quad (1)$$

where C_0 is the initial particle number exposure concentration before the implementation of mitigation measure, and C_{EMM} is the concentration after its implementation.

The industrial processes do not enable to perform always the measurement without mitigation because of safety requirements. The different approach for calculating the efficiency was applied when mitigation measures were already implemented (e.g., case study A). Namely, the emissions were monitored simultaneously in the emission source and in operator area and the total reduction of particle concentration was calculated according to Eq. 2,

$$E_{EMM} = (1 - \frac{C_{WA}}{C_{ES}}) \times 100 \tag{2}$$

where C_{WA} is the number concentration in the worker area and C_{ES} in the emissions source.

3. Results and discussion

3.1 Source substitution/elimination (C; Diesel engines emissions)

Mitigation measures: the measures implemented consisted of substitution of diesel forklifts (Toyota 2z, 42 kW, EU stage II clear) by electrical ones (STILL RX60-25, emission-free drive) to reduce indoor exposure to soot NPs.

Particle emissions: mean particle number concentrations were 1.1 $\times 10^5$/cm^3 in the worker area, with their mean diameter of 39 nm in the monitored range 10-420 nm. The peak of particle number concentrations in the breathing zone was greater than 2.5*10^3/cm^3 (1-min mean concentrations), corresponded to low mean particle diameters (30-40 nm), characteristic of diesel emissions (Kittelson et al., 2004; Morawska et al., 2008). The particle size distribution in the worker area was lower than 50 nm (83% of the particles) and 51% of them were lower than 30 nm.

Efficiency of the mitigation strategy: Figure 3 shows the comparison between particle number concentrations monitored in the breathing zone, during operation with diesel and with electrical forklift (during 1 h period). Measurements were recorded on two different days, with a time interval of one week. Only one type of forklift was evaluated on each of the days, initially the diesel and then the electrical ones. Background concentrations were monitored simultaneously in a background reference location in the plant, using a DiscMini monitor. This area was not directly affected by any process, and it was located >5m away from the forklift area. Results showed lower particle number concentrations when electric forklifts were used. The maximum exposure concentration (ca. 1*10^5/cm^3) was comparable to the lowest ones recorded when the diesel forklifts were not in operation. A reduction of 49% of particle concentration in the breathing zone, shown in Table 3, was calculated when electrical forklift was used instead of diesel one. This reduction is an average for 1 h monitoring period where forklifts were both operating and stationary. When focusing on the forklift driving intervals and by subtracting the background concentrations, the efficiency of source substitution was 92% (Table 3). It did not reach 100%, due to the fact that measurements were taken on different dates and because of the influence of secondary sources such as diesel engines working outdoors. The re-suspension of the previously deposited fine and coarse particles (with lower contributions in terms of particle number) by the electrical forklifts might have contributed as well.

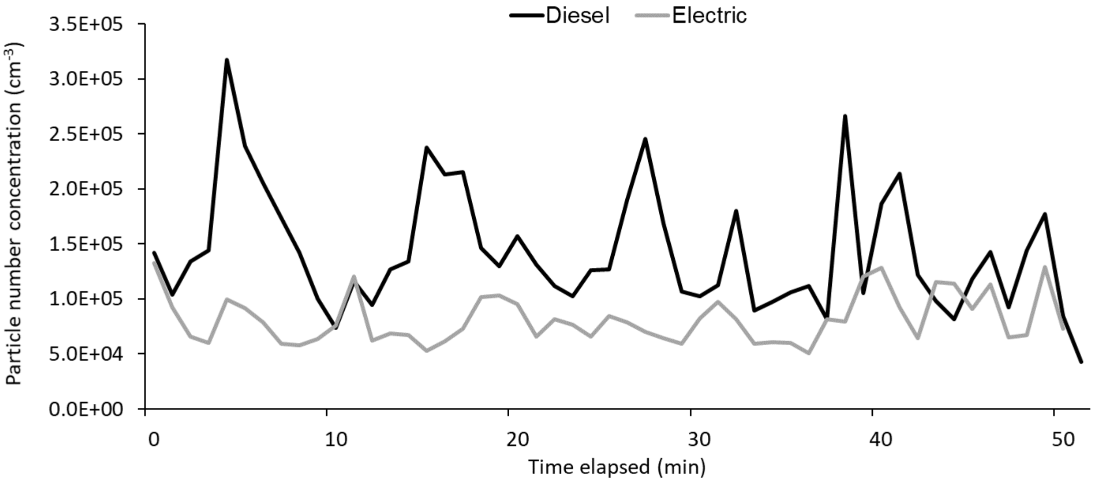

Figure 3. Particle number concentrations monitored in the worker breathing zone (scenario C), at operation using a diesel (black) and an electric (grey) forklift.

Table 3. Efficiency (reduction in particle number concentrations) of the mitigation strategies measured in operating conditions (NP: nanoparticle. LEV: local exhaust ventilation, air change per hour: ACH).

Mitigation measure	NP source	Experimental conditions	Efficiency (%)
Enhanced LEV with enclosure	Thermal spraying (A)	ACH=132 h^{-1}; door closed; exp. #2-#3	98.5-99.8%
Enhanced LEV with partial enclosure	Thermal spraying (A)	ACH=66 h^{-1}; door open; exp.#5	95.4%
LEV with partial enclosure	Thermal spraying (A)	ACH=33 h^{-1}; door open; exp.#4	85.6%
Enhanced LEV with partial enclosure	Thermal spraying (A)	ACH=66 h^{-1}; door close; exp.#1	99.3. %
LEV with partial enclosure	Laser ablation (B)	Extraction flowrate unavailable; partial enclosure	65.1%
Source substitution	Diesel forklifts (C)	Only for driving periods	91.5%
Source substitution	Diesel forklifts (C)	Average of driving and stationary periods, 1 hours	48.7%
Source isolation	Ceramic tile firing (D)	Enhanced sealing of the kiln	51.6%
Source isolation	Ceramic tile firing (D)	Optimal sealing of kiln and superior refractory condition	84.4%

3.2 Source isolation (D; Ceramic tile firing in a roller hearth kiln)

Mitigation measures: two strategies were implemented for assessing the effect of the source enclosure in scenario D: (i) kiln refurbishing by improving the sealing of 10 years old kiln; (ii) replacement of a conventional kiln by a new one of advanced technology and with optimized refractory conditions. To do so, three experimental campaigns were carried out.

Particle emissions: during the first of the three campaigns, in the conventional kiln without implementing any mitigation measure, the highest particle number concentrations were recorded in the zone of maximum temperature of the firing cycle (>8*10^5/cm^3; 46 nm; see Figure 4), which is the main emission area due to the highest temperatures recorded (Fonseca et al., 2016). Concentrations were constant over time in this region, 75% of the particles showed sizes smaller than 50 nm and 40% were smaller than 30nm, indicating nucleation as the main formation mechanism which is also consistent with the literature (Fonseca et al., 2016).

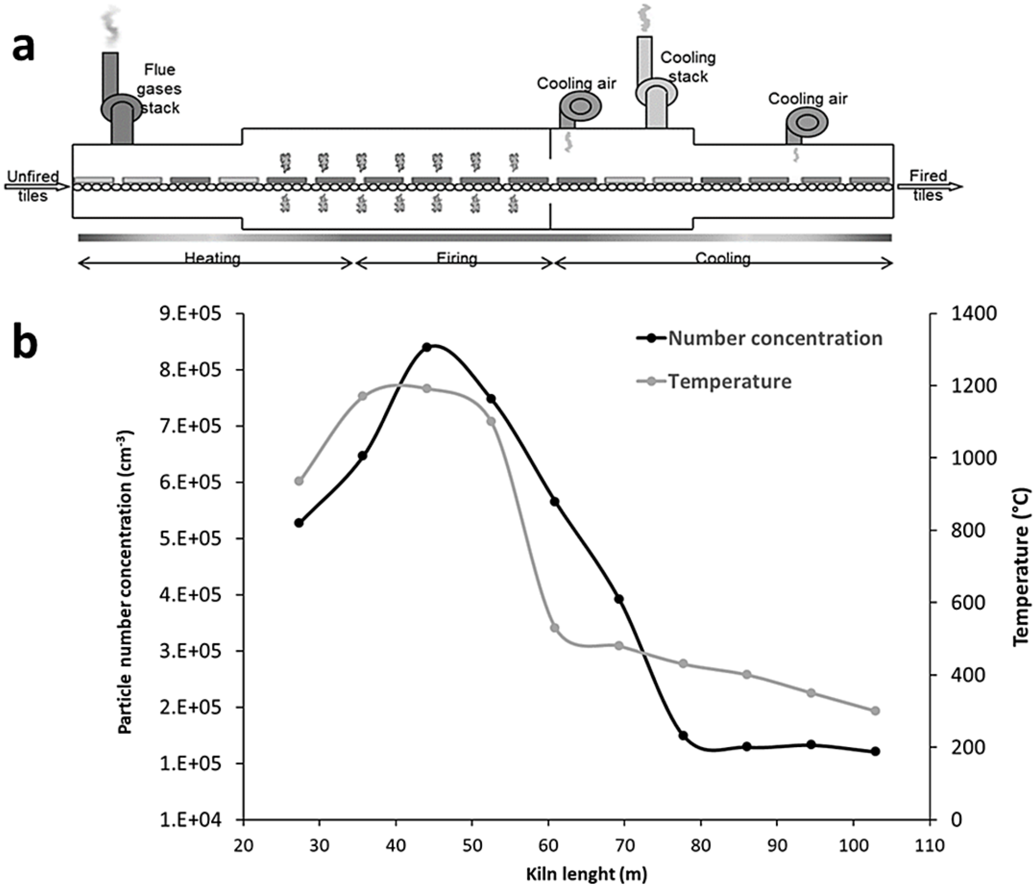

Figure 4. Schematic illustration a roller hearth kiln (scenario D) with the corresponding nanoparticle release (a) and temperature along the kiln (b).

Efficiency of the mitigation strategies: as a first stage to mitigate worker exposure to high NP concentrations, the maintenance and sealing of the old kiln in the firing zone were carried out. The efficiency of these measures was evaluated during the second monitoring campaign. Additionally, in a third stage, a new high-efficiency roller kiln was installed and its emission efficiency was also assessed. The reduction of NP emissions throughout the three different campaigns was observed (Figure S1, Supplementary material). The concentration for the old kiln dropped from 1×10^6/cm^3 to 5×10^5/cm^3 for the refurbished kiln and down to 1.6×10^5/cm^3 measured for the new, advanced kiln (Figure S1).

The adequate maintenance of the old kiln, including enhanced sealing, resulted in 51.6% of NP concentration reduction (Table 3). The particle number concentration decreased from 1×10^6 to 5×10^5/cm^3 along the wall of the kiln's firing zone. The use of new kiln reduced NP concentrations by 84.4%, compared to the old and refurbished one (Table 3). The concentration decreased from 1×10^6/ cm^3 to 1.6×10^5/ cm^3 as shown in Figure 5. These decreases were linked to the different conditions of the refractory materials, which were used to insulate the firing compartment of the kiln. Whereas the renovation of the conventional kiln was able to reduce particle release (52%, Table 3), this reduction was lower than that obtained from the operation of the advanced kiln with superior refractory sealing and energy efficiency, which proved to be also more efficient in terms of emissions reduction (84%, Table 3). In the cooling sections of the kilns (Figure 4a), results evidenced that the exposure concentrations around both kilns (conventional and advanced) were similar. Thus, the effective as well as targeted enclosure of the firing process, the optimum refractory condition and maintenance of the insulating materials are key parameters governing workplace exposure in ceramic tile firing facilities.

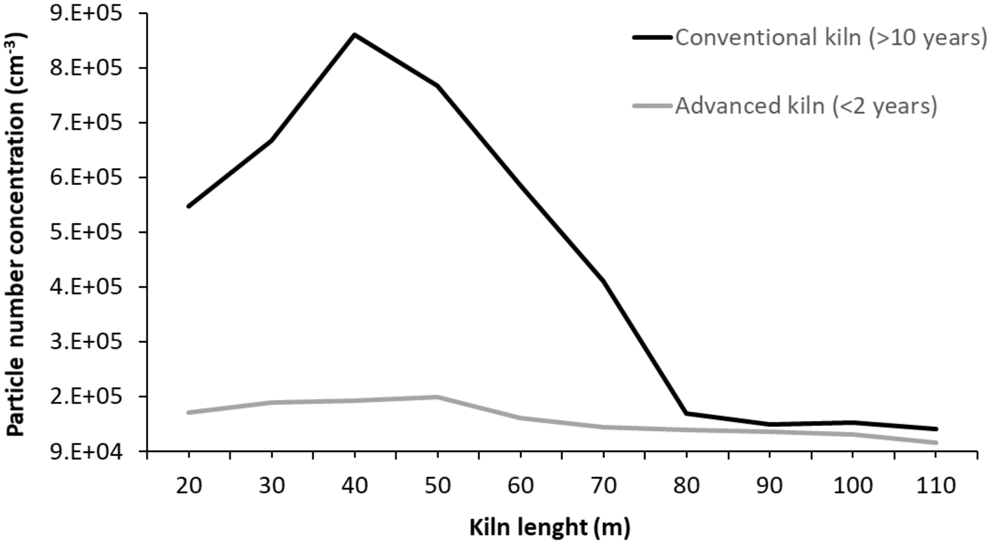

Figure 5. Emissions of particle in terms of number concentration along two kilns (scenario D): conventional (black curve) and advanced (grey curve). The peak at 45 m corresponds to the highest temperature zone (firing).

3.3 Engineering controls: ventilation and LEV system combined with source enclosure (A; thermal spraying deposition of coatings, and B; laser ablation of ceramic tiles)

The efficiency of specific ventilation and LEV combined with source enclosure measures was assessed in two particle emission scenarios described above, namely during: (A) thermal spraying deposition of coatings, and (B) laser ablation of ceramic tiles.

(A) Thermal spraying deposition of ceramic coatings

Mitigation measure: a LEV system was located directly above the APS area, extracting 24000 m^3/hour from three spraying rooms. Therefore, the extraction rate of the LEV fluctuated with the number of APS installations operating simultaneously. It should be noted that the maximum extraction rates can be considered high for such a pilot plant. The LEV system included a capturing hood covering the emission source and a duct without flanges with 0.36m diameter. An open hatch on the ceiling provided air supply to the spraying room when the LEV was active. The air exchange rate (ACH in Eq. 3) varied from 132 to 33 h^{-1} depending on the extraction flow rate of the LEV system and on the binary condition of the interior door (open/closed) influencing the total volume of affected area. The ACH was calculated according to Eq. 3:

$$\frac{Extraction\ flow\ (\frac{m^3}{h})}{Volume\ of\ affected\ area\ (m^3)} = ACH\ (h^{-1}) \tag{3}$$

Particle emissions: in total there were 30 spraying events, 11 for spraying micro-sized NiCrAlY and ZrO_2+(4mol%)Y_2O_3 powders and 19 times for spraying liquid precursors $Zn(NO_3)_2{\cdot}6H_2O$, $Zn(O_2CCH_3)_2$, $C_8H_{12}O_8Zr$). Table 4 summarises the details about representative spraying experiments, as well as the measured exposure concentrations in terms of particle number inside the spraying and the worker room. Mean particle number concentrations ranged between $3.7*10^5/cm^3$ - $1.5*10^6/cm^3$ and mean particle sizes were in the range 26-45 nm inside the spraying room, while in the operator area concentrations ranged from $3.3*10^3/cm^3$ to $5.4*10^4/cm^3$ (Table 4) and sizes from 32-59 nm. For all of the experiments, particle number concentrations were orders of magnitude higher inside the spraying room than in the operator area even when the door was open.

Table 4. Mean particle number concentrations inside the spraying room and in the exposure area (worker room), and experimental details for each of the experimental runs (scenario A, LEV: local exhaust ventilation, air change per hour: ACH).

Experiment parameters				**Particle number concentration (cm^{-3})**		
Run	**Feedstock**	**LEV flowrate (m^3/h)**	**ACH (h^{-1})**	**Interior door**	**Spraying room**	**Worker room**
#1	NiCrAlY	12000	66	closed	9.2×10^5	6.9×10^3
#2	NiCrAlY	24000	132	closed	1.5×10^6	3.3×10^3
#3	ZrO_2+4mol%Y_2O_3	24000	132	closed	6.6×10^5	5.2×10^3
#4	$Zn(NO_3)_2{\cdot}6H_2O$	12000	33	opened	3.7×10^5	5.4×10^4
#5	$Zn(NO_3)_2{\cdot}6H_2O$	24000	66	opened	5.0×10^5	2.3×10^4

Efficiency of the mitigation strategies: different ventilation and door configurations were tested. The most effective mitigation configuration corresponded to the highest ACH rate (132 h^{-1}, experimental runs #2 and 3, powder feedstocks; Table 4). In these experimental conditions the door was closed and the emissions generated inside the spraying room were not transferred to the operator room (Figure 6). The particle number concentrations did not demonstrate any statistically significant increase in the worker room, for both types of powders. Such experimental conditions resulted in about 99% reduction of particle number concentrations between spraying room and the worker – exposure – area (see Table 3).

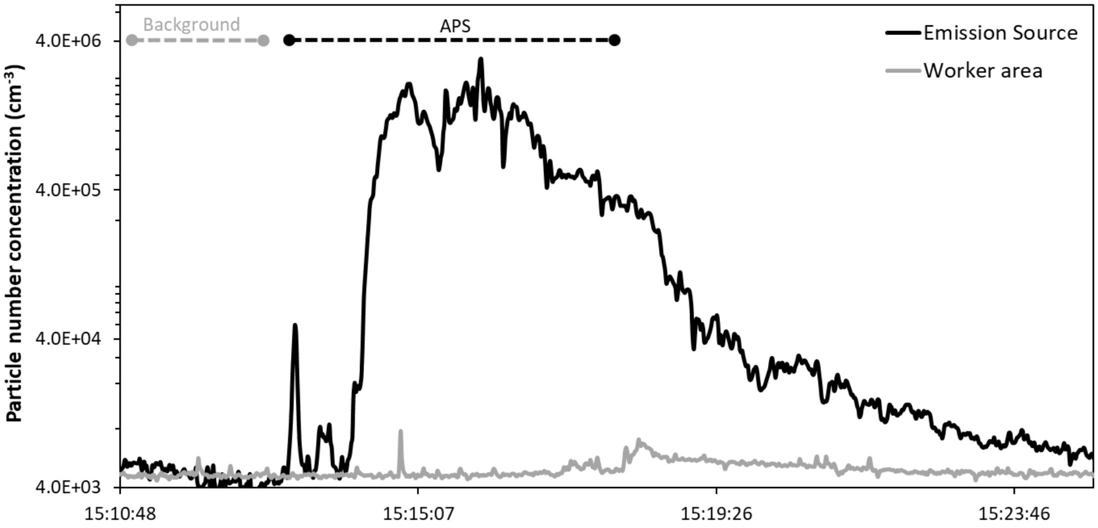

Figure 6. Particle number concentrations (10-700nm with DiscMini) for the experiment #2 inside the spraying room (emission source), and in the worker area (scenario A).

The experimental runs #1 and #2 used the same feedstock (powder) and were performed under the same enclosure conditions, while different ACH values were applied (#1: 66 h^{-1} and #2: 132 h^{-1}; Table 4). However, the efficiency of exposure reduction for the experimental runs #1 (99.3%) and #2 (98.5) were similar and approximately 99% indicating the significance of enclosure against fluctuations on the intensity (flowrate) of a continuously working LEV.

The experimental runs #4 and #5 (liquid-precursor feedstock), were carried out at ACHs of 33 and 66 h^{-1}, respectively and the interior door was open. As expected, when ACH had the lowest value (33 h^{-1}), mean exposure concentrations in the operator area had the highest value ($5.4*10^4/cm^3$; Table 4). Although, the peak concentrations were similar under both ACHs values (see Figure 7a), for ACH=33 h^{-1}, the particle number concentrations decreased at a slower rate than for ACH= 66 h^{-1} resulting in wider peaks with a higher potential for exposure impacts (Figure S2 in Supplementary material). When the air extraction rate was the highest (132 h^{-1}; Figure 7a; during spraying of powders), the peak particle number concentrations were lower than that measured during spraying of liquid precursors (lower ACH). It can be observed that the particle number concentrations decreased at a slower rate when powder was used as feedstock as opposed to liquid one, despite of ACH being almost 4 times higher (132 h^{-1} with powders vs. 33 h^{-1} with liquids; see Figure 7a). This evidenced the influence of the process parameters, as well as the technical mitigation measures implemented. Nevertheless, further research would be necessary to understand the influence of the use of powder or liquid feedstock.

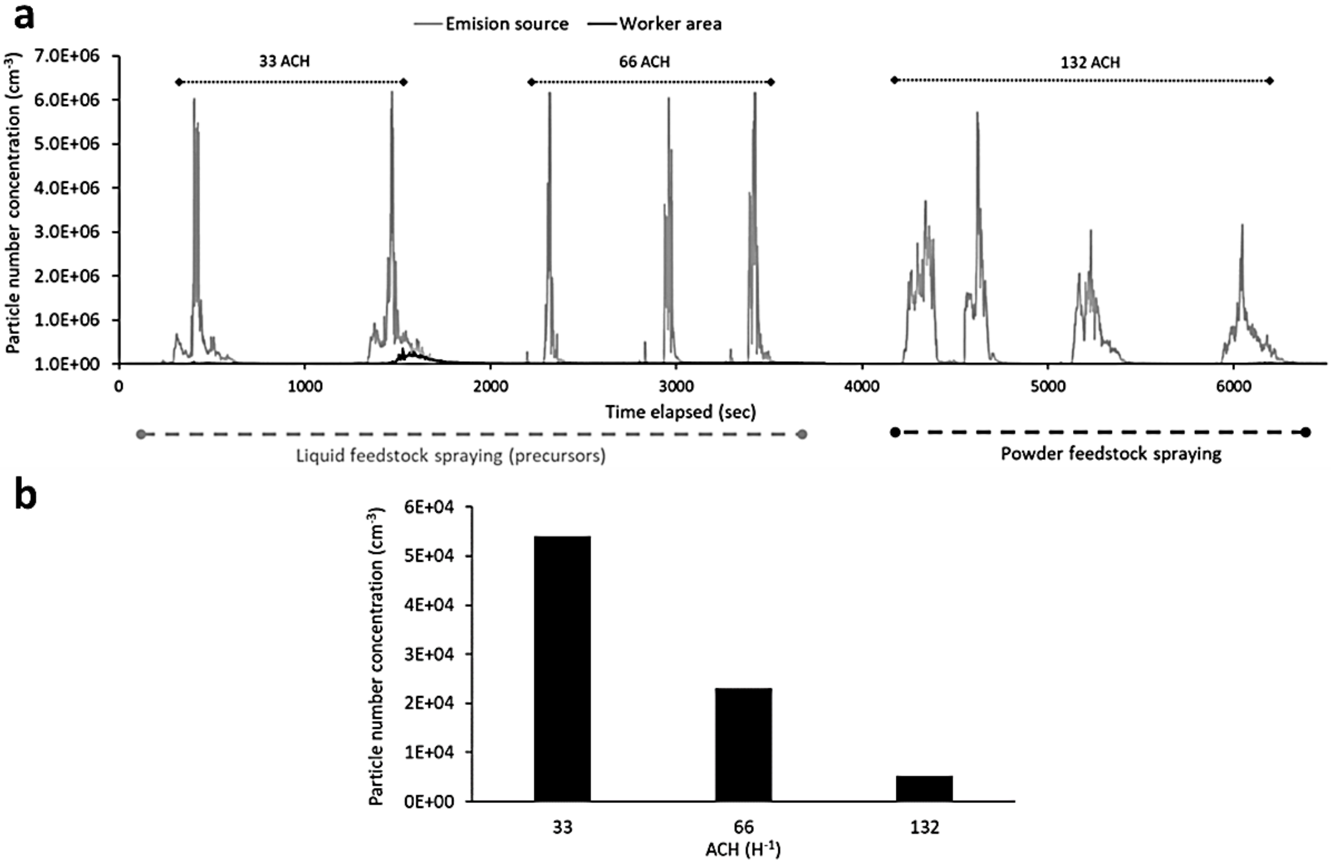

Figure 7. (a) Particle number concentrations (10-700nm with DiscMini) for the experiments #6, #7 and #5 from left to right, (b) number concentration in the worker area for different ACH values (scenario A).

In order to evaluate the influence of enclosure as mitigation measure, the experiments with the same LEV extraction rate (24000 m^3/h) and different door positions are compared in experimental runs #3 (powder feedstock) and #5 (liquid-precursor feedstock). Because of the air volumes were different when the door was open or closed, the ACH factor at the experimental run #3 was 132 h^{-1} and only half of this value, i.e. 66 h^{-1} during experimental runs #5 (liquid-precursor feedstock). During experimental run #3 (powder feedstock; ACH=132 h^{-1}) the mean efficiency of exposure reduction was 98.5%, while during experimental run #5 (liquid-precursor feedstock), with the door open and the same extraction flowrate (24000 m^3/h), the exposure reduction was 95.4% (see Table

3). It can be concluded that, for experimental runs #3 (powder feedstock) and #5 (liquid-precursor feedstock), the impact of the extraction flowrate on exposure mitigation was stronger than that of the enclosure (door open/closed). The difference in reduction efficiency becomes wider when experiments with lower extraction rate (12000 m^3/h) and different door positions are compared (#1 vs. #4; powder vs. liquid-precursor feedstock, respectively). The efficiency decreased to 85.6% during experiment run #4 (liquid-precursor feedstock), which was performed with the door open, while when the door was closed the efficiency was higher (99.3%; Table 3). According to this comparison (#1 vs. #4; powder vs. liquid-precursor feedstock, respectively) the enclosure has a higher influence in reducing exposure than the previous comparison (#3 vs. #5; powder vs. liquid-precursor feedstock, respectively), which is an indication that enclosure becomes more effective when LEV is less efficient, and vice versa. Similar conclusions were drawn by Salmatonidis et al., (2019) during the exposure assessment of thermal spraying processes at industrial scale; where it was demonstrated that despite a fully operating LEV, when the enclosure of the spraying booth was degraded, fugitive emissions significantly impacted exposure in the worker area.

Thus, a combination of different factors (process parameters-feedstock, air flow rate, and enclosure) should be taken into account to improve the efficiency of mitigation measures under real-world conditions. Nevertheless, the most efficient measure is the ACH (coupling LEV with enclosure) as can be observed in Figure 7b, where the reduction of particle number with increase of ACH is evidenced.

(B) Laser ablation of ceramic tiles

Mitigation measure: the laser engraving set up was equipped with a 5.6 m^3 capturing hood, partially enclosed, with an integrated LEV system operating with a fixed extraction flowrate (2000 $m^3\ h^{-1}$). The laser was located in an industrial building of 8000 m^3, naturally ventilated, where a previous screening (not shown) indicated that there were no additional significant NPs sources. Two experimental conditions were evaluated: with and without extraction.

Particle emissions: particles were generated during a repetitive batch process: each tile was ablated during approximately two minutes. Mean particle concentrations monitored in the exposure area reached $6{*}10^5/cm^3$ (maximum). Average concentrations (1-min) during the period with no extraction were $3.5{*}10^4/cm^3$ and mean particles size 175 nm (range 10-700 nm). When the LEV was fully operating the above values altered to $1.2{*}10^4/cm^3$ and 109 nm, respectively.

Effectiveness of the mitigation strategy: Figure 8 shows an evident reduction in particle number exposure concentrations, once the LEV system was activated, with an average efficiency of 65% over a 30-minute monitoring period (Table 3). The exposure reduction was lower than in case study A (with efficiency greater than 85%).The lower efficiency, compared to the thermal spraying, was probably due to worse enclosure in the laser ablation scenario and lower ventilation rate. This result shows the interdependence between extraction and source enclosure. Salmatonidis et al. (2018) demonstrated that during the laser ablation of ceramic tiles, lower extraction and no enclosure were sufficient to mitigate high particle emissions at laboratory-scale. Hence, since the scale of the scenarios might influence the effectiveness of control measures, the assessment in real industrial conditions becomes necessary.

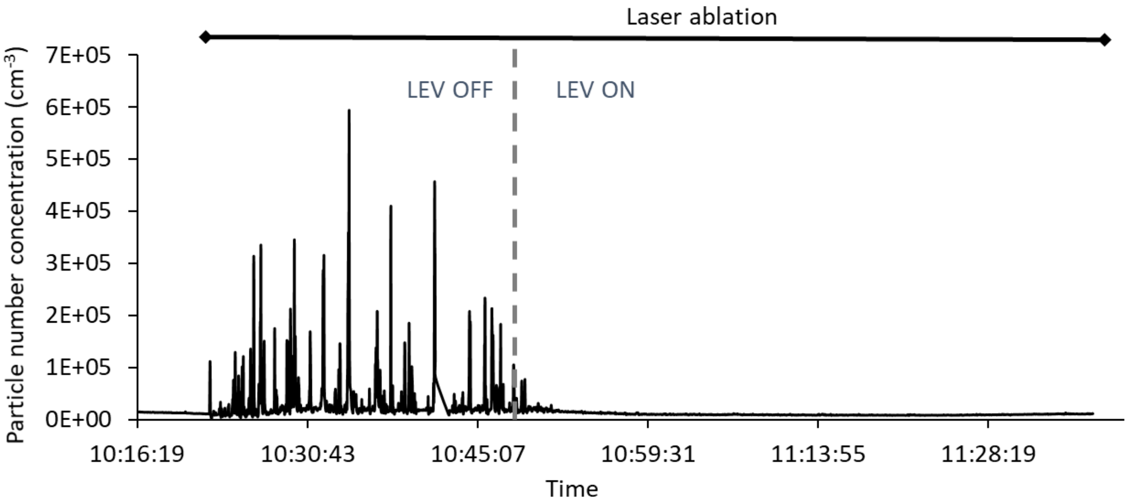

Figure 8. Particle number concentrations monitored with and without local exhaust ventilation (LEV; scenario A).

Table 5. Review of literature studies on the efficiency of ventilation systems for exposure reduction when dealing with manufactured nanomaterials (MNMs). The multiwalled carbon nanotubes (MWCNTs) had lengths between 1-20 nm and the D_p corresponds to their outer diameter.

Mitigation measure	Configuration	NP type	Size (nm)	Efficiency	Reference
Movable LEV system	-	Ag, Mn, Co	300	>99%	Old and Mehner, 2008.
Constant velocity hood	Constant hood face velocity = 0.5 m/s	Al_2O_3	200	Good performance	Tsai et al, 2010.
Constant flow hood	Constant airflow, hood face velocity varies inversely with height of sash opening	Al_2O_3	200	Low performance	Tsai et al, 2010.
Biological safety cabin		MWCNTs	D_p: 10-50	Good performance	Cena and Peters, 2011
Filters used in fume hoods (HEPA)	-	Ag	10	>99.99%	Kim et al, 2007

3.4 Comparison with literature studies

Literature data regarding the efficiency of technological measures applied for occupational exposure reduction is relatively scarce, especially under real-world industrial conditions Therefore, a comparison of the obtained results was carried out with a number of studies focusing on the effectiveness of ventilation systems used for exposure reduction to manufactured nanomaterials (Table 5). The studies shown in Table 5 were carried out at laboratory scale, simulating real operating conditions. In the present work, the efficiency of LEV systems was strongly depending on the volume of air in working room and on ventilation rates. The achieved exposure reductions were in the range 65%-99% being lower than 99% reduction reported by Kim et al., (2007) and by Old and Methner (2008). The studies of Cena and Peters (2011) and of Tsai et al., (2010) reported efficiencies only qualitatively, as “good” or “low”. This review evidences that quantitative, experimental and real-world assessments of the efficiency of mitigation strategies is missing in the literature devoted to occupational exposure and NP safety research. Our results highlight the interdependence of different mitigation strategies (e.g., LEV and source enclosure), which are frequently implemented simultaneously in real-world industrial scenarios. Unless this kind of scenarios are characterized in detail and for an ample number of NP emission sources, the implementation of exposure modelling tools will be strongly hindered.

4. Conclusions

The effectiveness of different mitigation measures for NP exposure reduction was assessed in four industrial settings. The following conclusions can be drawn:

- The efficiency of common engineering control mitigation measures such as local exhaust ventilation (LEV) and source enclosure can vary significantly depending on the intensity of LEV (flowrate), the total volume of air in the exposure area, the type of enclosure (e.g. partial, total), and their combinations. Adequate LEV configurations may reduce exposure concentrations (in terms of particle number) by 65-85% and even reach 99% by combining higher flow rates and enhanced enclosure.
- Adequate maintenance operations and enhanced sealing were applied to an industrial kiln used for firing ceramic tiles. Source isolation based on improved sealing in the firing compartment reduced exposure concentrations by 52%. In addition, a new kiln operating with an enhanced sealed combustion hearth minimised NP release in the worker area down to 84% of the measured exposure concentrations. In this case study, however, particle number concentrations remained high after the implementation of the mitigation strategies (ca. 10^5 cm^{-3}). In spite of the fact that the presence of workers in the kiln zone is limited, additional measures would be required to improve workers’ protection.
- The emissions from diesel engines significantly impact indoor the exposure to NPs. Substituting diesel with electric forklifts achieved a 92% reduction of particle number concentrations in breathing zone when the forklifts were in operation.

A review of the literature available evidenced the major need for real-world assessments of the efficiency of exposure mitigation strategies. One clear challenge identified is the interdependence of different strategies, which are frequently implemented simultaneously in industrial settings. The diversity of emission sources (stationary processes, moving vehicles, size of infrastructure, etc.)

contribute to the complexity of this type of assessment. However, these data are necessary as input for exposure modelling and risk assessment tools.

Conflicts of interest

The authors declare no conflict of interest relating to the material presented in this article. Its contents, including any opinions and/ or conclusions expressed, are solely those of the authors.

Acknowledgements

The authors gratefully acknowledge the collaboration of the European Ceramics Centre in Limoges. This work was carried out in the framework of the CERASAFE project (www.cerasafe.eu), with the support of SIINN ERA-NET (project id: 16), and was funded by the Spanish MINECO (PCIN-2015-173-C02-01). Partial funding from the "Generalitat de Catalunya" (project number: AGAUR 2017 SGR41) is also acknowledged.

References

Brines, M., Dall'Osto, M., Beddows, D.C.S., Harrison, R.M., Gómez-Moreno, F., Núñez, L., Art\'\iñano, B., Costabile, F., Gobbi, G.P., Salimi, F., Morawska, L., Sioutas, C., Querol, X., 2015. Traffic and nucleation events as main sources of ultrafine particles in high-insolation developed world cities. Atmos. Chem. Phys. 15, 5929–5945. https://doi.org/10.5194/acp-15-5929-2015

Brouwer, D., 2010. Exposure to manufactured nanoparticles in different workplaces. Toxicology 269, 120–127. https://doi.org/10.1016/j.tox.2009.11.017

Brouwer, D., Van Duuren-Stuurman, B., Berges, M., Jankowska, E., Bard, D., Mark, D., 2009. From workplace air measurement results toward estimates of exposure? Development of a strategy to assess exposure to manufactured nano-objects. J. Nanoparticle Res. 11, 1867–1881. https://doi.org/10.1007/s11051-009-9772-1

Brouwer, D.H., Gijsbers, J.H.J., Lurvink, M.W.M., 2004. Personal exposure to ultrafine particles in the workplace: Exploring sampling techniques and strategies. Ann. Occup. Hyg. 48, 439–453. https://doi.org/10.1093/annhyg/meh040

Cena, L.G., Peters, T.M., 2011. Characterization and control of airborne particles emitted during production of epoxy/carbon nanotube nanocomposites. J. Occup. Environ. Hyg. 8, 86–92. https://doi.org/10.1080/15459624.2011.545943

Conti, J.A., Killpack, K., Gerritzen, G., Huang, L., Mircheva, M., Delmas, M., Harthorn, B.H., Appelbaum, R.P., Holden, P.A., 2008. Health and safety practices in the nanomaterials workplace: Results from an international survey. Environ. Sci. Technol. 42, 3155–3162. https://doi.org/10.1021/es702158q

Donaldson, K., Tran, L., Jimenez, L.A., Duffin, R., Newby, D.E., Mills, N., MacNee, W., Stone, V., 2005. Combustion-derived nanoparticles: A review of their toxicology following inhalation exposure. Part. Fibre Toxicol. 2, 1–14. https://doi.org/10.1186/1743-8977-2-10

E.U., 2014. COUNCIL DIRECTIVE 98/24/EC. Off. J. Eur. Communities.

Ferrer, S., Mezquita, A., Gomez-Tena, M.P., Machi, C., Monfort, E., 2015. Estimation of the heat of reaction in traditional ceramic compositions. Appl. Clay Sci. 108, 28–39. https://doi.org/10.1016/j.clay.2015.02.019

Fonseca, A. S., Maragkidou, A., Viana, M., Querol, X., Hämeri, K., de Francisco, I., Estepa, C., Borrell, C., Lennikov, V., de la Fuente, G.F., 2016. Process-generated nanoparticles from ceramic tile sintering: Emissions, exposure and environmental release. Sci. Total Environ. 565, 922–932. https://doi.org/10.1016/j.scitotenv.2016.01.106

Fonseca, A S, Viana, M., Pérez, N., Alastuey, A., Querol, X., Kaminski, H., Todea, A.M., Monz, C., Asbach, C., 2016. Intercomparison of a portable and two stationary mobility particle sizers for nanoscale aerosol measurements. Aerosol Sci. Technol. 50, 653–668. https://doi.org/10.1080/02786826.2016.1174329

Fonseca, A.S., Viana, M., Querol, X., Moreno, N., de Francisco, I., Estepa, C., de la Fuente, G.F., 2015. Ultrafine and nanoparticle formation and emission mechanisms during laser processing of ceramic materials. J. Aerosol Sci. 88, 48–57. https://doi.org/10.1016/j.jaerosci.2015.05.013

Fransman, W., Schinkel, J., Meijster, T., Van Hemmen, J., Tielemans, E., Goede, H., 2008. Development and evaluation of an Exposure Control Efficacy Library (ECEL). Ann. Occup. Hyg. 52, 567–575. https://doi.org/10.1093/annhyg/men054

Gaines, L.L., Elgowainy, A., Wang, M.Q., 2008. Full fuel-cycle comparison of forklift propulsion systems. Argonne, IL. https://doi.org/10.2172/946421

Gerritzen, R.G., Huang, L., Killpack, K., Mircheva, M., Conti, J., 2006. Review of Safety Practices in the Nanotechnology Industry. Saf. Heal. 31.

Goede, H., Christopher-de Vries, Y., Kuijpers, E., Fransman, W., 2018. A Review of Workplace Risk Management Measures for Nanomaterials to Mitigate Inhalation and Dermal Exposure. Ann. Work Expo. Heal. 1–16. https://doi.org/10.1093/annweh/wxy032

Hämeri, K., Lähde, T., Hussein, T., Koivisto, J., Savolainen, K., 2009. Facing the key workplace challenge: Assessing and preventing exposure to nanoparticles at source. Inhal. Toxicol. 21, 17–24. https://doi.org/10.1080/08958370902942525

Hewett, P., Ganser, G.H., 2017. Models for nearly every occasion: Part I - One box models. J. Occup. Environ. Hyg. 14, 49–57. https://doi.org/10.1080/15459624.2016.1213392

Hussein, T., Kulmala, M., 2008. Indoor Aerosol Modeling: Basic Principles and Practical Applications. Water, Air, Soil Pollut. Focus 8, 23–34. https://doi.org/10.1007/s11267-007-9134-x

Kim, C.S., Bao, L., Okuyama, K., Shimada, M., Niinuma, H., 2006. Filtration efficiency of a fibrous filter for nanoparticles. J. Nanoparticle Res. 8, 215–221. https://doi.org/10.1007/s11051-005-9017-x

Kim, S.C., Harrington, M.S., Pui, D.Y.H., 2007. Experimental study of nanoparticles penetration through commercial filter media. J. Nanoparticle Res. 9, 117–125. https://doi.org/10.1007/s11051-006-9176-4

Kittelson, D.B., Watts, W.F., Johnson, J.P., 2004. Nanoparticle emissions on Minnesota highways. Atmos. Environ. 38, 9–19. https://doi.org/10.1016/j.atmosenv.2003.09.037

Kulmala, M., Petäjä, T., Ehn, M., Thornton, J., Sipilä, M., Worsnop, D.R., Kerminen, V.-M., 2014. Chemistry of Atmospheric Nucleation: On the Recent Advances on Precursor Characterization and Atmospheric Cluster Composition in Connection with Atmospheric New Particle Formation. Annu. Rev. Phys. Chem. 65, 21–37. https://doi.org/10.1146/annurev-physchem-040412-110014

Lee, M.H., McClellan, W.J., Candela, J., Andrews, D., Biswas, P., 2007. Reduction of nanoparticle exposure to welding aerosols by modification of the ventilation system in a workplace. J. Nanoparticle Res. 9, 127–136. https://doi.org/10.1007/s11051-006-9181-7

Mezquita, A., Boix, J., Monfort, E., Mallol, G., 2014. Energy saving in ceramic tile kilns: Cooling gas heat recovery. Appl. Therm. Eng. 65, 102–110. https://doi.org/10.1016/j.applthermaleng.2014.01.002

Morawska, L., Ristovski, Z., Jayaratne, E.R., Keogh, D.U., Ling, X., 2008. Ambient nano and ultrafine particles from motor vehicle emissions: Characteristics, ambient processing and implications on human exposure. Atmos. Environ. 42, 8113–8138. https://doi.org/10.1016/j.atmosenv.2008.07.050

Myojo, T., Nagata, T., Verbeek, J., 2017. The effectiveness of specific risk mitigation techniques used in the production and handling of manufactured nanomaterials: A systematic review. J. UOEH 39, 187–199. https://doi.org/10.7888/juoeh.39.187

Nazaroff, W.W., 2004. Indoor particle dynamics. Indoor Air, Suppl. 14, 175–183. https://doi.org/10.1111/j.1600-0668.2004.00286.x

Oberdorster, G., 2000. Pulmonary effects of inhaled ultrafine particles. Int. Arch. Occup. Environ. Health 74, 1–8. https://doi.org/10.1007/s004200000185

Oberdorster, G., Ferin, J., Gelein, R., Soderholm, S.C., Finkelstein, J., 1992. Role of the alveolar macrophage in lung injury: Studies with ultrafine particles. Environ. Health Perspect. 97, 193–199. https://doi.org/10.1289/ehp.9297193

Oberdörster, G., Sharp, Z., Atudorei, V., Elder, A., Gelein, R., Kreyling, W., Cox, C., 2004. Translocation of Inhaled Ultrafine Particles to the Brain. Inhal. Toxicol. 16, 437–445. https://doi.org/10.1080/08958370490439597

OECD, 2015. Harmonized Tiered Approach to Measure and Assess the Potential Exposure to Airborne Emissions of Engineered Nano-Objects and their Agglomerates and Aggregates at Workplaces. Ser. Saf. Manuf. Nanomater. No.55 55, JT03378848–JT03378848.

Old, L., Methner, M.M., 2008. Effectiveness of local exhaust ventilation (LEV) in controlling engineered nanomaterial emissions during reactor cleanout operations. J. Occup. Environ. Hyg. 5, D63–D69. https://doi.org/10.1080/15459620802059393

Pey, J., Querol, X., Alastuey, A., Rodríguez, S., Putaud, J.P., Van Dingenen, R., 2009. Source apportionment of urban fine and ultra-fine particle number concentration in a Western Mediterranean city. Atmos. Environ. 43, 4407–4415. https://doi.org/10.1016/j.atmosenv.2009.05.024

Pope, C.A., Dockery, D.W., 2006. Health effects of fine particulate air pollution: Lines that connect. J. Air Waste Manag. Assoc. 56, 709–742. https://doi.org/10.1080/10473289.2006.10464485

Pope, C.A., Dockery, D.W., Schwartz, J., 1995. Review of Epidemiological Evidence of Health Effects of Particulate Air Pollution. Inhal. Toxicol. 7, 1–18.

Ramachandran, G., Ostraat, M., Evans, D.E., Methner, M.M., O'Shaughnessy, P., D'Arcy, J., Geraci, C.L., Stevenson, E., Maynard, A., Rickabaugh, K., 2011. A strategy for assessing workplace exposures to nanomaterials. J. Occup. Environ. Hyg. 8, 673–685. https://doi.org/10.1080/15459624.2011.623223

Ribalta, C., Koivisto, A.J., López-Lilao, A., Estupiñá, S., Minguillón, M.C., Monfort, E., Viana, M., 2019. Testing the performance of one and two box models as tools for risk assessment of particle exposure during packing of inorganic fertilizer. Sci. Total Environ. 650, 2423–2436. https://doi.org/10.1016/j.scitotenv.2018.09.379

Salmatonidis, A., Ribalta, C., Sanfélix, V., Bezantakos, S., Biskos, G., Vulpoi, A., Simion, S., Monfort, E., Viana, M., 2019. Workplace Exposure to Nanoparticles during Thermal Spraying of Ceramic Coatings. Ann. Work Expo. Heal. 63, 91–106. https://doi.org/10.1093/annweh/wxy094

Salmatonidis, A., Viana, M., Pérez, N., Alastuey, A., de la Fuente, G.F., Angurel, L.A., Sanfélix, V., Monfort, E., 2018. Nanoparticle formation and emission during laser ablation of ceramic tiles. J. Aerosol Sci. 126, 152–168. https://doi.org/10.1016/j.jaerosci.2018.09.006

Schmid, O., Stoeger, T., 2017. Surface area is the biologically most effective dose metric for acute nanoparticle toxicity in the lung. J. Aerosol Sci. 113, 276. https://doi.org/10.1016/j.jaerosci.2017.09.017

Schulte, P., Geraci, C., Zumwalde, R., Hoover, M., Kuempe, E., 2008. Occupational risk management of engineered nanoparticles. J. Occup. Environ. Hyg. 5, 239–249. https://doi.org/10.1080/15459620801907840

Seaton, A., Tran, L., Aitken, R., Donaldson, K., 2010. Nanoparticles, human health hazard and regulation. J. R. Soc. Interface 7. https://doi.org/10.1098/rsif.2009.0252.focus

Tsai, S.J., Huang, R.F., Ellenbecker, M.J., 2010. Airborne nanoparticle exposures while using constant-flow, constant-velocity, and air-curtain-isolated fume hoods. Ann. Occup. Hyg. 54, 78–87. https://doi.org/10.1093/annhyg/mep074

Union, E., 2019. DIRECTIVE (EU) 2019/130 OF THE EUROPEAN PARLIAMENT AND OF THE COUNCIL. https://doi.org/http://eur-lex.europa.eu/pri/en/oj/dat/2003/l_285/l_28520031101en00330037.pdf

Van Broekhuizen, P., Van Veelen, W., Streekstra, W.H., Schulte, P., Reijnders, L., 2012. Exposure limits for nanoparticles: Report of an international workshop on nano reference values. Ann. Occup. Hyg. 56, 515–524. https://doi.org/10.1093/annhyg/mes043

Viana, M., Fonseca, A.S., Querol, X., López-Lilao, A., Carpio, P., Salmatonidis, A., Monfort, E., 2017. Workplace exposure and release of ultrafine particles during atmospheric plasma spraying in the ceramic industry. Sci. Total Environ. 599–600, 2065–2073. https://doi.org/10.1016/j.scitotenv.2017.05.132

Viana, M., Rivas, I., Reche, C., Fonseca, A.S., Pérez, N., Querol, X., Alastuey, A., Álvarez-Pedrerol, M., Sunyer, J., 2015. Field comparison of portable and stationary instruments for outdoor urban air exposure assessments. Atmos. Environ. 123, 220–228. https://doi.org/10.1016/j.atmosenv.2015.10.076

Viitanen, A.K., Uuksulainen, S., Koivisto, A.J., Hämeri, K., Kauppinen, T., 2017. Workplace measurements of ultrafine particles-A literature review. Ann. Work Expo. Heal. 61, 749–758. https://doi.org/10.1093/annweh/wxx049

Voliotis, A., Bezantakos, S., Giamarelou, M., Valenti, M., Kumar, P., Biskos, G., 2014. Nanoparticle emissions from traditional pottery manufacturing. Environ. Sci. Process. Impacts 16, 1489–1494. https://doi.org/10.1039/C3EM00709J

Wiesner, M.R., Lowry, G. V., Alvarez, P., Dionysiou, D., Biswas, P., 2006. Assessing the risks of manufactured nanomaterials. Environ. Sci. Technol. 40, 4336–4345. https://doi.org/10.1021/es062726m

Supplementary material

Effectiveness of nanoparticle exposure mitigation measures in industrial settings

Salmatonidis A., Sanfélix V., Carpio P., Pawłowski L., Viana M., Monfort E.

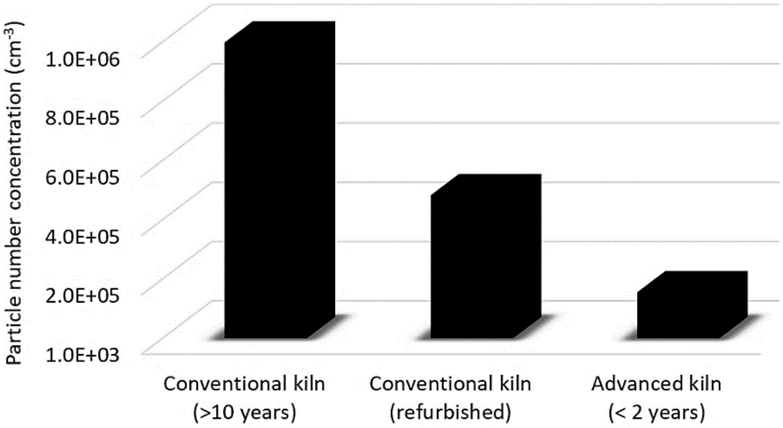

Figure S1. Evolution of emissions in terms of mean particle number concentration in three kilns having different isolations, refractory conditions and number of service years. The decreasing trend of particle release with improved isolation of the firing zone and refractory condition, can be observed.

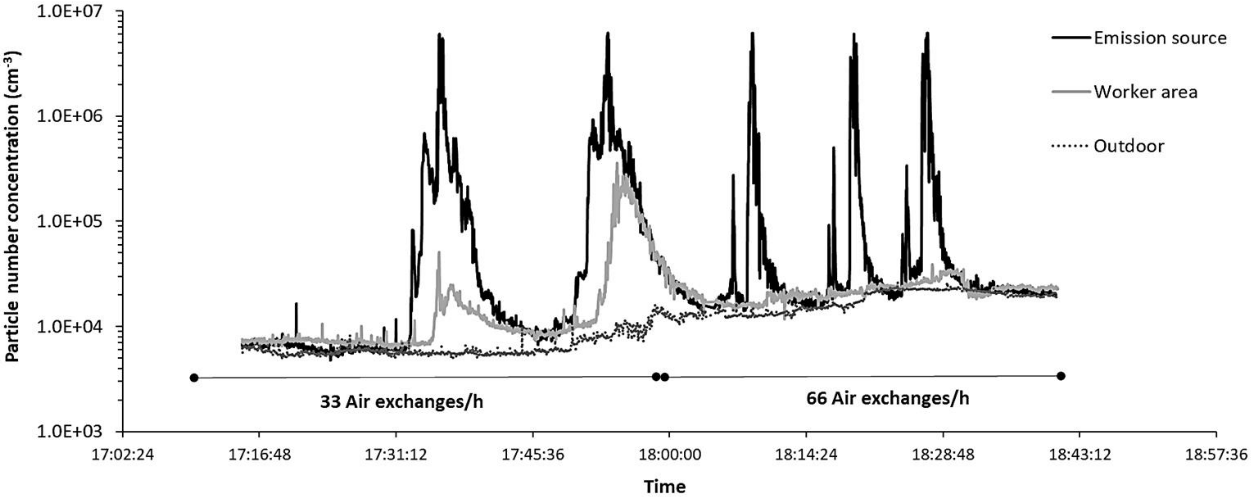

Figure S2. Emissions expressed in particle number concentrations monitored simultaneously during APS processing at the emission source (black curve), in the worker area (gray curve) and outdoor (doted curve). The experiments #4 and #5 have different LEV flow rates (12000/24000 m^3/h) but the same enclosure conditions (door open) under the spraying of the same feedstock (scenario A).

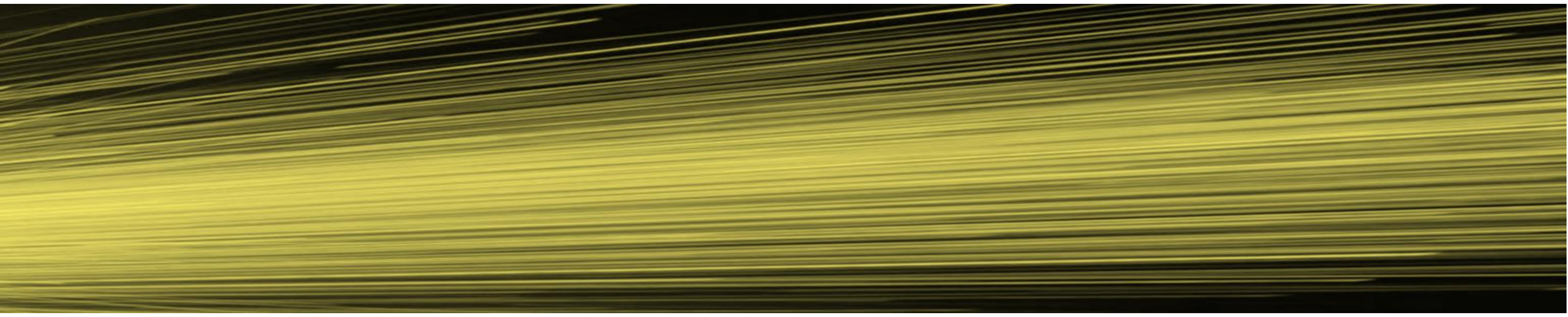

Chapter 5. **Discussion**

5. Discussion

This Discussion aims to integrate the results obtained in the scientific publications included in this PhD Thesis, with the aim to produce targeted and applied research of interest for the ceramic material processing at an industrial scale. Specifically, this chapter addresses the determinants of workplace exposure to nanoparticles (NP) by combining in an integrated approach all four research publications. The nanoparticle formation and release emission mechanisms were assessed, real-world industrial exposure scenarios were characterized, and the efficiency of mitigation strategies applicable at an industrial scale was quantified. It should be noted that although the real-world industrial scenarios are representative of worker exposure, there are certain limitations: no variations of the production scheduled was possible, several secondary-parallel processes were taking place simultaneously, and not all of the related information were available due to confidentiality issues.

5.1 Nanoparticle formation and emission mechanisms

As described in the Introduction, the main driver of workplace exposure is the presence of airborne pollutants (in this case, particles and NPs) in workplace air. In this work, two industrial activities were evaluated with a focus on NP emission mechanisms: (i) pulsed laser ablation (PLA; publication 1), and (ii) thermal spraying (Publication 2). PLA is used in the ceramic sector for surface structuring and decoration of ceramic tiles, and thermal spraying applies ceramic coatings on metallic substrates to enhance technical performance. Both processes are characterized by a high energy footprint, and thus have high potential for NP formation and release. NP concentrations were monitored in laser ablation and thermal spraying facilities in Spain and France, and the potential of these activities to impact workplace exposure was confirmed in this work. Table 5.1 presents a summary of the NP formation mechanisms identified during both industrial activities, as well as the nanoparticle concentration ranges monitored in terms of particle number and mass concentration.

Different particle emission mechanisms were identified for the two industrial activities assessed. Nanoparticle emissions were characterized by correlating particle release (number & mass concentration, size distribution) with fundamental ablation phenomena (melting & evaporation, melt drop expulsion, plasma plume generation, direct sublimation, shockwaves & grains ejection). Nucleation occurred when atoms, ions and clusters which emanated from the plasma plume (during laser ablation) acted as nuclei and formed secondary particles. Gaseous precursors emitted during laser ablation as well as during thermal spraying which may originate from direct sublimation (solid-to-gas) and from evaporation (liquid-to-gas), also formed new particles. In this context, the melting mechanism refers to the emissions originating from melt expulsion, the evaporation of melt, as well as sublimation and the subsequent condensation. The emission mechanisms were identified based on the size distribution of the particles released, as described in Publication 1 (Figure 5.1). Nanoparticle release after formation by nucleation showed sizes >20 nm and resulted in high particle number concentrations, but limited contributions in terms of particle mass. Conversely, the shockwaves mechanism released micron scaled particles with high mass and low number concentrations. The melting mechanism released particles in wide size range (20-700 nm), since it comprised different formation routes. It should be noted that for all the studied processes there is always a combination of phenomena taking place, which affect the mechanisms contributing to the emissions. Consequently, a mechanism was identified as dominant when it had the highest contribution in the emissions from the rest of the mechanisms involved. However, as shown in Publication 1 during laser ablation of ceramic tiles (i.e. alumina; UAW) with a near-IR laser two main mechanisms were identified as dominant (nucleation and melting), whereas a different combination (melting and shockwaves) contributed to emissions during ablation with mid-IR (i.e. glaze, GER).

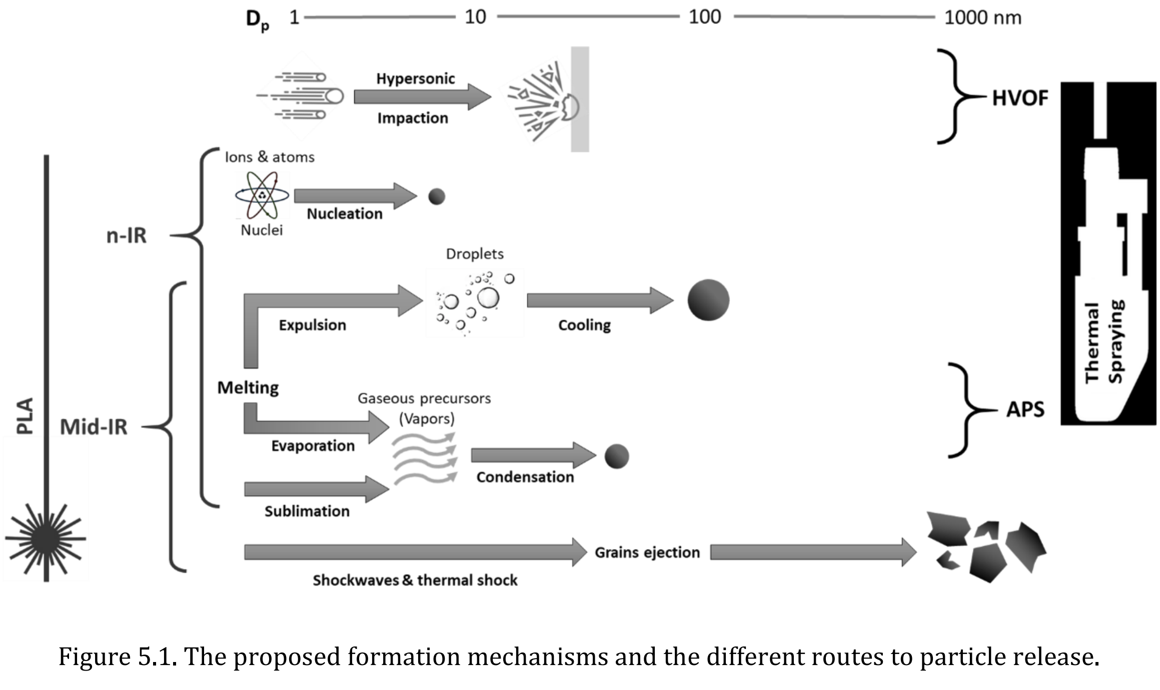

Figure 5.1. The proposed formation mechanisms and the different routes to particle release.

Table 5.1: Particle number concentrations from dominant mechanisms of different processes

Dominant mechanism	**Pulsed Laser Ablation**				**Thermal Spraying**			
	Particle number concentration (cm^{-3})							
	Near-IR		Mid-IR		HVOF		APS	
	Min	Max	Min	Max	Min	Max	Min	Max
Nucleation	3.7×10^{4}	2.4×10^{6}	-	-	-	-	-	-
Melting	1.5×10^{5}	2.4×10^{6}	8.4×10^{5}	1.5×10^{6}	-	-	9.2×10^{5}	2.0×10^{6}
Hypersonic impaction	-	-	-	-	2.9×10^{6}	3.8×10^{6}	-	-
Shockwave	-	-	1.6×10^{5}	1.7×10^{5}	-	-	-	-
	Particle mass concentration (µg m^{-3})							
	Near-IR (PM$_{2.5}$)		Mid-IR (PM$_{2.5}$)		HVOF (PM$_{2.5}$)		APS (PM$_{2.5}$)	
	Min	Max	Min	Max	Min	Max	Min	Max
Nucleation	5.8	15.2	-	-	-	-	-	-
Melting	13.6	1.8×10^{2}	7.3×10^{2}	4.5×10^{3}	-	-	1×10^{2}	1.8×10^{2}
Hypersonic impaction	-	-	-	-	1.2×10^{3}	1.4×10^{3}	-	-
Shockwave	-	-	1.7×10^{2}	4.5×10^{3}	-	-	-	-

Different emission mechanisms were identified for the two thermal spraying processes studied, melting for the APS and hypersonic impaction for the HVOF. The hypersonic impaction mechanism occurs when the micron-scaled feedstock particles impact on the target surface with supersonic velocities, resulting in the breakage or splintering of the original particles (micron-scaled feedstock) and the release of particles which are not deposited. The particles emitted may be nano-scaled but also micron-sized. The mechanisms identified contributed differently to particle number and mass concentrations. The maximum particle number concentrations monitored were mostly similar when particles were formed by nucleation, melting and hypersonic impaction, while in terms of particle mass concentrations the major contributing mechanisms were shockwaves and melting. With regard to the highest particle number concentrations monitored, instrumental issues should be noted as a limitation given that the concentrations reported in Table 5.1 are close or above the instruments' detection limits. In conclusion, it is interesting to note that while nucleation and hypersonic impaction mostly generated nanoparticle emissions (maximum concentration $2.4\text{x}10^{6}$ cm^{-3} and $3.8\text{x}10^{6}$ cm^{-3}, respectively), and the shockwave mechanism micro-scaled particles (171 µgPM$_{2.5}$ m^{-3}), melting contributed with particles across the entire particle size range to both particle metrics (181 µgPM$_{2.5}$ m^{-3}; 2.4×10^{6} cm^{-3}). The difference between the maximum and the minimum emissions may be used as an indication of the dependence of the emissions on the process parameters (Figure 5.2). According to the latter, the emissions by nucleation and melting can fluctuate significantly as they were affected by various process parameters, e.g., type of laser, energy input (laser/plasma settings), or composition and microstructure of the raw (tile/feedstock) material. Likewise, mean diameters of the emitted particles (10-700 nm) followed similar fluctuations (Figure 5.2). In the cases when nucleation – which released the smallest particles – was identified as the dominant mechanism, other mechanism (i.e. melting) also contributed to the total emissions increasing the mean particle diameters. Hypersonic impaction was the dominant mechanism only during HVOF, when all the process parameters were constant, and the mean diameters and the particle number concentrations showed minimal fluctuation (Figure 5.2). Similarly, there was only one specific case when the shockwaves mechanism was the only dominant mechanism (mid-IR, UPG), where the mean diameter was the largest and fluctuations were minimal. The melting mechanism, which can be dominant for both PLA and thermal spraying (APS) showed the highest fluctuations as it was influenced by the diverse parameters and the type of process.

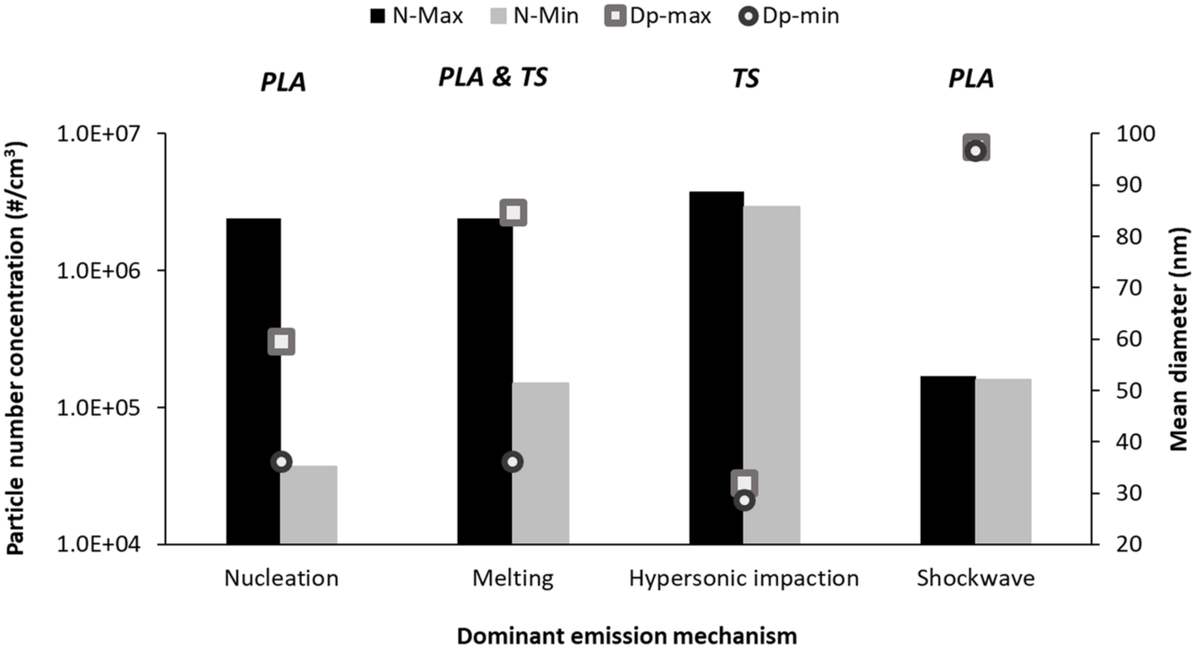

Figure 5.2 Emissions of the dominant mechanisms in terms of particle number concentration (N) and mean particle diameters (Dp), in relation to the laser ablation (PLA) and thermal spraying (TS) processes.

5.2 Exposure scenarios characterization

5.2.1. Exposure assessment

The exposure assessment activities in this Thesis focused on thermal spraying, which was performed at two different scales: pilot plant and industrial. Monitoring of exposure concentrations was also carried out in the laser ablation facility but, as discussed in Publication 1, exposure concentrations were not statistically significant as a result of the adequate implementation of mitigation measures. Thus, this section focuses only on the results obtained in the thermal spraying facilities.

Table 5.2 Qualitative characteristics (features) of the different exposure scales

Process features	**Pilot Plant**	**Industrial**
Workpiece sizes	Small (mm-cm)	Medium – large (cm-m)
Production system	Batch	Mass/serial
Automatization degree	Automated (robot)	Manual, semi-automated
Worker exposure	**Pilot Plant**	**Industrial**
Presence in spraying booth	Minimal presence	Constant presence
Workforce (number/unit)	<2	>4
Nanoparticle release	Fugitive emissions (ES to WA)	Fugitive emissions (ES to WA)

The main characteristics of the two thermal spraying scenarios are presented in Table 5.2. In the pilot-plant, small metallic platelets with diameters from several mm to a few cm were coated in a batch process. In the industrial plant, larger metal spheres of several cm were coated in a mass production mode; and in addition, metal workpieces of several meters in length were processed in a serial mode. The activity in the pilot-plant was fully automated, meaning that the presence of the worker inside the spraying booth was limited to inactivity periods (e.g., to remove the piece which was coated). On the contrary, at industrial scale the process was either manual (APS), where a worker was holding the spraying gun and had to change the workpiece after the completion of the coating; or semi-automated (HVOF), where the spraying was performed by a robot but the worker was required to enter the booth continuously to substitute the coated pieces with new uncoated ones. In both of the industrial processes (APS & HVOF) there was constantly at least one operator inside the spraying booth and occasionally more, when assistance was required. Thus, the spraying booths were considered in this work as emission sources (ES) but also as exposure areas. The general worker area (WA) was also an exposure area for the operators as well as for a broader workforce.

Figure 5.3 shows the NP exposure concentrations monitored in the two facilities in the emission source, worker area and background (ES, WA, BG, respectively), for the two types of thermal spraying techniques assessed. The aim was to characterize the exposure scenarios and assess the representativeness of the pilot plant scenario, with regard to actual industrial-scale spraying. At the emission sources, measured NP concentrations were comparable (>10^6 cm^{-3}; mean concentrations during spraying) for all the cases, and may be considered high (when compared with the current recommendation of nano-reference values, 40000 cm^{-3}). This is particularly relevant for the industrial scenarios because the worker presence was constant inside the booth, wearing though personal protective equipment (FPP3 mask in the case of HVOF, full helmet respirator during APS). Particle number concentrations remained high (up to 3.4×10^6 cm^{-3}) during in APS and HVOF spraying despite the continuously working extraction system. As mentioned, the workers in the pilot plant were not exposed directly to the high concentrations recorder inside the booth as the process was fully automated. Nevertheless, the high concentrations in the spraying booth of the pilot plant indicate that the level of exposure is mainly dependent from the energy footprint of process (thermal, high energy) rather than its scale (pilot plant or industrial).

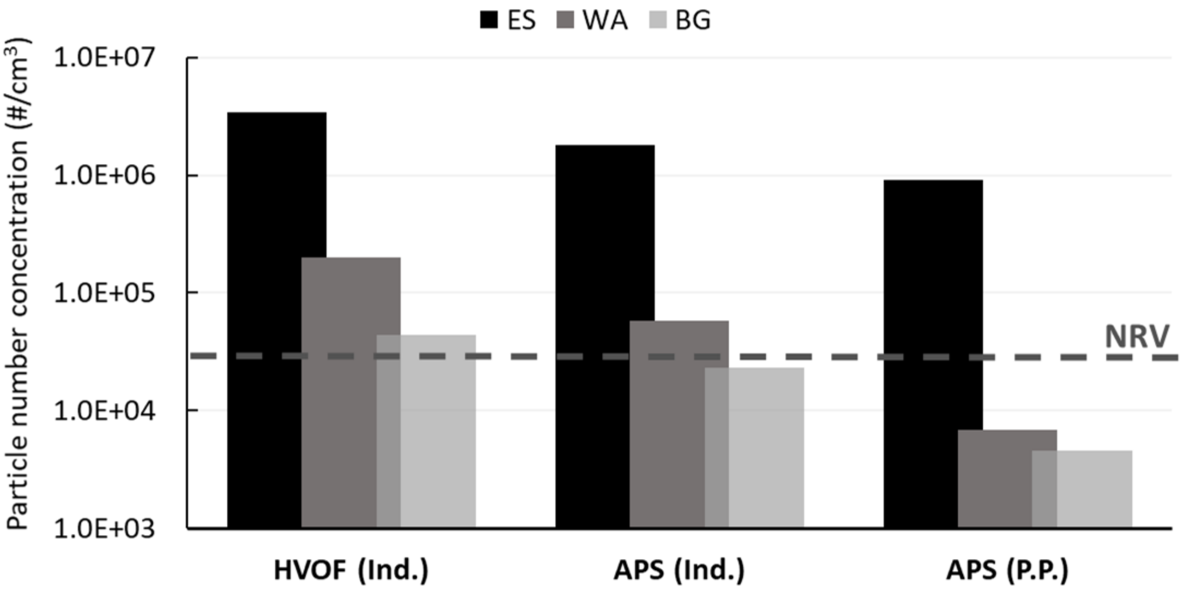

Figure 5.3. Thermal spraying exposure levels in terms of particle number concentrations in different locations and scales: industrial scale (Ind.), pilot-plant (P.P.); emission source (ES), worker area (WA), background reference (BG) and nano-reference values (NRVs).

In the worker area, on the other hand, particle number concentrations at pilot plant and industrial scale were lower by at least one order of magnitude due to the application of different mitigation measures. The workers operating in the worker area, which did not wear protective equipment in either of the scenarios, were exposed to concentrations in the range of 5.8×10^4 - 2×10^5 cm^{-3} at industrial scale and lower (6.9×10^3 cm^{-3}) in the pilot plant. The lower concentrations monitored in the pilot plant were mainly due to a more efficient enclosure (sealing) of the spraying booth. The concentrations monitored at industrial scale are still high when compared to the nano-reference values (Van Broekhuizen et al., 2012), while in the pilot plant they were lower than this recommendation. Furthermore, the number of workers potentially exposed was higher in the industrial facility than in the pilot plant (Table 5.2). When compared to background concentrations, in the case of HVOF the difference between worker area and background concentrations (1.6×10^5 cm^{-3}) was larger than in the case of APS (3.5×10^4 cm^{-3}), probably due to differences in the mitigation measures in place (more information in section 5.3 below) and evidencing larger impacts on exposure from this type of spraying technique. As for the pilot plant, exposure concentrations showed lower impacts from the spraying activities, when compared with background concentrations (2.3×10^3 cm^{-3}). Overall, the high concentrations monitored in the worker area in the industrial facility highlights the urgent need to raise awareness regarding nanoparticle exposures in industrial plants, to promote the use of personal protective equipment in areas which may initially not be considered as potential exposure scenarios. This work demonstrates that, contrarily to the current working style, protective equipment should be worn in the worker area and potentially even in other areas of the industrial facility. Regarding the pilot plant, it was concluded that the operating and exposure conditions were representative of actual industrial workplaces, and that the mitigation strategies in place were more efficient than in the specific industrial facility assessed. Finally, considering the above findings, the presence of workers inside the thermal spraying booths should be strongly discouraged.

5.2.2. Particle characterization

Physicochemical particle characterization techniques were applied to the airborne particles samples collected in the laser ablation and thermal spraying scenarios. As a consequence of the particle formation and release mechanisms described above, certain similarities but also clear differences were observed between both scenarios, with implications regarding exposure and potential health risks.

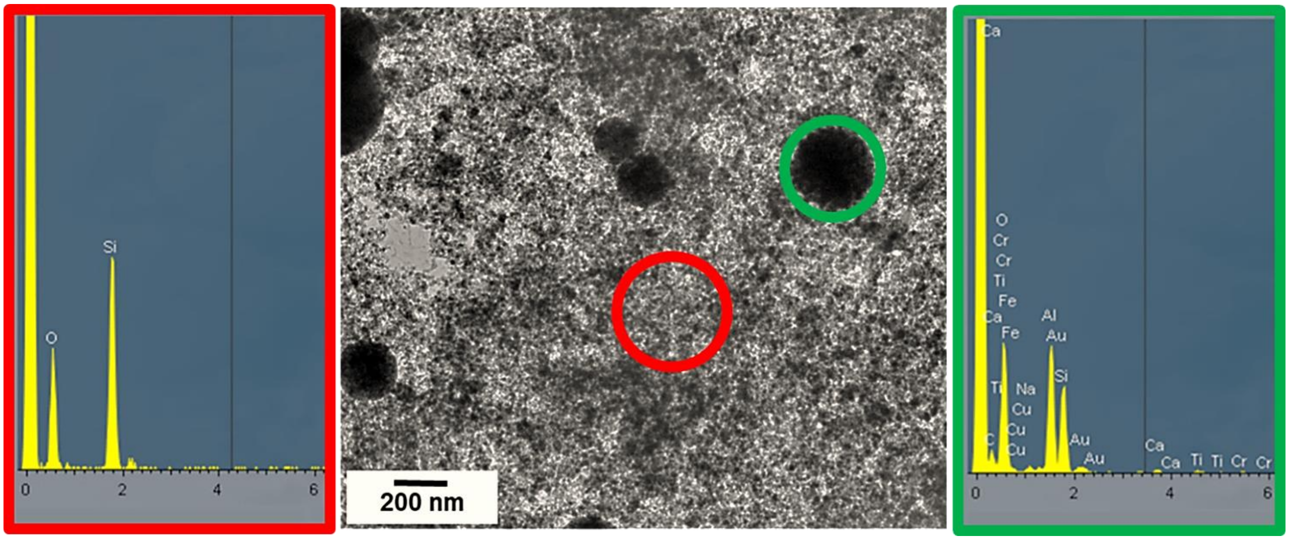

Figure 5.4. TEM image of the emitted particle from PLA of UPG tiles and the EDX analysis of the specific areas are shown with the respective frame colors.

Laser ablation

During laser ablation, ceramic tiles with different chemical composition were processed (publication 1): porcelain (UPG), alumina (UAW), biscuit porcelain (UBW) and glazed earthenware (GER). As expected, the chemical composition of the nanoparticles emitted generally resembled that of the source tiles. However, due to the characteristic thermal behaviors of the different elements in the tiles (e.g., different volatilization temperatures), certain tiles were characterized by the simultaneous emission of different nanoparticle types. This was the case, for instance, of porcelain tiles (UPG), which simultaneously released >15 nm SiO_2 NPs (Figure 5.4, red) and larger particles including a combination of the main chemical tracers of the UPG tile (Figure 5.4, green). SiO_2 nanoparticles were formed and released from UPG and not from other types of tiles probably due to microstructure characteristics of this type of tile. Another specific example was that of the glazed tiles (GER), where only the glaze material was treated, since the glaze has a thickness ca. 350-550 µm and the ablation depth was a few µm. Consequently, the nanoparticles emitted were mainly composed of Zn oxides, which sourced from an amorphous phase of the glaze. Overall, the majority of particles emitted with diameters >1 µm had spherical or spheroid shapes, regardless the type of tile ablated, while particles <1 µm were fractal-like. These results evidence the high variability of chemical and morphological properties of particles emitted during laser ablation of ceramic tiles, and the need for further targeted, experimental studies in real-world scenarios in order to characterize exposures and minimize potential health risks.

Thermal spraying

TEM images of particles collected inside the APS spraying booth are shown in Figure 5.5. Chain-like agglomerates of primary particles with different particle sizes (5 to 20 nm) can be observed (Figure 5.5). The spherical or spheroid shape of nanoparticles (Figure 5.5), can be an indication that they might have originated from melting-evaporation and the consequent condensation. Moreover, these nanoparticles were found to have a composition similar to that of the feedstock, i.e., Ti-Al oxides and Cr-Ni depending on the coating (two different feedstocks were applied).

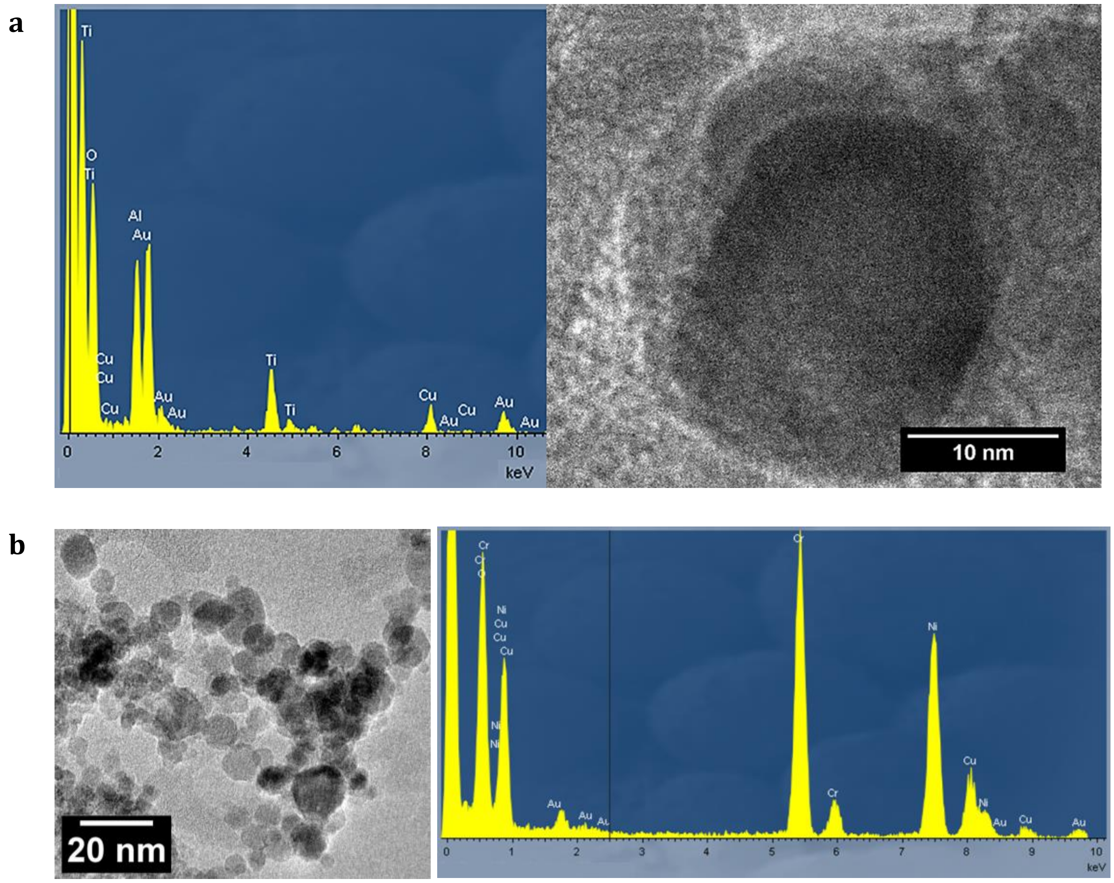

Figure 5.5. TEM image of the emitted particle from APS with (a) Al_2O_3-TiO_2 and (b) Cr-Ni feedstocks

Particles sampled from the other booth (HVOF) are shown in the TEM images in Figure 5.6. The agglomerates in Figure 5.6 are distinctively different from the ones observed in the case of APS (Figure 5.5). Irregularly-shaped particles with diameters 5-40 nm appear to be strongly aggregated, resembling nanoparticles which have undergone collisions. The latter could be an indication that nanoparticles were emitted directly as aggregates formed by breakage or splintering of partially melted micro-scaled particles (feedstock), when impacted at hypersonic velocities on the surface being coated, confirming the emission mechanism described above (section 5.1). The chemical composition of the particles emitted was similar to that of the micron-sized feedstock used (W-Cr-Ni-C), verifying that thermal spraying was the source of the sampled particles and of worker exposure.

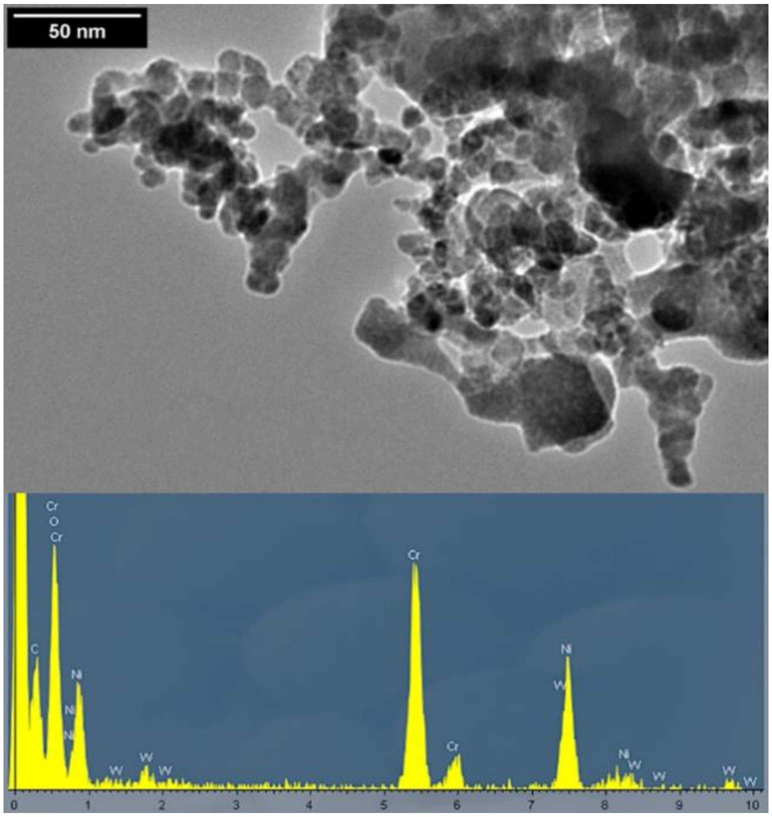

Figure 5.6. TEM image of the emitted particle from HVOF *with WC-Cr-Co-Ni feedstock*

Finally, the hygroscopic properties of the particles emitted during thermal spraying was assessed. This analysis was only possible for the industrial thermal spraying scenario, due to the logistical complexity of the instrument used. The hydrophobic/hydrophilic properties of the aerosol emitted during spraying were assessed using an HTDMA. Particles with mobility diameters of 30 and 90 nm were preselected (dry) and subsequently were exposed to high relative humidity (RH 87%), after which their size distribution was measured again. The aim of this analysis was to test the usefulness of the HTDMA as a tool to discriminate, in real-time, thermal spraying emissions from workplace background particle concentrations. The basic assumption was that, due to their different chemical compositions and aging process, the hygroscopic behavior of thermal spraying and background aerosols would also be different and this would facilitate their discrimination in the workplace.

Results evidenced that 30-nm (electrical mobility diameter) particles originating from the plasma processes exhibited hygroscopicities which did not differ significantly from other aerosols sampled when there was no spraying activity. However, taking into account that 30-nm particles were observed by the HTDMA only during working hours, their presence has to be attributed to nanoparticle emissions during spraying activity. Nevertheless, further research is necessary in order to understand the potential influence of soot particles emitted during the HVOF on these measurements. The 90-nm particles, on the other hand, were hydrophobic at 87% RH. This allowed to clearly distinguish them from other aerosols of the same dry size, which were present in the workplace. In conclusion, the information provided by the HTDMA can complement existing methods for exposure assessment to process-generated nanoparticles, as changes in particle size upon inhalation may alter their deposition patterns inside the human respiratory system.

Results evidence that exposure in both facilities assessed was driven by nanoparticles formed unintentionally during thermal spraying, referred to as process-generated nanoparticles. The concentrations of the released nanoparticles in terms of number were barely affected by the different sizes of the micro-scaled feedstock material. This result highlights the relevance of process-generated nanoparticles released during high-energy industrial activities, given their potential for significant impacts on workplace exposure.

5.3 Exposure mitigation

The results from the experimental work in this Thesis, integrated in the sections above, point to the need for dedicated and efficient exposure mitigation measures in industrial settings. Specifically, for the thermal process in the ceramic sector, frequently-applied technologies release (unintentionally) high concentrations of process-generated nanoparticles, as described above. The variety of industrial activities results in a wide variety of potential mitigation strategies, which in addition depend on the specific industrial scenario under assessment. Furthermore, the actual efficiency of each mitigation strategy depends on its implementation. Because of this complexity, this Thesis aimed to expand the knowledge on the efficiency and applicability of exposure mitigation strategies for the ceramic sector.

The ultimate goal was to provide quantitative estimates of the particle removal efficiency of specific mitigation strategies implemented in industrial facilities from the ceramic sector.

As described in Publication 4, this work started with a review of the scientific literature available, which highlighted three major research gaps:

- The scientific literature is scarce on exposure assessments for process-generated NPs, when compared to engineered NPs or fine and coarse particles.
- While a significant number of studies on the effectiveness of personal protective equipment is available for laboratory-scale testing, less information is available on the effectiveness of technical measures.
- Generalizing case-study results is complex, which implies the need for more experimentally monitored case studies.

Based on these results, four exposure scenarios were assessed in this Thesis, with the aim to quantify the effectiveness of the mitigation strategies in place:

- Thermal spraying deposition of ceramic coatings: local exhaust ventilation (LEV) and source enclosure (improved sealing of the booth) and personal protective equipment (PPE)
- Laser ablation of ceramic tiles: local exhaust ventilation (LEV)
- Diesel engine emissions (forklifts): source substitution by using electrically-powered forklifts
- Ceramic tile firing in a roller hearth kiln: source enclosure by enhanced sealing of the kiln

The efficiency of mitigation measures was expressed as the reduction of exposure to NPs, before and after the implementation of the mitigation measures. The exposure reductions were characterized in terms of particle number concentrations, and for nine different exposure scenarios. Results evidenced that particle number removal efficiencies, tested in this Thesis, ranged from 48.7% up to 99.8% (Figure 5.7).

The highest efficiency was achieved by the combined use of a strong LEV with an efficient enclosure (99.8%) during thermal spraying scenario (APS-pilot plant). This efficiency was adequate to limit the transport of fugitive emissions and prohibit any statistically significant increase of nanoparticles concentration to the worker area. For the other thermal spraying process (HVOF-industrial) the application of LEV achieved a lower efficiency (90.5%), since fugitive emissions from the emission source were transported in the worker area due to the partial enclosure implemented. Partial enclosure but with a less effective LEV (lower flowrate) showed even lower efficiency (65.1%; Figure 5.7) in an industrial scale laser ablation scenario. The efficiency of masks (PPE) was tested under real-working conditions and high exposure concentrations during thermal spraying (HVOF), and it was found that particle number concentrations in the worker breathing zone (inside the mask) were 86.7% lower than outside the mask.

Source substitution, where diesel powered forklifts were substituted with electrically powered ones, achieved a 91.5% reduction of exposure concentrations in the worker breathing zone. If the background concentrations are not subtracted from the calculations, the efficiency is significantly lower (48.7%). The latter indicates that contribution of secondary and outdoor sources to worker exposure, considerably influence the resulting data. Efficiency of 84.4% was calculated for the source isolation of the roller hearth kiln. The principal of the latter mitigation strategy was to insulate the kiln with refractory furnishing in order to limit fugitive emissions. Degraded isolation of the kiln, due to heavy use, showed the minimum efficiency in terms of mitigation (51.6%; Figure 5.7). The mitigation efficiency was influenced by the refractory conditions of the insulating materials.

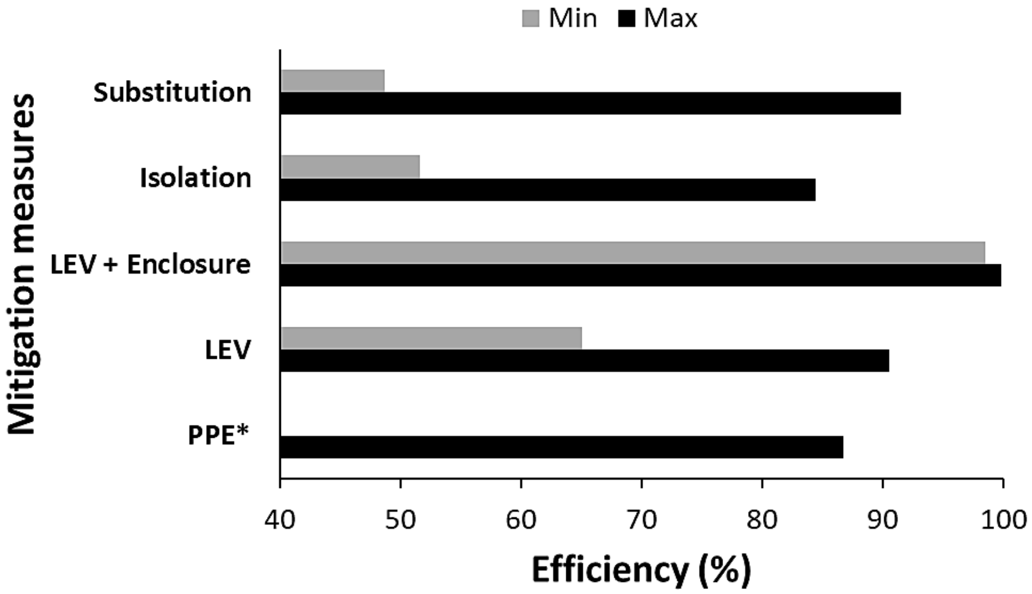

Figure 5.7. Efficiency of the mitigation measures assessed for the reduction of exposure concentrations, in terms of particle number concentrations. *The only value for PPE corresponds to one case study as described in publication 2.

The results in this work evidence that, even though the hierarchy of controls (Schulte et al., 2008) dictates the priority for the implementation of risk management strategies, this does not necessarily mean that the order of the mitigation measures is based on their efficiency. It should be noted that different measures overlapped in some of the scenarios (e.g., LEV and partial source enclosure were operating in parallel in the APS scenario), and thus the efficiencies reported are at times representative of a combination of measures.

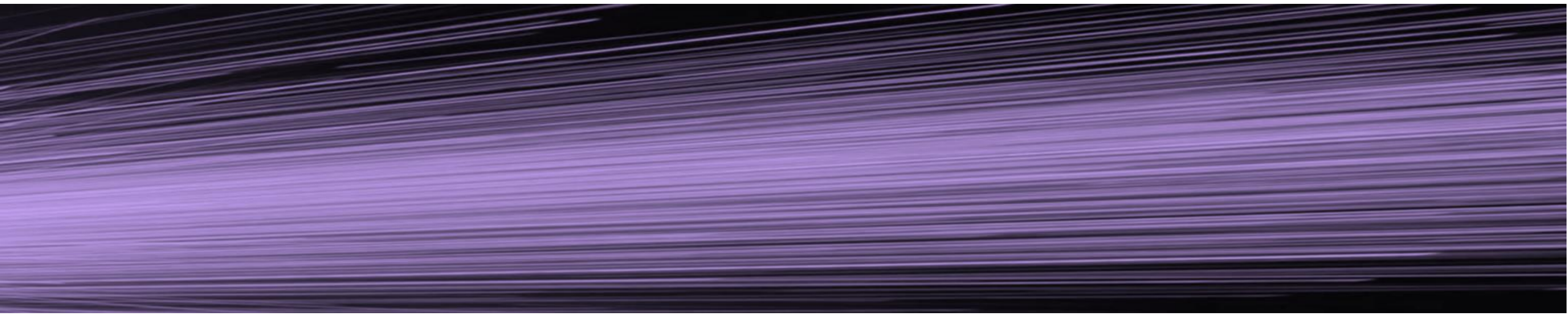

Chapter 6. **Conclusions**

6. Conclusions

This PhD Thesis addresses occupational exposure to nanoparticles during selected activities (laser ablation and thermal spraying) characteristic of the ceramic industry. An integrated approach is followed, which covers nanoparticle formation and release mechanisms, exposure assessment at industrial- and pilot-plant scales, and quantifying the efficiency of exposure mitigation measures. The ultimate goal of this work was to contribute in improving nanosafety of industrial processes by reducing potential risks. The main conclusions and recommendations extracted are summarized below.

6.1. Particle formation and release mechanisms

Among the broad variety of activities and characteristic processes of the ceramic industry, laser ablation and thermal spraying were selected as representative of advanced thermal technologies applied in this industrial sector. Due to their high energy footprint, these activities are known to generate high particle (fine and nano) concentrations, with potentially high impacts on worker exposure. The following particle formation and release mechanisms were identified and characterized in the framework of this PhD Thesis:

1) Pulsed laser ablation (PLA) of ceramic tiles

PLA is a highly versatile technique with broad applications, which may be carried out with diverse parametrizations which in turn impact NP formation and release. The main parameters found to influence particle emissions during ablation of ceramic tiles were the type of laser and the energy settings, as well as the type of tile and their physico-chemical surface properties. Particle emissions were driven by:

- Particle nucleation, in terms of particle number concentrations in the size range >10 nm.
- Mechanical shockwaves, in terms of particle mass concentrations (>100 nm).
- Ceramic tile melting and droplet expulsion, in terms of particle mass and number concentrations, as this mechanism generated droplets with a wide range of particle diameters (40-700 nm). It should be noted that the melting mode comprised also agglomerates and

aggregates of smaller particles. Agglomerates have a wide range of sizes depending on the primary size of the particles as well as the number of particles clustered.

- Evidently, the chemical composition of the emitted particles depends on the ablated ceramic tile. However, not all of the emitted particles had the same composition as the respective tile. Nanoparticles composed only by certain of the tile elements may be released, for instance SiO_2 nanoparticles were emitted during the ablation of porcelain tiles.
- Regarding the influence of the type of laser, a combination of mechanisms was found to contribute to particle number emissions. The near-IR laser generated particles by means of nucleation and melting, whereas the mid-IR laser produced particles through melting and mechanical shockwaves.

2) Thermal spraying of ceramic coatings

The thermal spraying processes studied in this work (APS, HVOF) were seen to generate high particle concentrations in terms of mass and number concentrations:

- Atmospheric Plasma Spraying was characterized by high temperatures ($5\text{-}20\times10^3$ °C) and relatively low projection velocities (200-500 m/s). During APS the feedstock is melted and metal vapors are oxidized by entrained air and condense in the cold zone of the jet, a mechanism which results in nanoparticle formation. Nanoparticles emitted by APS mainly had spherical shapes as they mostly originated from condensation of gaseous or liquid precursors.
- High Velocity Oxy-Fuel spraying was characterized by high velocities (up to 1500 m/s) and relatively lower temperatures (2.9×10^3 °C). In this case the feedstock was not entirely melted, and particles were driven with supersonic speeds towards the workpiece. Nanoparticles (mean D_p: ca. 30 nm) with irregular shapes were detected, suggesting that they were formed during supersonic destructive collisions. An additional emission route could be the fugitive emission of submicron particles, which would not be deposited on the substrate as they would simply disperse inside the booth.

The main recommendations extracted regarding particle formation and release mechanisms are:

- The size distribution of particles emitted during laser ablation of tiles is dependent on the type of tile and laser used. Thus, the proper understanding of the link between process parameters (type of laser and tile) and the resulting size distribution of particles emitted may aid in the adequate design of exposure mitigation strategies.

- While the number and mean particle size of particles emitted during thermal spraying was mostly similar for both spraying techniques (APS and HVOF), particle morphology was markedly different depending on the temperature and projection velocity of the spraying technique. As a result, the morphological characterization of particles in the worker area may serve as a useful tool to identify the main sources of particle exposures, in thermal spraying settings.

6.2. Exposure scenarios

Thermal spraying was assessed at pilot plant and industrial scale as a source of workplace exposures to nanoparticles. Exposures were characterized using online and offline techniques, and with a focus on different aerosol metrics including particle number and mass concentrations, size distribution, chemical composition and hygroscopicity. Results evidenced that:

- APS (assessed at pilot plant and industrial scale): particle emissions in terms of number concentration were comparable at both scales (>10^6 cm^{-3}), evidencing the potential for occupational exposures generated by this industrial activity. The impact on worker exposure was markedly lower at pilot plant scale: while exposure levels were high (5.8×10^4 particles cm^{-3}) and above the nano-reference values (NRV, 4×10^4 cm^{-3}) at industrial scale, they were <NRVs in the pilot plant. Exposures were lower due to two main factors: the absence of worker presence inside the spraying booths (which was not the case at industrial scale), and the better implementation of mitigation strategies (mainly, source enclosure) in the pilot plant.
- HVOF (assessed at industrial scale): high particle number concentrations (>10^6 cm^{-3}) were recorded inside the thermal spraying booth (ES), which should also be considered an exposure area given that the operator was frequently present inside the booth. Exposure concentrations in the worker area (WA) were lower by one order of magnitude in terms of number (10^4-10^5 cm^{-3}) and up to a factor of 4 in terms of PM_1 (44-100 µg m^{-3}).
- In terms of particle mass concentrations, and at industrial scale, particle mass concentrations showed differences as a function of the spraying technique: PM_1 concentrations were higher in the HVOF booth (6.4×10^2 µg m^{-3}) than during APS (6.1 µg m^{-3}). This contrasts with particle number concentrations, which were similar irrespective of the spraying technique and the feedstock material applied. Results suggest that particle mass concentrations were mostly

driven by fugitive emissions of the feedstock material under both spraying techniques, and in addition by impaction mechanisms in the HVOF booth.

- A size distribution analysis demonstrated that the majority of particles emitted during APS and HVOF were between 26-90 nm, evidencing that spraying was a major source of nanoparticles in terms of total number concentration.
- The nanoparticles released exhibited a markedly different hygroscopic behaviour when compared to background aerosols: nanoparticles emitted during thermal spraying were found to be hygrophobic, in contrast with more hygrophillic background particles. Due to these characteristic properties they can be easily distinguished, on a real-time basis with the HTDMA, allowing fast identification of particle emission hotspots or accidental releases. This would contribute to streamlining and tailoring particle exposure assessments in workplace scenarios.

The main recommendations extracted are:

- Thermal spraying activities have high potential to for nanoparticle (and fine particle) release to workplace air. However, guidelines and regulations for occupational health refer mainly to mass concentrations, and not to particle number concentration which would be a more relevant metric for nanoparticle exposures. Thus, in order to protect workers against nanoparticle exposures, risk management measures are of paramount importance.
- Exposure may be fully mitigated at laboratory scale with adequately designed and implemented strategies (e.g., in the case of laser ablation of tiles, a local exhaust ventilation system). At pilot plant and industrial scales (e.g., during thermal spraying), full mitigation of exposures is more complex and requires a combination of technological and non-technological measures.
- During thermal spraying, the presence of the operator/worker inside the spraying booth during the spraying activity should be avoided at all times.
- In thermal spraying scenarios, exposure mitigation strategies should cover different particle size ranges: in both APS and HVOF scenarios strategies should focus on nanoparticles as well as fine particles (<100 nm and >1 μm).

6.3. Mitigation measures

The effectiveness of different mitigation strategies was assessed under different exposure scenarios:

- Source substitution was applied by eliminating diesel engines and exchanging them with electric ones, resulting to an efficiency of 92%. Based on the concept of substituting or eliminating a source, the efficiency should have been 100%. However, in real-world industrial scenarios it is challenging to distinguish one source from secondary and parallel ones, and also to discriminate it from outdoor and background concentration. Thus, the calculated efficiencies may be influenced from the above conditions.
- Source isolation measures achieved efficiencies from 52% (enhanced sealing) to 84% (optimal sealing and superior refractory condition); depending on the characteristics of the insulating (refractory) material, type of kiln (conventional or advanced) and time of service (new or old).
- Engineering controls such as local exhaust ventilation, source enclosure and their combinations were quantified. Different LEV configurations may reduce exposure concentrations in terms of particle number by 65-85% and even reach 99% by combining higher flow rates and enhanced enclosure.
- The efficiency of personal protective equipment (PPE; face masks) was evaluated under real-working conditions. The concentrations in the worker breathing zone (inside the mask) were reduced by 87% when compared to the emission source ones. However, the breathing zone concentrations were still high (4×10^5 cm^{-3}).

The main recommendations extracted are:

- Personal protective equipment: offers protection only to the individual wearing it and there are several variables which may affect the performance of a respirator (e.g. fitting, breathing rate); therefore, solely PPE may not offer adequate protection and should always be used in combination with additional mitigation measures.
- The diversity of potential sources and activities in industrial workplaces dictates the need for tailored mitigation measures.

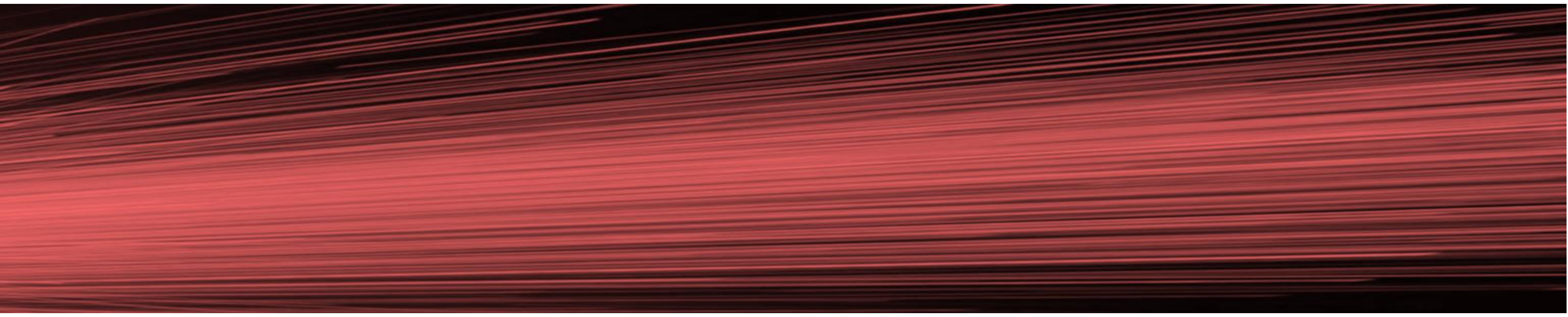

Chapter 7. **Limitations and future work**

7. Limitations and future work

7.1. Limitations

7.1.1. Technical limitations

- During the experimental campaigns performed in the framework of this Thesis different instruments were used (SMPS, CPC, DiSCmini, NanoScan-SMPS). These instruments are based on different measuring principles: SMPS and NanoScan DMAs classify particles based on their electrical mobility, CPCs count particles by optical detectors; whereas DiSCmini uses an electrometer to count particles. Furthermore, it was not always possible to have the same time resolutions, the standard measurement error and the detection limits for each instrument were different.

- Particle number concentrations monitored at the emission sources (near field) were markedly high (>1×10^{6} cm^{-3}), which meant that the maximum particle number concentration limit of the instruments – as stated by the manufacturers – were exceeded. This resulted in inhomogeneous degrees of uncertainty across the different datasets. The solution to this problem would be the use of a dilution system upstream to all instruments, which would have reduced uncertainties at high concentrations. However, the application of a dilution system introduces additional practical difficulties during campaigns in real-world occupational settings: (i) it can be applied to stationary instruments but it is rather complex for personal monitors; (ii) portable instruments and monitors can operate autonomously (battery operated) and the dilutors should be able follow; and (iii) either all the instruments need to have a common inlet or several dilutors would be needed.

7.1.2. Operational and methodological limitations

- In real-world occupational settings and industrial facilities there is a strict operational/production schedule that needs to be followed and some exposure monitoring gaps may arise. An approach that combines stationary and personal monitoring may contribute to a comprehensive monitoring strategy. Nevertheless, such an approach would require increased number of instruments/monitors.

- Exposure monitoring is dependent on the monitoring location: particle concentrations show high spatial-temporal variability, which means that source representability is a relevant issue. Thus, it is essential to ensure the collection of sufficient case details, including repetitions to guarantee a representative exposure assessment. Furthermore, it is especially relevant to focus exposure assessments on the modeling of aerosol processes driving exposures (sources), so that the understanding of the processes may contribute to the design of effective and targeted mitigation strategies.

7.2. Future work

7.2.1. Application of the data to models

- The research performed in this PhD Thesis produced analytical data on particle exposure, emission mechanisms, properties of the emitted particles and efficiency of mitigation measures. These high resolution case-and task-specific data may have added value if used in modeling approaches. They may be used for validation and calibration of models that predict exposure (e.g. one/two box models). The information on the hygroscopicity of nanoparticles could help develop the next generation inhalation-deposition models. Since the characteristics of the inhaled particles change at the elevated relative humidity within the human respiratory tract, new models could use this as a new variable in order to increase their representability and accuracy. Furthermore, risk assessment and control banding tools could use the available data to update their libraries and databases.

7.2.2. Application of the results to health risks and prevention

- In the framework of this PhD Thesis and specifically during the second thermal spraying experimental campaign (publication 3), process-generated nanoparticle samples were collected on filters and also in liquid suspension. This was achieved using an aerosol concentrator (versatile aerosol condensation enrichment system: VACES), with which size segregated samples were obtained (fine, ultrafine and coarse). Filter samples were chemically characterized by ICP MS/AES and XRF, while liquid samples were used for toxicological assessment by means of ALI (air-liquid interface). The results obtained from these analyses, which are not included in this PhD Thesis, may create an intersection on the interpretation between exposure and health data combining exposure assessment, chemical composition and hygroscopicity of aerosols with the toxicological response. This will be a holistic as well comprehensive analysis of a real case of exposure-risk-hazard due to nanoparticle release.

- The data in this Thesis also has potential for application in risk assessment. The case specific data can indicate hotspots of potential hazards to sectors which are not directly related to nanomaterials and nanotechnology, but where workers are exposed to high concentrations of nanoparticles. This can increase understanding of possible symptoms and facilitate risk identification. Moreover, it may contribute to the definition of relevant OEL values or other legislative regulations.
- Finally, the dissemination of the major findings and their potential health implications to the workers directly affected can be paramount for their safety. The understanding of the immediate risks along with the proper training on how to avoid them, can result in safer operational practices among the workforce.

References

ACGIH, 1995. Threshold Limit Values for Chemical Substances and Physical Agents and Biological Exposure Indices. Cincinnati, Ohio.

Agarwal, J.K., Sem, G.J., 1980. Continuous flow, single-particle-counting condensation nucleus counter. J. Aerosol Sci. 11, 343–357. https://doi.org/https://doi.org/10.1016/0021-8502(80)90042-7

Allen, G., Sioutas, C., Koutrakis, P., Reiss, R., Lurmann, F.W., Roberts, P.T., 1997. Evaluation of the TEOM® Method for Measurement of Ambient Particulate Mass in Urban Areas. J. Air Waste Manag. Assoc. 47, 682–689. https://doi.org/10.1080/10473289.1997.10463923

Alofs, D.J., Balakumar, P., 1982. Inversion to obtain aerosol size distributions from measurements with a differential mobility analyzer. J. Aerosol Sci. 13, 513–527. https://doi.org/10.1016/0021-8502(82)90017-9

Araujo, J.A., Barajas, B., Kleinman, M., Wang, X., Bennett, B.J., Gong, K.W., Navab, M., Harkema, J., Sioutas, C., Lusis, A.J., Nel, A.E., 2008. Ambient particulate pollutants in the ultrafine range promote early atherosclerosis and systemic oxidative stress. Circ. Res. 102, 589–596. https://doi.org/10.1161/CIRCRESAHA.107.164970

Asbach, C., Alexander, C., Clavaguera, S., Dahmann, D., Dozol, H., Faure, B., Fierz, M., Fontana, L., Iavicoli, I., Kaminski, H., MacCalman, L., Meyer-Plath, A., Simonow, B., van Tongeren, M., Todea, A.M., 2017. Review of measurement techniques and methods for assessing personal exposure to airborne nanomaterials in workplaces. Sci. Total Environ. 603–604, 793–806. https://doi.org/10.1016/j.scitotenv.2017.03.049

Asbach, C., Clavaguera, S., Todea, A.M., 2016. Measurement Methods for Nanoparticles in Indoor and Outdoor Air, in: Viana, M. (Ed.), Indoor and Outdoor Nanoparticles: Determinants of Release and Exposure Scenarios. Springer International Publishing, Cham, pp. 19–49. https://doi.org/10.1007/698_2015_423

Balakrishnan, K., Dey, S., Gupta, T., Dhaliwal, R.S., Brauer, M., Cohen, A.J., Stanaway, J.D., Beig, G., Joshi, T.K., Aggarwal, A.N., Sabde, Y., Sadhu, H., Frostad, J., Causey, K., Godwin, W., Shukla, D.K., Kumar, G.A., Varghese, C.M., Muraleedharan, P., Agrawal, A., Anjana, R.M., Bhansali, A., Bhardwaj, D., Burkart, K., Cercy, K., Chakma, J.K., Chowdhury, S., Christopher, D.J., Dutta, E., Furtado, M., Ghosh, S., Ghoshal, A.G., Glenn, S.D., Guleria, R., Gupta, R., Jeemon, P., Kant, R., Kant, S., Kaur, T., Koul, P.A., Krish, V., Krishna, B., Larson, S.L., Madhipatla, K., Mahesh, P.A., Mohan, V., Mukhopadhyay, S., Mutreja, P., Naik, N., Nair, S., Nguyen, G., Odell, C.M., Pandian, J.D., Prabhakaran, D., Prabhakaran, P., Roy, A., Salvi, S., Sambandam, S., Saraf, D., Sharma, M., Shrivastava, A., Singh, V., Tandon, N., Thomas, N.J., Torre, A., Xavier, D., Yadav, G., Singh, S., Shekhar, C., Vos, T., Dandona, R., Reddy, K.S., Lim, S.S., Murray, C.J.L., Venkatesh, S., Dandona, L., 2019. The impact of air pollution on deaths, disease burden, and life expectancy across the states of India: the Global Burden of Disease Study 2017. Lancet Planet. Heal. 3, e26–e39. https://doi.org/10.1016/S2542-5196(18)30261-4

Basinas, I., Jiménez, A.S., Galea, K.S., Tongeren, M. van, Hurley, F., 2018. A Systematic Review of the Routes and Forms of Exposure to Engineered Nanomaterials. Ann. Work Expo. Heal. 62, 639–662. https://doi.org/10.1093/annweh/wxy048

Bello, D., Wardle, B.L., Yamamoto, N., Guzman DeVilloria, R., Garcia, E.J., Hart, A.J., Ahn, K., Ellenbecker, M.J., Hallock, M., 2009. Exposure to nanoscale particles and fibers during machining of hybrid advanced composites containing carbon nanotubes. J. Nanoparticle Res. 11, 231–249. https://doi.org/10.1007/s11051-008-9499-4

BéruBé, K., Balharry, D., Sexton, K., Koshy, L., Jones, T., 2007. COMBUSTION-DERIVED NANOPARTICLES: MECHANISMS OF PULMONARY TOXICITY. Clin. Exp. Pharmacol. Physiol. 34, 1044–1050. https://doi.org/10.1111/j.1440-1681.2007.04733.x

Boverhof, D.R., Bramante, C.M., Butala, J.H., Clancy, S.F., Lafranconi, W.M., West, J., Gordon, S.C., 2015. Comparative assessment of nanomaterial definitions and safety evaluation considerations. Regul. Toxicol. Pharmacol. 73, 137–150. https://doi.org/10.1016/j.yrtph.2015.06.001

Brand, P., Havlicek, P., Steiners, M., Holzinger, K., Reisgen, U., Kraus, T., Gube, M., 2013a. Exposure of healthy subjects with emissions from a gas metal arc welding process: Part 1 - Exposure technique and external exposure. Int. Arch. Occup. Environ. Health 86, 25–30. https://doi.org/10.1007/s00420-012-0739-7

Brand, P., Lenz, K., Reisgen, U., Kraus, T., 2013b. Number size distribution of fine and ultrafine fume particles from various welding processes. Ann. Occup. Hyg. 57, 305–313. https://doi.org/10.1093/annhyg/mes070

Brouwer, D., 2010. Exposure to manufactured nanoparticles in different workplaces. Toxicology 269, 120–127. https://doi.org/10.1016/j.tox.2009.11.017

Brouwer, D., Berges, M., Virji, M.A., Fransman, W., Bello, D., Hodson, L., Gabriel, S., Tielemans, E., 2012. Harmonization of measurement strategies for exposure to manufactured nano-objects; Report of a workshop. Ann. Occup. Hyg. 56, 1–9. https://doi.org/10.1093/annhyg/mer099

Brouwer, D., Van Duuren-Stuurman, B., Berges, M., Jankowska, E., Bard, D., Mark, D., 2009. From workplace air measurement results toward estimates of exposure? Development of a strategy to assess exposure to manufactured nano-objects. J. Nanoparticle Res. 11, 1867–1881. https://doi.org/10.1007/s11051-009-9772-1

Brouwer, D.H., Gijsbers, J.H.J., Lurvink, M.W.M., 2004. Personal exposure to ultrafine particles in the workplace: Exploring sampling techniques and strategies. Ann. Occup. Hyg. 48, 439–453. https://doi.org/10.1093/annhyg/meh040

Burtscher, H., 2005. Physical characterization of particulate emissions from diesel engines: a review. J. Aerosol Sci. 36, 896–932. https://doi.org/10.1016/j.jaerosci.2004.12.001

Buzea, C., Pacheco, I.I., Robbie, K., 2007. Nanomaterials and nanoparticles: Sources and toxicity. Biointerphases 2, MR17–MR71. https://doi.org/10.1116/1.2815690

CEN, 1993. Workplace Atmospheres - Size Fraction Definitions for Measurement of Airborne Particles. Belgium.

Cena, L.G., Chisholm, W.P., Keane, M.J., Chen, B.T., 2015. A Field Study on the Respiratory Deposition of the Nano-Sized Fraction of Mild and Stainless Steel Welding Fume Metals. J. Occup. Environ. Hyg. 12, 721–728. https://doi.org/10.1080/15459624.2015.1043055

Chen, D., Pui, D.Y.H., Hummes, D., Fissan, H., Quant, F.R., Sem, G.J., 1996. Nanometer differential mobility analyzer (Nano-DMA): Design and numerical modeling. J. Aerosol Sci. 27, S137–S138. https://doi.org/10.1016/0021-8502(96)00141-3

Chen, M., Wang, H., Sun, Q., Yu, F., Wang, Y., Wan, W., Wang, C., Gui, H., Liu, J., Lü, L., 2019. Simulation of Miniature PDMA for Ultrafine-Particle Measurement. Atmosphere (Basel). 10, 116. https://doi.org/10.3390/atmos10030116

Chow, J.C., 1995. Measurement methods to determine compliance with ambient air quality standards for suspended particles. J. Air Waste Manag. Assoc. 45, 320–382.

https://doi.org/10.1080/10473289.1995.10467369

Colomban, P., 2013. The Destructive/Non-Destructive Identification of Enameled Pottery, Glass Artifacts and Associated Pigments—A Brief Overview. Arts 2, 77–110. https://doi.org/10.3390/arts2030077

Conti, J.A., Killpack, K., Gerritzen, G., Huang, L., Mircheva, M., Delmas, M., Harthorn, B.H., Appelbaum, R.P., Holden, P.A., 2008. Health and safety practices in the nanomaterials workplace: Results from an international survey. Environ. Sci. Technol. 42, 3155–3162. https://doi.org/10.1021/es702158q

D'Anna, A., 2009. Combustion-formed nanoparticles. Proc. Combust. Inst. 32, 593–613. https://doi.org/10.1016/j.proci.2008.09.005

Debia, M., Bakhiyi, B., Ostiguy, C., Verbeek, J.H., Brouwer, D.H., Murashov, V., 2016. A Systematic Review of Reported Exposure to Engineered Nanomaterials. Ann. Occup. Hyg. 60, 916–935. https://doi.org/10.1093/annhyg/mew041

Deepshikha, S., Srinivasan, J., 2010. Discriminating between natural and anthropogenic aerosol contributions to optical depth over Afro-Asian region. Atmos. Sci. Lett. 11, 307–312. https://doi.org/10.1002/asl.299

Demou, E., Stark, W.J., Hellweg, S., 2009. Particle emission and exposure during nanoparticle synthesis in research laboratories. Ann. Occup. Hyg. 53, 829–838. https://doi.org/10.1093/annhyg/mep061

Ding Y., Kuhlbusch T.A.J., Van Tongeren M, Jiménez AS, Tuinman I., Chen R., Alvarez I.L, Mikolajczyk U., Nickel C., Meyer J, Kaminski H, Wohlleben W, Stahlmecke B., Clavaguera S., Riediker M., 2017. Airborne engineered nanomaterials in the workplace—a review of release and worker exposure during nanomaterial production and handling processes. *J. Hazard. Mat.* 322, 17–28. https://doi.org/10.1016/j.jhazmat.2016.04.075

Donaldson, K., Brown, D., Clouter, A., Duffin, R., MacNee, W., Renwick, L., Tran, L., Stone, V., 2002. The Pulmonary Toxicology of Ultrafine Particles. J. Aerosol Med. 15, 213–220. https://doi.org/10.1089/089426802320282338

Donaldson, K., Stone, V., Clouter, A., Renwick, L., MacNee, W., 2001a. Ultrafine particles. Occup. Environ. Med. 58, 211–216. https://doi.org/10.1136/oem.58.3.211

Donaldson, K., Stone, V., Seaton, A., Macnee, W., 2001b. Ambient particle inhalation and the cardiovascular system: potential mechanisms. Environ. Health Perspect. 109, 523–527. https://doi.org/sc271_5_1835 [pii]

Donaldson, K., Tran, L., Jimenez, L.A., Duffin, R., Newby, D.E., Mills, N., MacNee, W., Stone, V., 2005. Combustion-derived nanoparticles: A review of their toxicology following inhalation exposure. Part. Fibre Toxicol. 2, 1–14. https://doi.org/10.1186/1743-8977-2-10

E.U., 2014. COUNCIL DIRECTIVE 98/24/EC. Off. J. Eur. Communities.

Eleftheriadis, K., Ochsenkuhn, K.M., Lymperopoulou, T., Karanasiou, A., Razos, P., Ochsenkuhn-Petropoulou, M., 2014. Influence of local and regional sources on the observed spatial and temporal variability of size resolved atmospheric aerosol mass concentrations and water-soluble species in the Athens metropolitan area. Atmos. Environ. 97, 252–261. https://doi.org/10.1016/j.atmosenv.2014.08.013

Elihn, K., Ulvestad, B., Hetland, S., Wallén, A., Randem, B.G., 2008. Exposure to ultrafine particles in asphalt work. J. Occup. Environ. Hyg. 5, 771–779. https://doi.org/10.1080/15459620802473891

Epp, J., 2016. X-ray diffraction (XRD) techniques for materials characterization, in: Materials Characterization Using Nondestructive Evaluation (NDE) Methods. Elsevier, pp. 81–124. https://doi.org/10.1016/B978-0-08-100040-3.00004-3

EU, 2011. RECOMMENDATIONS ON THE DEFINITION OF NANOMATERIAL. Off. J. Eur. Union L 275/38.

EU, 1989. 89/336/EEC. Off. J. Eur. Communities 139, 1–8.

Evans, D.E., Heitbrink, W.A., Slavin, T.J., Peters, T.M., 2008. Ultrafine and respirable particles in an automotive grey iron foundry. Ann. Occup. Hyg. 52, 9–21. https://doi.org/10.1093/annhyg/mem056

Ferin, J., Oberdörster, G., Penney, D.P., 1992. Pulmonary Retention of Ultrafine and Fine Particles in Rats. Am. J. Respir. Cell Mol. Biol. 6, 535–542. https://doi.org/10.1165/ajrcmb/6.5.535

Fierz, M., Houle, C., Steigmeier, P., Burtscher, H., 2011. Design, calibration, and field performance of a miniature diffusion size classifier. Aerosol Sci. Technol. 45, 1–10. https://doi.org/10.1080/02786826.2010.516283

Flagan, R.C., 1998. History of Electrical Aerosol Measurements. Aerosol Sci. Technol. 28, 301–380. https://doi.org/10.1080/02786829808965530

Fonseca, A.S., 2016. Exposure characterisation and source of nanoparticles in workplace enviroments. University of Barcelona.

Fonseca, A.S., Kuijpers, E., Kling, K.I., Levin, M., Koivisto, A.J., Nielsen, S.H., Fransman, W., Fedutik, Y., Jensen, K.A., Koponen, I.K., 2018. Particle release and control of worker exposure during laboratory-scale synthesis, handling and simulated spills of manufactured nanomaterials in fume hoods. J. Nanoparticle Res. 20. https://doi.org/10.1007/s11051-018-4136-3

Fonseca, A.S., Maragkidou, A., Viana, M., Querol, X., Hämeri, K., de Francisco, I., Estepa, C., Borrell, C., Lennikov, V., de la Fuente, G.F., 2016a. Process-generated nanoparticles from ceramic tile sintering: Emissions, exposure and environmental release. Sci. Total Environ. 565, 922–932. https://doi.org/10.1016/j.scitotenv.2016.01.106

Fonseca, A.S., Viana, M., Pérez, N., Alastuey, A., Querol, X., Kaminski, H., Todea, A.M., Monz, C., Asbach, C., 2016b. Intercomparison of a portable and two stationary mobility particle sizers for nanoscale aerosol measurements. Aerosol Sci. Technol. 50, 653–668. https://doi.org/10.1080/02786826.2016.1174329

Fonseca, A.S., Viana, M., Querol, X., Moreno, N., de Francisco, I., Estepa, C., de la Fuente, G.F., 2015. Ultrafine and nanoparticle formation and emission mechanisms during laser processing of ceramic materials. J. Aerosol Sci. 88, 48–57. https://doi.org/10.1016/j.jaerosci.2015.05.013

Fonseca, A.S., Viitanen, A.K., Koivisto, A.J., Kangas, A., Huhtiniemi, M., Hussein, T., Vanhala, E., Viana, M., Querol, X., Hameri, K., 2014. Characterization of exposure to carbon nanotubes in an industrial setting. Ann. Occup. Hyg. 59, 586–599. https://doi.org/10.1093/annhyg/meu110

Gabay, C., Kushner, I., 1999. ACUTE-PHASE PROTEINS AND OTHER SYSTEMIC RESPONSES TO INFLAMMATION. N. Engl. J. Med. 340, 448–454.

Gebhart, J., 2001. Optical direct-reading techniques: light intensity systems. Wiley-Interscience,New York, NY, New York.

Gerritzen, R.G., Huang, L., Killpack, K., Mircheva, M., Conti, J., 2006. Review of Safety Practices in the Nanotechnology Industry. Saf. Heal. 31.

Goede, H., Christopher-de Vries, Y., Kuijpers, E., Fransman, W., 2018. A Review of Workplace Risk

Management Measures for Nanomaterials to Mitigate Inhalation and Dermal Exposure. Ann. Work Expo. Heal. 1–16. https://doi.org/10.1093/annweh/wxy032

Göhler, D., Stintz, M., Hillemann, L., Vorbau, M., 2010. Characterization of nanoparticle release from surface coatings by the simulation of a sanding process. Ann. Occup. Hyg. 54, 615–624. https://doi.org/10.1093/annhyg/meq053

Graczyk, H., Lewinski, N., Zhao, J., Concha-Lozano, N., Riediker, M., 2015. Characterization of Tungsten Inert Gas (TIG) Welding Fume Generated by Apprentice Welders. Ann. Occup. Hyg. 60, 205–219. https://doi.org/10.1093/annhyg/mev074

GRIMM Aerosol Technik GmbH, n.d. MINI WIDE RANGE AEROSOL SPECTROMETER-Model 1371 [WWW Document]. www.GRIMM-aerosol.com. URL https://www.grimm-aerosol.com/products-en/indoor-air-quality/the-wide-range-hybrid/1371/

Gu, J., Wensing, M., Uhde, E., Salthammer, T., 2019. Characterization of particulate and gaseous pollutants emitted during operation of a desktop 3D printer. Environ. Int. 123, 476–485. https://doi.org/10.1016/j.envint.2018.12.014

Hagen, D.E., Alofs, D.J., 1983. Linear Inversion Method to Obtain Aerosol Size Distributions from Measurements with a Differential Mobility Analyzer. Aerosol Sci. Technol. 2, 465–475. https://doi.org/10.1080/02786828308958650

Halperin, W.E., 1996. The role of surveillance in the hierarchy of prevention. Am. J. Ind. Med. 29, 321–323. https://doi.org/10.1002/(SICI)1097-0274(199604)29:4<321::AID-AJIM8>3.0.CO;2-R

Hermann, M., Wehner, B., Bischof, O., Han, H.S., Krinke, T., Liu, W., Zerrath, A., Wiedensohler, A., 2007. Particle counting efficiencies of new TSI condensation particle counters. J. Aerosol Sci. 38, 674–682. https://doi.org/10.1016/j.jaerosci.2007.05.001

Hewitt, G.W., 1957. The charging of small particles for electrostatic precipitation. Trans. Am. Inst. Electr. Eng. Part I Commun. Electron. 76, 300–306. https://doi.org/10.1109/TCE.1957.6372672

Hinds, W.C., 1999. Aerosol technology: properties, behavior, and measurement of airborne particles. John Wiley & Sons.

Hoek, G., Boogaard, H., Knol, A., De Hartog, J., Slottje, P., Ayres, J.G., Borm, P., Brunekreef, B., Donaldson, K., Forastiere, F., Holgate, S., Kreyling, W.G., Nemery, B., Pekkanen, J., Stone, V., Wichmann, H.E., Van Der Sluijs, J., 2010. Concentration response functions for ultrafine particles and all-cause mortality and hospital admissions: Results of a European expert panel elicitation. Environ. Sci. Technol. 44, 476–482. https://doi.org/10.1021/es9021393

Hoppel, W.A., 1978. Determination of the aerosol size distribution from the mobility distribution of the charged fraction of aerosols. J. Aerosol Sci. 9, 41–54. https://doi.org/10.1016/0021-8502(78)90062-9

Ibald-Mulli, A., Wichmann, H.-E., Kreyling, W., Peters, A., 2002. Epidemiological Evidence on Health Effects of Ultrafine Particles. J. Aerosol Med. 15, 189–201. https://doi.org/10.1089/089426802320282310

Invernizzi, N., 2011. Nanotechnology between the lab and the shop floor: What are the effects on labor? J. Nanoparticle Res. 13, 2249–2268. https://doi.org/10.1007/s11051-011-0333-z

ISO, 1995. ISO 7708:1995-Air quality - Particle size fraction definitions for health-related sampling.

Jenkins, N.T., Eagar, T.W., Pierce, G., 2005. Particle Size Distribution of Gas Metal and FLux Cored Arc Welding Fumes. Scan. Electron Microsc. 156–163.

Jenner, M., 1995. The politics of London air John Evelyn's Fumifugium and the Restoration. Hist. J. 38, 535–551. https://doi.org/10.1017/S0018246X00019968

Jiménez, A.S., Tongeren, M. Van, Cherrie, J.W., 2011. A review of monitoring methods for inhalable hardwood dust.

Kaluza, S., Balderhaar, J. kleine, Orthen, B., Honnert, B., Jankowska, E., Pietrowsk, P., Gracia Rosell, M., Tanarro, C., Tejedor, J., Zugasti, A., 2013. Workplace exposure to nanoparticles, EU-OSHA.

Kaminski, H., Beyer, M., Fissan, H., Asbach, C., Kuhlbusch, T.A.J., 2015. Measurements of nanoscale TiO2and Al2O3in industrial workplace environments – Methodology and results. Aerosol Air Qual. Res. 15, 129–141. https://doi.org/10.4209/aaqr.2014.03.0065

Kim, B., Lee, J.S., Choi, B.S., Park, S.Y., Yoon, J.H., Kim, H., 2013. Ultrafine particle characteristics in a rubber manufacturing factory. Ann. Occup. Hyg. 57, 728–739. https://doi.org/10.1093/annhyg/mes102

Kim, J.J., American Academy of Pediatrics Committee on Environmental Health, 2004. Ambient air pollution: health hazards to children. Pediatrics 114, 1699—1707.

https://doi.org/10.1542/peds.2004-2166

Knibbs, L.D., Cole-Hunter, T., Morawska, L., 2011. A review of commuter exposure to ultrafine particles and its health effects. Atmos. Environ. 45, 2611–2622. https://doi.org/10.1016/j.atmosenv.2011.02.065

Knutson, E.O., Whitby, K.T., 1975. Aerosol classification by electric mobility: apparatus, theory, and applications. J. Aerosol Sci. 6, 443–451. https://doi.org/10.1016/0021-8502(75)90060-9

Kohli, R., 2012. Chapter 3 - Methods for Monitoring and Measuring Cleanliness of Surfaces, in: Kohli, R., Mittal, K.L. (Eds.), Developments in Surface Contamination and Cleaning. William Andrew Publishing, Oxford, pp. 107–178. https://doi.org/https://doi.org/10.1016/B978-1-4377-7883-0.00003-1

Koivisto, A.J., Aromaa, M., Mäkelä, J.M., Pasanen, P., Hussein, T., Hämeri, K., 2012a. Concept To Estimate Regional Inhalation Dose of Industrially Synthesized Nanoparticles. ACS Nano 6, 1195–1203. https://doi.org/10.1021/nn203857p

Koivisto, A.J., Aromaa, M., Mäkelä, J.M., Pasanen, P., Hussein, T., Hämeri, K., Koivisto, A.J., Aromaa, M., Mäkelä, J.M., Hussein, T., 2012b. Concept To Estimate Regional Inhalation Dose of Industrially Synthesized Nanoparticles. ACS Nano 6, 1195–1203. https://doi.org/10.1021/nn203857p

Koivisto, A.J., Hussein, T., Niemelä, R., Tuomi, T., Hämeri, K., 2010. Impact of particle emissions of new laser printers on modeled office room. Atmos. Environ. 44, 2140–2146. https://doi.org/https://doi.org/10.1016/j.atmosenv.2010.02.023

Koivisto, A.J., Jensen, A.C.Ø., Kling, K.I., Nørgaard, A., Brinch, A., Christensen, F., Jensen, K.A., 2017. Quantitative material releases from products and articles containing manufactured nanomaterials: Towards a release library. NanoImpact 5, 119–132. https://doi.org/10.1016/j.impact.2017.02.001

Koivisto, A.J., Jensen, A.C.Ø., Levin, M., Kling, K.I., Maso, M.D., Nielsen, S.H., Jensen, K.A., Koponen, I.K., 2015. Testing the near field/far field model performance for prediction of particulate matter emissions in a paint factory. Environ. Sci. Process. Impacts 17, 62–73. https://doi.org/10.1039/c4em00532e

Koivisto, A.J., Kling, K.I., Levin, M., Fransman, W., Gosens, I., Cassee, F.R., Jensen, K.A., 2016. First order risk assessment for nanoparticle inhalation exposure during injection molding of polypropylene composites and production of tungsten-carbide-cobalt fine powder based upon pulmonary inflammation and surface area dose. NanoImpact 6, 30–38. https://doi.org/10.1016/j.impact.2016.11.002

Koponen, I.K., Koivisto, A.J., Jensen, K.A., 2015. Worker exposure and high time-resolution analyses of process-related submicrometre particle concentrations at mixing stations in two paint factories. Ann. Occup. Hyg. 59, 749–763. https://doi.org/10.1093/annhyg/mev014

Kuhlbusch, T.A.J., Asbach, C., Fissan, H., Göhler, D., Stintz, M., 2011. Nanoparticle exposure at nanotechnology workplaces: A review. Part. Fibre Toxicol. 8, 1–18. https://doi.org/10.1186/1743-8977-8-22

Kuhlbusch, T.A.J., Wijnhoven, S.W.P., Haase, A., 2018. Nanomaterial exposures for worker, consumer and the general public. NanoImpact 10, 11–25. https://doi.org/10.1016/j.impact.2017.11.003

Landrigan, P.J., 2017. Air pollution and health. Lancet Public Heal. 2, e4–e5. https://doi.org/10.1016/S2468-2667(16)30023-8

Landrigan, P.J., Fuller, R., Acosta, N.J.R., Adeyi, O., Arnold, R., Basu, N., Baldé, A.B., Bertollini, R., Bose-O'Reilly, S., Boufford, J.I., Breysse, P.N., Chiles, T., Mahidol, C., Coll-Seck, A.M., Cropper, M.L., Fobil, J., Fuster, V., Greenstone, M., Haines, A., Hanrahan, D., Hunter, D., Khare, M., Krupnick, A., Lanphear, B., Lohani, B., Martin, K., Mathiasen, K. V., McTeer, M.A., Murray, C.J.L., Ndahimananjara, J.D., Perera, F., Potočnik, J., Preker, A.S., Ramesh, J., Rockström, J., Salinas, C., Samson, L.D., Sandilya, K., Sly, P.D., Smith, K.R., Steiner, A., Stewart, R.B., Suk, W.A., van Schayck, O.C.P., Yadama, G.N., Yumkella, K., Zhong, M., 2017. The Lancet Commission on pollution and health. Lancet 391. https://doi.org/10.1016/S0140-6736(17)32345-0

Lehnert, M., Pesch, B., Lotz, A., Pelzer, J., Kendzia, B., Gawrych, K., Heinze, E., Van Gelder, R., Punkenburg, E., Weiss, T., Mattenklott, M., Hahn, J.U., Möhlmann, C., Berges, M., Hartwig, A., Brüning, T., 2012. Exposure to inhalable, respirable, and ultrafine particles in welding fume. Ann. Occup. Hyg. 56, 557–567. https://doi.org/10.1093/annhyg/mes025

Lelieveld, J., Evans, J.S., Fnais, M., Giannadaki, D., Pozzer, A., 2015. The contribution of outdoor air pollution sources to premature mortality on a global scale. Nature 525, 367–371. https://doi.org/10.1038/nature15371

Lelieveld, J., Klingmüller, K., Pozzer, A., Pöschl, U., Fnais, M., Daiber, A., Münzel, T., 2019. Cardiovascular disease burden from ambient air pollution in Europe reassessed using novel hazard ratio functions. Eur. Heart J. 1590–1596. https://doi.org/10.1093/eurheartj/ehz135

Liu, B.Y.H., Kim, C.S., 1977. On the counting efficiency of condensation nuclei counters. Atmos. Environ. 11, 1097–1100. https://doi.org/10.1016/0004-6981(77)90240-2

Liu, B.Y.H., Pui, D.Y.., 1974a. A submicron aerosol standard and the primary, absolute calibration of the condensation nuclei counter. J. Colloid Interface Sci. 47, 155–171. https://doi.org/10.1016/0021-9797(74)90090-3

Liu, B.Y.H., Pui, D.Y.H., 1974b. Electrical neutralization of aerosols. J. Aerosol Sci. 5, 465–472. https://doi.org/10.1016/0021-8502(74)90086-X

Manoli, E., Voutsa, D., Samara, C., 2002. Chemical characterization and source identificatio/napportionment of fine and coarse air particles in Thessaloniki, Greece. Atmos. Environ. 36, 949–961.

Maynard, A.D., Aitken, R.J., 2007. Assessing exposure to airborne nanomaterials: Current abilities and future requirements. Nanotoxicology 1, 26–41. https://doi.org/10.1080/17435390701314720

McMurry, P.H., 2000a. A review of atmospheric aerosol measurements. Atmos. Environ. 34, 1959–1999. https://doi.org/10.1016/S1352-2310(99)00455-0

McMurry, P.H., 2000b. The history of condensation nucleus counters. Aerosol Sci. Technol. 33, 297–322. https://doi.org/10.1080/02786820050121512

Mills, N.L., Miller, M.R., Lucking, A.J., Beveridge, J., Flint, L., Boere, A.J.F., Fokkens, P.H., Boon, N.A., Sandstrom, T., Blomberg, A., Duffin, R., Donaldson, K., Hadoke, P.W.F., Cassee, F.R., Newby, D.E., 2011. Combustion-derived nanoparticulate induces the adverse vascular effects of diesel exhaust inhalation. Eur. Heart J. 32, 2660–2671. https://doi.org/10.1093/eurheartj/ehr195

Monsé, C., Hagemeyer, O., Raulf, M., Jettkant, B., van Kampen, V., Kendzia, B., Gering, V., Kappert, G., Weiss, T., Ulrich, N., Marek, E.-M., Bünger, J., Brüning, T., Merget, R., 2018. Concentration-dependent systemic response after inhalation of nano-sized zinc oxide particles in human volunteers. Part. Fibre Toxicol. 15, 8. https://doi.org/10.1186/s12989-018-0246-4

Morawska, L., He, C., Johnson, G., Jayaratne, R., Salthammer, T., Wang, H., Uhde, E., Bostrom, T., Modini, R., Ayoko, G., McGarry, P., Wensing, M., 2009. An Investigation into the Characteristics and Formation Mechanisms of Particles Originating from the Operation of Laser Printers. Environ. Sci. Technol. 43, 1015–1022. https://doi.org/10.1021/es802193n

NIOSH, 2013. Protecting the Nanotechnology Workforce. Cincinnati, OH: U.S.

O'Dowd, C.D., De Leeuw, G., 2007. Marine aerosol production: A review of the current knowledge. Philos. Trans. R. Soc. A Math. Phys. Eng. Sci. 365, 1753–1774. https://doi.org/10.1098/rsta.2007.2043

Oberdörster, G., Oberdörster, E., Oberdörster, J., 2005a. Nanotoxicology: An Emerging Discipline Evolving from Studies of Ultrafine Particles. Environ. Health Perspect. 113, 823–839. https://doi.org/10.1289/ehp.7339

Oberdörster, G., Oberdörster, E., Oberdörster, J., 2005b. Nanotoxicology: An emerging discipline evolving from studies of ultrafine particles. Environ. Health Perspect. 113, 823–839. https://doi.org/10.1289/ehp.7339

Oberdörster, G., Utell, J.M., 2002. Ultrafine Particles in the Urban Air: To the Respiratory Tract—And Beyond? Environ. Health Perspect. 110, 440–441. https://doi.org/10.2788/678452

OECD, 2015. Harmonized Tiered Approach to Measure and Assess the Potential Exposure to Airborne Emissions of Engineered Nano-Objects and their Agglomerates and Aggregates at Workplaces. Ser. Saf. Manuf. Nanomater. No.55 55, JT03378848–JT03378848.

OJIMA, J., 2012. Gaseous Contaminant Distribution in the Breathing Zone. Ind. Health 50, 236–238. https://doi.org/10.2486/indhealth.MS1314

Pey, J., Querol, X., Alastuey, A., Forastiere, F., Stafoggia, M., 2013. African dust outbreaks over the Mediterranean Basin during 2001–2011: PM10 concentrations, phenomenology and trends, and its relation with synoptic and mesoscale meteorology. Atmos. Chem. Phys. 13, 1395–1410. https://doi.org/10.5194/acp-13-1395-2013

Pope, C.A., Dockery, D.W., Schwartz, J., 1995. Review of Epidemiological Evidence of Health Effects of Particulate Air Pollution. Inhal. Toxicol. 7, 1–18.

Querol, X., Alastuey, A., Ruiz, C.R., Artiñano, B., Hansson, H.C., Harrison, R.M., Buringh, E., Ten Brink, H.M., Lutz, M., Bruckmann, P., Straehl, P., Schneider, J., 2004a. Speciation and origin of PM10 and PM2.5 in selected European cities. Atmos. Environ. 38, 6547–6555. https://doi.org/10.1016/j.atmosenv.2004.08.037

Querol, X., Alastuey, A., Viana, M.M., Rodriguez, S., Artiñano, B., Salvador, P., Garcia Do Santos, S., Fernandez Patier, R., Ruiz, C.R., De La Rosa, J., Sanchez De La Campa, A., Menendez, M., Gil, J.I., 2004b. Speciation and origin of PM10 and PM2.5 in Spain. J. Aerosol Sci. 35, 1151–1172. https://doi.org/10.1016/j.jaerosci.2004.04.002

Querol, X., Viana, M., Alastuey, A., Amato, F., Moreno, T., Castillo, S., Pey, J., de la Rosa, J., Sánchez de la Campa, A., Artíñano, B., Salvador, P., García Dos Santos, S., Fernández-Patier, R., Moreno-Grau, S., Negral, L., Minguillón, M.C., Monfort, E., Gil, J.I., Inza, A., Ortega, L.A., Santamaría, J.M., Zabalza, J., 2007. Source origin of trace elements in PM from regional background, urban and industrial sites of Spain. Atmos. Environ. 41, 7219–7231. https://doi.org/10.1016/j.atmosenv.2007.05.022

Rader, D.J., McMurry, P.H., 1986. Application of the tandem differential mobility analyzer to studies of droplet growth or evaporation. J. Aerosol Sci. 17, 771–787. https://doi.org/10.1016/0021-8502(86)90031-5

Ramachandran, G., 2008. Toward better exposure assessment strategies - The new NIOSH initiative. Ann. Occup. Hyg. 52, 297–301. https://doi.org/10.1093/annhyg/men025

Raynor, P.C., Cebula, J.I., Spangenberger, J.S., Olson, B.A., Dasch, J.M., D'Arcy, J.B., 2012. Assessing Potential Nanoparticle Release During Nanocomposite Shredding Using Direct-Reading Instruments. J. Occup. Environ. Hyg. 9, 1–13. https://doi.org/10.1080/15459624.2012.633061

Ribalta, C., Koivisto, A.J., Salmatonidis, A., López-Lilao, A., Monfort, E., Viana, M., 2019. Modeling of High Nanoparticle Exposure in an Indoor Industrial Scenario with a One-Box Model. Int. J. Environ. Res. Public Health 16, 1695. https://doi.org/10.3390/ijerph16101695

Saber, A.T., Jacobsen, N.R., Jackson, P., Poulsen, S.S., Kyjovska, Z.O., Halappanavar, S., Yauk, C.L., Wallin, H., Vogel, U., 2014. Particle-induced pulmonary acute phase response may be the causal link between particle inhalation and cardiovascular disease. Wiley Interdiscip. Rev. Nanomedicine Nanobiotechnology 6, 517–531. https://doi.org/10.1002/wnan.1279

Sadik, O.A., 2013. Anthropogenic nanoparticles in the environment. Environ. Sci. Process. Impacts 15, 19–20. https://doi.org/10.1039/c2em90063g

Salmatonidis, A., Ribalta, C., Sanfélix, V., Bezantakos, S., Biskos, G., Vulpoi, A., Simion, S., Monfort, E., Viana, M., 2019a. Workplace Exposure to Nanoparticles during Thermal Spraying of Ceramic Coatings. Ann. Work Expo. Heal. 63, 91–106. https://doi.org/10.1093/annweh/wxy094

Salmatonidis, A., Viana, M., Biskos, G., Bezantakos, S., 2019b. Hygroscopic behaviour of UFPs emitted during thermal spraying, submited to the Journal of Aerosol Science (under review).

Salmatonidis, A., Viana, M., Pérez, N., Alastuey, A., de la Fuente, G.F., Angurel, L.A., Sanfélix, V., Monfort, E., 2018. Nanoparticle formation and emission during laser ablation of ceramic tiles. J. Aerosol Sci. 126, 152–168. https://doi.org/10.1016/j.jaerosci.2018.09.006

Sanfélix, V., Monfort, E., López-Lilao, A., Estupiñá, S., Viana, M., Salmatonidis, A., Guaita, L., Nácher, F., M.C.Bellés, Ribera, A., 2018. Emissions of Nanoparticles Generated in the Ceramic Process, in: Qualicer 2018. Castellon, pp. 1–11.

Savolainen, K., Alenius, H., Norppa, H., Pylkkänen, L., Tuomi, T., Kasper, G., 2010a. Risk assessment of engineered nanomaterials and nanotechnologies-A review. Toxicology 269, 92–104. https://doi.org/10.1016/j.tox.2010.01.013

Savolainen, K., Pylkkänen, L., Norppa, H., Falck, G., Lindberg, H., Tuomi, T., Vippola, M., Alenius, H., Hämeri, K., Koivisto, J., Brouwer, D., Mark, D., Bard, D., Berges, M., Jankowska, E., Posniak, M., Farmer, P., Singh, R., Krombach, F., Bihari, P., Kasper, G., Seipenbusch, M., 2010b. Nanotechnologies, engineered nanomaterials and occupational health and safety - A review. Saf. Sci. 48, 957–963. https://doi.org/10.1016/j.ssci.2010.03.006

Schaming, D., Remita, H., 2015. Nanotechnology: from the ancient time to nowadays. Found. Chem. 17, 187–205. https://doi.org/10.1007/s10698-015-9235-y

Schmid, O., Stoeger, T., 2017. Surface area is the biologically most effective dose metric for acute nanoparticle toxicity in the lung. J. Aerosol Sci. 113, 276. https://doi.org/10.1016/j.jaerosci.2017.09.017

Schulte, P., Geraci, C., Zumwalde, R., Hoover, M., Kuempe, E., 2008. Occupational risk management of engineered nanoparticles. J. Occup. Environ. Hyg. 5, 239–249. https://doi.org/10.1080/15459620801907840

Schulte, P.A., Geraci, C.L., Murashov, V., Kuempel, E.D., Zumwalde, R.D., Castranova, V., Hoover, M.D., Hodson, L., Martinez, K.F., 2014. Occupational safety and health criteria for responsible development of nanotechnology. J. Nanoparticle Res. 16. https://doi.org/10.1007/s11051-013-2153-9

Schulte, P.A., Roth, G., Hodson, L.L., Murashov, V., Hoover, M.D., Zumwalde, R., Kuempel, E.D., Geraci, C.L., Stefaniak, A.B., Castranova, V., Howard, J., 2016. Taking stock of the occupational safety and health challenges of nanotechnology: 2000–2015. J. Nanoparticle Res. 18, 1–21. https://doi.org/10.1007/s11051-016-3459-1

Sowards, J., Lippold, J., Dickinson, D., Ramirez, A., 2008. Characterization of Welding Fume from SMAW Electrodes — Part I. Weld. JOURNAL-NEW YORK 87.

Šrám, R.J., Binková, B., Dejmek, J., Bobak, M., 2005. Ambient Air Pollution and Pregnancy Outcomes: A Review of the Literature. Environ. Health Perspect. 113, 375–382. https://doi.org/10.1289/ehp.6362

Stephens, B., Azimi, P., El, Z., Ramos, T., 2013. Ultra fi ne particle emissions from desktop 3D printers. Atmos. Environ. 79, 334–339. https://doi.org/10.1016/j.atmosenv.2013.06.050

Stoeger, T., Reinhard, C., Takenaka, S., Schroeppel, A., Karg, E., Ritter, B., Heyder, J., Schulz, H., 2006. Instillation of six different ultrafine carbon particles indicates a surface area threshold dose for acute lung inflammation in mice. Environ. Health Perspect. 114, 328–333. https://doi.org/10.1289/ehp.8266

Stolzenburg, M.R., McMurry, P.H., 1991. An ultrafine aerosol condensation nucleus counter. Aerosol Sci. Technol. 14, 48–65. https://doi.org/10.1080/02786829108959470

Tritscher, T., Beeston, M., Zerrath, A.F., Elzey, S., Krinke, T.J., Filimundi, E., Bischof, O.F., 2013. NanoScan SMPS-A novel, portable nanoparticle sizing and counting instrument. J. Phys. Conf. Ser. 429. https://doi.org/10.1088/1742-6596/429/1/012061

Tsai, S.J., Ada, E., Isaacs, J.A., Ellenbecker, M.J., 2009. Airborne nanoparticle exposures associated with the manual handling of nanoalumina and nanosilver in fume hoods. J. Nanoparticle Res. 11, 147–161. https://doi.org/10.1007/s11051-008-9459-z

U.S.C., 1970. OCCUPATIONAL SAFETY AND HEALTH ACT OF 1970.

van Broekhuizen, P., 2017. Applicability of provisional NRVs to PGNPs and FCNPs. Amsterdam. https://doi.org/10.13140/RG.2.2.18241.25445

van Broekhuizen, P., van Broekhuizen, F., Cornelissen, R., Reijnders, L., 2011. Use of nanomaterials in the European construction industry and some occupational health aspects thereof. J. Nanoparticle Res. 13, 447–462. https://doi.org/10.1007/s11051-010-0195-9

Van Broekhuizen, P., Van Broekhuizen, F., Cornelissen, R., Reijnders, L., 2012a. Workplace exposure to nanoparticles and the application of provisional nanoreference values in times of uncertain risks. J. Nanoparticle Res. 14. https://doi.org/10.1007/s11051-012-0770-3

Van Broekhuizen, P., Van Veelen, W., Streekstra, W.H., Schulte, P., Reijnders, L., 2012b. Exposure limits for nanoparticles: Report of an international workshop on nano reference values. Ann. Occup. Hyg. 56, 515–524. https://doi.org/10.1093/annhyg/mes043

Viana, M., Fonseca, A.S., Querol, X., López-Lilao, A., Carpio, P., Salmatonidis, A., Monfort, E., 2017. Workplace exposure and release of ultrafine particles during atmospheric plasma spraying in the ceramic industry. Sci. Total Environ. 599–600, 2065–2073. https://doi.org/10.1016/j.scitotenv.2017.05.132

Viana, M., Kuhlbusch, T.A.J., Querol, X., Alastuey, A., Harrison, R.M., Hopke, P.K., Winiwarter, W., Vallius, M., Szidat, S., Prévôt, A.S.H., Hueglin, C., Bloemen, H., Wåhlin, P., Vecchi, R., Miranda, A.I., Kasper-Giebl, A., Maenhaut, W., Hitzenberger, R., 2008. Source apportionment of particulate matter in Europe: A review of methods and results. J. Aerosol Sci. 39, 827–849. https://doi.org/10.1016/j.jaerosci.2008.05.007

Viana, M., Pey, J., Querol, X., Alastuey, A., de Leeuw, F., Lükewille, A., 2014. Natural sources of atmospheric aerosols influencing air quality across Europe. Sci. Total Environ. 472, 825–833. https://doi.org/10.1016/j.scitotenv.2013.11.140

Viitanen, A.K., Uuksulainen, S., Koivisto, A.J., Hämeri, K., Kauppinen, T., 2017. Workplace measurements of ultrafine particles-A literature review. Ann. Work Expo. Heal. 61, 749–758. https://doi.org/10.1093/annweh/wxx049

Voiland, A., 2010. Aerosols: Tiny Particles, Big Impact [WWW Document]. NASA, Earth Obs. URL https://earthobservatory.nasa.gov/features/Aerosols/page1.php

Voliotis, A., Bezantakos, S., Giamarelou, M., Valenti, M., Kumar, P., Biskos, G., 2014. Nanoparticle emissions from traditional pottery manufacturing. Environ. Sci. Process. Impacts 16, 1489–1494. https://doi.org/10.1039/C3EM00709J

von Glasow, R., 2010. Atmospheric chemistry in volcanic plumes. Proc. Natl. Acad. Sci. 107, 6594–6599. https://doi.org/10.1073/pnas.0913164107

Warheit, D.B., Webb, T.R., Sayes, C.M., Colvin, V.L., Reed, K.L., 2006. Pulmonary Instillation Studies with Nanoscale TiO2 Rods and Dots in Rats: Toxicity Is not Dependent upon Particle Size and Surface Area. Toxicol. Sci. 91, 227–236. https://doi.org/10.1093/toxsci/kfj140

Warren, B.E., 1990. X-ray Diffraction. Courier Corporation.

WHO, 2016. Ambient air pollution: A global assessment of exposure and burden of disease. Geneva.

WHO, W.H.O., 2017. WHO Guidelines on Protecting Workers from Potential Risks of Manufactured Nanomaterials. World Health Organization, Geneva.

Wiedensohler, A., Birmili, W., Nowak, A., Sonntag, A., Weinhold, K., Merkel, M., Wehner, B., Tuch, T., Pfeifer, S., Fiebig, M., Fjäraa, A.M., Asmi, E., Sellegri, K., Depuy, R., Venzac, H., Villani, P., Laj, P., Aalto, P., Ogren, J.A., Swietlicki, E., Williams, P., Roldin, P., Quincey, P., Hüglin, C., Fierz-Schmidhauser, R., Gysel, M., Weingartner, E., Riccobono, F., Santos, S., Grüning, C., Faloon, K., Beddows, D., Harrison, R., Monahan, C., Jennings, S.G., O'Dowd, C.D., Marinoni, A., Horn, H.G., Keck, L., Jiang, J., Scheckman, J., McMurry, P.H., Deng, Z., Zhao, C.S., Moerman, M., Henzing, B., De Leeuw, G., Löschau, G., Bastian, S., 2012. Mobility particle size spectrometers: Harmonization of technical standards and data structure to facilitate high quality long-term observations of atmospheric particle number size distributions. Atmos. Meas. Tech. 5, 657–685. https://doi.org/10.5194/amt-5-657-2012

Wiedensohlet, A., Orsini, D., Covert, D.S., Coffmann, D., Cantrell, W., Havlicek, M., Brechtel, F.J., Russell, L.M., Weber, R.J., Gras, J., Hudson, J.G., Litchy, M., 1997. Intercomparison Study of the Size-Dependent Counting Efficiency of 26 Condensation Particle Counters. Aerosol Sci. Technol. 27, 224–242. https://doi.org/10.1080/02786829708965469

Williams, D.B., Carter, C.B., 2009. Transmission Electron Microscopy, Second. ed. Springer Science& Business Media, New York,.

Winklmayr, W., Reischl, G.P., Lindner, A.O., Berner, A., 1991. A new electromobility spectrometer for the measurement of aerosol size distributions in the size range from 1 to 1000 nm. J. Aerosol Sci. 22, 289–296. https://doi.org/10.1016/S0021-8502(05)80007-2

Young, R.A., 1993. The rietveld method. Oxford University Press.

Zartarian, V., Bahadori, T., McKone, T., 2005. Adoption of an official ISEA glossary. J. Expo. Anal. Environ. Epidemiol. 15, 1–5. https://doi.org/10.1038/sj.jea.7500411

Zhang, S.H., Akutsu, Y., Russell, L.M., Flagan, R.C., Seinfeld, J.H., 1995. Radial differential mobility analyzer. Aerosol Sci. Technol. 23, 357–372. https://doi.org/10.1080/02786829508965320

Zhou, Y., Kong, X., Chen, A., Cao, S., 2015. Investigation of Ultrafine Particle Emissions of Desktop 3D Printers in the Clean Room. Procedia Eng. 121, 506–512. https://doi.org/10.1016/j.proeng.2015.08.1099

Zimmer, A.T., Biswas, P., 2001. Characterization of the aerosols resulting from arc welding processes. J. Aerosol Sci. 32, 993–1008. https://doi.org/https://doi.org/10.1016/S0021-8502(01)00035-0

Zimmer, A.T., Maynard, A.D., 2002. Investigation of the aerosols produced by a high-speed, hand-held grinder using various substrates. Ann. Occup. Hyg. 46, 663–672. https://doi.org/10.1093/annhyg/mef089

Annex: Abbreviations and Acronyms

Abbreviation	**Description**
ACGIH	American Conference of Governmental Industrial Hygienists
ACH	Air Changes per Hour
APS	Atmospheric Plasma Spraying
BG	Background
BZ	Breathing zone
CEN	European Committee for Standardization
CPC	Condensation Particle Counter
CyI	The Cyprus Institute
DiSCmini	Diffusion Size Classifier miniature
DMA	Differential Mobility Analyzer
Dp	Particle Diameter
ECHA	European Chemical Agency
EDX	Energy Dispersive X-ray
ENP	Engineered Nanoparticles
ES	Emission Source
EU	European Union
GER	Glazed Earthenware Red tile
HVOF	High Velocity Oxy-Fuel spraying
ICMA	Aragon Material Science Institute

ICRP	International Commission on Radiological Protection
Ind.	Industrial
ISO	International Organization for Standardization
ITC	Institute for Ceramic Technology
LDSA	Lung Deposited Surface Area
LEV	Local Exhaust Ventilation
mid-IR	middle Infrared
MNMs	Manufactured Nanomaterials
N	Total Particle Number Concentration
N.A.	Not Available
n-ENP	Non-Engineered Nanoparticles
NF	Near Field
NIOSH	National Institute for Occupational Safety and Health
n-IR	near Infrared
NRV	Nano-Reference Values
OECD	Organization for Economic Cooperation and Development
OEL	Occupational Exposure Limits
OPC	Optical Particle Counter
OPS	Optical Particle Sizer
PGNPs	Process Generated Nanoparticles
PLA	Pulsed Laser Ablation
PM	Particulate Matter
P.P.	Pilot Plant

PPE	Personal Protective Equipment
RH	Relative Humidity
SER	Social Economic Council of Netherland
SMPS	Scanning Mobility Particle Sizer
TEM	Transmission Electron Microscopy
TS	Thermal Spraying
TSP	Total Suspended Particles
UAW	Unglazed Alumina White tile
UBW	Unglazed Biscuit White tile
UFP	Ultrafine Particles tile
UPG	Unglazed Porcelain Grey
WA	Worker Area
WHO	World Health Organization

Acknowledgements

The current PhD Thesis was carried out in the framework of the CERASAFE project (www.cerasafe.eu), with the support of SIINN ERA-NET (project id: 16), and was funded by the Spanish MINECO (PCIN-2015-173-C02-01). Additional support from project MAT2016-79866-R (AEI/FEDER, UE) and from the 'Generalitat de Catalunya' (project number: AGAUR 2017 SGR41) is also acknowledged. Furthermore, the Aragón Materials Science Institute (ICMA - Universidad de Zaragoza, CSIC), the European Ceramics Centre in Limoges, the Cyprus Institute (CyI) and TM COMAS (http://www.tmcomas.com) are kindly thanked for their committed cooperation.

I would like to gratefully thank my supervisors, Dr. Mar Viana for the great opportunity that she gave me and her flawless supervision and unconditioned support; and Prof. Dr. Eliseo Monfort for making a huge effort to overcome the kilometric distance every time I sought his assistance and guidance during my PhD candidateship. Thanks to your professionalism and scientific expertise, these last three years were highly productive as well as educating for me. I would also like to thank my tutor at the University of Barcelona (Faculty of Chemistry) Dr. Angels Sahuquillo Estrugo for her kind support and advice every time I requested her assistance.

Kind acknowledgements to all the co-authors of the scientific papers included in this Thesis. My sincere gratitude to Prof. Dr. George Biskos and to Dr. Spyros Bezantakos from the CyI for their help and cooperation during the experimental, analytical and scripting part of my PhD. My warmest appreciations to Prof. Dr. German de la Fuente and Prof. Dr. Luis Alberto Angurel from ICMA, for substantially supporting my work by providing their scientific expertise as well as the facilities and means to perform my experimental work. My honest thanks to Prof. Dr. Andres Alastuey and Dr. Noemi Perez from IDAEA-CSIC, for aiding my work by providing advance equipment (i.e. instruments), scientific, technical and organizational support. Prof. Dr. Pawlowski and Dr. Pablo Carpio are also acknowledged for their collaboration. To my trustworthy coworkers Dr. Vicenta (Tica) Sanfelix from ITC in Castellon and Dr. Carla Ribalta from IDAEA-CSIC, thank you very much for your constant help and committed cooperation. I would also like to thank Prof. Dr. Simon Simion and Dr. Adriana Vulpoi from the Babeș-Bolyai University in Romania.

My sincere appreciation to Prof. Dr. Xavier Querol for leading by example and providing inspiration to carry out scientific research at the top level. Special thanks to my colleague and compatriot Dr.

Angeliki Karanasiou for all her help before and during my work at IDAEA-CSIC. I would like to express my thanks to my friends and colleagues Dr. Fulvio Amato and Dr. Maria Izquierdo for their continuous help and support. Many thanks for all their help to Dr. Cristina Reche and Garay Sosa, two of the most kind, helpful and generous colleagues one can have. I would also like to acknowledge a team of specialized colleagues: Natalia Moreno, Mercè Cabañas, Rafael Bartrolí, Silvia Martínez, Rebeca Vazquez and Diana Blanco for their remarkable technical support in the analytical laboratories. To all of my fellow colleagues at the EGAR group of IDAEA-CSIC: Dr. Teresa Moreno, Dr. Marco Pandolfi, Dr. Patricia Córdoba, Marina Ealo, Dr. Aurelio Tobias, Elena Martínez, Dr. Gloria Titos, Amaia Fernandez, Jesús Yus, Pedro Trechera, Marten in't Veld, Marta Via, Dr. Maria-Cruz Minguillón, Cristina Carnerero and whoever I might be forgetting, thank you for creating a wonderful working environment.

For the artwork on the cover of this Thesis, I thank my friend Akis Hondas (Ink's_Sins©). I owe gratitude to my parents for supporting my education throughout the years. Above all, I am entirely grateful to my family, which I thank for everything.